The role of age and complement in CD8$^+$ T cell function during human metapneumovirus (HMPV) infection

by

Olivia B. Parks

Bachelor of Science, University of Pittsburgh, 2018

Submitted to the Graduate Faculty of the

School of Medicine in partial fulfillment

of the requirements for the degree of

Doctor of Philosophy

University of Pittsburgh

2024

UNIVERSITY OF PITTSBURGH

SCHOOL OF MEDICINE

This dissertation was presented

by

Olivia B. Parks

It was defended on

January 8, 2024

and approved by

Committee Chair: Lawrence P. Kane, PhD, Professor and Vice Chair for Education, Immunology

Beibei Bill Chen, PhD, Professor, Pulmonary, Allergy and Critical Care Medicine

Rachel A. Gottschalk, PhD, Assistant Professor, Immunology

Anita K. McElroy, MD, PhD, Assistant Professor, Pediatrics

Thesis Advisor/Dissertation Director: John V. Williams, MD, Professor, Pediatrics and Microbiology & Molecular Genetics

The role of age and complement in CD8$^+$ T cell function during human metapneumovirus (HMPV) infection

Olivia B. Parks, PhD

University of Pittsburgh, 2024

Human metapneumovirus (HMPV) is a leading cause of severe respiratory disease in young children <5yrs old, older adults >65yrs old, and the immunocompromised. HMPV immunity is incomplete with re-infections occurring throughout childhood and adulthood. Re-infections usually result in mild, self-resolving disease except in the elderly, who are at risk for severe disease and co-morbidities. The aged immune response to respiratory viruses such as HMPV is not fully understood. Aging studies have identified marked CD8$^+$ T cell dysfunction due to cell-intrinsic epigenetic changes in gene expression and subsequent function. Thus, we hypothesized that age-related CD8$^+$ T cell dysfunction contributes to severe respiratory disease in the aged host. We found that aged mice produced fewer HMPV tetramer$^+$ CD8$^+$ T cells, which had higher PD-1 expression and other inhibitory receptors and were less polyfunctional with decreased granzyme B. Previous studies have also identified an integral role of PD-1/L signaling in CD8$^+$ T cell function in a young host. Blockade of PD-1/L signaling improves CD8$^+$ T cell antiviral function in young mice. We further hypothesized that PD-1/L signaling was also critical to rejuvenate exhausted CD8$^+$ T cells in the aged host. We found that removal of PD-1 improved granzyme B production and reduced the accumulation of cytotoxic tissue-resident memory CD8$^+$ T cells in the aged host. In a concurrent study, we investigated other regulators of CD8$^+$ T cell function during HMPV infection. Notably, we found that the complement protein, C1q, produced by inflammatory monocytes modulates CD8$^+$ T cell antiviral function through the receptor, gC1qR. Taken together, this work explores the relationship between severe respiratory disease in an aged mouse model

and $CD8^+$ T cell function upon primary infection and re-challenge, the role of PD-1/L signaling in aged $CD8^+$ T cell antiviral function, and identifies C1q as a novel regulator of $CD8^+$ T cell function.

Table of Contents

List of Tables

List of Figures

List of Appendix Figures

Preface

Alexander Fleming once said “One sometimes finds what one is not looking for”. I was assigned Alexander Fleming for a history paper in 8th grade and I became inspired by his journey as a physician and discovery of penicillin. To me he represented the discovery and excitement that comes with medicine and research, which culminated in one of the greatest medical advancements in our history.

I’m reminded of this quote while I write my dissertation because I never saw myself pursuing a dual MD/PhD degree. I always knew I wanted to be a neonatologist, but if it wasn’t for several key people along the way, I would not have realized my passion for both research and academic medicine. I want to thank Toby Yanowitz, MD, MS and Misty Good, MD, MS for supporting and guiding me through high school and college to ultimately apply into the MD/PhD program at Pitt Med. Misty especially opened up many doors for me along the way when I worked with her in Jay Kolls’ lab at Children’s Hospital.

I also want to thank my career advisor, Craig Byersdorfer, MD/PhD for helping me with my MSTP application and encouraging me to apply into the MSTP program as a second year medical student. Not only has he been a fantastic career advisor, but he and his lab became collaborators in my PhD work which developed into a vital part of my thesis project. I know that the skills and techniques I learned in his lab will stay with me in all my future immunology research.

The biggest lesson I learned during graduate school was that science is all about taking chances, trying new things, making mistakes, and learning from them. I was lucky to be a part of John Williams’ lab where I was surrounded by people who were collegial, supportive, and just

altogether good people. I want to thank Jie Lan, PhD for introducing me to the world of flow cytometry, Yu Zhang, PhD for teaching me cell culture and Williams lab virology techniques, Sara Walters, MS for teaching me all about mice, breeding patterns, and colony maintenance, Moni Johnson, MS for patiently ordering all of my lab supplies and helping me with qPCR, and Taylor Eddens, MD/PhD for being a fantastic mentor both for my project and for everything related to the CHP PedSDP program. I also want to thank Megan Freeman, MD/PhD for being a strong female role model and for connecting me with Williams lab alumnus, John Erickson, MD/PhD. Even though we've never met in person, John has become an incredibly influential mentor, making significant scientific contributions to my third F30 submission and two of my papers. It has been an honor learning from him and I am grateful to have established this connection as I continue my training. Lastly, I want to especially thank my mentor, John Williams, MD, for helping me with all *three* of my F30 submissions, continually editing and offering experiment suggestions for each of the three arms of my project, and for always being available for any and all career advice. In the Williams lab, I've learned so many crucial skills in experimental design, grant writing, collaborating, and problem solving when experiments don't go quite the way you planned, all of which I can carry with me and build upon in my future research.

I often have said that my mom deserves an honorary PhD for all that she has done to support me along my journey. She has never said no to listening to another presentation, proofreading my emails, or giving advice on situations that have arose at every stage of my journey. I truly would not have been able to do any of this without her and I am forever grateful.

As someone who is interested in going into neonatology, I never saw myself pursuing a PhD and I certainly never saw myself studying the aged immune response. However, the

knowledge, connections, and mentors that I have gained along the way during graduate school just goes to show that sometimes “one [really] does find what one is not looking for”.

1.0 Introduction

1.1 Human Metapneumovirus: The Pathogen

1.1.1 Epidemiology

Human metapneumovirus (HMPV) was first discovered in 2001 in the Netherlands from nasopharyngeal samples of 28 children with lower respiratory illness (1). Like other respiratory pathogens, HMPV has a seasonal distribution, but in temperate regions tends to peak 1-2 months later than RSV and influenza, which have the highest prevalence in the winter months (1, 2).

Nearly all children worldwide are seropositive for human metapneumovirus (HMPV) by age five and reinfections occur throughout adult life, leading to mild, self-resolving disease (1, 3). Children under two years old, immunocompromised individuals at all ages or those who have pre-existing pulmonary conditions (i.e. asthma or emphysema), and the elderly are at the greatest risk of severe disease (1, 4).

HMPV infections in children worldwide account for 6-40% of all acute respiratory illness (1, 5-7). The peak hospitalization age for HMPV infection in children is 6-12 months (1, 3). Studies have found that the majority of young adults <65 yrs who are hospitalized for HMPV have underlying conditions such as cystic fibrosis or lymphoma (1, 8, 9). Adults >65 yrs old represent an equal or larger proportion of HMPV-associated hospitalizations compared to children <5 yrs old (8). A retrospective study over nine years found that older adults accounted for 45.9% of

hospitalizations for HMPV infection (median age 74) while 35.1% were children <5 yrs old (8). These findings indicate the significant burden that HMPV infections place on young and aged individuals.

1.1.2 Transmission & Clinical Features

HMPV is spread from direct or close contact with HMPV infected individuals or contaminated objects (i.e. fomites). HMPV RNA can be detected in the respiratory tract five days to two weeks after symptom onset (10). Common presenting symptoms of HMPV disease include fever, cough, and rhinorrhea with 50% of cases also reporting wheezing (3). Infants and the elderly have higher risk of hospitalization and death from HMPV (3). Adults hospitalized for HMPV infection typically present with pneumonia and a spectrum of upper and lower respiratory tract symptoms (e.g. cough, wheeze, dyspnea) (11). Viral or bacterial co-infections with HMPV are common, especially in the elderly population. Usually, viral co-infections do not increase disease severity in the elderly (12). However bacterial co-infections can increase the risk of co-morbidities (i.e. pneumonia) and mortality (8, 13-15).

1.1.3 Diagnosis

The presenting symptoms of HMPV infection are indistinguishable from other respiratory viral infections. The virus grows slowly in culture, so culture is not a reliable means for diagnosis of HMPV infections.

Methods of HMPV detection include: nucleic acid amplification tests such as RT-qPCR, cell culture, enzyme immune-assay (EIA), direct immunofluorescent-antibody (IFA) test, and enzyme-linked immunosorbent assay (ELISA) (2). RT-qPCR and cell culture can directly detect virus, infected cells can be detected via IFA, while the host response to infection is best measured through serologic tests EIA and ELISA. Most of these are not commonly used since they lack the sensitivity and specificity of RT-qPCR (2). Serologic testing is useful for epidemiologic studies especially when combined with RT-qPCR (10, 16). Therefore, the gold standard for diagnosis in the clinical setting is RT-qPCR, for which there are several commercially available multiplex kits (17-19).

1.1.4 Virology of HMPV

HMPV is an enveloped, negative-sense, non-segmented, single-stranded RNA virus (1). HMPV belongs to the *Pneumoviridae* subfamily along with respiratory syncytial virus (RSV), which is distinct from but related to the *Paramyxoviridae* family (1). The HMPV genome is comprised of approximately 13,000 nucleotides (1). There are eight genes which encode nine proteins: N (nucleoprotein), P (phosphoprotein), M (matrix protein), F (fusion protein), M2 (M2-1 and M2-2 proteins), SH (small hydrophobic protein), G (attachment glycoprotein), and L (large polymerase protein) (1). **Fig. 1-2** depicts the gene arrangement, length, and function of the nine proteins.

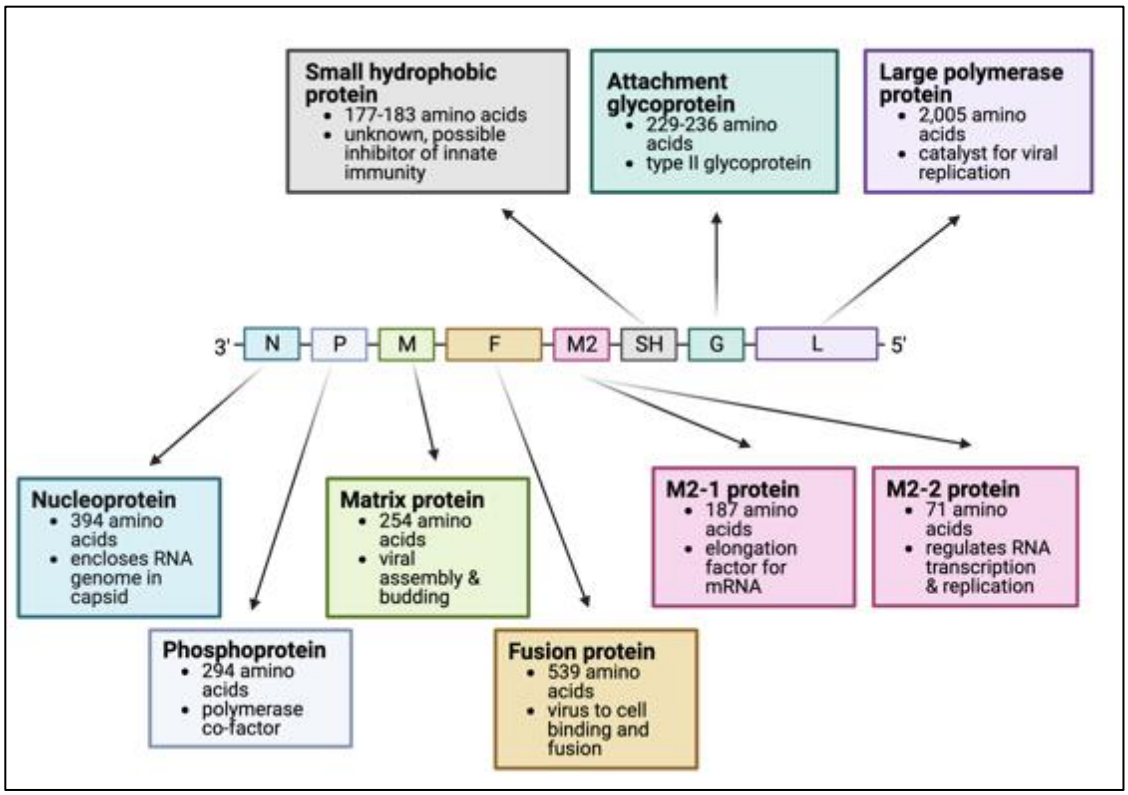

Figure 1-1. HMPV genome

A schematic of the HMPV genome showing each gene and the cooresponding proteins they transcribe.

HMPV has a long propagation time of up to fourteen days and is difficult to grow in culture, requiring trypsin for adequate *in vitro* replication (20). HMPV grows optimally in LLC-MK2 (rhesus kidney) cells, creating cytopathic effects (20).

Phylogenetic evolutionary analyses suggest that HMPV derived from Avian metapneumovirus about 200-400 years ago (21-24). Avian metapneumovirus infects turkeys, chickens, and ducks with a 100% morbidity rate, but low mortality (25). Of the four subtypes of avian metapneumovirus, HMPV is most closely related to avian subtype C, which was discovered in the United States in 1996 (26). However, HMPV appears to be now fully adapted to humans and cannot form a productive infection in birds (26).

There are two main genetic lineages of HMPV, A and B, which are each divided into two clades (i.e. A1, A2, B1, and B2) (21-23, 27). The dominant lineage of HMPV can vary each year, but all HMPV genes are highly conserved in these four clades (21). There is cross-protection and cross-neutralization between clades, which suggests that HMPV isolates from these clades are not distinct serotypes (28-30).

HMPV primarily infects ciliated airway epithelial cells and some innate immune cells including monocyte-derived dendritic cells (MDDCs) (31). HMPV initially replicates in the upper respiratory tract, but has the ability to spread to the bronchioles and alveoli in the lower respiratory tract (32). The viral F and G proteins are the primary mediators of attachment to airway epithelial cells (32). HMPV enters cells in a dynamin-dependent manner by clathrin-mediated endocytosis before fusing with endosomes (33). In the HMPV F protein there is an invariant arginine-glycine-aspartate (RGD) motif that binds to the integrin $\alpha V\beta 1$ and other RGD-binding integrins to promote attachment and endocytosis of HMPV into the airway epithelial cell (33). HMPV infection is only productive when the F protein is expressed and the virus is capable of infecting airway epithelial cells even in the absence of G protein expression, indicating that F protein facilitates infection of the upper respiratory tract independent of G protein (34).

1.1.5 Immune response to HMPV

Innate Immune Response

HMPV infection of airway epithelial cells induces the RIG-I/MAVS signaling pathways, which causes IRF and NK-κB activation, leading to pro-inflammatory cytokine gene expression (35). In

addition, infected airway epithelial cells express viral RNAs that is recognized by toll-like receptors (TLRs) TLR3, TLR7, and TLR8 in innate immune cells, in particular in dendritic cells (DCs) (35). DCs are one of the first cell types to encounter and respond to HMPV, thus facilitating further innate cell recruitment to the lung and priming of naïve $CD4^+$ and $CD8^+$ T cells in the draining lymph nodes. Neutrophils (36), eosinophils (37, 38), DCs (39), and monocytes/macrophages (40) have all been implicated in the innate immune response to HMPV. However, natural killer cells (NK cells) do not significantly contribute to acute viral clearance during HMPV infection (41).

Type I interferon (IFNα and IFNβ) signaling is critical in the acute phase of respiratory viral infection. Type I interferon act via autocrine and paracrine signaling to activate ISGs to promote an antiviral response in cells at the site of infection (35). Type I IFNs are produced primarily by infected airway epithelial cells as well as plasmacytoid DCs (pDCs) upon viral infection. Alveolar macrophages (AM) are also capable of becoming infected with HMPV and can produce IFN (32). Type I IFN then binds to the IFNαR receptor on innate immune cells, primarily DCs, activating a signaling cascade leading to phosphorylation of STAT1/2 which promotes transcription of ISGs (35). ISGs are viral sensors so the upregulation during infection allows more cells to detect the virus (42). This process also regulates the recruitment of innate immune cells, particularly neutrophils and inflammatory monocytes, to the lung early in infection (36).

HMPV and RSV are all capable of inhibiting IFN expression during infection (43). The HMPV small hydrophobic (SH) protein impairs IFN production by inhibiting STAT1 phosphorylation (44, 45). Innate immunity has been shown to exacerbate HMPV disease. A phenomenon still being

explored is that mice with the IFNα receptor genetically ablated ($IFNAR^{-/-}$ mice) exhibited less severe disease, reduced lung inflammation, diminished viral spread in lung epithelial cells, and mounted higher antibody titers compared to wild-type (WT) mice (43).

There is also a nexus between IFNAR expression and programmed cell death-ligand 1 (PD-L1) expression on DCs and interstitial macrophages (IMs) (43). Type I IFNs play a role in shaping the adaptive immune response by inducing expression of PD-L1 on DCs (43). DCs and IMs from $IFNAR^{-/-}$ mice have decreased PD-L1 expression compared to WT mice and there were fewer DCs recruited to the lung in $IFNAR^{-/-}$ mice (43). Despite the improved clinical outcome in $IFNAR^{-/-}$ mice, $IFNAR^{-/-}$ $CD8^{+}$ T cells were more functionally impaired, which could be due to the upregulation of another inhibitory receptor - T cell immunoglobulin and mucin-domain containing-3 (TIM-3) expression (43).

Overall, the innate immune response to HMPV infection is important to control viral replication in the upper airways and activate the adaptive immune response to ultimately form a memory T cell compartment.

Adaptive Immune Response

B and T lymphocytes have distinct roles in the adaptive immune response. B lymphocytes mediate the humoral arm of the adaptive immune response primarily by producing antibodies against viral antigens. T lymphocytes regulate the cell-mediated response by coordinating with antigen presenting cells (APCs) such as dendritic cells (DCs) to produce cytotoxic $CD8^{+}$ T cells that can recognize and kill virally infected cells. Despite seropositivity reaching 100% of children

worldwide by five years of age, reinfections occur often throughout childhood and adult life (46), suggesting that humoral immunity is insufficient to protect against reinfections. Neutralizing antibodies primarily target the HMPV F protein (47). The neutralizing capacity of HMPV antibodies is less robust compared to antibodies against RSV F protein (47). In addition, neutralizing F protein antibodies isolated from memory B cells post-HMPV infection appear to be less dominant against the antigen (47), which indicates that the humoral response is insufficient to protect fully against re-infections (48). Therefore the T cell-mediated arm of the adaptive immune system is important in preventing severe disease, particularly in vulnerable populations including infants, the elderly, and immunocompromised (49, 50).

$CD4^+$ and $CD8^+$ T cell depletion studies in mice show that $CD4^+$ T cells contribute to lung pathology and clinical disease after HMPV infection (51). Removing $CD4^+$ T cell help resulted in impaired antibody production (51). Despite this, mice that lacked $CD4^+$ T cells were still able to clear virus, indicating that $CD8^+$ T cells were the primary cell type responsible for clearance of HMPV (46, 51).

$CD8^+$ T cells in the lung become functionally impaired by day seven post-infection (p.i.), a state characterized by decreased effector function (i.e. IFNγ, granzyme B) and upregulation of inhibitory receptors (i.e. PD-1, TIM-3, LAG-3) (52). Notably, $CD8^+$ T cells at day seven p.i. during HMPV infection have a similar gene expression profile compared to canonically exhausted $CD8^+$ T cells on day 30 during chronic LCMV infection (52). Despite vaccinating mice with virus-like particles (VLPs) expressing the HMPV F and M proteins, $CD8^+$ T cells still upregulated inhibitory

receptors, including programmed cell death protein 1 (PD-1) and exhibited functional impairment in degranulation (53).

PD-1 signaling has often been described as a "brake" that regulates $CD8^+$ T cell function (54). Tumor-infiltrating $CD8^+$ T cells that have high PD-1 expression are usually described as being "exhausted" (55). Therefore, one modality of cancer immunotherapy uses PD-1/L1 blockade to improve the function of exhausted tumor-infiltrating $CD8^+$ T cells (56). This checkpoint blockade therapy has also been extended to chronic viral infections, where a similar population of exhausted $CD8^+$ T cells accumulates due to chronic antigen stimulation (57).

PD-1 is expressed ubiquitously on NK cells, B cells, and both $CD4^+$ and $CD8^+$ T cells (58). PD-1 also plays an important role in regulating $CD8^+$ T cell function during HMPV infection (46). PD-1 interacts with ligands PD-L1 and PD-L2, which are expressed on a variety of cells including innate immune cells, antigen-presenting cells, and airway epithelial cells (59, 60). During HMPV infection, $CD8^+$ T cells upregulate PD-1 on the cell surface, which interacts directly with its ligands to inhibit phosphorylation of ZAP70 and PI3K, by initiating recruitment of the phosphatases SHP1 and SHP2 (58). ZAP70 and PI3K are direct downstream mediators of TCR signal transduction (58). In this way, PD-1 exerts its inhibitory effects to prevent the activation of $CD8^+$ T cells during HMPV infection, which contributes to the $CD8^+$ T cell functional impairment and exhaustion-like phenotype observed during initial infection and re-challenge (46, 52, 61, 62).

PD-1 also serves as an activation marker on T regulatory $CD4^+$ (Treg) cells (63). Tregs have temporally distinct roles during HMPV infection. Treg depletion two days p.i. results in increased

$CD8^+$ T cell function and production of more virus-specific $CD8^+$ T cells (63). In contrast, depleting Tregs prior to infection impairs $CD8^+$ tetramer production and causes delayed viral clearance (63).

Taken together, numerous studies have shown that $CD8^+$ T cells are an integral part of the adaptive immune response to HMPV. In particular, targeting the PD-1 pathway on $CD8^+$ T cells may be a potential therapeutic to optimize $CD8^+$ T cell function and ameliorate severe disease.

1.1.6 Treatment & Vaccine Development

Currently, the first line treatment option for HMPV infection is supportive therapy. However, there are several therapeutic options tested *in vitro* and in animal models that exhibit potential for preventing or ameliorating severe HMPV disease.

Immunoglobulins have been developed as therapeutic options for HMPV in animal models. The HMPV-specific human Fab DS7, human monoclonal antibody, caused a dose-dependent reduction in viral titer in the lungs of cotton rats (64, 65). In addition, an antibody that targets the HMPV fusion F protein, Mab338, was effective both before infection, as prevention, and after infection as a therapeutic option (66-68). In animal models, Mab338 reduced viral titer and neutralized all four subgroups of HMPV (65).

Fusion inhibitors have also been considered as treatment options. Several fusion inhibitors show efficacy *in vitro* in blocking HMPV replication. In BALB/c mice, the HRA2 fusion inhibitors administered with a lethal HMPV infection protected against severe disease and mortality (69).

Another group found that HR-1 peptides were able to inhibit HMPV post-infection, making them potentially useful after exposure in patient populations particularly vulnerable to severe HMPV infection (70).

Ribavirin is active against a broad spectrum of RNA and DNA viruses. Case reports suggest that combination treatment of ribavirin and polyclonal intravenous immune globulin (IVIG) ameliorates severe HMPV infection (71-73). However, there are no randomized controlled trials to confirm these findings. Ribavirin and IVIG are expensive, and a small particle aerosol generator is required to administer ribavirin, creating logistical challenges (74). Ribavirin is also a teratogen, which limits its use in the clinical setting (74).

RNA interference (RNAi) represents yet another approach for treatment of HMPV infections, although not necessarily practical in humans due to the cytokine storm this treatment can induce (75). One study showed that small interfering RNA (siRNA) can target the G gene of HMPV *in vitro* (76). While siRNA against G protein did not have a significant effect on viral growth in these experiments, it still has potential to impact HMPV gene replication, since G protein is critical for HMPV viral replication.

There are currently no licensed vaccines available for HMPV. Transgenic mice for the human HLA MHC-I allele B*07:02 (HLA-B7) were used to screen $CD8^+$ T cell epitopes for the HMPV F, M, and N proteins to identify potential vaccine antigens (77). Other avenues of vaccine development include: inactivated vaccines (78, 79), viral protein-based vaccines (80), and live attenuated vaccines (81). HMPV F protein is the most promising candidate for a protein-based

vaccine (80). Inactivated vaccines led to increased pulmonary disease and a robust Th2 response upon HMPV rechallenge in mice? (78, 79), which make them less promising candidates. When mice received an intraperitoneal injection of F protein coupled with a retroviral core particle carrier, there was a decrease in mortality and an increase in neutralizing antibody production to both homologous and heterologous HMPV strains (80). Finally, a live attenuated HMPV vaccine candidate has been approved for human trials (81).

In all, there are numerous therapeutics that show promising results both *in vitro* and *in vivo* in animal models to target severe disease in vulnerable populations, such as the elderly. Furthermore, there are also useful tools available to promote HMPV vaccine development.

1.2 Respiratory Viral Infections in The Elderly

Adapted from:

Respiratory Virus Immune Response in the Aged Host

Olivia B. Parks[1], Anusha Kalavacharla[1], John V. Williams[1,#]

[1] Department of Pediatrics, University of Pittsburgh School of Medicine, Pittsburgh, PA, USA

In preparation for publication in *Frontiers Immunology*

Respiratory viral infections (RVI) in the elderly are a major cause of morbidity and mortality, comprising 13-31% of all respiratory illnesses documented in this population (82-85). By 2050, it

is projected that adults >60 years old will comprise 22% of the population worldwide (86). Prior to the COVID-19 pandemic, RVI in the elderly placed a significant burden on the US healthcare system. The average annual direct medical costs in the US calculated from several influenza seasons was approximately $10.4 billion, with 64% of this cost allocated to individuals 65 years and older (87). Since the pandemic began, patients 50 years and older infected with SARS-CoV-2 comprised greater than 94% of the deaths (88). In 2020 alone, $6.3 billion were spent on Medicare costs for COVID-19-related hospitalizations (89). Thus, both before and after the COVID-19 pandemic, RVI take a significant toll on the healthcare system and quality of life of older adults.

Lower respiratory tract infections caused by influenza virus and respiratory syncytial virus (RSV) are leading causes of hospitalization of elderly patients, resulting in approximately 53,800 deaths annually in those 65 and above in the US (83, 84, 90). Further, up to 90% of all influenza-related deaths in the US each year occur in the elderly (91). Rhinovirus and human metapneumovirus (HMPV) are also common causes of severe LRI affecting the aged population (92). There is a significant RVI burden in nursing homes, with an average LRI affecting 1.4-2.8/1000 resident days (82, 93). One retrospective study of over 2000 subjects hospitalized for LRI identified RSV in >10% of individuals ≥65 and 8% among those 50-64 years (94, 95). Another study of hospitalizations due to HMPV over nine winter seasons found that 46% were individuals >65yrs while 35% were children <2 years (8). This study also concluded that HMPV and parainfluenza viruses 1-4 (PIV) had similar prevalence, accounting for LRI that were not caused by RSV or influenza virus (8).

Studies in nursing homes have confirmed serious outcomes from LRI in the elderly, with one study reporting a case-fatality rate of 8% among 480 residents with confirmed LRI (93). These effects are compounded by the fact that many elderly patients suffering from LRI have atypical presentations such as anorexia, confusion, dizziness, and ataxia (84, 96), which increase the risk for late diagnosis and treatment (83). Patients that are clinically suspected of LRI may have false negative rapid antigen detection tests since these tests are less sensitive in elderly patients (83). A recent study also found that HMPV and COVID-19 share similar clinical presentations, underscoring the importance of accurate diagnosis and testing especially in the elderly population (97). Due to the atypical presentation and delay in diagnosis of LRI in the elderly, antiviral therapy may not be provided in a timely fashion (98). In addition, secondary bacterial infection is a common complication of LRI, found in about 10-30% of elderly patients infected with respiratory viruses such as influenza virus or RSV (98-102).

Research into the aging immune system has identified changes in both innate and adaptive immune cells that lead to decreased function using *in vitro* and *in vivo* models. Leukocytes are rapidly dividing cells and therefore suffer disproportionately from the genetic effects of aging, including genomic instability, epigenetic changes, and deteriorating telomeres (91). Impaired leukocyte function leads to immunosenescence, a compensatory chronic pro-inflammatory state, as well as immune cell exhaustion. The culmination of this disequilibrium in inflammatory and immune cell response leads to delayed viral clearance, viral dissemination to the lower respiratory tract, and an overall increased risk of morbidity and mortality.

1.3 The Immune System in the Aging Lung

Increased age affects virtually every aspect of the immune system. Specifically, monocytes, macrophages, and $CD8^+$ T cells undergo several age-related phenotypic changes that affect their function in the aged host particularly during respiratory virus infection.

1.3.1 Monocytes & Macrophages

Expression of the monocyte lineage marker CD68 is decreased in bone marrow from aged mice, indicating a decrease in macrophage precursors (103, 104). Accordingly, scRNA-seq analysis in aged mice shows reduced fetal-derived tissue-resident macrophages particularly in the lung (105). Aged mice had unchanged levels of circulating bone-marrow derived myeloid cells but increased expression of pro-inflammatory genes such as *Ccl5* and *Gdf15 (105)*. Interferon (IFN)γ-stimulated macrophages from aged mice expressed 50% less major histocompatibility complex (MHC) class II compared to young cells (103, 106)**.** Studies on circulating monocytes in the peripheral blood of elderly patients revealed that aged individuals had increased $CD14^+$ $CD16^+$ pro-inflammatory monocytes, in line with studies in aged mice (107-109). When aged monocytes from elderly humans were stimulated with TLR4 they exhibited impaired phagocytosis and increased intracellular tumor necrosis factor (TNF) production, indicating impaired monocyte function (107). Thus, both murine and human aged monocytes and macrophages exhibit defects in signaling, MHC-II expression, and phagocytosis.

Alveolar and interstitial macrophages represent the first line of defense in the lung against RVI (32, 110). These macrophages are the primary producers of pro-inflammatory cytokines such as

TNF, IL-6, and IL-8 that serve an essential role in controlling respiratory viruses such as RSV and influenza (32, 111, 112). Alveolar macrophages (AM) are a self-renewing population of tissue-resident macrophages that primarily serve an anti-inflammatory role to phagocytose foreign particles and secrete anti-inflammatory cytokines such as TGF-β and IL-10 to control the inflammatory immune response by neighboring cells (113). Interstitial macrophages (IM) are a unique subset of macrophages that derive from circulating monocytes (113). They secrete immunoregulatory cytokines such as IL-10, present antigen via MHC-II, and control Th2 allergic inflammation (113). Influenza infection of aged mice showed a decreased number of macrophages localizing to the lung as well as down-regulation of cell cycling pathways in AM (114). A recent study used heterochronic adoptive transfer and parabiosis techniques to determine that the aged lung microenvironment may prevent AM from proliferating during influenza infection, thus contributing to delayed viral clearance (115). In addition, Blacher *et al* found that aged macrophages had decreased expression of Kruppel-like factor 4 (KLF4) which regulates circadian clock genes in macrophages (116). Age-associated downregulation of KLF4 in aged macrophages could prevent diurnal trafficking of these cells from the bone marrow to sites of infection (116). Furthermore, gene expression analysis revealed only 53 genes undergoing rhythmic transcription in aged macrophages compared to 680 genes in macrophages from young mice (116). Humans 65 and older who were carriers of certain KLF4 hypomorphic alleles KLF4 were more prone to developing infections and had increased mortality compared to younger individuals who were non-carriers (116).

Taken together, there are distinct changes in the inflammatory profile and gene expression signature of monocytes and macrophages in the aged host, particularly in the lung

microenvironment where it has been heavily studied. This contributes to the increased susceptibility of elderly patients to respiratory viral infections.

1.3.2 Inflammaging

The "Inflammaging Hypothesis" is an explanation of immunosenescence (117) and refers to the observation that the aged host exhibits increased basal levels of pro-inflammatory cytokines, most notably C-reactive protein (CRP), TNF, IL-1β, and IL-6, and an impaired anti-inflammatory response (117-119) (**Fig. 1-3**). It is posited that inflammaging is the "first hit" leading to a heightened proinflammatory state, which predisposes the aged individual to a second hit consisting of an absence of 'robust' immune response genes and a presence of 'frail' genes. This heightens susceptibility to infection or systemic disease (119). This two-hit hypothesis helps explain the pathogenesis of multisystem conditions such as atherosclerosis, diabetes, Alzheimer's, and most importantly for this discussion, immune dysfunction and increased risk of severe RVI in the elderly patient (119-121). In addition to this two-hit hypothesis, a decrease in cortisol production and impaired function of the Hypothalamus-Pituitary-Adrenal (HPA) axis shifts the balance from an anti-inflammatory to a pro-inflammatory response (122). Chronic inflammation in the aged host is strongly associated with a greater incidence of chronic disease and decreased immune response to infection leading to increased mortality and prolonged hospital stay (123-127). Studies in aged humans, particularly centenarians, have shown that chronic inflammation is counteracted by anti-inflammaging cytokines such as IL-1Ra, IL-4, IL-10, and TGF-β1 (117). When this balance between pro and anti-inflammatory cytokines is lost, inflammaging dominates, leading to an impaired immune response and increased susceptibility to RVI.

Aged mice (>18 months) have elevated levels of pro-inflammatory cytokines at baseline compared to young adult mice (2-6 months) (119, 123, 128). This imbalance leads to chronic inflammation and multisystem pathological effects (129). Franceschi *et al* suggested there is a threshold, which varies between individuals, for which the pro-inflammatory state is beneficial, promoting immune cell maturation and immunological memory (119, 130). When the basal pro-inflammatory response surpasses this threshold, the beneficial effects of inflammation are lost, and the detrimental pathological effects of inflammation dominate. This promotes a shift towards more pro-inflammatory macrophages and further perpetuates an impaired antiviral response leading to severe LRI in the aged host. Individuals who live to extreme age, such as centenarians, may have an inherently higher threshold for this pro-inflammatory shift (119, 131-133).

Chronic cytomegalovirus (CMV) infection, which is latent in most adults, can lead to an accumulation of cellular debris and chronic inflammation (130, 134). CMV infection promotes a pro-inflammatory microenvironment that accelerates immunosenescence and inflammaging (130, 135). In the presence of the inflammaging microenvironment, innate immune receptors such as TLRs and NOD-like receptors (NLRs) respond to more danger associated molecular proteins (DAMPS) which are a result of misfolded proteins, nucleic acids, and apoptotic cells. TLRs and NLRs have increased basal activation from these DAMPS and produce more inflammatory cytokines (130, 136).

In conjunction with inflammaging, there are substantial epigenetic and metabolic changes that occur in innate immune cells, particularly monocytes and macrophages (137) (**Fig. 1-3**). Upon each encounter with pathogens, these innate immune cells are reprogrammed via long noncoding

RNAs (lnRNAs) and modifications of histones (i.e. H3K4me3) to upregulate glycolysis and oxidative phosphorylation (137). When the same pathogen is encountered again, these modified innate immune cells are able to respond more quickly and robustly to the pathogen. Studies have shown that BCG vaccination in humans can enhance trained immunity via heterologous protection and promote increased expression of myeloid genes in HSCs (138).

Taken together, inflammaging represents a critical part of the aging immune system. Further studies are needed to elucidate the interaction between inflammaging and trained immunity during RVI in the aged host.

1.3.3 $CD8^+$ T lymphocytes

$CD8^+$ T lymphocytes are a crucial component of the immune response to HMPV and other respiratory viruses. Studies of the human T cell response to influenza vaccine found that $CD8^+$ T lymphocytes in the elderly patient failed to produce adequate levels of $CD8^+$ effector cytokines, granzyme B, and IFNγ (91, 139, 140) (**Fig. 1-3**). The inhibitory receptor programmed cell death protein 1 (PD-1), which is associated with lung T cell impairment during RVI (46, 141), was upregulated at baseline on T cells of uninfected, otherwise healthy, aged mice compared to their young counterparts (142) (**Fig. 1-3**).

Although the $CD8^+$ T cell population is markedly increased in the aged host, sometimes comprising as much as 70-80% of the total $CD3^+$ T cell population, these cells have reduced T cell receptor diversity and impaired $CD8^+$ T cell response in a murine influenza model (143, 144). In addition, with increasing age there is a decline in naïve T cells (T_N) and an increase in virtual

memory T cells (T_{VM}) (145). T_{VM} are a subset of antigen inexperienced $CD8^+$ T cells that express high levels of CD44 and the receptors for IL-15 and IL-17 (145). T_{VM} are rapid responders to antigen in young mice, but with increased age these T_{VM} exhibit decreased function and a senescence profile (145). One group found that aged T_{VM} failed to proliferate upon stimulation, had impaired accumulation of cyclin D1, and increased expression of Bcl-2 in both *in vitro* and *in vivo* studies (145). Furthermore, adoptive transfer of aged $CD8^+$ T cells into young mice failed to recover the T_{VM} rapid response to antigen that was observed in young mice.

Overall, these findings support that there are significant deficits in $CD8^+$ T lymphocytes with increasing age. The central hypothesis of this thesis is that age-dependent defects in $CD8^+$ T cells contribute to severe HMPV disease in the aged host.

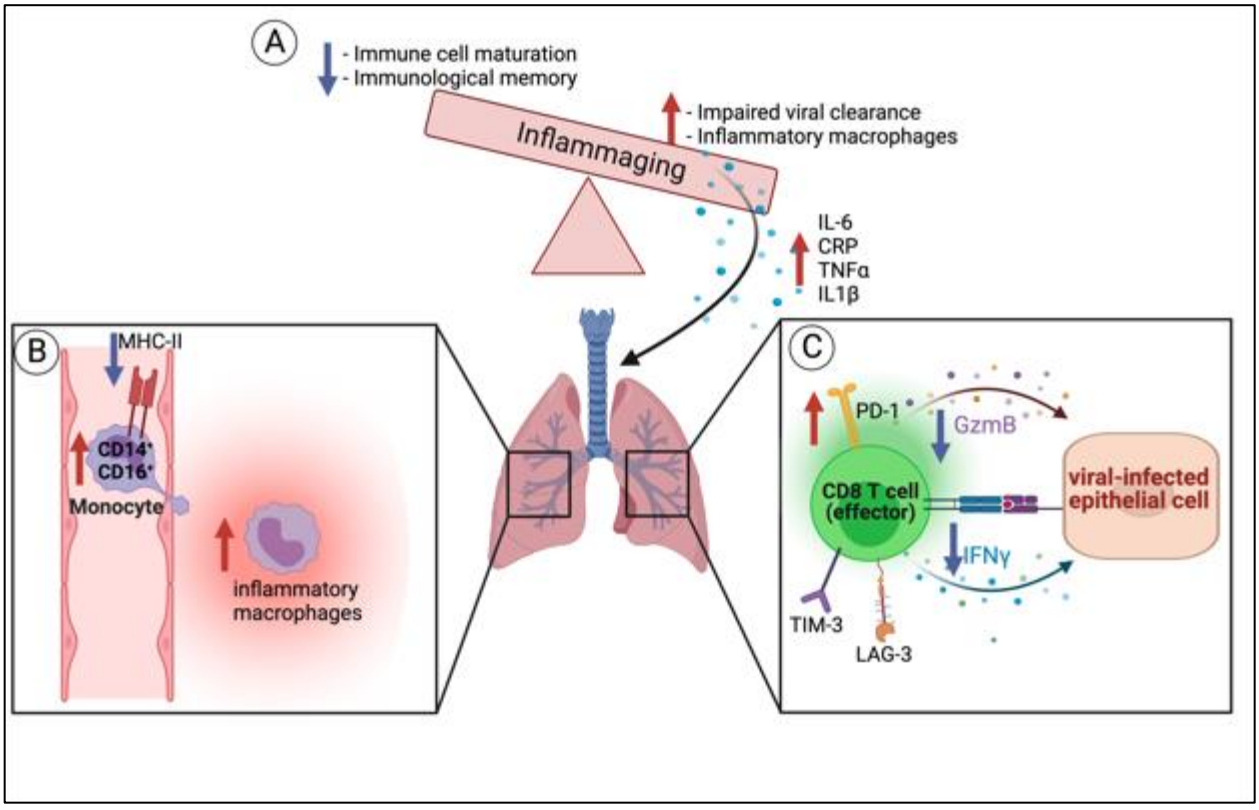

Figure 1-2. The immune system in the aging lung.

(A) Aging is associated with a skewing towards increased production of inflammatory cytokines and macrophages, leading to impaired viral clearance. **(B)** The aged host produces more $CD14^+$ $CD16^+$ inflammatory macrophages that circulate in the bloodstream and migrate to inflamed tissues, such as the lung. **(C)** $CD8^+$ T cells that were primed in the lymph node migrate to the site of infection in the lung. Aged $CD8^+$ T cells upregulate inhibitory receptors such as PD-1, TIM-3, and LAG-3 and have decreased production of antiviral cytokines granzyme B and IFNγ. Abbreviations: IL-6: Interleukin-6, CRP: C-reactive protein, TNFα: tumor necrosis factor α, IL-1β: Interleukin-1 β, MHC-II: Major histocompatibility complex-II, PD-1: Programmed cell death protein 1, TIM-3: T cell immunoglobulin and mucin domain-containing protein 3, LAG-3: Lymphocyte-Activation Gene 3.

2.0 Terminally Exhausted CD8$^+$ T Cells Contribute to Age-Dependent Severity of Respiratory Virus Infection

Adapted from:

Terminally exhausted CD8$^+$ T cells contribute to age-dependent severity of respiratory virus infection

Olivia B. Parks[1], Taylor Eddens[2], Jorna Sojati[1], Jie Lan[1], Yu Zhang[1], Tim D. Oury[3], Manda Ramsey[4], John J. Erickson[5], Craig A. Byersdorfer[4], John V. Williams[1,6,#]

[1]Department of Pediatrics, Division of Infectious Diseases, University of Pittsburgh School of Medicine, Pittsburgh, PA, USA

[2]Department of Pediatrics, Division of Allergy/Immunology, University of Pittsburgh School of Medicine, Pittsburgh, PA, USA

[3]Department of Pathology, University of Pittsburgh School of Medicine, Pittsburgh, PA, USA

[4]Department of Pediatrics, Division of Blood and Marrow Transplant and Cellular Therapies, University of Pittsburgh School of Medicine, Pittsburgh, PA, USA

[5]Department of Pediatrics, Division of Neonatology and Pulmonary Biology, Cincinnati Children's Hospital Medical Center, University of Cincinnati School of Medicine, Cincinnati, OH, USA

[6]Institute for Infection, Inflammation, and Immunity in Children (i4Kids), Pittsburgh, PA, USA

These data are reported in *Immunity & Ageing*, 2023. doi: 10.1186/s12979-023-00365-5

2.1 Abstract

Background: Lower respiratory tract infections are a leading cause of severe morbidity and mortality among older adults. Despite ubiquitous exposure to common respiratory pathogens throughout life and near universal seropositivity, antibodies fail to protect effectively the elderly. Therefore, we hypothesized that severe respiratory illness in the elderly is due to deficient $CD8^+$ T cell responses.

Results: Here, we establish an aged mouse model of human metapneumovirus infection (HMPV). Aged C57BL/6 mice exhibit worsened weight loss, clinical disease, lung pathology and delayed viral clearance compared to young adult mice. Aged mice generate fewer lung-infiltrating HMPV epitope-specific $CD8^+$ T cells. Those that do expand demonstrate higher expression of PD-1 and other inhibitory receptors and are functionally impaired. Transplant of aged T cells into young mice and vice versa, as well as adoptive transfer of young versus aged $CD8^+$ T cells into *Rag1*$^{-/-}$ recipients, recapitulates the HMPV aged phenotype, suggesting a cell-intrinsic age-associated defect. HMPV-specific aged $CD8^+$ T cells exhibit a terminally exhausted $TCF1/7^-$ TOX^+ $EOMES^+$ phenotype. We confirmed similar terminal exhaustion of aged $CD8^+$ T cells during influenza viral infection.

Conclusions: This study identifies terminal $CD8^+$ T cell exhaustion as a mechanism of severe disease from respiratory viral infections in the elderly.

Keywords: Respiratory viral infection, aged immune response, viral immunology

2.2 Introduction: Aged CD8$^+$ T cells and RVIs

Respiratory viral infections are a leading cause of mortality worldwide, occurring predominantly in children <2 years, adults >65 years, and the immunocompromised (1). Human metapneumovirus (HMPV) is a leading cause of acute lower respiratory infections, with nearly 100% of children becoming seropositive by five years of age (1). Despite universal early exposure, re-infections of HMPV occur throughout adult life, but usually result in mild, self-resolving respiratory disease (1). However, elderly individuals infected with HMPV are at risk for increased morbidity and mortality associated with HMPV pneumonia and both bacterial and viral co-infections; in some studies, HMPV is as common among older adults as influenza and respiratory syncytial virus (RSV) (11, 49, 146, 147).

There are limited data on HMPV immune responses and pathogenesis in humans, which comes primarily from study of young children (3, 4, 148, 149). Previous studies using young adult mouse HMPV models showed that CD8$^+$ T cells help mediate viral clearance and protective immunity (46, 52, 61, 62). However, CD8$^+$ T cell responses are constrained during acute respiratory virus infection by coordinated signaling of cell surface inhibitory receptors, predominantly programmed cell death-1 (PD-1) and lymphocyte activation gene 3 (LAG-3), which remain upregulated even after viral clearance (46). The persistent co-expression of these receptors, particularly PD-1, leads to a state of functional impairment during acute respiratory virus infection manifested by

diminished degranulation and cytokine production such as IFNγ, and delayed viral clearance (46, 52, 61, 62).

The aging immune system is characterized by a functional decline in virtually all immune cells, coupled with an increase in basal pro-inflammatory cytokine production, a state that has been termed “inflammaging” (117, 130). Gene expression analysis at the single cell level has revealed distinct transcriptional and epigenetic changes in immune cells in both mice and humans as they age (150, 151). Bulk $CD8^+$ T cells in aged mice show increased expression of the transcription factors thymocyte selection-associated high mobility group box protein (TOX) and eomesodermin (EOMES), changes that promote terminal differentiation of $CD8^+$ T cells (150, 152, 153). A subset of murine $CD8^+$ T cells have increased production of granzyme K with increased age, which contributes to the inflammatory microenvironment (150). In addition, murine $CD8^+$ tissue-resident memory T cells (T_{RM}) have been identified as the cause of lung inflammation and fibrosis during viral pneumonia in aged mice (154). $CD8^+$ T cell responses to influenza have been studied in aged mice (155, 156) and older humans (157-159). Low granzyme B production by influenza-specific cytolytic T lymphocytes (CTL) from elderly humans correlated with lower protection against influenza and has been considered a marker for optimal protective vaccine responses in humans (157, 158). Another report described decreased degranulation but lower PD-1 expression on influenza-specific $CD8^+$ T cells from aged humans (158, 159). However, one limitation of human studies is the use of viral peptide stimulation instead of tetramers, the former of which fails to detect unresponsive virus-specific $CD8^+$ T cells.

We developed an aged mouse model of HMPV infection to explore the contributions of both age and virus-specific $CD8^+$ T cells to protection and disease. We found that aged HMPV-infected mice exhibited worse clinical disease, delayed viral clearance, and enhanced lung pathology compared with young mice. Virus-specific $CD8^+$ T cells in aged mice were fewer, expressed higher levels of PD-1 and other inhibitory receptors, and exhibited markedly decreased granzyme B production. Reciprocal transplant of aged T cells into young mice and vice versa, as well as adoptive transfer of aged or young $CD8^+$ T cells into *Rag1*$^{-/-}$ mice, confirmed this was a $CD8^+$ T cell-intrinsic age-associated defect. Similarly, influenza-infected aged mice lost more weight, produced fewer tetramer$^+$ $CD8^+$ T cells, had impaired granzyme B production, and accumulated more Tcf1/7$^-$ Tox$^+$ Eomes$^+$ $CD8^+$ T cells. Collectively, these results identify a population of dysregulated and dysfunctional terminally exhausted $CD8^+$ T cells in the aged host which contributes to the severity of multiple respiratory viral diseases in this population.

2.3 Materials & Methods

2.3.1 Mice and viral infection

C57BL/6 (B6), congenic CD45.1, and *Rag1*$^{-/-}$ mice were purchased from The Jackson Laboratory. All animals were bred and maintained in specific pathogen-free conditions in accordance with the University of Pittsburgh Institutional Animal Care and Use Committee. 6-7wks and 70-71wks female animals were used in all experiments. HMPV (pathogenic clinical strain TN/94-49, genotype A2) was grown and titered in LLC-MK2 cells as previously described (160). In select experiments, influenza virus strain A/34/PR/8 (PR8) was grown in MDCK cells and titered on

LLC-MK2 cells as in (46). For all experiments, mice were anesthetized with isoflurane in a heated chamber and infected intratracheally with 2.0 x 10^6 PFU HMPV or 500 PFU PR8 in 100 μL volume. Mock-infected mice were inoculated with the same volume of sterile PBS. Viral titers for HMPV infected mice were measured by plaque assay as previously described (160, 161). Clinical scoring of mice was performed by at least two individuals independently with one point given for each of the following signs: hunched, huddled, rapid breathing, lethargy, or ruffled fur.

Bronchoalveolar lavage (BAL)

BAL was harvested as in described (162). Briefly, mice were euthanized and their trachea exposed, cannulated with a blunt tipped syringe needle, and secured in place using suture. Lungs were flushed with 1mL BAL buffer (sterile PBS, 0.5% Fetal Bovine Serum (FBS), 1:250 0.5M EDTA) at least four times. BAL was spun down at 500xg for 10min. Supernatant was collected for Luminex. ACK lysis buffer (1 ml) was added to the cell pellet. After 1min, 1 mL of RPMI/10% FBS was added and spun down at 500xg for 5 min. Cells were resuspended in RPMI/10% FBS and used for flow cytometry staining.

2.3.2 Histopathologic score

10% formalin was injected into a section of the lower left lung lobe and stored in 10% formalin in histology cassettes (Fisher Scientific B851000WH). Tissue sections were stained with H&E by the UPMC Children's Hospital of Pittsburgh Histology Core and slides were imaged and scored in a blinded fashion at 200X magnification. Scoring criteria per field included: 0: no inflammation; 1: <25% inflammation; 2: 25-50% inflammation; 3: 50-75% inflammation; 4: >75% inflammation. To generate the histopathologic score, the score for each sample was added and divided by the total number of fields analyzed.

2.3.3 Antibody treatment

$CD8^+$ T cell depletion: One day prior to infection, aged and young B6 mice were treated with 300μg in sterile PBS of αCD8 (BioXCell BE0061) or rat isotype control (BioXCell BE0090) via intraperitoneal injections. Mice were injected with 150 μg of αCD8 or rat isotype control every other day post-infection.

2.3.4 IFNγ ELISpot assay

ELISpot assay and analysis was performed as previously described (46, 163) adding HMPV N_{11-18} peptide. Influenza NP366 peptide served as control.

2.3.5 Flow cytometry staining

Single cell suspension: Mice were euthanized and the right lung harvested. The lung was cut into 2mm segments using scissors in Eppendorf tubes. Lung tissue was resuspended in RPMI/10% FBS in tissue culture tubes and incubated for 1 hr at 37°C with DNAse and collagenase. After enzymatic digestion, the lung was filtered through 70 μm filters, spun down at 1500rpm for 5min, and the pellet resuspended in 2mL ACK Lysis Buffer (Gibco A10492-01) for 1min. 10 mL RPMI/10%FBS was added after ACK Lysis and cells were spun down at 1500rpm for 5min. Cells then underwent either tetramer staining or *ex vivo* peptide stimulation.

Tetramer staining: Cells were incubated with FACS/dasatinib for 30 min before adding APC conjugated N_{11-18} or BV421 conjugated M_{94-102} tetramers 1:200 in FACS/dasatinib for 90 min. Cells were then spun down at 1500rpm for 3min and washed 1x with FACS buffer.

Ex vivo peptide stimulation: 100μL of cells were added to a flat-bottom 96-well tissue culture plate. The following was added to cells: 100μL of 200μM N11 HMPV peptide or NP366 for irrelevant control diluted 1:10 in RPMI/10% FBS, 6μL CD107a-PE, and 22μL BFA (BD Cat. #51-2301KZ)/Monensin (BD Cat. #2092KZ). In addition, 1:1000 PMA/ionomycin instead of peptide was added to one aliquot of cells for a positive control. Cells were incubated for 5hrs at 37ºC.

For both conditions: After either tetramer staining or peptide stimulation, cells were stained with Live/Dead dye 1:1000 in PBS for 12 min, washed 1x with PBS, and blocked with αCD16/32 Fc block (Tonbo Biosciences Cat. #70-0161-M001) 1:100 in FACS buffer for 10 min. For surface staining, cells were stained with surface antibody 1:100 in BD Brilliant Stain Buffer (BD Cat. #566349) buffer for 30 min at 4ºC. Cells were spun down at 1500rpm for 3min and washed 1x with FACS buffer.

Intracellular cytokine staining: After cells were stained for surface antibodies, cells were fixed for 30min with eBioscience™ Foxp3/Transcription Factor Staining Buffer Set (ThermoFisher 00-5523-00) at 4ºC, spun down at 1640rpm for 3min, washed 1x with Foxp3 Fix/Perm Buffer, and stained with 6 uL/antibody in Foxp3 Fix/Perm Buffer for 1hr at 4ºC. Cells were spun down at 1640rpm for 3 min, washed 1x with FACS buffer, resuspended in FACS buffer, and stored in the dark at 4ºC until they were analyzed on the Cytek® Aurora multispectral flow cytometer.

Intracellular transcription factor staining: For transcription factor staining, cells were fixed for 18hrs in Foxp3 Fix/Perm at 4ºC. After fix/perm, cells were washed 1x with Foxp3 Fix/Perm Buffer and stained with 2.5μL antibody in Foxp3 Fix/Perm Buffer for 1 hr at 4ºC.

After intracellular staining, cells were spun down at 1640rpm for 3min, washed 1x with FACS buffer, resuspended in FACS buffer with 100 μL BioLegend Precision Count Beads™ (BioLegend Cat. #424902) and run on the Cytek® Aurora multispectral flow cytometer. A full list

of antibodies used in all experiments is shown in Supplemental Table 1. Fluorescence minus one (FMO) controls were used for all inhibitory receptors and transcription factors. For HMPV tetramer staining, Flu NP366-APC and HLA-B-35:01-BV421 tetramers were used as the irrelevant controls. Any irrelevant tetramer background staining was subtracted from the final tetramer frequency. Unstained cells from each experiment were fixed for 20 min in 2% PFA and used on the flow cytometer to minimize autofluorescence. Data analysis was performed with Flowjo (v10.8.1). Boolean gating in FlowJo was used to assess inhibitory receptor and functional cytokine co-expression. Patterns were visualized using the SPICE program (NIAID). All antibodies used in this study are listed in **Table 1**.

Table 1. Aurora Cytek Full Panels

Cell marker	Fluorophore	Species	Catalog Number	Clone
Both plates				
CD19	BV785	rat	115543	6D5
CD3e	BUV395	hamster	565992	145-2C11
CD4	AF700	rat	100536	RM4-5
CD44	APC-Cy7	rat	560568	IM7
CD62L	BUV563	rat	741230	MEL-14
CD8a	AF532	rat	58-0081-80	53-6.7
CD45.1	BV510	mouse	110741	A20
CD45.2	BUV496	mouse	741092	104
Tetramer plate only				
Foxp3	PerCP-Cy5.5	rat	45-5773-82	FJK-16s
T-bet	PE	mouse	644809	4B10

GATA-3	BV711	mouse	565449	L50-823
Rorγt	AF647	mouse	562682	Q31-378
EOMES	AF488	mouse	53-4875-82	Dan11mag
TOX	eFluor^{TM}660	mouse	50-6502-82	TXRX10
TCF-7/TCF-1	R718	mouse	567587	S33-966
BCL6	BUV661	mouse	568062	K112-91
PD-1 (CD279)	PE-Cy7	rat	109110	RMP1-30
TIM-3 (CD366)	BV605	rat	119721	RMT3-23
LAG-3 (CD223)	BUV805	rat	748540	C9B7W
2B4 (CD244.1)	BUV737	rat	749155	C9.1
HMPV M94 Class I tetramer	BV421	--	From NIH	--
HMPV N11 Class I tetramer	APC	--	From NIH	--
Peptide stimulation plate only				
Perforin	FITC	rat	11-9392-82	eBioOMAK-D
Granzyme B	PE-Cy5.5	rat	35-8898-80	NGZB
IFNγ	BV650	rat	505831	XMG1.2
CD107a (LAMP1)	PE	rat	121611	1D4B
IL-2	APC	rat	503810	JES6-5H4

2.3.6 Bone marrow transplant

Irradiation: The day prior to transplant, recipient mice were conditioned with 10-11 cGy total body irradiation in two split doses four hours apart from an X-ray source (MultiRad 350, Precision X-Ray Irradiation). Irradiated mice were placed on an immunocompromised rack in animal facility, given sterile autoclaved water, and supplied with irradiated food.

BM single cell suspension: Femur and tibia from *Rag1*$^{-/-}$ mice were harvested, tissue removed, and clean cuts made at either bone end. Using a 25G needle, marrow was flushed from the bone into a conical tube using D-10 media (10% FBS, 1% Pen Strep antibiotics, 1% L-glutamine, 1% MEM Non-Essential Amino Acids, 0.1% 50mM β-mercaptoethanol). BM was spun down at 350xg for 5min and cell pellet was filtered through 70μm strainer, washed 2x with 5mL sterile PBS, and counted on BD Accuri™ cytometer.

B and T cell magnetic column selection: For B and T lymphocyte magnetic column selection, spleen and lymph nodes (inguinal, peritoneal, and submandibular) were collected from B6 and congenic CD45.1 donor mice either 6-7wks or 70-71wks. All lymph nodes and each spleen per mouse were passed through 70 um strainer, spun down at 350xg for 5min, pooled together through a 40um strainer, and spun down again at 350xg for 5min. The spleen/lymph node single cell suspension were combined from two mice and resuspended in 900μL aMACs buffer at which point cells were incubated with CD90.2 microbeads or CD19-biotin and biotin labeled microbeads and run over LS column (Miltenyi 130-042-401) per Miltenyi instructions. Plunge was collected from the columns, spun down at 350xg for 5 min, and cell pellet was washed with 5mL sterile 1XPBS x2. Cells were counted on BD Accuri™ cytometer.

Tail vein injections: $1x10^7$ T, B, and *Rag1*$^{-/-}$ BM cells were resuspended per ml of sterile PBS, followed by injection of 200 μL of cells ($2x10^6$ of each cell type) into irradiated recipient mice via tail vein injection.

2.3.7 CD4$^+$ and CD8$^+$ T cell adoptive transfer

CD4 and CD8 biotinylated antibodies along with anti-biotin microbeads were used to positively select CD4 and CD8 subsets of T cells for use in combination experiments. $1x10^6$ CD4 and $1x10^6$ CD8 T cells were combined per mouse, with the remainder of the cell populations as outlined above.

2.3.8 scRNAseq Data Analysis

CD8$^+$ T cell scRNAseq dataset from lungs of mice and humans was kindly shared with us from Maxim Artyomov: https://www.synapse.org/#!Synapse:syn22255433/wiki/604556 and was generated as described in (150).

2.3.9 Statistical analysis

Data analysis was performed using Prism version 9.0 (GraphPad Software). Comparisons between 2 groups were performed using an unpaired 2-tailed Student's *t* test. Multiple group comparisons were performed using a 1-way or 2-way ANOVA as appropriate. A *P* value less than 0.05 was considered significant. Error bars in each graph represent SEM.

2.3.10 Declarations & Acknowledgements

Ethics Approval: All animals were maintained in accordance with *Guide for the Care and Use of Laboratory Animals* (NIH publication no. 85-23. Revised 1985) and were handled according to protocols approved by the University of Pittsburgh Subcommittee on Animal Care (IACUC).

Consent for publication: Not applicable.

Availability of data and materials: The datasets used and/or analyzed during the current study are available from the corresponding author on reasonable request.

Competing interests: JVW serves on the Scientific Advisory Board of Quidel and an Independent Data Monitoring Committee for GlaxoSmithKline, neither involved in the present work. All other authors declare no conflicts of interest.

Funding: Supported by NIH AI085062 (JVW), F30 HL159915-01A1 (OBP), T32 GM-008208 (OBP, JS), K12 HD000850 (TE), and the Henry L. Hillman Foundation (JVW). We thank the University of Pittsburgh Unified Flow Core for help with flow cytometry.

Author Contributions: OBP: conceived, designed, and performed experiments, acquired and analyzed data, and wrote manuscript. TE: performed experiments, revised manuscript. JS: performed experiments, revised manuscript. JL: contributed analytic tools, revised manuscript. YZ: contributed analytic tools, revised manuscript. TDO: acquired and analyzed data, revised manuscript. MR: contributed analytic tools, performed experiments. JJE: conceived and designed experiments, revised manuscript. CAB: conceived, designed, and performed experiments, interpreted data, revised manuscript. JVW: conceived and designed experiments, interpreted data, and revised manuscript.

Acknowledgements: We thank Anita McElroy, MD/PhD for discussion of the project and results. We thank the NIH Tetramer Core Facility (contract number 75N93020D00005) for providing tetramers. The authors have no additional financial interests.

2.4 Results

2.4.1 HMPV-infected aged mice exhibit more severe disease.

To establish an aged mouse model for HMPV, young (6-7wks) and aged (70-71wks) C57BL/6 (B6) mice were infected with HMPV TN/94-49. This strain causes mild, self-resolving disease in young adult BL/6 mice with minimal weight loss, transient lung inflammation, and viral clearance by day 7-9 post-infection (p.i.) (46, 52, 61, 62). Young infected mice in the current experiments similarly exhibited a mild phenotype, while aged infected mice lost significantly more weight (**Fig 2-1A**) and displayed higher clinical illness scores (**Fig 2-1B**). Aged mice had higher viral titers at day seven p.i. and delayed viral clearance, with 50% of aged mice having detectable viral titer at day nine p.i. (**Fig 2-1C**). Moreover, aged mice retained enhanced lung inflammation late in HMPV infection as evidenced by peribronchial and perivascular infiltrates and increased histopathology scores (**Fig 2-1D-F**).

$CD8^+$ T cells contribute to viral clearance of HMPV in young mice (46, 52, 61, 62). To test the role that $CD8^+$ T cells play in aged mice, $CD8^+$ T cells were depleted from young and aged mice. Mice received αCD8 depleting antibody (Ab) or isotype control Ab via intraperitoneal injection one day prior to HMPV infection and every other day p.i.. $CD8^+$ depletion was confirmed via flow

cytometry with representative flow plots shown at day five p.i. (**Appendix Fig 1A)**. Aged mice again lost significantly more weight compared to young mice, but $CD8^+$ depletion did not result in further weight loss in either age group (**Fig 2-1G**). CD8 depletion in aged mice had no major impact on viral titer, although aged mice depleted of $CD8^+$ T cells tended to have higher viral titers on day five p.i. compared to young $CD8^+$ depleted mice, and a trend towards higher titer on day nine p.i. compared to aged isotype control (**Fig 2-1H**). There was no difference in $CD19^+$ $B220^+$ B cells between isotype and $CD8^+$ depleted groups of either age (**Appendix Fig 1B & C**). However, there was a significant increase in the absolute number of $CD4^+$ T cells in aged CD8-depleted mice (**Appendix Fig 1C**). The lack of differences in young mice with $CD8^+$ depletion is most likely because HMPV viral clearance is mediated by multiple cell types. For example, a prior study found that $CD4^+$ T cells could compensate for a lack of $CD8^+$ T cells and contribute to viral clearance in young mice infected with HMPV (51). Collectively, these data reveal enhanced susceptibility and more severe clinical illness in aged HMPV-infected mice, with a trend towards delayed viral clearance in aged mice depleted of $CD8^+$ T cells.

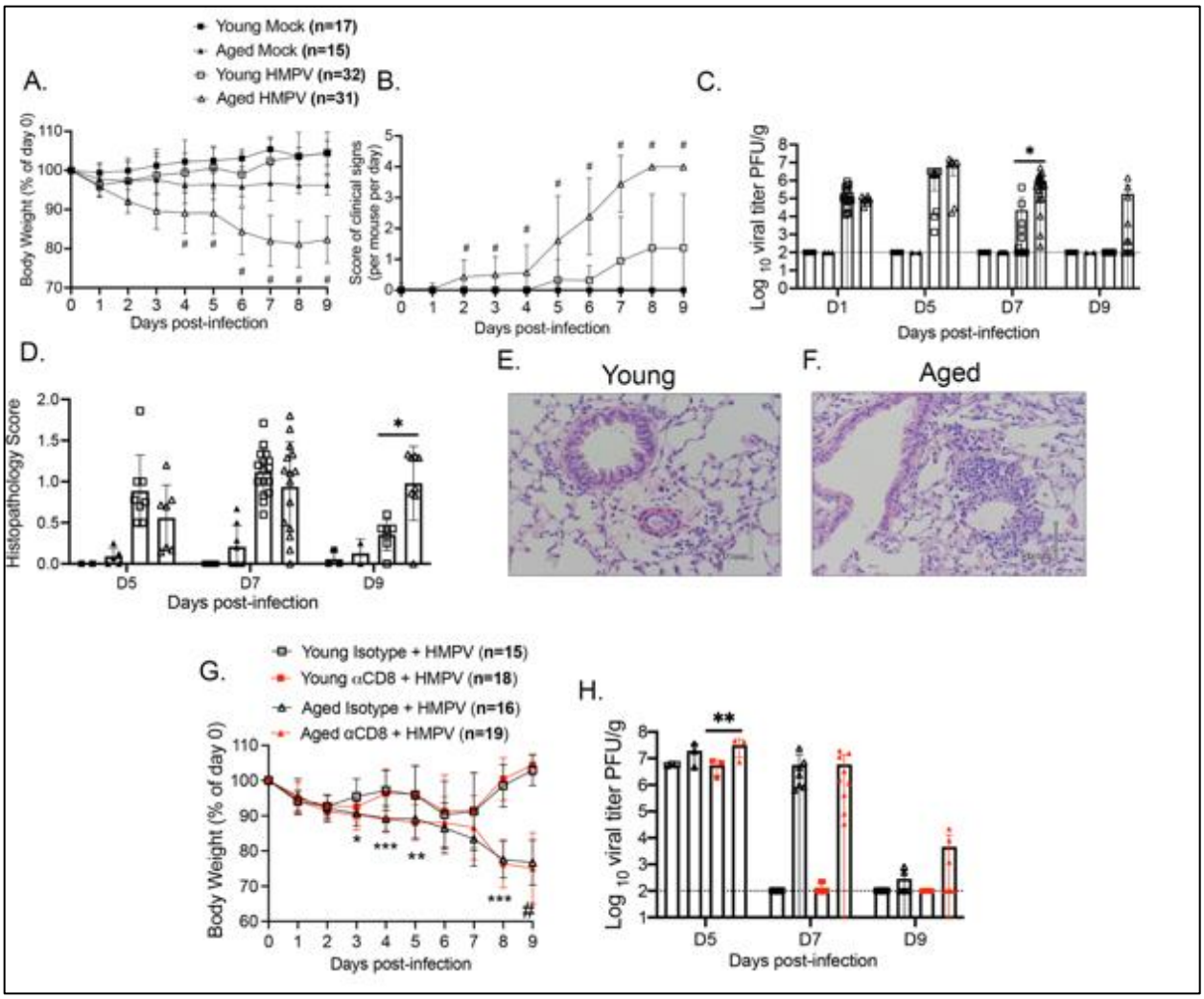

Figure 2-1. Aged mice had more severe HMPV disease and delayed viral clearance

(A) Aged infected mice lost more weight during HMPV infection, P<0.0001 days 4-9 p.i. for aged vs. young HMPV. **(B)** Aged mice had more severe clinical signs throughout infection. Clinical signs included: hunched, rapid breathing,lethargy, and ruffled fur with one point given for each sign observed. Two individuals independently scored each mouse daily and average score was calculated, P<0.0001 on day 2-9 p.i. for aged vs. young HMPV. **(C)** Aged mice had delayed HMPV clearance. Viral titer in lung in PFU/g was quantified using plaque assay and normalized to lung weight. Dotted line indicates limit of detection (LOD). **(D)** Aged infected mice accumulated more inflammatory infiltrates in the perivascular and peribronchial spaces in the lung by day 9 p.i. The histopathology score: average score per section field by a group-blinded experienced lung pathologist. 0 = no inflammation, 1 = <25% inflammation, 2 = 25-50% inflammation, 3 = 50-75% inflammation, and 4 = >75% inflammation. **(E & F)** Representative lung histology at day 9 p.i. **(G)** Aged and young TN/94-49 HMPV infected mice were treated with either αCD8 blocking

antibody (Ab) or rat isotype control Ab. Aged vs. young isotype groups weight loss significant at days 3, 4, 8, and 9 p.i; aged vs. young αCD8 groups significant at days 4, 5, 8, and 9 p.i. **(H)** Aged αCD8 mice tended to have delayed viral clearance compared to young αCD8 mice. Dotted line indicates LOD. Number of mice per group at D5, D7, and D9, respectively: Aged isotype (n= 3,7,6), Young isotype (n= 3,7,6), Aged αCD8 (n= 3, 9, 7), Young αCD8 (n=3,8,7). Number of mice per group below LOD at D5, D7, and D9, respectively: Aged isotype (n= 0/3,0/7,4/6), Young isotype (n= 0/3,7/7,6/6), Aged αCD8 (n= 0/3,0/9,4/7), Young αCD8 (n= 0/3,6/8,7/7). *P<0.05,**P<0.01, ***P<0.001, #=****P<0.0001, one or two-way ANOVA.

2.4.2 Aged mice generate fewer HMPV-specific CD8$^+$ T cells in the lung

We next quantified HMPV-specific CD8$^+$ T cell responses in the lungs of young versus aged mice. We used MHC-I tetramers bearing one of the immunodominant H2-K^b HMPV epitopes, $N_{11\text{-}18}$ (46). At day seven post-infection, aged HMPV infected mice produced fewer epitope-specific CD8$^+$ tetramer$^+$ (tet$^+$) T cells compared to young infected mice in both lung and bronchoalveolar lavage (BAL) (**Fig 2-2A-C**). Similar findings were observed for a different HMPV epitope, $M_{94\text{-}102}$, with a significant decrease in the percentage of tet$^+$ cells in both lung and BAL, and only a trend in absolute cell number (**Appendix Fig 2**). These findings demonstrate that the reduced number of HMPV-specific cells in aged mice was not unique to a single epitope. While virus-specific CD8$^+$ T cells were reduced in aged mice, the absolute number of bulk CD8$^+$ T lymphocytes was not different between the two groups (**Appendix Fig 3A**). These findings suggest that changes in aged mice were specific to infection-induced, lung-infiltrating, virus-reactive CD8$^+$ T cells. Similarly, no difference in absolute number of CD8$^+$ tet$^+$ T cells was noted in the draining lymph nodes or spleen between young and aged mice, though there were modestly increased but rare tetramer-specific cells in the aged spleens (**Appendix Fig 3B-D**). These findings indicate that

HMPV-specific $CD8^+$ T cells in aged mice were primed to a similar degree in lymphoid organs compared to young HMPV-infected mice and did not exhibit migration defects.

To test whether aged mice possess reduced epitope-specific $CD8^+$ T cell precursors or an intrinsic ability to differentiate into effector cells, we performed tetramer enrichment of spleen and peripheral lymph nodes (combined to facilitate detection of rare precursors) in naïve aged and young mice. Aged mice had fewer epitope-specific precursor $CD8^+$ T cells compared to young mice (**Fig 2-2D-F**). We then quantified total $CD44^-$ $CD62L^+$ naïve $CD8^+$ T cells (T_N) in the lung of naïve aged and young mice and found that aged mice had substantially fewer T_N compared to young mice (**Appendix Fig 4A-B**). Upon infection, aged mice failed to robustly increase $CD44^+$ $CD62L^-$ T effector $CD8^+$ T cells (T_{EM}) (**Appendix Fig 4A-C**). Collectively, these data indicate significantly reduced naïve $CD8^+$ T cell precursors and a diminished capacity to differentiate into effector cells in aged mice.

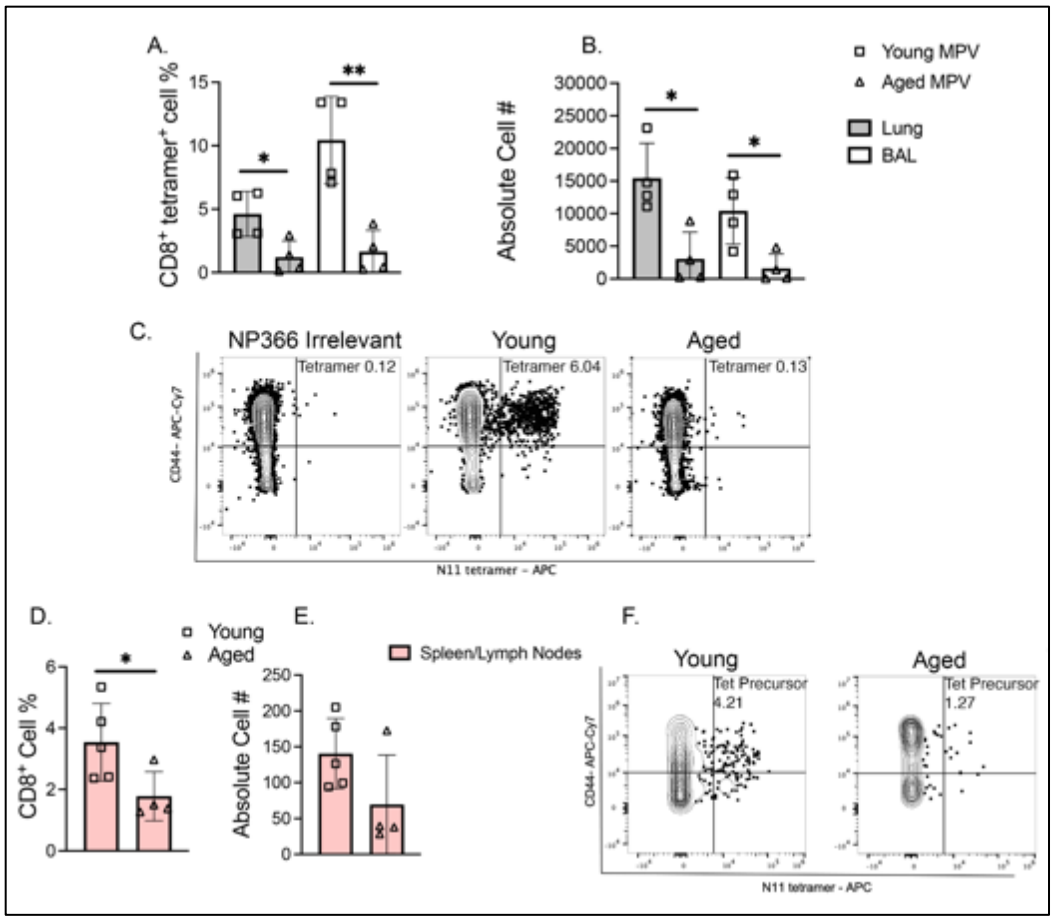

Figure 2-2. Aged mice produce fewer HMPV-specific CD8$^+$ T cells in the lung.

(A, B) Aged infected mice had decreased CD8$^+$ N11 tetramer$^+$ cells in lung (shaded bars) and BAL (open bars) compared to young infected mice at day 7 post-infection. Both N11 percent of CD8$^+$ tetramer$^+$ T cells and absolute cell number is shown. Absolute cell number was calculated by BioLegend Precision Counting Beads. **(C)** Representative flow plots from aged and young infected lung, respectively. **(D-E)** Aged uninfected mice had fewer tetramer precursor cells in the spleen and lymph nodes compared to young uninfected mice. Tetramer precursors were enriched from uninfected mouse spleen and lymph node via magnetic column selection using APC-labeled beads. **(F)** Representative flow plots of CD8$^+$ tetramer precursor cells shown. *P<0.05, **P<0.01, unpaired t-test.

2.4.3 Aged HMPV-specific CD8$^+$ T cells co-express inhibitory receptors and produce less granzyme B

In addition to numerical differences and changes in differentiation potential of virus-specific CD8$^+$ T cells, we sought to characterize functional attributes of aged compared with young CD8$^+$ T cells. We previously showed in young adult mice that lung CD8$^+$ tet$^+$ cells upregulated numerous inhibitory receptors by day seven p.i. and that PD-1 significantly contributed to CD8$^+$ T cell functional impairment (46, 52, 61, 62). The fraction of HMPV N11-specific CD8$^+$ T cells co-expressing the inhibitory receptors PD-1, TIM-3, LAG-3, and 2B4 increased in the BAL of aged mice at day seven post-infection (**Fig 2-3A & Fig 2-3B blue pie slice**). The number of CD8$^+$ tet$^+$ T cells expressing just one inhibitory receptor (orange pie slice) was also increased in aged CD8$^+$ tet$^+$ T cells (**Fig 2-3B)**. Additionally, aged HMPV-specific CD8$^+$ cells expressed more PD-1 on a per cell basis as measured by mean fluorescence intensity (MFI) (**Fig 2-3C**). These results indicate that aged virus-specific CD8$^+$ T cells more highly co-express the inhibitory receptors PD-1, TIM-3, LAG-3, and 2B4, which could contribute to decreased ability of these cells to combat infection (46, 52, 61, 62).

To test whether aged CD8$^+$ T cells were functionally impaired during HMPV infection, we quantified intracellular cytokine production and degranulation in aged CD8$^+$ T cells from infected mice following restimulation with HMPV epitope peptides (46). Following restimulation, aged CD8$^+$ T cells displayed significantly decreased granzyme B production compared to young CD8$^+$ T cells in the lung, with a similar trend in BAL (**Fig 2-3D**). There was also decreased production of IFNγ by aged CD8$^+$ T cells in BAL (**Fig 2-3D**). Representative flow plots and histograms of granzyme B production in the lung are shown in **Fig 2-3E & F**. Combinatorial analysis based on

expression of granzyme B, IFNγ, TNF, CD107a, and perforin revealed that aged CD8$^+$ T cells were significantly less polyfunctional with many more aged cells exhibiting zero measured functions (**Fig 2-3G)**. Taken together, these data indicate not only are HMPV-specific CD8$^+$ T cells quantitatively reduced in aged mice, but they also co-express numerous inhibitory receptors and are functionally impaired.

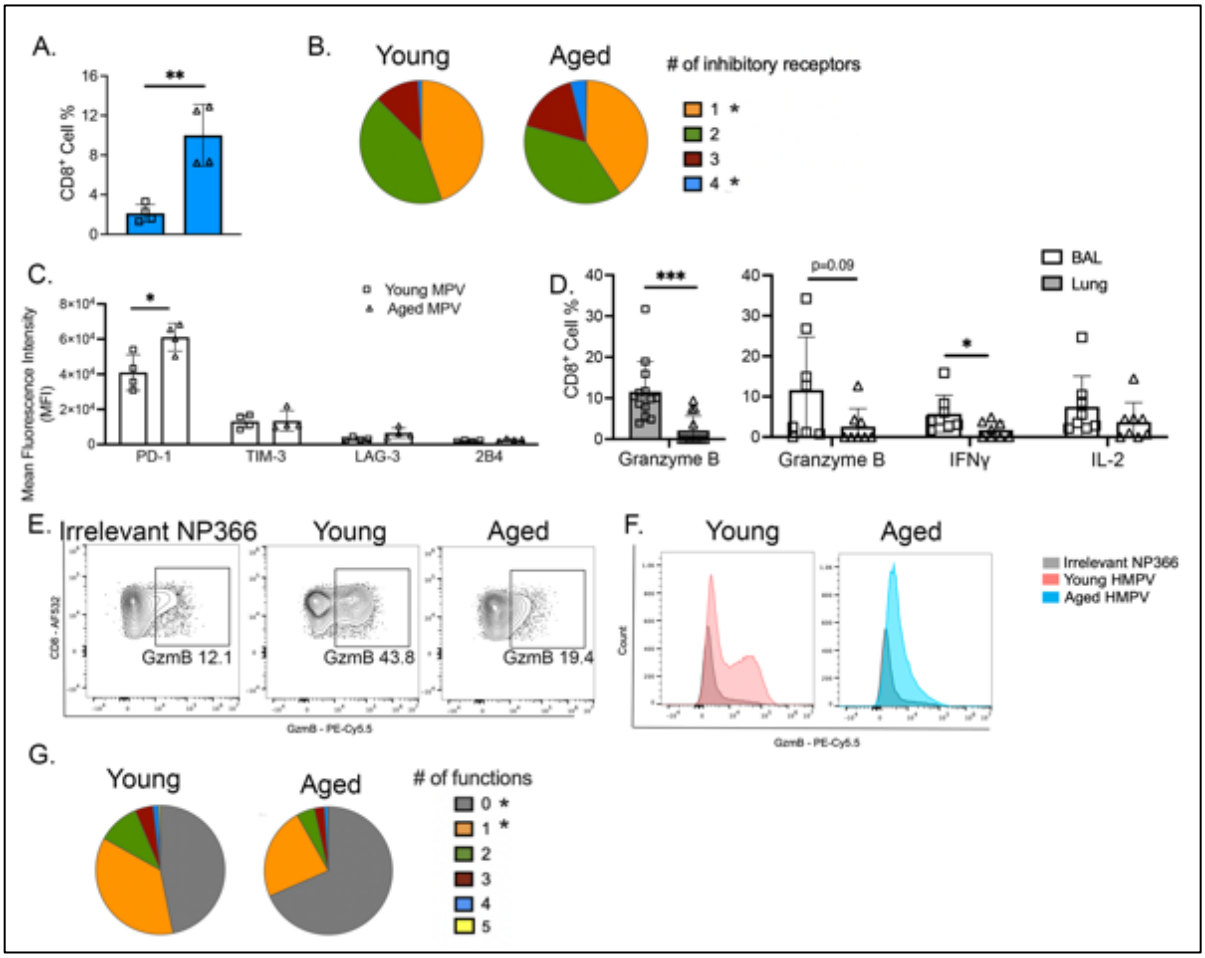

Figure 2-3. Aged HMPV-specific CD8$^+$ T cells co-express inhibitory receptors and produce less granzyme B

(A) CD8$^+$ N11 tet$^+$ cells from aged infected mice had increased expression of all 4 inhibitory receptors PD-1, TIM-3, LAG-3, and 2B4 compared to young infected mice. **(B)** Pie charts represent SPICE software analysis of inhibitory receptor co-expression on CD8$^+$ N11 tet$^+$ T cells in BAL of infected aged and young mice on day 7 post-infection. Asterisks indicate statistically significant differences between aged and young. **(C)** Aged CD8$^+$ tet$^+$ cells in BAL had increased mean fluorescence intensity (MFI) of PD-1 at day 7 post-infection while there was no difference in MFI in

other inhibitory receptors. **(D)** $CD8^+$ cells from aged infected mice had decreased production of granzyme B in lung (shaded bars). In BAL (open bars) aged $CD8^+$ T cells produced significantly less IFNγ with a trend towards decreased production of granzyme B and IL-2. **(E & F)** Representative flow plots and histograms of granzyme B production in aged and young infected lung at day 7 post-infection with NP366 flu irrelevant as control. **(G)** Aged $CD8^+$ T cells in lung were less polyfunctional. Functional markers measured: granzyme B, IFNγ, TNF, perforin, and CD107a. *P<0.05, **P<0.001, unpaired t-test.

2.4.4 Aged T cells transplanted into young mice recapitulate the aged immune response to HMPV.

To test whether $CD8^+$ T cell impairment in aged mice was due to T cell-intrinsic defects or systemic age-dependent dysfunction, we used two complementary approaches. We first used chimeric bone marrow (BM) transplantation. Aged and young CD45.2 mice were lethally irradiated and adoptively transplanted with either young or aged CD45.1 T cells, along with young B cells and BM from young *Rag1*$^{-/-}$ mice (to reconstitute the non-B, non-T cell hematopoietic compartment). Engraftment of donor cells and successful ablation of recipient cells was confirmed at five weeks post-transplant (**Appendix Fig 5A-C**) and was equal in all groups in both transplant models, as assessed by percentages of circulating and localized (lung, BAL) donor cells, on the day of euthanasia (**Appendix Fig 5A-C**). There was a significant difference in recipient cell frequencies, but no significant differences in donor cell engraftment (**Appendix Fig 5A-C**). At six weeks post-transplant, the mice were infected with HMPV and $CD8^+$ T cell response analyzed on day seven p.i. For clarity, the experimental groups are referred to as: age of T cells → age of host (i.e., young T cells into an aged host = $Y_T \rightarrow A_H$) (**Fig 2-4A**). $A_T \rightarrow Y_H$ had a significantly diminished $CD8^+$ tet^+ response compared to $Y_T \rightarrow Y_H$ while $Y_T \rightarrow A_H$ produced more $CD8^+$ tet^+ cells compared to $A_T \rightarrow A_H$ (**Fig 2-4B-D**). $Y_T \rightarrow A_H$ mice had more $CD8^+$ tet^+ cells that expressed no inhibitory receptors and

fewer $CD8^+$ tet^+ cells that expressed at least one inhibitory receptor compared to $A_T \rightarrow A_H$ (**Fig 2-4E**). There was a trend towards increased inflammation measured by higher histopathological score in $A_T \rightarrow Y_H$ compared to $Y_T \rightarrow A_H$ (**Appendix Fig 5D-F**).

We next evaluated the function of the transplanted $CD8^+$ T cells via *ex vivo* HMPV peptide stimulation, as in **Fig 2-3**. Y_T $CD8^+$ T cells exhibited increased granzyme B production independent of the age of the host (**Fig 2-4F**). The percentage of functional $CD8^+$ HMPV-specific cells was calculated by dividing the percentage of granzyme B^+ $CD8^+$ T cells by the percentage of tet^+ cells, which was also increased in Y_T $CD8^+$ T cells (**Fig 2-4G**). Boolean gating of granzyme B, CD107a, IFNγ, TNF, and perforin revealed that $Y_T \rightarrow A_H$ mice tended to have more polyfunctional $CD8^+$ T cells compared to $A_T \rightarrow Y_H$ (**Fig 2-4H**).

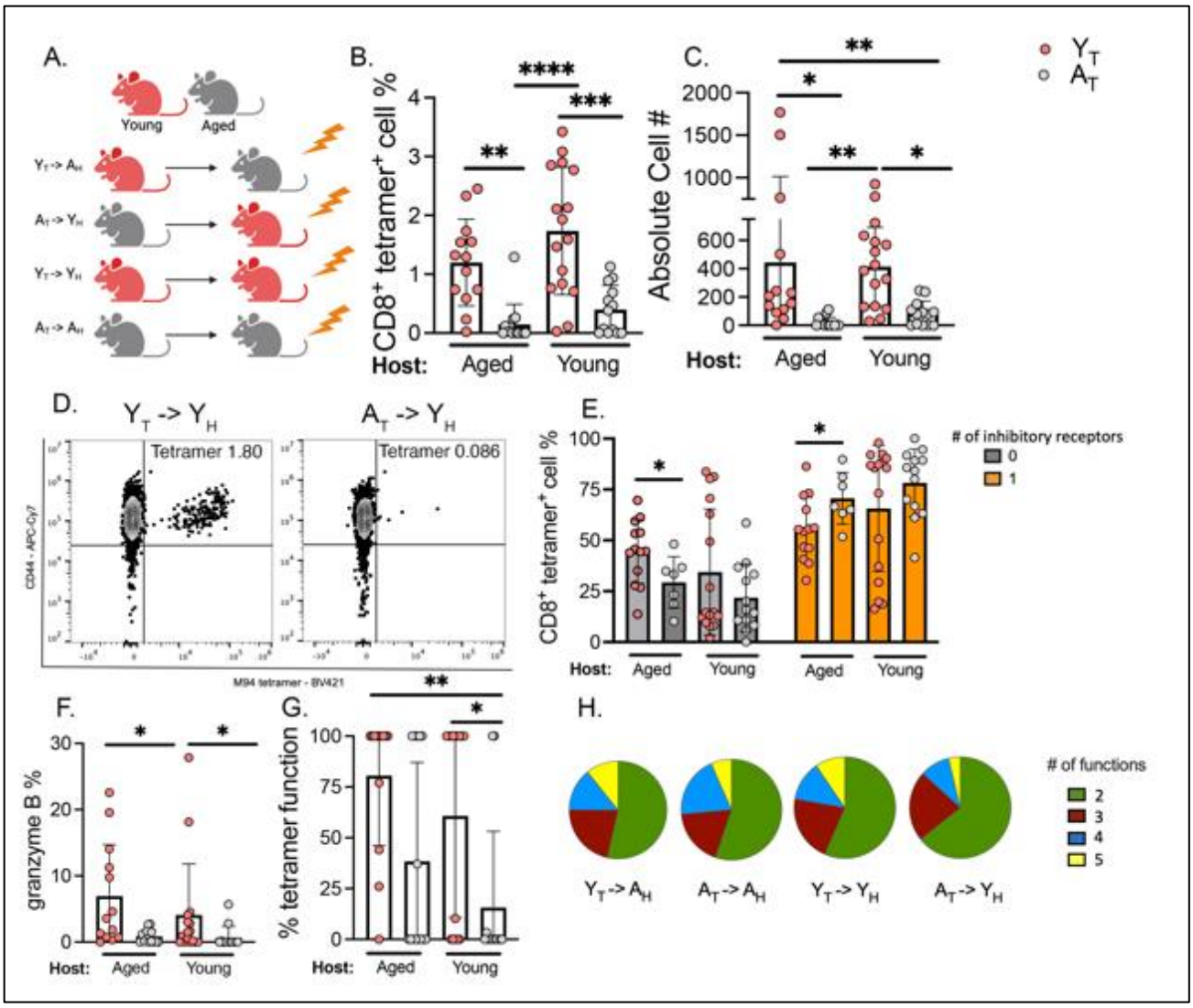

Figure 2-4. Aged T cells transplanted into young mice recapitulated aged CD8⁺ T cell phenotype.

(A) Syngeneic transplant experimental design. Lethally irradiated CD45.2 aged mice were reconstituted with T lymphocytes from young or aged CD45.1 donors, young B cells, and *Rag1*$^{-/-}$ BM. **(B, C)** Aged mice that received young T lymphocytes (i.e. Y_T -> A_H) had improved CD8⁺ tetramer⁺ response compared to A_T -> A_H control. A_T -> Y_H had a diminished tetramer response compared to Y_T -> Y_H **(D)** Representative flow plots of tetramer staining. **(E)** Combinatorial analysis of PD-1, TIM-3, LAG-3, and 2B4 inhibitory receptors revealed that A_T -> Y_H had increased percent of CD8⁺ T cells that expressed 0 inhibitory receptors and decreased percent of CD8⁺ T cells that expressed at least 1 inhibitory receptor compared to A_T -> A_H. **(F)** Percentage of CD8⁺ T cells expressing granzyme B. **(G)** Percent functional virus-specific CD8⁺ T cells was calculated by dividing the percentage of granzyme B⁺ CD8⁺ T cells by the

percentage of tet^+ cells. **(H)** Boolean analysis of polyfunctionality of $CD8^+$ T cells. Functional markers measured: granzyme B, IFNγ, TNF, perforin, and CD107a. *P<0.05, **P<0.005, ****P<0.0001, one-way ANOVA.

The second approach to test whether the age-dependent $CD8^+$ T cell defects were cell-intrinsic involved adoptive transfer of purified $CD8^+$ T cells from young or aged donors into a young *Rag1*$^{-/-}$ host, which avoided any potential effects of irradiation and BM reconstitution (**Fig 2-5A**). Similar reduction in the percentage of epitope-specific $CD8^+$ T cells was noted in the adoptive transfer model of $A_{CD8\ T} \rightarrow Y_H$ which had a diminished $CD8^+$ tet^+ response compared to $Y_{CD8\ T} \rightarrow Y_H$ (**Fig 2-5B-D**). Aged $CD8^+$ T cells transferred to young *Rag1*$^{-/-}$ recipients also displayed significantly reduced granzyme B production (**Fig 2-5E, F**), a decreased percentage of functional granzyme B^+ $CD8^+$ T cells (**Fig 2-5G**), and fewer polyfunctional $CD8^+$ T cells (**Fig 2-5H-K**). Collectively, these findings from complementary experimental approaches reveal a cell-intrinsic age-related defect in $CD8^+$ T cells leading to impaired generation and diminished functionality of HMPV-specific $CD8^+$ T cells.

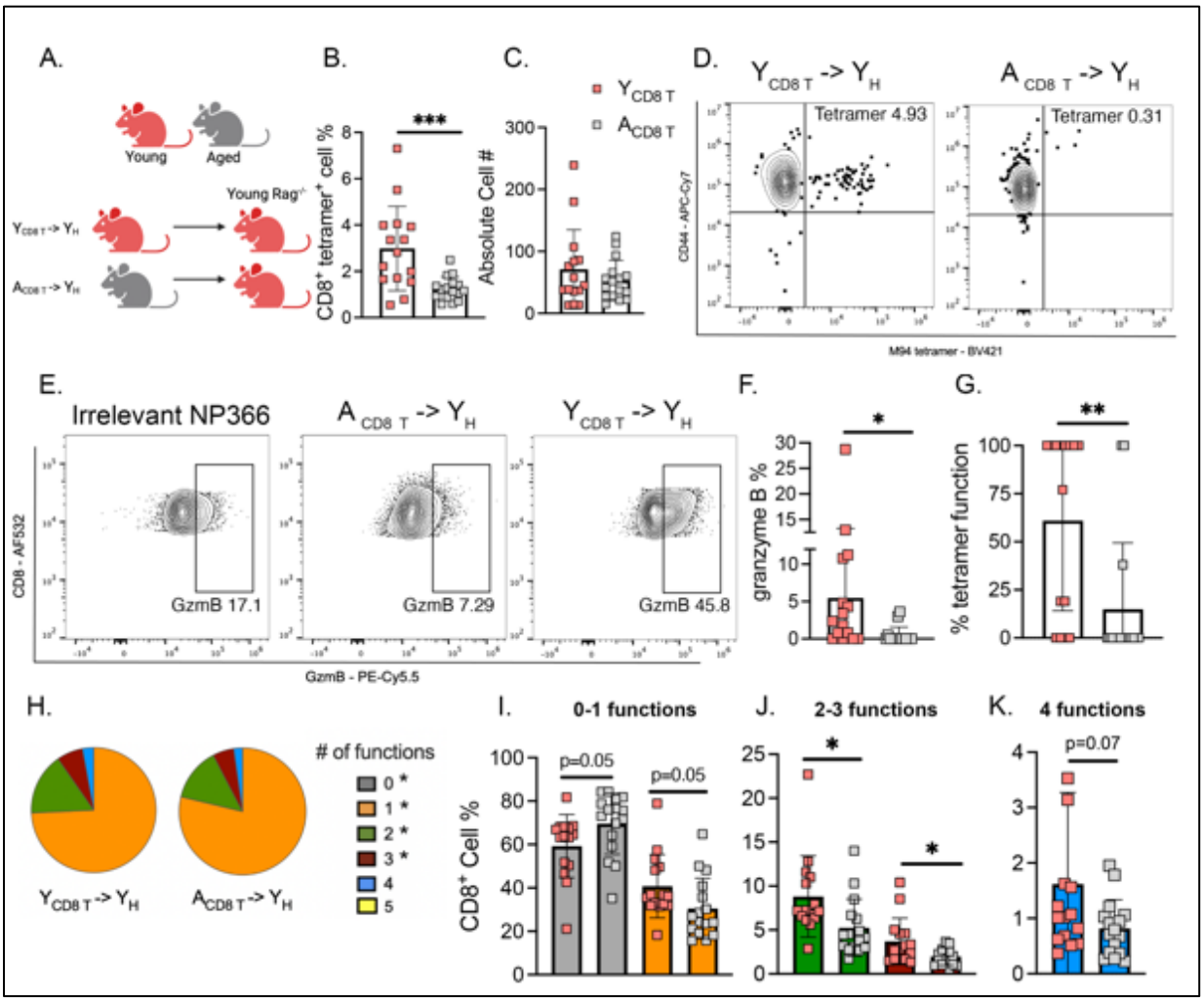

Figure 2-5. Aged CD8$^+$ T cells in *Rag1*$^{-/-}$ mice recapitulated aged immune response to HMPV

(A) CD8$^+$ T cell adoptive transfer experimental design. Aged or young CD8$^+$ T lymphocytes were isolated and adoptively transferred along with young CD4$^+$ T and B lymphocytes into young *Rag1*$^{-/-}$ recipients. **(B, C)** *Rag1*$^{-/-}$ recipients with aged CD8$^+$ T lymphocytes (i.e., $A_{CD8\ T}$ -> Y_H) had a significantly diminished epitope-specific CD8$^+$ T cell response compared to $Y_{CD8\ T}$ -> Y_H control. **(D)** Representative flow plots of tetramer staining. **(E-G)** $A_{CD8\ T}$ -> Y_H produced less granzyme B and had fewer granzyme B functional CD8$^+$ tet$^+$ T cells. **(H-K)** $A_{CD8\ T}$ -> Y_H had significantly fewer polyfunctional CD8$^+$ T lymphocytes as measured by combinatorial analysis of cytokines/markers of degranulation and SPICE analysis. The percentage of functional virus-specific CD8$^+$ tetramer$^+$ cells was calculated by dividing the percentage of granzyme B$^+$ CD8$^+$ T cells by the percentage of tet$^+$ cells. Functional markers measured: granzyme B, IFNγ, TNF, perforin, and CD107a. *P<0.05, **P<0.01, ***P<0.005, unpaired t-test or one-way ANOVA.

2.4.5 Aged $CD8^+$ T cells exhibit a terminally exhausted phenotype resistant to reinvigoration by PD-1 blockade and 4-1BB treatment

Given the high degree of functional impairment and expression of numerous cell surface inhibitory receptors, we hypothesized that age-related terminal exhaustion was a contributing factor to the impaired function of aged $CD8^+$ T cells, even when transplanted into young mice. To test this, we first measured baseline expression of *Eomes*, *Tox*, and *Tcf7* in HMPV-infected aged and young mice since these transcription factors are key in characterizing terminal exhaustion (150, 164). There was a striking increase in exhausted $Tcf7^-$ $Eomes^+$ Tox^+ bulk $CD8^+$ T cells (T_{EX}) (**Fig 2-6A**) and an increase toward more N11 epitope-specific $Tcf7^-$ $Eomes^+$ Tox^+ $CD8^+$ T cells in aged versus young mice at day seven p.i. (**Fig 2-6B**). Representative gating is shown in **Appendix Fig 6**. To determine if this phenotype represented an exhausted $CD8^+$ T cell as opposed to a transiently impaired state, we depleted $CD4^+$ T cells from aged and young HMPV-infected mice. Previous studies have shown that $CD4^+$ T cells prevent $CD8^+$ T cell exhaustion (165, 166). Therefore, depleting $CD4^+$ T cells would be predicted to promote $CD8^+$ T cell exhaustion, similar to chronic antigen stimulation models (i.e. chronic viral infection, cancer). Aged CD4 depleted mice had a similar population of Tox^+ $Eomes^+$ $CD8^+$ T cells as isotype control treated mice of the same age (**Fig 2-6C**). These findings indicate that this population of T_{EX} $CD8^+$ T cells represents a CD8-intrinsic exhausted state.

We next examined $CD8^+$ T_{EX} cells in the BM chimera transplanted groups to determine whether the aged $CD8^+$ T_{EX} phenotype was dependent upon the age of the host. We saw a marked increase in the T_{EX} population in the $A_T \rightarrow Y_H$ mice compared to the $Y_T \rightarrow Y_H$ mice, with a similar striking increase in T_{EX} in $A_T \rightarrow A_H$ compared to $Y_T \rightarrow A_H$ in both bulk and epitope-specific $CD8^+$ T cells

(**Fig 2-6D, F**). The adoptive transfer model of aged or young $CD8^+$ T cells into *Rag1*$^{-/-}$ mice also demonstrated an increase in T_{EX} in $A_{CD8\ T} \rightarrow Y_H$ in both bulk and tetramer$^+$ $CD8^+$ T cells (**Fig 2-6E, G**). Taken together, these findings suggest that a key cell-intrinsic driver of aged $CD8^+$ T cell dysfunction is terminal exhaustion, which cannot be reversed by transplanting aged $CD8^+$ T cells into a young host.

Using publicly available datasets from a prior study (150) in which scRNAseq was performed on lungs from naïve, uninfected young and aged mice, as well as on PBMCs from young and aged healthy humans, we found a similar T_{EX} $CD8^+$ population in aged murine lung (**Fig 2-6H & 2-6I**). Aged $CD8^+$ T cells from both uninfected mice and humans had decreased *Tcf7* expression (**Fig 2-6J; 2-6M**) while aged $CD8^+$ T cells from mice also upregulated *Tox* (**Fig 2-6K**) and *Eomes* (**Fig 2-6L**). Furthermore, in our model, aged lung $CD8^+$ T lymphocytes, following *ex vivo* peptide stimulation, produced significantly less IFNγ compared to young lung lymphocytes (**Fig 2-6N & O**). Taken together, these findings support the existence of a T_{EX} $CD8^+$ T cell population in aged mice that is functionally impaired and which cannot be reinvigorated by transplantation into a young host.

We next sought to uncover whether aged $CD8^+$ T cell exhaustion could be reversed, and function restored, by existing therapeutics. To this end, we administered a PD-1 blocking antibody (αPD-1), a 4-1BB agonist, or both to aged mice, which were then infected with HMPV. These approaches have previously been shown to rejuvenate exhausted T cells in cancer models (167, 168), and PD-1:PD-L blockade restored $CD8^+$ T cell function in HMPV-infected young adult mice (61, 62). However, none have been described in the setting of HMPV infection of aged individuals. Using

our previously established ELISpot assay for assessing response to inhibitory receptor blockade (61), we found that lung lymphocytes from aged mice produced less IFNγ compared to young mice (**Appendix Fig 7A-C**) and this response was not improved by PD-1 blockade and/or 4-1BB treatment in aged mice (**Appendix Fig 7A-C**). These data indicate that aged CD8$^+$ T cells are resistant to functional reinvigoration with checkpoint inhibitors that have shown clinical efficacy in humans and mice for reversing T cell exhaustion in other settings.

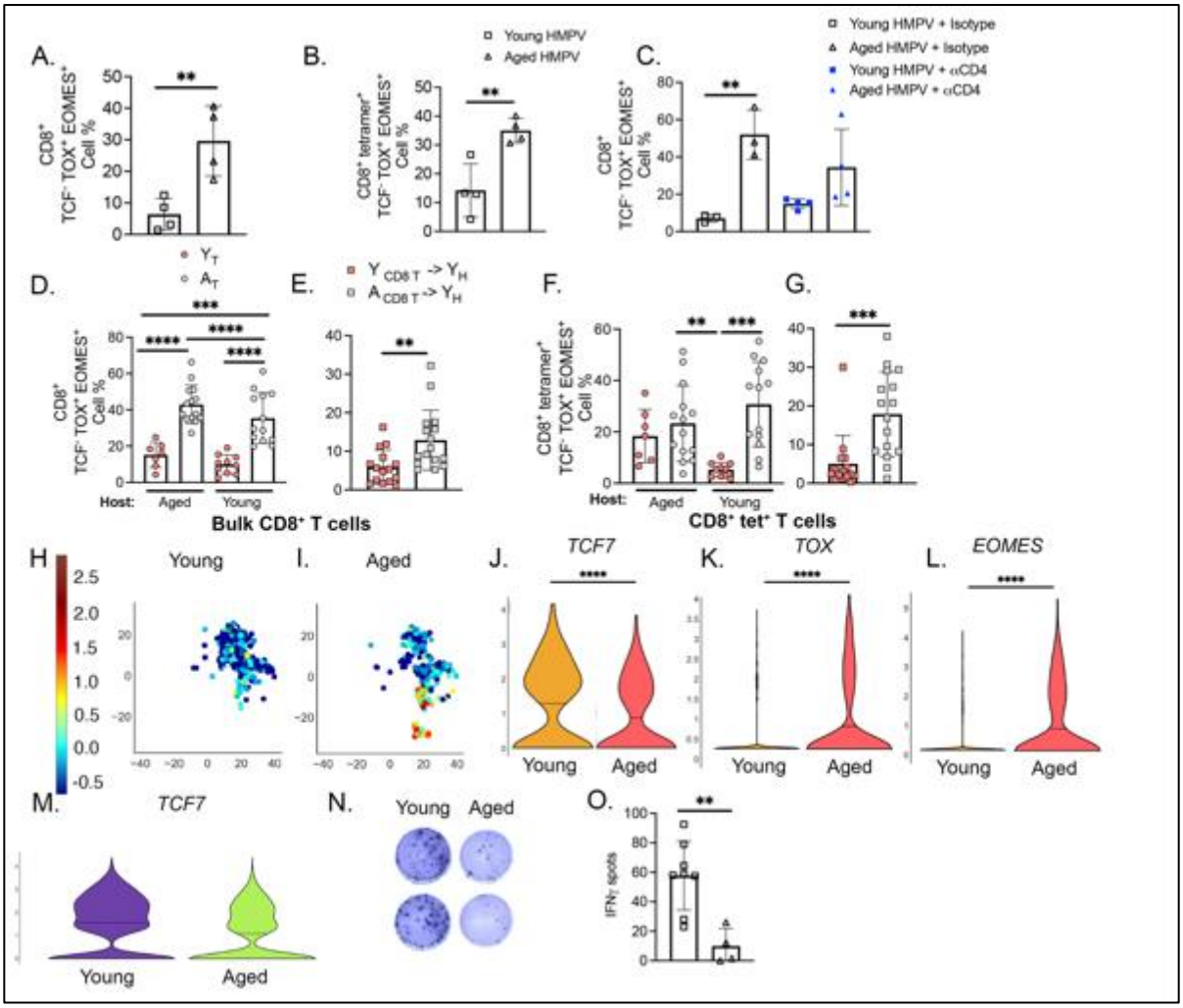

Figure 2-6. Aged CD8$^+$ T cells exhibit terminally exhausted phenotype

(A, B) Aged mice at day 7 p.i. had expanded population of terminally exhausted CD8$^+$ T cells (T_{EX}) in both bulk CD8$^+$ T cells and CD8$^+$ N11 tet$^+$ T lymphocytes. T_{EX} CD8$^+$ T cells are defined as Tcf7$^-$ Eomes$^+$ Tox$^+$. **(C)** Aged CD4 depleted mice expressed similar levels of Tox and Eomes on CD8$^+$ T cells compared to isotype treated mice. Young CD4

depleted mice did have a trend towards increased expression of Tox and Eomes on $CD8^+$ T cells. **(D & F)** A_T -> Y_H accumulated T_{EX} bulk and HMPV-specific $CD8^+$ T lymphocytes to a similar degree as A_T -> A_H control while Y_T -> A_H and Y_T-> Y_H had reduced T_{EX} populations. **(E & G)** A similar T_{EX} $CD8^+$ population in both bulk and epitope-specific $CD8^+$ T lymphocytes was seen in the $A_{CD8\ T}$ -> Y_H adoptive transfer model. **(H & I)** scRNAseq on naive young and aged mice revealed similar expression patterns of Tox and Eomes in $CD8^+$ T cells from aged lung. **(J-L)** Violin plots of Tcf7, Tox, and Eomes expression, respectively, in murine lung $CD8^+$ T cells in both age groups. **(M)** Violin plot of TCF7 expression in PBMCs from healthy aged and young humans. **(N)** Representative IFN-g ELISpot image. **(O)** IFN-f spot number significantly decreased in aged mice. *P<0.05, **P<0.01, ***P<0.001, ****P<0.0001, unpaired t-test or one-way ANOVA.

2.4.6 Influenza-infected aged mice had improved $CD8^+$ T cell response and accumulated terminally exhausted $CD8^+$ T cells

We sought to determine if this intrinsic $CD8^+$ T cell terminal exhaustion and functional impairment was generalizable to other respiratory viruses. Aged mice infected with influenza tended to lose more weight by day eight and nine p.i. (**Fig 2-7A**) and also produced fewer influenza-specific $CD8^+$ T cells (**Fig 2-7B-C**). Aged influenza-infected mice failed to produce granzyme B or have any granzyme B functional tet^+ $CD8^+$ T cells (**Fig 2-7D-F**). There was also a striking accumulation of aged $CD8^+$ T cells that were Tox^+ $Eomes^+$ (**Fig 2-7G-H**). Furthermore, aged $CD8^+$ T cells were functionally impaired, producing less IFNγ at day 7 p.i. (**Fig 2-7I & J**). These findings underscore that the aged mouse phenotype of functionally impaired, exhausted $CD8^+$ T cells is present in response to multiple respiratory viral infections.

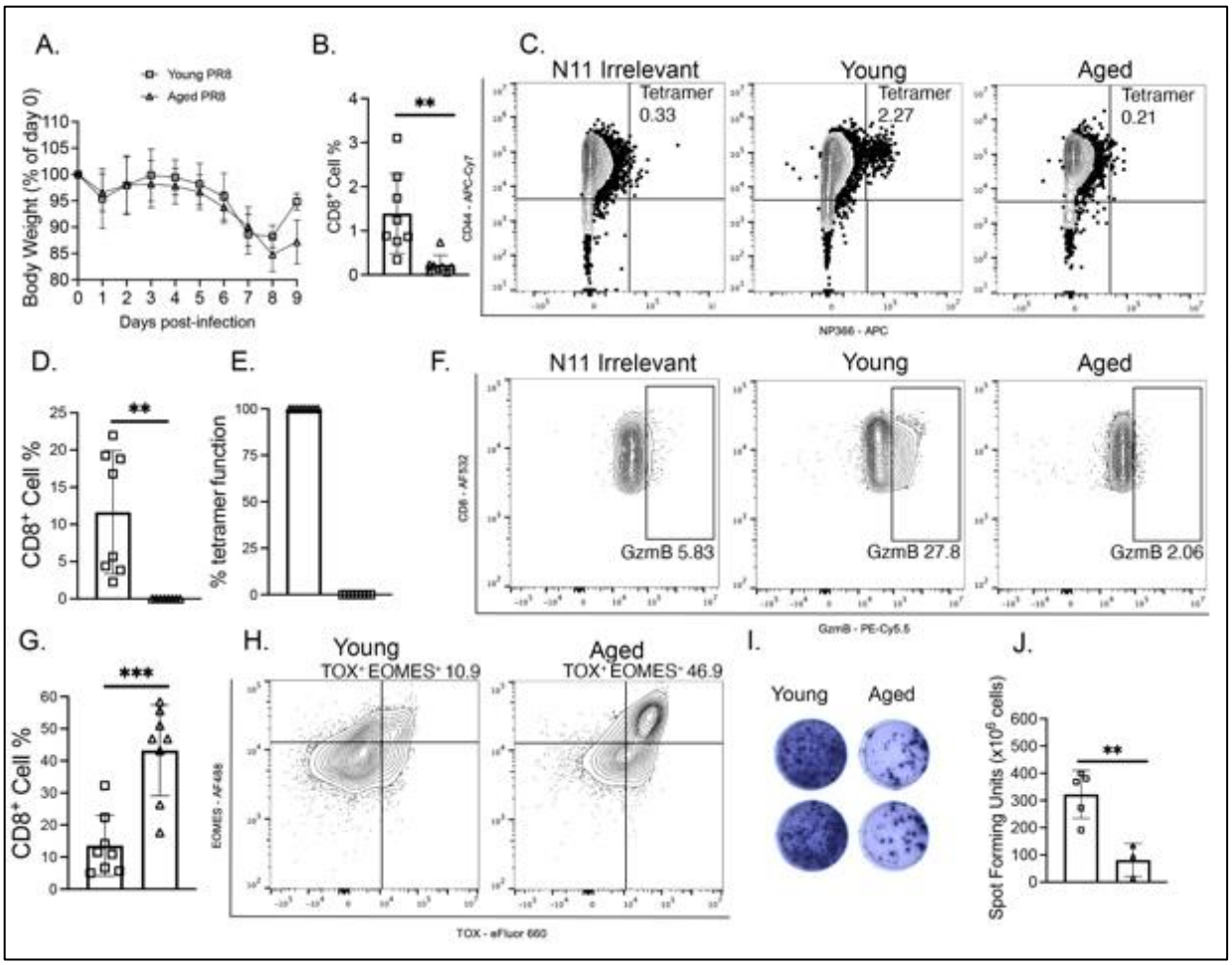

Figure 2-7. Influenza infected aged mice had impaired and terminally exhausted CD8$^+$

(A) Aged infected mice tended to lose more weight by day 9 p.i. **(B)** Aged mice produced fewer tet$^+$ CD8$^+$ T cells at day 7 p.i. **(C)** Representative flow plots of NP366 flu tetramer staining at day 7 p.i. **(D)** Aged CD8$^+$ T cells failed to produce granzyme B. **(E)** Aged CD8$^+$ T cells had no granzyme B functional tet$^+$ T cells. **(F)** Representative granzyme B staining at day 7 p.i. **(G)** Aged mice accumulated more Tcf7$^-$ Tox$^+$ Eomes$^+$ CD8$^+$ T cells compared to young infected mice at day 7 p.i. **(H)** Representative staining of Tox$^+$ Eomes$^+$ CD8$^+$ T cells. **(I)** Representative images of ELISpot. **(J)** Aged mice had minimal IFNγ production, *P<0.05, **P<0.01, ***P<0.005, unpaired t-test.

2.5 Discussion

Here, we examined the aged $CD8^+$ T cell response to HMPV using a newly established mouse model. We found that aged mice exhibit enhanced disease and delayed viral clearance compared with young mice. Aged mice also generate fewer lung resident virus-specific T cells, possibly due to reduced precursor frequency or differentiation potential, and those that do develop are functionally impaired. Furthermore, the T cell phenotype in aged mice is intrinsic to the $CD8^+$ T cell compartment, with a terminal exhaustion phenotype that was also found in single cell analysis (150) from naïve, uninfected, aged mice and healthy, aged humans, further supporting our findings. Functionally, aged $CD8^+$ T cells were resistant to reinvigoration by PD-1 checkpoint inhibitor and 4-1BB treatment. Moreover, this age-related $CD8^+$ T cell exhaustion contributes to increased disease severity caused by multiple respiratory viruses, including HMPV and influenza.

These findings have important implications for our understanding of severe lower respiratory tract infections in the elderly, which is a leading worldwide cause of morbidity and mortality in this vulnerable population (11, 147). One previous study reported increased weight loss, enhanced viral burden, and elevated pro-inflammatory cytokine production in 18-month-old HMPV-infected BALB/c mice compared to 6-7 week-old mice (169). In that report, HMPV-infected aged and young mice had similar numbers of pulmonary $CD8^+$ T cells, although antigen specificity and function were not assessed. We developed an aged mouse model that recapitulated aspects of severe HMPV illness observed in humans. Depletion of $CD8^+$ T cells in aged and young mice during infection revealed that $CD8^+$ T cells are not solely responsible for weight loss and viral clearance since we observed no difference in weight loss between isotype treated and CD8 depleted groups of either age, with minimal difference in viral clearance. These findings are consistent with

a previous study showing the dual role of $CD8^+$ and $CD4^+$ T cells in viral clearance (51). In our study, we focused on the $CD8^+$ T cell response to HMPV, acknowledging that viral clearance and weight loss during infection are multifactorial processes. We did find that aged $CD8^+$ T cells are intrinsically impaired, which contributed to a diminished adaptive immune response and more severe disease. $CD8^+$ T cell dysfunction has also been observed in other lower respiratory infections in elderly humans, including influenza (157) and COVID-19 (170), supporting our findings.

We found that aged mice produced significantly fewer HMPV-specific $CD8^+$ T cells in the lung and BAL. This has been reported in aged mice infected with influenza (155), but has not been shown for HMPV previously. Our findings suggest that this decrease in epitope-specific $CD8^+$ T cells was not due to impaired migration, as there was no epitope-specific aged $CD8^+$ T cell accumulation in the draining lymph nodes or spleen. Aged uninfected mice had a diminished pool of naïve $CD44^-$ $CD62L^+$ $CD8^+$ T cells, which may lead to the reduced number of naïve $CD8^+$ T cells and the limited capacity of these naïve $CD8^+$ T cells to differentiate into T_{EM}. Depletion of naïve T cells in aged antigen-experienced mice leading to a limitation of antigen-specific precursor repertoire has been described for both $CD4^+$ and $CD8^+$ T cells (171, 172). A previous study using vaccina virus characterized virus-specific precursors and determined their importance to confer protective T cell immunity (173). Thus, the important finding of fewer epitope-specific precursor $CD8^+$ T cells in our model in uninfected aged mice further supports and underscores an age-dependent diminished virus-specific $CD8^+$ T cell response to HMPV infection (167, 174).

Virus-specific $CD8^+$ T cells in aged mice infected with HMPV expressed more inhibitory receptors and were less polyfunctional compared to those from young mice. Notably, aged $CD8^+$ T cells had a striking decrease in granzyme B production, a phenomenon that has been described for other aged mouse models using single cell RNA sequencing analysis (150) as well as in elderly humans infected with COVID-19 (170). Our results show that HMPV-infected aged mice produced fewer virus-specific $CD8^+$ T cells that also expressed more inhibitory receptors and were deficient in granzyme B production and IFNγ secretion, thus explaining many features of the aged HMPV phenotype.

We used two complementary models, syngeneic transplant and adoptive transfer, to determine whether this aged $CD8^+$ T cell phenotype was due to a cell-intrinsic or host-dependent extrinsic cause. With both approaches, we observed that aged $CD8^+$ T cells exhibited decreased function regardless of whether the recipient host was young or aged. Similarly, young $CD8^+$ T cells did not show any impairment when transplanted into an aged host. Previous studies support these findings by showing that transplants of aged bone marrow or aged $CD8^+$ T cells alone into a young host is insufficient for the aged immune cells to be rejuvenated (150, 175). Collectively, these results indicate that the aged $CD8^+$ T cell phenotype we observe in response to HMPV infection originates primarily from a cell-intrinsic source. Of note, transfer of young $CD8^+$ T cells into aged mice by either transplant approach did not fully recapitulate all immunologic, virologic, and pathologic features of T cells in young mice during primary HMPV infection. This could be due to immunologic alteration secondary to the irradiation and transfer procedures, the semi-permissive nature of murine models for human pathogens, or a contribution of aging in the somatic cell compartment. Ongoing work is exploring the last possibility.

Since HMPV causes an acute infection, we thought it unlikely that HMPV disease was causing classical $CD8^+$ T cell exhaustion that has been described in chronic infection (176) and cancer models (167, 177). Rather, the aged microenvironment may promote a terminal exhaustion-like state in $CD8^+$ T cells, which then impairs the immune response when the aged host is exposed to HMPV. Previous studies have shown a baseline increase in *Eomes* and *Tox* with a decrease in *TCF1/7* on $CD8^+$ T cells in both uninfected aged mice (150) and aged humans (159, 178). In our study, we found that aged mice, both uninfected and infected, accumulated a large population of $Tcf7^-$ $Eomes^+$ Tox^+ $CD8^+$ T cells (i.e., T_{EX}) compared to young mice, which correlated with a loss of IFNγ production in aged mice. This finding was recapitulated in the transplant and adoptive transfer models, where aged bulk and, importantly, virus-specific $CD8^+$ T cells retained this T_{EX} phenotype despite being transferred into young hosts. Conversely, young $CD8^+$ T cells did not acquire a T_{EX} phenotype when transferred into an aged host. When aged and young HMPV-infected mice were depleted of CD4 T cells to promote $CD8^+$ T cell exhaustion, there was no significant increase in the population of $Tcf7^-$ Tox^+ $Eomes^+$ $CD8^+$ T cells between isotype and $CD4^+$ depleted aged mice, indicating that the $CD8^+$ T_{EX} phenotype observed during HMPV infection was canonical exhaustion. Importantly, we observed an increase, although not statistically significant in $Tcf7^-$ Tox^+ $Eomes^+$ $CD8^+$ T cells in young CD4-depleted HMPV-infected mice compared to young isotype control. We may not have seen a robust increase in $Tcf7^-$ Tox^+ $Eomes^+$ $CD8^+$ T cells in young CD4-depleted mice because our model is an acute viral infection while other studies (165, 166) use CD4 depletion as a synergistic approach along, with a cancer or chronic infection model, to promote $CD8^+$ T cell exhaustion. Overall, these findings suggest an

age-dependent progression of $CD8^+$ T cells to a terminally exhausted phenotype, which limits antiviral $CD8^+$ T cell responses.

Terminal exhaustion has been partially reversible in other models of T cell exhaustion in which there is chronic antigen stimulation or a tumor microenvironment. In mice chronically infected with the Clone-13 strain of lymphocytic choriomeningitis (LCMV), $Tcf7^+$ $CD8^+$ T cells were identified as the $CD8^+$ T cell subset responsive to PD-1 blockade (179). PD-1 blockade and 4-1BB treatment were also able to reverse $CD8^+$ T cell exhaustion in cancer models (167, 180). In our model, we identified a subset of $CD8^+$ T cells in the aged host that possess transcriptional markers resembling T_{EX} found in these chronic infection and cancer models. However, unlike cancer (174, 180) and chronic viral infection (179), attempts to reverse the T_{EX} phenotype in aged $CD8^+$ T cells using PD-1 blocking and/or 4-1BB agonist antibodies were not successful. Taken together, the data from the current experiments suggest that age-dependent changes in $CD8^+$ T cells related to viral infection may be irreversible and thus represent a true terminal exhaustion phenotype similar to chronic antigen stimulation models. These data point towards a need to identify other targets or novel approaches to therapy. Future studies will focus on understanding why checkpoint inhibitors fail to improve the immune response in the aged host and finding additional treatments that can be used.

2.6 Conclusions

Here we present evidence that a major contributor to severe HMPV disease in older adults is due to age-dependent, cell-intrinsic $CD8^+$ T cell dysfunction. Aged mice exhibited a diminished virus-

specific response to both HMPV and influenza with decreased T cell functionality, which led to clinical and virologic consequences. We identified an accumulation of terminally exhausted $CD8^+$ T cells in the aged host during both HMPV and influenza, which was not meaningfully restored with checkpoint inhibitor treatment. These findings have important implications for severe respiratory virus infections among elderly individuals, as well as older adults with cancer receiving checkpoint inhibitor therapy who acquire respiratory viral infections. Additionally, these findings provide further insight into the pathophysiology of severe respiratory viral infection among older adults and our model builds a foundation for future studies to improve the aged immune response to respiratory viruses and vaccines.

3.0 Human Metapneumovirus Reinfection in Aged Mice Recapitulates Increased Disease Severity in Elderly Humans Infected With Human Metapneumovirus

Olivia B. Parks[*], Taylor Eddens[†], Yu Zhang[*], Tim D. Oury[‡], Anita McElroy[*,¶,||], John V. Williams[*,¶,||]

Affiliations:

[*]Department of Pediatrics, Division of Infectious Diseases, University of Pittsburgh School of Medicine, Pittsburgh, PA, USA

[†]Department of Pediatrics, Division of Allergy/Immunology, University of Pittsburgh School of Medicine, Pittsburgh, PA, USA

[‡]Department of Pathology, University of Pittsburgh School of Medicine, Pittsburgh, PA, USA

[¶]Institute for Infection, Inflammation, and Immunity in Children (i4Kids), Pittsburgh, PA, USA

[||]Center for Vaccine Research, University of Pittsburgh School of Medicine, Pittsburgh, PA USA

Corresponding Author:

Olivia B. Parks

University of Pittsburgh

Rangos Research Building

4401 Penn Avenue

Pittsburgh, PA 15224

Phone: 412-692-8298

Email: obp1@pitt.edu

Competing Interest Statement: JVW serves on the Scientific Advisory Board of Quidel and an Independent Data Monitoring Committee for GlaxoSmithKline, neither involved in the present work. All other authors declare no conflicts of interest.

Keywords: Respiratory viral infection, aged immune response, viral immunology

These data are reported in *ImmunoHorizons, 2023:* doi: 10.4049/immunohorizons.2300026

[1] Supported by NIH AI085062 (JVW), F30HL159915 (OBP), T32 GM008208 (OBP), T32 AI089443 (YZ), K12 HD000850 (TE), and the Henry L. Hillman Foundation (JVW).

3.1 Abstract

Human metapneumovirus (HMPV) is a leading cause of respiratory infection in adults >65 years. Nearly all children worldwide are seropositive for HMPV by five years of age, but re-infections occur throughout life and there is no licensed vaccine. Recurrent HMPV infection is mild and self-resolving in immunocompetent individuals. However, elderly individuals develop severe respiratory disease upon HMPV re-infection that leads to a high risk of morbidity and mortality. In this study, we developed a mouse model to mirror HMPV re-infection in elderly humans. C57BL/6J mice were infected with HMPV at 6-7wks old, aged in house, and re-challenged with high-dose virus at 70wks. Aged re-challenged mice had profound weight loss similar to primary infected mice, increased lung histopathology, and accumulated cytotoxic $CD8^+$ $CD44^+$ $CD62L^-$ $CD69^+$ $CD103^+$ memory cells despite having undetectable lung virus titer. When aged mice 14 months p.i. or young mice five weeks p.i. were restimulated with HMPV cognate antigen to mimic epitope vaccination, aged mice had an impaired $CD8^+$ memory response. Convalescent serum transfer from young naïve or five weeks post-infection into aged mice on day of infection did not protect. Aged mice vaccinated with UV-inactivated HMPV also exhibited diminished protection and poor $CD8^+$ memory response compared to young mice. These results suggest that aged individuals with HMPV re-infection have a dysregulated $CD8^+$ memory T cell response that fails to protect and actually exacerbates disease. Moreover, aged mice exhibited a poor memory response to either epitope peptide or UV-inactivated vaccination, suggesting that aged $CD8^+$ T cell dysfunction presents a barrier to effective vaccination.

3.2 Introduction: Aged CD8$^+$ T cell memory response

Human metapneumovirus (HMPV) is a leading cause of respiratory infection in children <2 years, adults >65, and the immunocompromised (1, 181). Despite children reaching 100% HMPV seroprevalence worldwide by five years of age, reinfections occur throughout life but these usually manifest as mild, self-resolving illness (1, 181). However, HMPV infection in the elderly can result in severe disease with an increased risk of mortality and comorbidities such as bacterial pneumonia (8, 182-184). HMPV prevalence in older adults is similar to influenza and respiratory syncytial virus (RSV), underscoring the burden of these viruses in the aged population (147). The contribution of immune memory response to HMPV in the aged host is not well understood (94, 147, 182, 185). One study using primary infection of 18-month-old BALB/c mice compared to 6-seven week-old mice found that HMPV-infected aged mice had increased weight loss, viral burden, and elevated pro-inflammatory cytokine production (169). However, memory T cell formation and response to HMPV re-exposure were not assessed. Previous studies have also shown that increased age leads to a progressive decline in function of several immune cell types which contributes to impaired cell-mediated responses and maintenance of memory T cells, leading to poor vaccine responses (186, 187). Thus, impaired immune memory in older adults may contribute to severity of HMPV reinfection and represents a gap in our knowledge.

Aged humans accumulate a population of CD69$^+$ CD8$^+$ tissue-resident memory (T_{RM})-like cells in the lung that is not present in young adults (188). This population of T cells is the main driver of chronic lung sequelae and fibrosis in aged mice infected with influenza virus (154, 189). Moreover, depletion of CD8$^+$ T_{RM} following primary influenza virus infection in aged mice led to decreased

inflammatory monocyte recruitment and diminished lung fibrosis (154), indicating a role for $CD8^+$ T_{RM} in lung damage following influenza infection.

In addition to altered T cell function, humoral immunity is affected by age. Older adults have a diminished antibody response to inactivated influenza vaccine (190) that is enhanced by adjuvanted and high-dose vaccines (191, 192). HMPV reinfections do occur in older adults, despite the presence of humoral immunity (193). Furthermore, re-infection by RSV in humans and mice can occur despite high neutralizing antibody titer (94, 194). These data underscore that humoral immunity alone is not sufficient to provide protection against HMPV in the aged host. We thus sought to define the $CD8^+$ T cell memory response in the aged host and elucidate cell-mediated mechanisms of severe HMPV re-infection.

Here, we established an aged mouse model that mimics re-infection in elderly humans, using mice correlated in age to a human >65 years (195). Mice 6-7 weeks old were infected with HMPV, aged, and re-challenged with high-dose virus fourteen months after primary infection. Aged re-challenged mice had no detectable virus in lungs, yet exhibited severe weight loss and accumulated $CD8^+$ $CD69^+$ $CD103^+$ T cells with more potent cytotoxic functions than both aged and young primary infected mice. HMPV epitope vaccination of aged mice fourteen months p.i. proved to be ineffective at inducing a $CD8^+$ memory response. Furthermore, vaccination strategies with UV-inactivated virus or HMPV cognate peptide five weeks prior to infection with live virus did not improve outcomes in aged mice. Overall, these data show the aged mouse HMPV re-challenge model resembles what is reported in elderly humans. These results also underscore the poor vaccine response in the aged host and show that while immune memory reduced detectable lung

virus, it did not protect against disease in aged mice, and in fact induced immune-mediated lung damage.

3.3 Materials & Methods

3.3.1 Mice and viral infection

C57BL/6 (B6) mice were purchased from The Jackson Laboratory. All animals were bred and maintained in specific pathogen-free conditions in accordance with the University of Pittsburgh Institutional Animal Care and Use Committee. 6-7 week-old and 70-71 week-old female animals were used in all experiments. HMPV (pathogenic clinical strain TN/94-49, genotype A2) was grown and titered in LLC-MK2 cells as previously described (160). For all experiments, mice were anesthetized with isoflurane in a heated chamber and infected intratracheally with either $2.0x10^6$ or $1.0x10^7$ PFU in 100 μL, depending on the experiment. Mock-infected mice were inoculated with the same volume of sterile PBS. Viral titers were measured by plaque assay as previously described (160, 161). To generate UV-inactivated HMPV virus, TN/94-49 virus stock was placed in a sterile 6-well tissue culture dish and placed in the Stratagene® 1800 UV Stratalinker run automatic cross-linking (1200x100μJ) for 3x10 min intervals, gently agitating the dish in between each dose. UV-inactivated virus was titered via plaque assay to confirm no replicating virus was present.

3.3.2 CD45.2 IV labeling

Mice were administered 4 μg of CD45.2-BUV496 (BD Cat# 741092) in 200 μL sterile PBS via tail vein injection and were euthanized 3 mins. post-injection as in (154).

3.3.3 N11/LPS Treatment

Mice were administered 100ug HMPV N11 peptide (GenScript Peptide Sequence: LSYKHAIL) and 10 μg LPS (Sigma Cat# L2360) in 200 μL sterile PBS via intraperitoneal injection. Daily weights were taken and mice were euthanized 5 days post-treatment.

3.3.4 Histopathologic score

10% formalin was injected into a section of the lower left lung lobe and stored in 10% formalin in histology cassettes (Fisher Scientific B851000WH). Tissue sections were stained with H&E or Picrosirius red stain by the UPMC Children's Hospital of Pittsburgh Histology Core and slides were imaged at 200X magnification. Scoring criteria for H&E slides per field included: 0: no inflammation; 1: <25% inflammation; 2: 25-50% inflammation; 3: 50-75% inflammation; 4: >75% inflammation. To generate the histopathologic score, the score for each sample was added and divided by the total number of fields analyzed.

3.3.5 IFNγ ELISpot assay

ELISpot assay and analysis was performed as previously described (46, 163). In select experiments, 10 μg of αPD-1 mAb (BioXCell Cat# BE0033-2), agonist 4-1BB mab (BioXCell Cat# BE0239), a combination of both, or rat IgG2a isotype control (BioXCell Cat# BE0089) were added to ELISpot wells along with HMPV N_{11-18} peptide. Influenza NP366 peptide (GenScript Peptide Sequence: ASNENMETM) served as control.

3.3.6 IgG HMPV ELISA

1μg of TN/94-49 HMPV in 1x ELISA coating buffer (BioLegend Cat# 421701) was plated per well overnight at 4°C. The remainder of the ELISA was performed as in (196).

3.3.7 Luminex

Lung homogenates were clarified by centrifugation (10,000xg for 10min) and analyzed via ProcartaPlex™ Cytokine & Chemokine 36-Plex Panel 1A (Cat# EPX360-26092-901) per manufacturer's instructions.

3.3.8 Convalescent serum transfer

Serum was harvested from young mock or HMPV infected mice 5 wks p.i. by terminal bleed. 200μL of serum was passively transferred into mice as described in (197).

3.3.9 Flow cytometry staining

Single cell suspension: Mice were euthanized and the right lung harvested. The lung was cut into 2 mm segments using scissors, resuspended in RPMI/10% FBS, and incubated for 1hr at 37°C with DNAse and collagenase. After digestion, the lung was filtered through 70μm filters, spun at 1500rpm for 5 min, and the pellet resuspended in 2mL ACK Lysis Buffer (Gibco A10492-01) for 1 min. 10 mL RPMI/10%FBS was added after ACK Lysis and cells were spun at 1500rpm for 5min. Cells then underwent either tetramer staining or *ex vivo* peptide stimulation.

Tetramer staining: Cells were incubated with 1:2000 100mg dasatinib in 1XPBS/1% FBS (FACS) for 30 min before adding APC conjugated $N_{11\text{-}18}$ 1:200 in FACS/dasatinib for 90 min. Cells were then spun down at 1500rpm for 3min and washed 1x with FACS buffer.

Ex vivo peptide stimulation: 100 μL of cells were added to a flat-bottom 96-well tissue culture plate. The following was added to cells: 100 μL of 200 μM N11 HMPV peptide or NP366 for irrelevant control diluted 1:10 in RPMI/10% FBS, 6 μL CD107a-PE, and 22 μL BFA (BD Cat. #51-2301KZ)/Monensin (BD Cat. #2092KZ). In addition, 1:1000 PMA/ionomycin instead of peptide was added to one aliquot of cells for a positive control. Cells were incubated for 5hrs at 37°C.

For both conditions: After either tetramer staining or peptide stimulation, cells were stained with Live/Dead dye 1:1000 in PBS for 12 min, washed 1x with PBS, and blocked with αCD16/32 Fc block (Tonbo Biosciences Cat. #70-0161-M001) 1:100 in FACS buffer for 10min. For surface staining, cells were stained with surface antibody 1:100 in BD Brilliant Stain Buffer (BD Cat. #566349) buffer for 30min at 4°C. Cells were spun at 1500rpm for 3 min and washed 1x with FACS buffer.

Intracellular cytokine staining: After cells were stained for surface antibodies, cells were fixed for 30min with eBioscience™ Foxp3/Transcription Factor Staining Buffer Set (ThermoFisher 00-5523-00) at 4°C, spun at 1640rpm for 3 min, washed 1x with Foxp3 Fix/Perm Buffer, and stained with 6uL/antibody in Foxp3 Fix/Perm Buffer for 1hr at 4°C. Cells were spun at 1640rpm for 3min, washed 1x with FACS buffer, resuspended in FACS buffer, and stored in the dark at 4°C until they were analyzed on the Cytek® Aurora multispectral flow cytometer.

Intracellular transcription factor staining: For transcription factor staining, cells were fixed for 18 hrs in Foxp3 Fix/Perm at 4°C. After fix/perm, cells were washed 1x with Foxp3 Fix/Perm Buffer and stained with 2.5 μL antibody in Foxp3 Fix/Perm Buffer for 1 hr at 4°C.

After intracellular staining, cells were spun down at 1640rpm for 3 min, washed 1x with FACS buffer, resuspended in FACS buffer with 100 μL BioLegend Precision Count Beads™ (BioLegend Cat. #424902) and run on the Cytek® Aurora multispectral flow cytometer. A full list of antibodies used in all experiments is shown in **Table 1** with additional antibodies specific for this study in **Table 2**. Fluorescence minus one (FMO) controls were used for all inhibitory receptors and transcription factors. For HMPV tetramer staining, influenza NP366-APC tetramers were used as irrelevant controls. Any irrelevant tetramer background staining was subtracted from the final tetramer frequency. Unstained cells from each experiment were fixed for 20 min in 2% PFA and used on the flow cytometer to minimize autofluorescence. Data analysis was performed with Flowjo (v10.8.1). Boolean gating in FlowJo was used to assess inhibitory receptor and functional cytokine co-expression. Patterns were visualized using the SPICE program (NIAID).

Table 2. Memory T cell markers

Cell marker	Fluorophore	Species	Catalog Number	Clone
CD69*	BV510	hamster	104532	H1.2F3
CD69*	PE-Cy5	hamster	104510	H1.2F3
CD103	BUV661	rat	741504	M290

*across the experiments, two different fluorochromes of CD69 were unintentionally used. However, both CD69 antibodies are identical clones.

3.3.10 Statistical analysis

Data analysis was performed using Prism version 9.0 (GraphPad Software). Comparisons between 2 groups were performed using an unpaired 2-tailed Student's *t* test or Mann-Whitney as appropriate. Multiple group comparisons were performed using a 1-way or 2-way ANOVA as appropriate with correction for multiple comparisons (Dunnett test). A *P* value less than 0.05 was considered significant. Error bars in each graph represent SEM.

3.3.11 Study Approval

All animals were maintained in accordance with *Guide for the Care and Use of Laboratory Animals* (NIH publication no. 85-23. Revised 1985) and were handled according to protocols approved by the University of Pittsburgh Subcommittee on Animal Care (IACUC).

3.3.12 Author contributions

OBP: conceived, designed, and performed experiments, acquired and analyzed data, and wrote manuscript. TE: contributed analytic tools, revised manuscript. YZ: contributed analytic tools, revised manuscript. AM conceived and designed experiments, revised manuscript. TDO: acquired and analyzed data, revised manuscript. JVW: conceived and designed experiments, interpreted data, and revised manuscript.

3.4 Results

3.4.1 Aged mice re-challenged with virus 14 months after primary infection exhibit reduced virus in lung yet more severe disease.

Since most older adults with HMPV are seropositive from prior infection (193), we developed a re-infection model where 6-7wk old B6 mice were infected with 2x106 PFU of TN/94-49 HMPV, aged in-house for 64 weeks, and re-challenged with $1x10^7$ PFU TN/94-49 at 70-71wks. The TN/94-49 strain at dose 2x106 PFU causes mild, self-resolving disease in young adult B6 mice with minimal weight loss, transient lung inflammation, and viral clearance by day 7-9 post-infection (p.i.), fully protecting against challenge for >8 weeks (61). Thus, we chose to re-challenge mice with a higher dose of 1x107 PFU TN/94-49 to overcome immunity from their prior infection (**Fig 3-1A**). Aged mice re-challenged with a higher dose of virus lost weight to a similar degree as aged and young mice receiving primary infection of 1x107 PFU, and all mice were euthanized at day 5 p.i. due to extreme weight loss (**Fig 3-1B**). Despite the severe weight loss

similar to primary infected mice, aged re-challenged mice had no detectable titer in lungs at day 5 p.i. (**Fig 3-1C**). Additionally, aged mice that were previously infected had a significant HMPV IgG antibody response, which increased further upon re-challenge (**Fig 3-1D**). Aged re-challenged mice had increased collagen deposition within the alveolar parenchyma indicative of lung fibrosis compared to aged primary infected mice (**Fig 3-1E-F**). Aged re-challenged mice also tended to have more inflammatory infiltrates in lungs (**Fig 3-1G-I**).

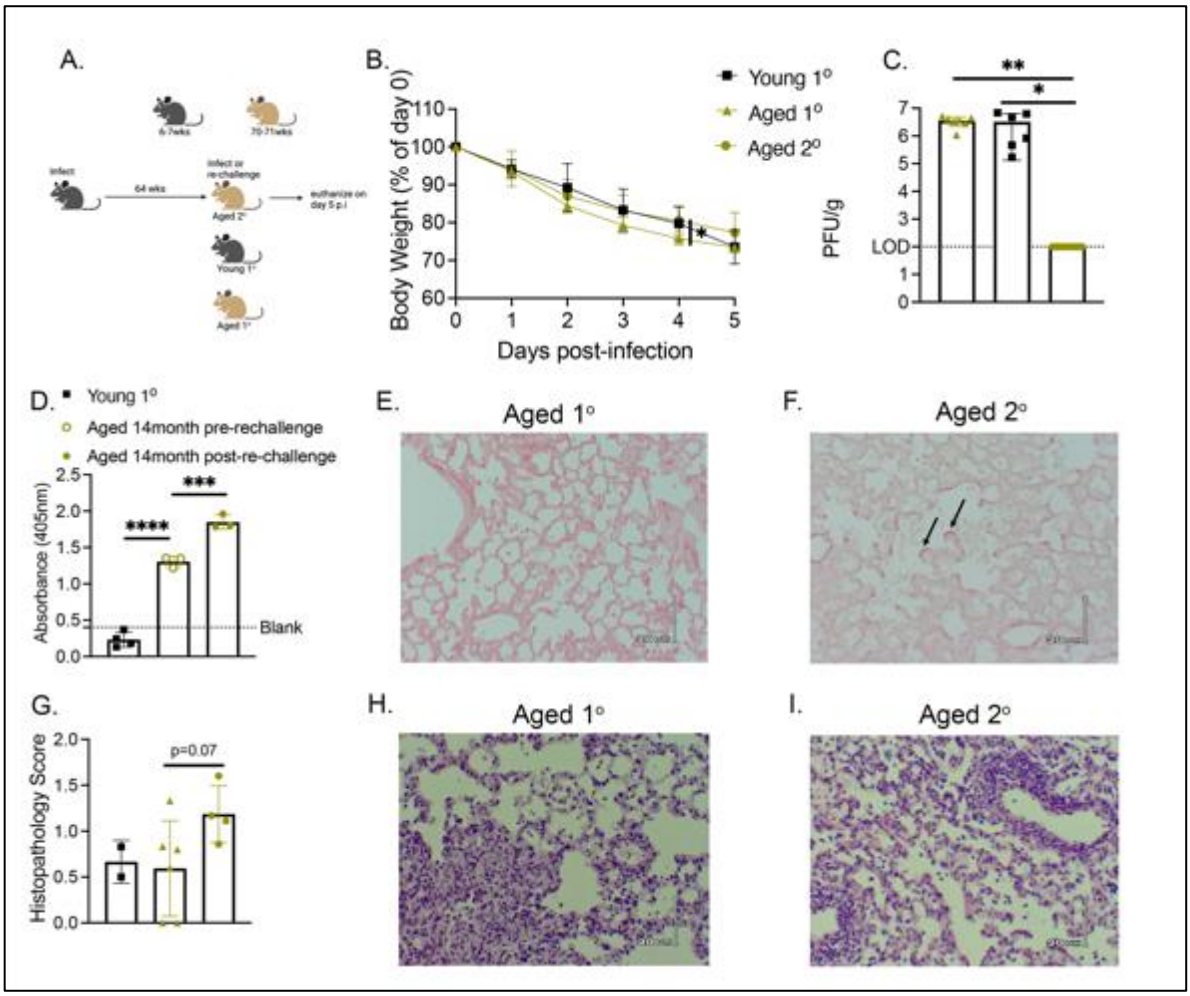

Figure 3-1. Aged mice re-challenged with virus 14 months after primary infection exhibit reduced virus in lung yet more severe disease

(A) Experimental schematic **(B)** Aged mice re-challenged with $1x10^7$ PFU had increased weight loss day 5 p.i. similar to aged and young primary infected mice with the same dose. **(C)** Aged re-challenged mice cleared virus by day 5 p.i.

(D) Aged re-challenged mice had significantly increased HMPV IgG antibody pre re-challenge compared to young primary infected mice at day 5 p.i. There was also a significant increase in IgG antibody post re-challenge as measured by absorbance via HMPV-specific ELISA. **(E, F)** Aged re-challenged mice have increased linear fibrosis in the alveolar parenchyma denoted by black arrows. **(G)** Aged re-challenged mice tended to have increased pathology scores and inflammation in the lung. **(H, I)** Representative histology images. Data in **B** and **C** represent 3 independent experiments with 2-3 mice per experiment. Data in **D** and **G** represent 1 independent experiment. *P<0.05, **P<0.01, ***P<0.005, ***P<0.0001, one- or two-way ANOVA.

3.4.2 Aged re-challenged mice accumulate $CD44^+$ $CD62L^-$ $CD69^+$ $CD103^+$ memory $CD8^+$ T cells that have increased cytotoxic function

Aged mice produced fewer tetramer$^+$ (tet^+) $CD8^+$ T cells following primary HMPV infection compared to young primary infected mice (**Fig 3-2A; Appendix Fig 8A**). However, aged mice re-challenged fourteen months after primary infection had increased tet^+ $CD8^+$ T cells compared to primary infection in both age groups (**Fig 3-2A; Appendix Fig 8A**). Aged re-challenged mice had significantly more $CD44^+$ $CD62L^-$ effector $CD8^+$ T cells and significantly fewer $CD44^-$ $CD62L^+$ $CD8^+$ T cells compared to young mice (**Appendix Fig 8B-C**). Aged re-challenged mice accumulated significantly more tet^+ memory $CD8^+$ T cells as defined by $CD44^+$ $CD62L^-$ $CD69^+$ $CD103^+$ expression (**Fig 3-2B-C; Appendix Fig 8D**). Upon *ex vivo* peptide restimulation, $CD8^+$ T cells from aged re-challenged mice produced significantly more granzyme B (**Fig 3-2D; 3-2G**) and tended to degranulate more as measured by CD107a (**Fig 3-2E**). In addition, memory $CD8^+$ T cells in aged re-challenged mice were more functional, having increased granzyme B production (**Fig 3-2F**). There was no difference in the percentage or absolute number of $CD19^+$ B or $CD4^+$ T cells between groups (**Appendix Fig 8E-F**). Gating strategies shown in **Appendix Fig 9**. In addition, we found increased concentration of T cell chemoattractants, including CCL2, CCL3,

CCL7, and CXCL2 in the lungs of aged, primary infected mice late in HMPV infection, which could explain the accumulation of $CD8^+$ T cells in the lung of aged mice (**Appendix Fig 10A-B**). Taken together, aged re-challenged mice exhibited severe disease and lung inflammation despite undetectable virus in lung. Furthermore, aged re-challenged mice accumulated significantly more tet^+ memory $CD8^+$ T cells with increased cytotoxic function, suggesting immune-mediated disease.

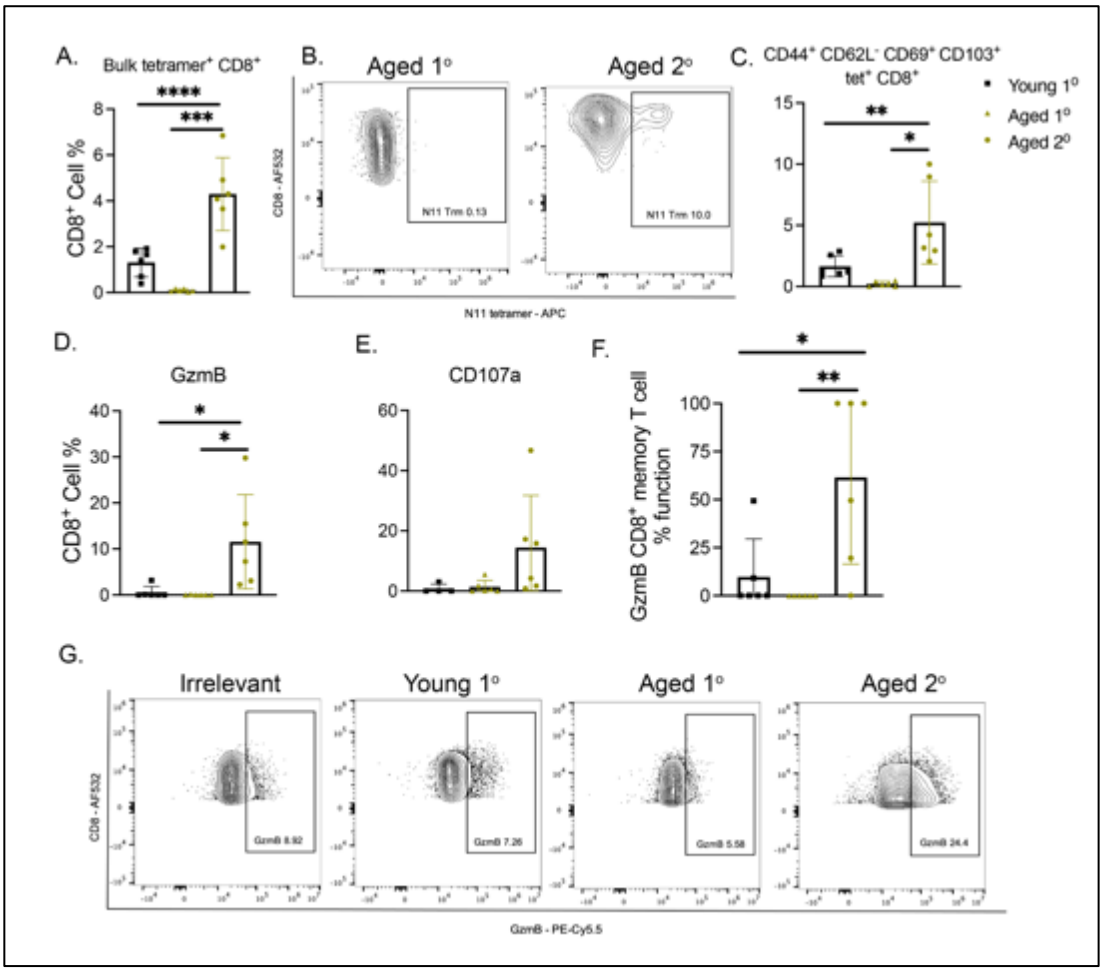

Figure 3-2. Aged re-challenged mice accumulate $CD44^+$ $CD62L^-$ $CD69^+$ $CD103^+$ memory $CD8^+$ T cells that have increased cytotoxic function.

(A) Aged re-challenged mice produced more, but aged primary infected mice produced significantly fewer, tet^+ $CD8^+$ T cells compared to young primary infected mice. **(B-C)** Aged re-challenged mice accumulated significantly more virus-specific $CD44^+$ $CD62L^-$ $CD69^+$ $CD103^+$ $CD8^+$ T cells in lung compared to aged and young primary infected

mice. **(D-E)** Upon *ex vivo* peptide restimulation, aged re-challenged mice produced significantly more granzyme B and tended to degranulate more as measured by CD107a staining. **(F)** Significantly more of the $CD44^+$ $CD62L^-$ $CD69^+$ $CD103^+$ $CD8^+$ T cells were functional in producing granzyme in the aged re-challenged mice. This was calculated by granzyme B cells percent divided by memory $CD8^+$ T cell percent. **(G)** Representative flow plots of granzyme B staining. Data represent 3 independent experiments with 5-6 mice per experiment *P<0.05, **P<0.01, ***P<0.005, ***P<0.0001, one-way ANOVA.

3.4.3 Serum from young mice five weeks post-infection did not protect aged or young mice against HMPV infection.

Considering that aged mice re-challenged with virus fourteen months after primary infection had undetectable lung viral titer, we questioned whether the humoral response neutralized the virus upon re-infection to abort replication. To test the role of the humoral response during HMPV infection, serum was collected from either naïve or HMPV-infected young mice five weeks p.i.. Naïve or HMPV serum was injected into aged or young mice on the day of infection (**Fig 3-3A**). Aged mice that received naïve serum lost significantly more weight on days three and four p.i. compared to young mice with naïve serum (**Fig 3-3B**). There was no difference in viral titer between all four groups (**Fig 3-3C**). Aged mice that received either naïve or HMPV serum produced fewer tet^+ $CD8^+$ T cells compared to young mice (**Fig 3-3D**). While young mice injected with HMPV serum had significantly fewer tet^+ $CD8^+$ compared to young mice injected with naïve serum (**Fig 3-3D**). Aged mice produced fewer $CD44^+$ $CD62L^-$ $CD69^+$ $CD103^+$ $CD8^+$ T cells in the lung regardless of serum given (**Fig 3-3E-F**). Young mice that received HMPV serum did have modest increase in memory $CD8^+$ T cells compared to young mice with naïve serum (**Fig 3-3E-F**). Aged $CD8^+$ T cells in both groups produced less granzyme B via *ex vivo* peptide stimulation (**Fig 3-3G**). In addition, aged T cells stimulated with class I peptide in ELISpot produced less IFNγ

regardless of serum type (**Fig 3-3H-I**). Young mice did tend to produce more IFNγ when given HMPV serum compared to aged mice with HMPV serum (**Fig 3-3H-I**). In an attempt to improve the aged $CD8^+$ T cell IFNγ response, PD-1 blockade or 4-1BB co-stimulation were added to the *ex vivo* peptide stimulation, both of which have been used to potentiate $CD8^+$ T cells in cancer models (167, 174, 180). However, neither treatment increased IFNγ production in aged $CD8^+$ T cells **(Fig 3-3H-I)**. Taken together, these data suggests that the humoral response is only partially protective in young mice but suggests that the weight loss in aged mice is not mediated by HMPV-specific antibody. These data would support the idea that cellular immunity, such as dysfunctional $CD8^+$ T cells, are critical drivers of immunopathology rather than humoral immunity.

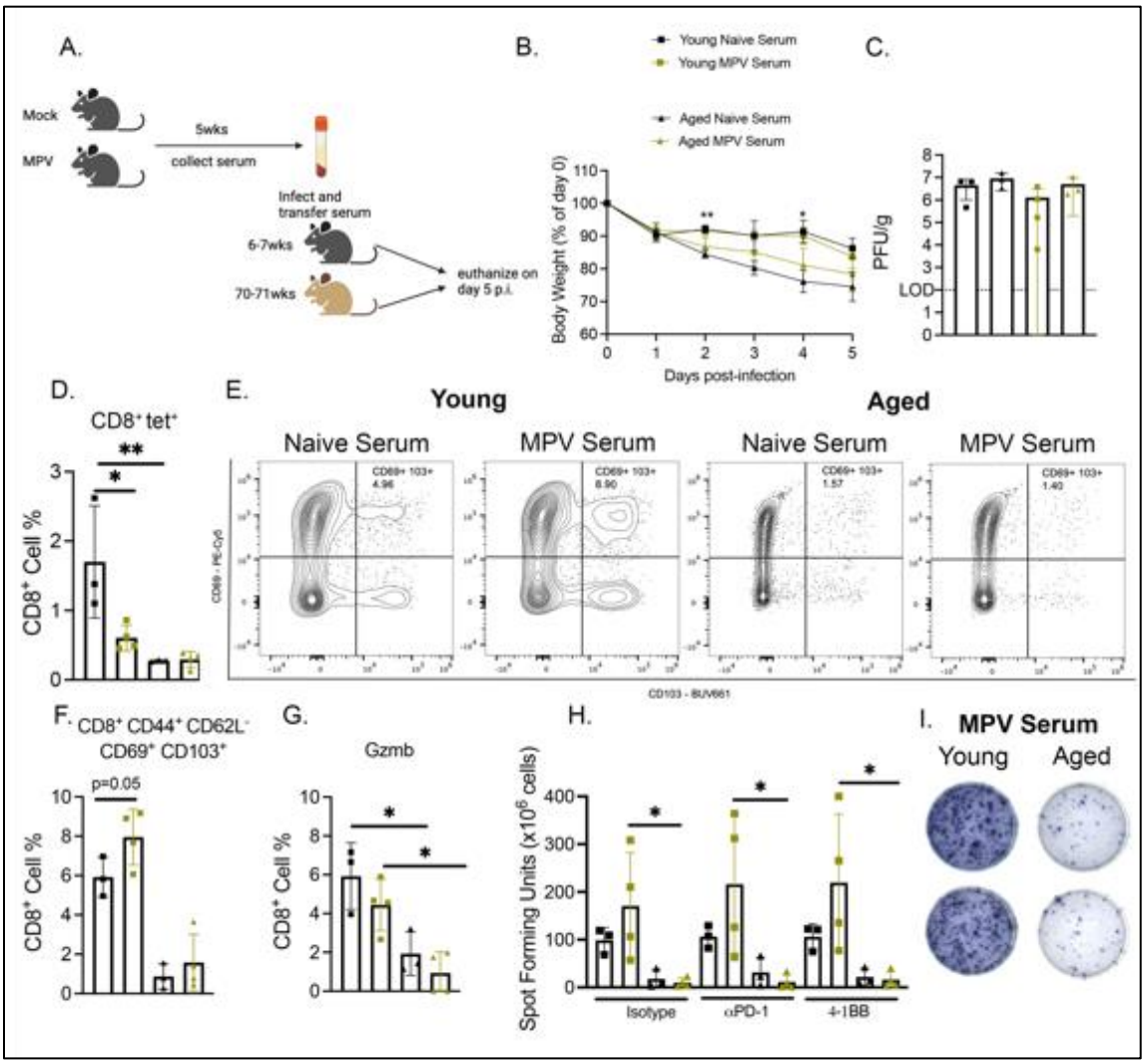

Figure 3-3. Serum from young mice 5wk p.i. did not protect aged or young mice against HMPV infection.

(A) Schematic of experimental design. **(B)** Aged mice that received naive serum lost more weight at day 2 and 4 p.i. **(C)** There was no difference in viral titer between any of the age groups. **(D)** Aged mice produced fewer $CD8^+$ tet^+ T cells regardless of whether they received naive or MPV serum. **(E-F)** Aged mice also produced fewer $CD44^+$ $CD62L^-$ $CD69^+$ $CD103^+$ $CD8^+$ memory T cells regardless of serum treatment. **(G)** Aged $CD8^+$ T cells from both groups produced significantly less granzyme B compared to young mice. **(H-I)** Aged $CD8^+$ T cells also produced less IFNγ as measured by ELISpot. Data represents 1 independent experiment with 3-4 mice per group. *P<0.05, **P<0.01, ***P<0.005, ***P<0.0001, one-way ANOVA.

3.4.4 Aged mice display impaired contraction of $CD8^+$ T cells in the lung 40 days post-infection

We next sought to compare differences in T cell memory formation between young and aged mice and identify lung tissue-resident $CD8^+$ T cells more precisely. Aged and young mice were infected with $1x10^6$ PFU HMPV and 40 days p.i., injected IV with CD45.2 antibody and immediately euthanized (**Fig 3-4A**). Using this *in vivo* labeling method, tissue resident cells stain negative for CD45.2 while cells trafficking to the lung from the blood stain positive (198). Aged mice accumulated significantly more $CD45.2^-$ $CD8^+$ T lymphocytes, consistent with T_{RM}, in the lung (**Fig 3-4B-D**). There was a trend towards an increase in frequency of $CD45.2^-$ $CD44^+$ $CD62L^-$ $CD69^+$ $CD103^+$ T_{RM} cells in young mice (**Appendix Fig 10C**). However, by absolute cell number, aged mice accumulated more of these $CD8^+$ T_{RM} in the lung (**Fig 3-4E**). While there was no significant difference in the frequency or absolute number of bulk tet^+ $CD8^+$ T cells between the age groups (**Fig 3-4F; Appendix Fig 10D**), aged mice produced more $CD45.2^-$ tet^+ $CD8^+$ T cells (**Fig 3-4G**). Both bulk and tet^+ aged $CD45.2^-$ $CD8^+$ T had increased mean fluorescence intensity (MFI) and percentage of cells expressing PD-1 compared to young mice (**Fig 3-4H; Appendix Fig 10E**). This led us to consider whether treating lung lymphocytes with PD-1 blockade and 4-1BB stimulation would impact $CD8^+$ T cell function in this model. *Ex vivo* peptide restimulation of lung lymphocytes revealed that aged mice exhibited significantly more IFNγ-producing cells compared to young mice (**Fig 3-4I-J**). However, PD-1 blockade, 4-1BB agonist treatment, or the combination did not change IFNγ production in either age group (**Fig 3-4I)**. There was no difference in HMPV IgG production between aged and young mice (**Appendix Fig 10F**). These results suggest that aged mice accumulate $CD45.2^-$ $CD8^+$ T_{RM}s in the lung following primary

infection and that these aged CD8$^+$ T cells have increased cytotoxic function that is not restrained by PD-1 or 4-1BB signaling.

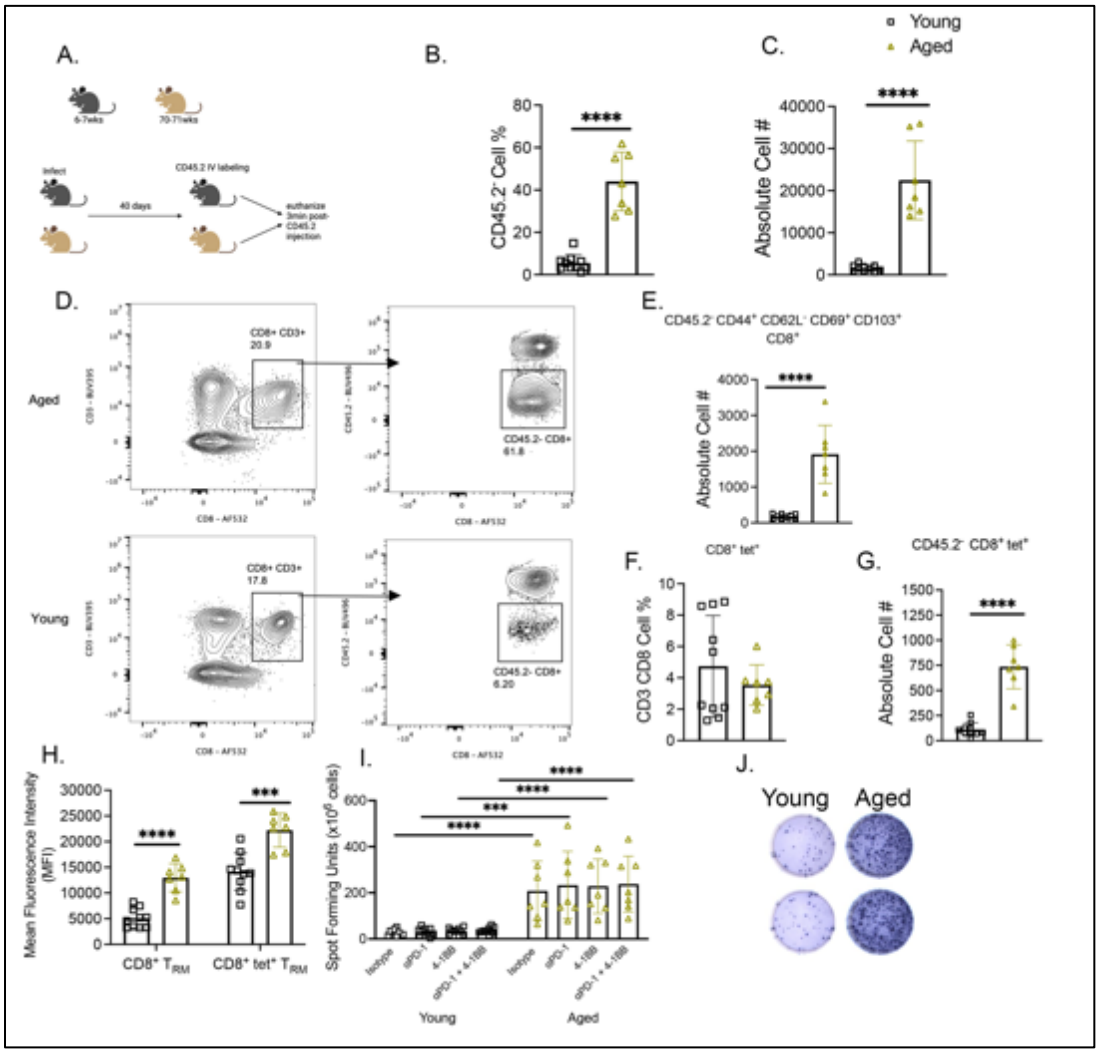

Figure 3-4. Aged mice failed to contract CD45.2$^-$ CD8$^+$ T cells in the lung 40 days p.i.

(A) Experimental design schematic. **(B-C)** Aged mice had significantly more CD45.2$^-$ CD8$^+$ T cells in the lung via CD45.2 IV labeling at day 40 p.i. compared to young mice. **(D)** Representative gating of CD45.2 staining. **(E)** Aged mice had increased absolute number of CD45.2$^-$ CD44$^+$ CD62L$^-$ CD69$^+$ CD103$^+$ CD8$^+$ (i.e. T_{RM}) T cells. **(F)** There was no difference in CD8$^+$ tet$^+$ frequency between age groups. **(G)** Aged mice had increased absolute number of CD45.2$^-$ CD8$^+$ tet$^+$ T cells in lung. **(H)** PD-1 MFI expression was increased on aged bulk CD8$^+$ and tet$^+$ T_{RM} cells in the lung. **(I-J)** Aged lung T lymphocytes had significant IFNg production after *ex vivo* peptide stimulation. Data

represent 2 independent experiments with 3-5 mice per experiment. ***P<0.005, ***P<0.0001, unpaired t-test or one-way ANOVA.

3.4.5 Aged mice restimulated with HMPV peptide/LPS adjuvant lost more weight and had diminished $CD8^+$ memory response.

Elderly humans have a poor response to vaccines (199-201). We aimed to use this aged mouse model to elucidate the $CD8^+$ T cell memory response. Aged mice fourteen months p.i. or young mice five weeks p.i. were vaccinated with HMPV cognate peptide antigen for a dominant $K^b/N_{11–19}$ (N11) epitope (46, 61) adjuvanted with LPS via intraperitoneal injection (**Fig 3-5A**). fThis model was designed to mimic what would occur if elderly humans received epitope or inactivated vaccination for a virus they had previously been exposed to. Aged mice lost significantly more weight compared to young mice (**Fig 3-5B**) and accumulated fewer bulk and tet^+ memory $CD8^+$ T cells in the lung (**Fig 3-5C-E; Appendix Fig 11A**). Aged mice also produced fewer tet^+ $CD8^+$ T cells compared to young mice (**Appendix Fig 11B**), as we observed in aged mouse primary infection (**Fig 3-2A**). There was no difference in the absolute number of $CD8^+$ T cells in the lung between the age groups (**Appendix Fig 11C**), which ruled out a global impairment in aged $CD8^+$ T cell production. Since aged mice exhibited a diminished $CD8^+$ memory response to peptide stimulation in this model, we hypothesized that HMPV cognate antigen and LPS adjuvant did not adequately activate the $CD8^+$ T cell response in aged mice. To test this hypothesis, we assessed inhibitory receptor expression on $CD8^+$ memory T cells. Combinatorial analysis of PD-1, TIM-3, LAG-3, and 2B4 expression on bulk $CD8^+$ memory T cells revealed that the majority of memory CD8 T cells from young mice had increased expression of only one inhibitory receptor (**Appendix Fig 11D**), while aged mice co-expressed two or three of these receptors (**Fig 3-5F**), but neither age

group expressed all four (**Appendix Fig 11E**). Analysis of CD44 and CD62L expression on $CD8^+$ T cells showed that aged mice had increased $CD44^+$ $CD62L^-$ $CD8^+$ T effector cells and a significantly diminished pool of $CD44^-$ $CD62L^+$ $CD8^+$ T cells (**Appendix Fig 11F**). Furthermore, *ex vivo* HMPV peptide stimulation ELISpot revealed that aged mice generated significantly fewer IFNγ-producing cells compared to young mice whether treated with PD-1 blockade, 4-1BB agonist treatment, or both (**Fig 3-5G-H**). These results indicate that aged mice mounted an impaired $CD8^+$ memory response when re-challenged with HMPV cognate peptide antigen in the absence of viral infection.

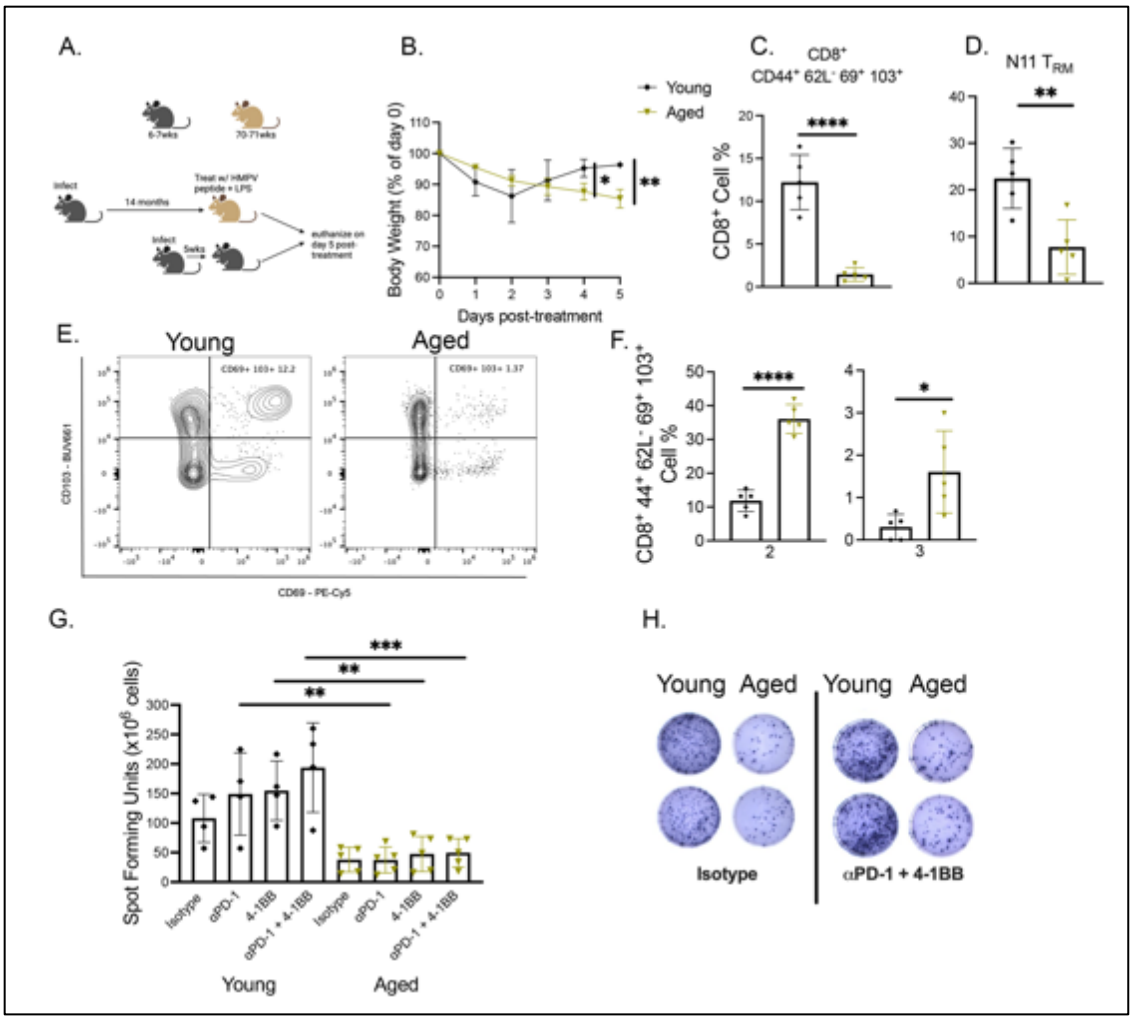

Figure 3-5. Aged mice restimulated with HMPV-peptide/LPS adjuvant lost more weight and had diminished CD8$^+$ memory response.

(A) Experimental design. **(B)** Aged mice restimulated with HMPV N11 peptide + LPS lost significantly more weight post-treatment. **(C-E)** Aged restimulated mice had diminished bulk and virus-specific CD8$^+$ T_{RM} response. **(F)** CD8$^+$ CD44$^+$ CD62L$^-$ CD69$^+$ CD103$^+$ T cells from aged restimulated mice co-expressed significantly more inhibitory receptors PD-1, TIM-3, LAG-3, and 2B4 based on combinatorial analysis. **(G-H)** Aged restimulated mice produced less IFN at baseline in *ex vivo* peptide stimulation and failed to increase IFNg production with PD-1, 4-1BB or combination therapy. Data represent 1 experiment with 5 mice per experiment. *P<0.05, **P<0.01, ***P<0.005, ***P<0.0001, unpaired t-test .

To further test this vaccine strategy, we vaccinated aged and young mice with HMPV cognate peptide/LPS, waited five weeks, then re-challenged with live virus, and assessed the $CD8^+$ memory response (**Fig 3-6A**). Aged mice tended to lose more weight post-infection (**Fig 3-6B**) and have more virus in lungs (**Fig 3-6C**). Aged mice produced fewer tet^+ $CD8^+$ T cells (**Fig 3-6D-E**) as well as $CD44^+$ $CD62L^-$ $CD69^+$ $CD103^+$ $CD8^+$ memory T cells (**Fig 3-6F-H**), and tet^+ $CD8^+$ memory T cells (**Fig 3-6I-J**). In addition, aged vaccinated mice produced less IFN via *ex vivo* peptide stim which was not improved with PD-1 blockade or 4-1BB co-stimulation (**Fig 3-6K-L**). Taken together, these results indicate that HMPV cognate peptide/LPS is an ineffective vaccine in aged mice.

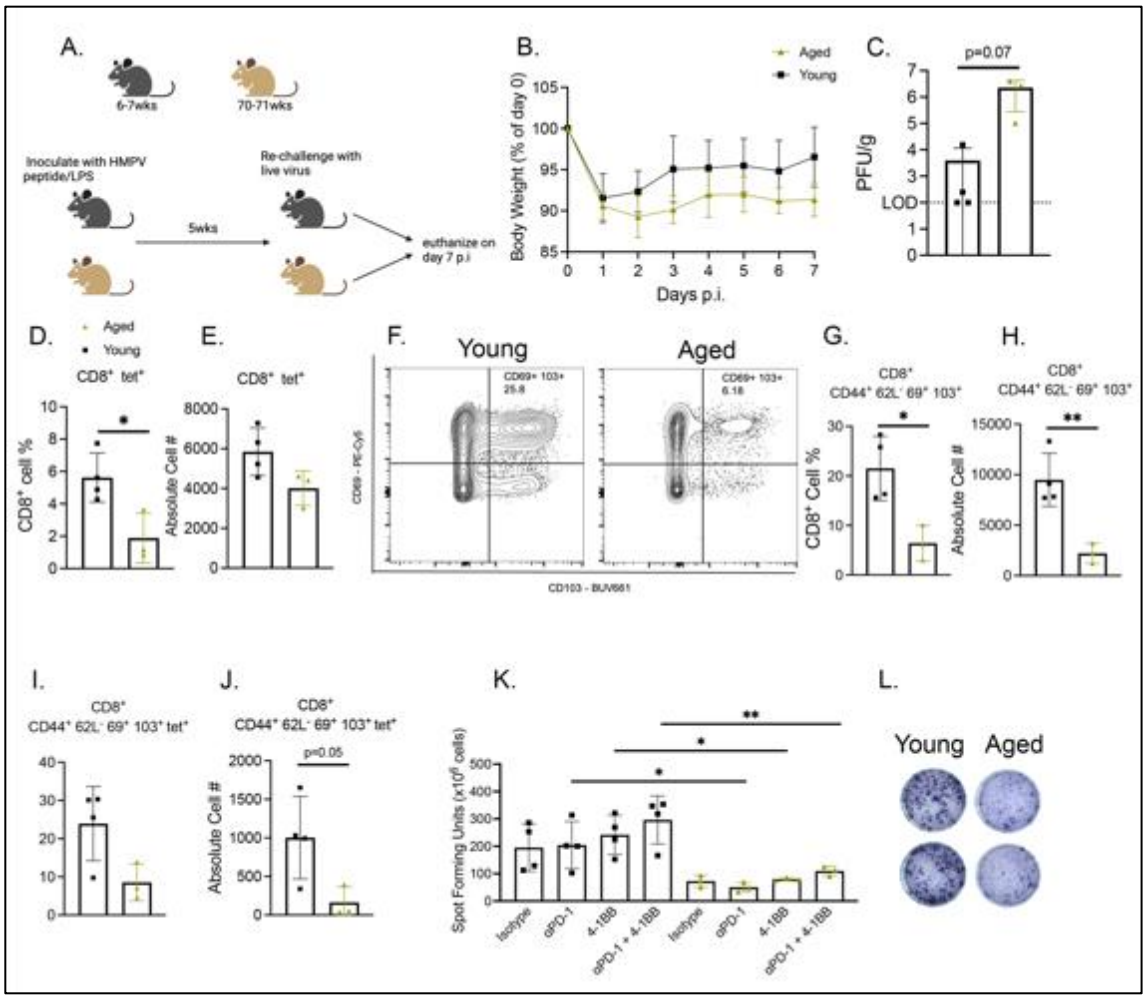

Figure 3-6. Aged mice vaccinated with HMPV cognate peptide prior to infection had poor CD8$^+$ memory response.

(A) Schematic of experimental design. **(B)** Aged vaccinated mice tended to lose more weight post-infection. **(C)** Aged vaccinated mice also tended to have higher titer in lung. **(D-E)** Aged mice produced fewer tet$^+$ CD8$^+$ T cells. **(F-H)** Aged vaccinated mice also produced fewer CD8$^+$ CD44$^+$ CD62L$^-$ CD69$^+$ CD103$^+$ memory T cells compared to young mice. **(I-J)** Aged vaccinated mice tended to also have fewer tet$^+$ memory CD8$^+$ T cells. **(K-L)** Aged CD8$^+$ T cells also produced less IFNg as measured by *ex vivo* peptide stim ELISpot. Data represent 1 independent experiment with 3-4 mice per experiment. *P<0.05, **P<0.01, unpaired t-test .

3.4.6 Aged mice vaccinated with UV-inactivated HMPV exhibited severe HMPV disease and poor $CD8^+$ memory response.

We have shown that re-challenged aged mice develop severe disease and lung inflammation while accumulating dysfunctional $CD8^+$ T_{RM}. Conversely, non-replicating peptide + LPS injection given as vaccination prior to or post HMPV infection did not stimulate an adequate $CD8^+$ T cell response in aged mice. Since vaccination of older individuals is a highly desirable preventive strategy, we next aimed to assess the aged $CD8^+$ memory response in another vaccination model. Aged 70-71 week or young 6-7 week-old B6 mice were primed with either PBS, $2x10^6$ PFU live virus, or an equivalent volume of UV-inactivated virus followed by re-challenge five weeks later with live virus (**Fig 3-7A**). Aged mice primed with UV-inactivated virus lost significantly more weight post-rechallenge compared to aged mice primed with live virus (**Fig 3-7B**). Aged mice "primed" with only PBS (thus undergoing primary infection) tended to have higher viral burden in lung compared to young primary infected mice (**Fig 3-7C**), a phenomenon we have previously observed (manuscript submitted). Aged mice vaccinated with UV-inactivated virus had significantly higher viral titer compared to young UV-vaccinated mice, which lacked detectable lung virus (**Fig 3-7C**). Aged and young mice primed with live virus had undetectable titer in lungs (**Fig 3-7C**). ELISA showed a robust IgG response by both aged and young mice primed with live virus (**Fig 3-7E**). However, aged mice vaccinated with UV-inactivated HPMV had negligible IgG response (**Fig 3-7E**). Young mice vaccinated with UV-inactivated HMPV had a significantly greater IgG response compared to aged UV-vaccinated mice, but still less than young mice primed with live virus (**Fig 3-7E**).

We next assessed the lung $CD8^+$ memory T cell response to this vaccination model. Aged mice vaccinated with UV-inactivated HMPV had a significantly decreased bulk $CD8^+$ memory T cell response compared to young mice while mice of both age groups primed with live virus had a robust bulk $CD8^+$ memory T cell response (**Fig 3-7D; F**). There was also a modest but not significant increase in tet^+ $CD8^+$ memory T cells in young mice primed with live virus compared with aged mice (**Fig 3-7G**). Representative flow plots of $CD69^+$ and $CD103^+$ staining are shown in **Fig 3-7D**. Since we observed this difference in $CD8^+$ memory T cells between the age groups and based on vaccination or live virus priming, we performed combinatorial analysis to assess PD-1, TIM-3, LAG-3, and 2B4 inhibitory receptor co-expression on $CD8^+$ memory T cells. Aged and young vaccinated mice had significantly increased co-expression of 3 inhibitory receptors compared to aged and young mice primed with live virus with no significant difference in 0, 1, 2, or 4 inhibitory co-expression (**Appendix Fig 11G-H**). Taken together, these data indicate that vaccinating aged mice with UV-inactivated virus led to less effective IgG antibody production and more impaired $CD8^+$ memory T cells, resulting in increased weight loss and delayed viral clearance. Without the inflammation that normally accompanies a live viral infection, UV-inactivated virus did not mount a robust cell-mediated and humoral response in aged mice, which could explain the poor vaccine response in older adults.

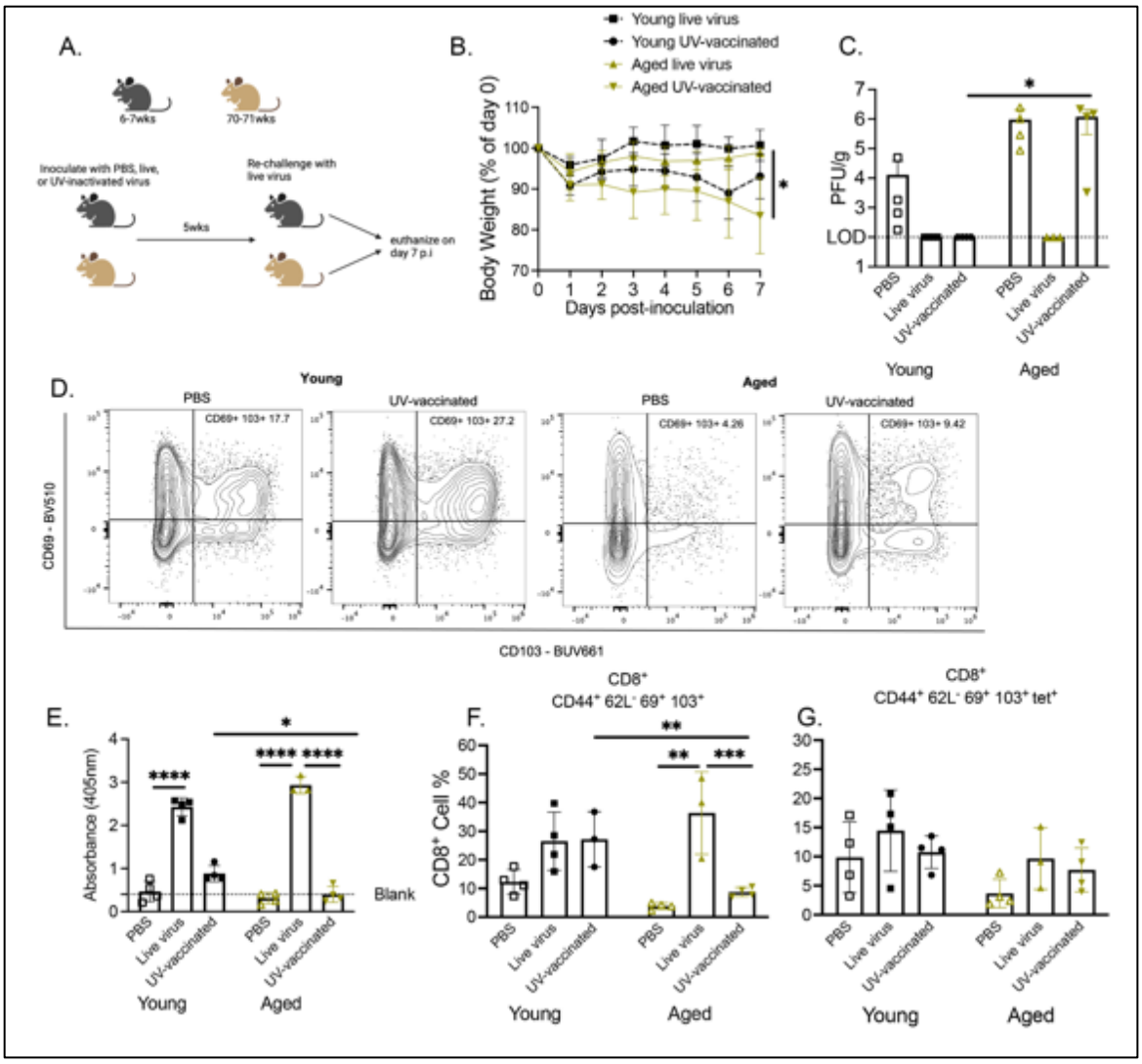

Figure 3-7. Aged mice vaccinated with UV-inactivated HMPV exhibited severe HMPV disease and poor CD8$^+$ memory response.

(A) Schematic of experimental design. **(B)** Aged mice primed with UV-inactivated virus and re-challenged with live virus lost significantly more weight post-infection compared to aged mice primed with live virus. **(C)** Aged mice primed with UV-inactivated virus had significantly higher viral titer at day 7 post-infection. **(D)** Aged and young mice primed with live virus mounted a robust IgG antibody response compared to UV-inactivated virus priming. **(E-F)** Aged mice primed with UV-inactivated virus had significantly decreased CD8$^+$ CD44$^+$ CD62L$^-$ CD69$^+$ CD103$^+$ cell percent compared to aged mice primed with live virus or young mice primed with UV-inactivated virus. There was no significant difference in virus-specific memory CD8$^+$ T cells. **(G)** Representative flow plots of CD69 and CD103

staining. Data represent 2 independent experiments with 2-3 mice per experiment. *P<0.05, **P<0.01, ***P<0.005, ****P<0.0001, one-way ANOVA.

3.5 Discussion

In this study, we developed an HMPV re-challenge aged mouse model to recapitulate human disease, where initial exposure occurs in childhood and re-exposure occurs again later in life. We found that aged re-challenged mice developed severe disease comparable to primary infected aged and young mice despite undetectable lung virus titer. Aged re-challenged mice had a robust antibody response, suggesting this protected against lung virus replication. Nonetheless, aged re-challenged mice exhibited more severe disease, lung inflammation and fibrosis, and increased cytotoxic $CD8^+$ T cell response, all suggesting immune-mediated pathology. Aged re-challenged mice did exhibit a greater number of lung $CD8^+$ T_{RM}, but these cells demonstrated enhanced effector functions. We also observed an increase in chemoattractants in the aged lung late in HMPV infection (i.e. days 7-9), which could explain, in part, the accumulation of lung $CD8^+$ T cells in aged mice. We further show that the humoral response is not fully protective against HMPV infection as even young mice given serum from young mice 5wks post MPV infection had only a small decrease in lung viral titer.

We previously showed that PD-1 signaling restrains antiviral $CD8^+$ T cell functions in young adult mice (46, 52, 61, 62). However, aged re-infected mice $CD8^+$ T cells demonstrated strong effector function in the presence or absence of PD-1 blockade. Similarly, 4-1BB agonists restore function to exhausted T cells in some cancer models (167, 174, 180), but blocking this pathway had no

effect on the aged antiviral $CD8^+$ T cells. Importantly, there was also no effect of PD-1 blockade or 4-1BB agonist in young mice at day 40 p.i. One explanation for these findings in young mice could be that young mice contracted their memory $CD8^+$ T cell population in the lung by day 40 p.i., minimizing any differences that these agents would produce. When young mice were re-stimulated with HMPV peptide/LPS, causing the memory $CD8^+$ T cell population to expand, they exhibited a trend towards increased IFNγ production with PD-1/4-1BB combination, supporting our previous findings of PD-1 signaling in young mice (46, 52, 61, 62). In contrast, aged mice failed to respond to PD-1 blockade of 4-1BB agonist treatment in either model. Collectively, these data suggest that older mice developed a strong but ultimately dysfunctional and perhaps unregulated memory $CD8^+$ T cell response. Similar to our findings, in aged mice infected with influenza, cytotoxic $CD8^+$ $CD69^+$ T_{RM} accumulated up to 60 days post-primary infection and caused significant lung inflammation and fibrosis (154). These findings suggest that HMPV severe respiratory disease in the elderly could, in part, be driven by these cytotoxic dysfunctional $CD8^+$ memory T cells.

To test HMPV vaccination strategies, aged and young previously infected mice were re-challenged with HMPV cognate peptide antigen fourteen months or five weeks after primary infection. We hypothesized that a non-replicating immune memory stimulus with HMPV peptide plus LPS would result in an improved immune response in aged re-challenged mice and induce a milder(?) cytotoxic T cell response. However, aged mice restimulated with HMPV cognate antigen mounted a poor $CD8^+$ T_{RM} response characterized by co-expression of more inhibitory receptors and production of less IFNγ. In our complementary vaccination approach, aged mice primed with HMPV cognate peptide plus LPS also had a poor memory response upon re-challenge with live

virus. In contrast, the robust accumulation of $CD8^+$ memory T cells with low inhibitory receptor expression we observed in young mice is similar to our previous vaccination strategies using virus-like particles (VLPs) (202) or dendritic cell vaccination (52). LPS alters the immune response in female mice that are twelve months old (203), so it is possible that using LPS as an adjuvant was detrimental to the immune response in aged mice, leading to an impaired $CD8^+$ memory response and weight loss. These findings in HMPV peptide re-stimulated aged mice may help to explain why elderly humas exhibit a poor response to vaccines against viruses they have previously been exposed to. Overall, these data suggest that there is an intrinsic defect in the aged $CD8^+$ memory T cell population that causes immunopathology upon re-exposure to either live virus or HMPV peptide vaccination later in life.

Older adults mount a poor memory response to many vaccines and as a result adjuvanted or high-dose vaccines are often required to elicit protection in these individuals (190-192). Currently, there is no licensed HMPV vaccine, although we and others have tested vaccine strategies in rodents (52, 202, 204), non-human primates (205, 206), and humans (207, 208). UV-inactivated vaccines have been tested in mice for other respiratory viruses and elicited promising results (209, 210). Therefore, we tested whether a UV-inactivated HMPV vaccine approach might elicit robust T cell-mediated immunity in aged mice. Aged mice previously vaccinated with UV-inactivated HMPV exhibited severe disease upon exposure to live HMPV, with increased weight loss and delayed viral clearance compared to young mice. In addition, aged, vaccinated mice had a lower IgG antibody response and a diminished $CD8^+$ memory T cell response with increased co-expression of inhibitory receptors. Thus, vaccinating aged mice with UV-inactivated HMPV virus was inadequate to protect against exposure to live HMPV virus. These findings underscore the

dysfunctional $CD8^+$ memory T cell response in the aged host and emphasize the importance of optimizing respiratory virus vaccine strategies in this vulnerable population. One recent study showed improved protection against RSV after elderly humans were vaccinated with $AS01_E$-adjuvanted RSV F protein (211). These findings suggest possible HMPV vaccine strategies to pursue in future studies with the aged mouse model described here. Future studies are also warranted to elucidate the mechanism behind the poor memory response to a UV-inactivated vaccine in aged mice.

Taken together, we developed a novel fourteen month re-challenge mouse model that resembles viral re-infections in elderly humans. We demonstrate multiple ways to use this model to elucidate the aged immune response to re-challenge. This aged mouse model of HMPV re-infection also provides insight into the contribution of $CD8^+$ memory T cells to severe HMPV disease in aged re-challenged mice. Furthermore, this model will be useful to optimize vaccine development in this vulnerable population.

3.5.1 Acknowledgements

We thank the University of Pittsburgh Unified Flow Core for help with flow cytometry. We thank the NIH Tetramer Core Facility (contract number 75N93020D00005) for providing tetramers.

4.0 PD-1 impairs CD8$^+$ T cell granzyme B production in aged mice during acute viral respiratory infection

Olivia B. Parks[*], Danielle Antos[*], Taylor Eddens[†], Sara Walters[*], Monika Johnson[*], Tim D. Oury[‡], Rachel A. Gottschalk[+], John J. Erickson[}], John V. Williams[*,¶,‖]

Affiliations:

[*]Department of Pediatrics, Division of Infectious Diseases, University of Pittsburgh School of Medicine, Pittsburgh, PA, USA

[†]Department of Pediatrics, Division of Allergy/Immunology, University of Pittsburgh School of Medicine, Pittsburgh, PA, USA

[‡]Department of Pathology, University of Pittsburgh School of Medicine, Pittsburgh, PA, USA

[+]Department of Immunology, University of Pittsburgh School of Medicine, Pittsburgh, PA, USA

[}]Department of Pediatrics, Division of Neonatology and Pulmonary Biology, Cincinnati Children's Hospital Medical Center, University of Cincinnati School of Medicine, Cincinnati, OH, USA

[¶]Institute for Infection, Inflammation, and Immunity in Children (i4Kids), Pittsburgh, PA, USA

[‖] **Corresponding Author:**

John V. Williams, MD

University of Pittsburgh

Rangos Research Building

4401 Penn Avenue

Pittsburgh, PA 15224

Phone: 412-692-8298

Email: jvw@chp.edu

Competing Interest Statement: JVW previously served on the Scientific Advisory Board of Quidel and an Independent Data Monitoring Committee for GlaxoSmithKline, neither involved in the present work. All other authors declare no conflicts of interest.

Keywords: Respiratory viral infection, aged immune response, viral immunology

These data are reported in *ImmunoHorizons, 2023:* doi: 10.4049/immunohorizons.2300094

Funding: NIH AI085062 (JVW), Henry L. Hillman Foundation (JVW), 5F30HL159915 and T32 GM008208 (OBP), K12 HD000850 (TE).

4.1 Abstract

$CD8^+$ T cell dysfunction contributes to severe respiratory viral infection outcomes in older adults. $CD8^+$ T cells are the primary cell type responsible for viral clearance. With increasing age, $CD8^+$ T cell function declines in conjunction with an accumulation of cytotoxic tissue resident memory (T_{RM}) $CD8^+$ T cells. Given the importance of PD-1 regulating $CD8^+$ T cells during acute and chronic infections, we sought to elucidate the role of PD-1 signaling on the function of aged $CD8^+$ T cells and accumulation of $CD8^+$ T_{RM} cells during acute viral respiratory tract infection. PD-1 blockade or genetic ablation in aged mice yielded improved $CD8^+$ T cell granzyme B production comparable to young mice during HMPV and influenza viral infections. Syngeneic transplant and adoptive transfer strategies revealed that improved granzyme B production in aged *Pdcd1*$^{-/-}$ $CD8^+$ T cells was primarily cell-intrinsic, as aged WT $CD8^+$ T cells did not have increased granzyme B production when transplanted into young hosts. PD-1 signaling promotes accumulation of cytotoxic $CD8^+$ T_{RM} cells in aged mice. PD-1 blockade in aged mice during re-challenge infection resulted in improved clinical outcomes that paralleled reduced accumulation of $CD8^+$ T_{RM} cells. These findings suggest that PD-1 signaling impairs $CD8^+$ T cell granzyme B production and contributes to $CD8^+$ T_{RM} accumulation in the aged lung. These findings also have implications for future research investigating PD-1 checkpoint inhibitors as a potential therapeutic option for elderly patients with severe respiratory viral infections.

4.2 Introduction: The Role of PD-1 Signaling

Lower respiratory infections contribute to increased morbidity and mortality in adults >65 years of age (1). Human metapneumovirus (HMPV) is a leading cause of acute lower respiratory tract infection and occurs with a similar incidence amongst older adults as influenza and respiratory syncytial virus (RSV) (11, 49, 146, 147). Despite universal exposure to HMPV and 100% seropositivity worldwide by five years of age, recurrent infections occur throughout life, especially in adults >65 years of age, where reinfection can cause severe respiratory disease (11, 49, 146, 147).

Increased age is associated with a widespread decline in immune cell function and a subsequent increase in basal pro-inflammatory cytokine production, referred to as "inflammaging" (117, 130). In addition, aged mice and humans have increased levels of pro-inflammatory $GZMK^+$ $CD8^+$ T cells (150), terminally differentiated $CD8^+$ T cells expressing thymocyte selection-associated high mobility group box protein (TOX) and eomesodermin (EOMES) (150, 152, 153), as well as tissue-resident memory $CD8^+$ T cells (T_{RM}) that propagate lung inflammation and fibrosis (154).

$CD8^+$ T cells are the primary mediators of HMPV clearance (46, 52, 61, 62). Nonetheless, during HMPV infection virus-specific $CD8^+$ T cells upregulate inhibitory receptors such as programmed cell death-1 (PD-1) and lymphocyte activation gene 3 (LAG-3) (46). PD-1 expression impairs $CD8^+$ T cell degranulation and cytokine production during HMPV infection (46, 52, 61, 62). Studies in aged mice revealed that virus-specific $CD8^+$ T cells and antiviral functions, particularly granzyme B production, decline with age, impacting the immune response to respiratory viruses (155, 157, 170, 212). We found that aged mice infected with HMPV displayed more severe clinical

disease, delayed viral clearance, and exacerbated lung inflammation compared to young mice (213). Aged HMPV-infected mice also generated fewer virus-specific $CD8^+$ T cells, which possessed a terminally differentiated phenotype characterized by a loss of expression of transcription factor 7 (Tcf7, which encodes the TF Tcf1) and increased expression of Tox and Eomes, along with significantly decreased granzyme B production (150, 152, 153, 213). Upon HMPV re-challenge, aged mice exhibited severe disease, and accumulated cytotoxic $CD8^+$ T_{RM}s (214).

PD-1 blockade has been used successfully to rejuvenate "stem-cell like" exhausted $CD8^+$ T cells in lymphocytic choriomeningitis virus (LCMV) chronic infection (179, 215) and cancer models (216, 217). Immune checkpoint inhibitors targeting PD-1 signaling have comparable efficacy in both young adults and elderly humans with metastatic solid tumors, indicating that the aged immune system has the capacity to respond to PD-1 blockade (218). In young mice infected with HMPV, PD-1 neutralization or genetic ablation resulted in improved $CD8^+$ T cell function and improved viral clearance (46, 52, 61, 62). In addition, abrogating PD-1 signaling during influenza virus infection improved viral clearance and increased $CD8^+$ T cell production of IFNγ and granzyme B (219). PD-1 signaling has been implicated in optimal $CD8^+$ memory T cell formation following influenza infection, suggesting that the timing of PD-1 blockade during acute viral infection is important to enhance $CD8^+$ T cell function while not impairing memory formation (220). However, the effects of PD-1 blockade on the aged $CD8^+$ T cell response and T_{RM} formation during HMPV infection is poorly understood.

Here, we sought to elucidate the role of PD-1 signaling on virus-specific $CD8^+$ T cell function and memory T_{RM} formation in aged mice. We found that aged *Pdcd1*$^{-/-}$ mice had improved $CD8^+$ T cell granzyme B production during either HMPV or influenza infection. This increase in function was primarily cell-intrinsic, since aged *Pdcd1*$^{-/-}$ $CD8^+$ T cells transplanted into young congenically marked recipients had improved antiviral function compared to aged WT $CD8^+$ T cells. In addition, aged *Pdcd1*$^{-/-}$ mice did not accumulate cytotoxic $CD8^+$ T_{RM} cells at day 40 post-infection, which was in contrast to the detrimental accumulation of cytotoxic $CD8^+$ T_{RM} cells in aged WT mice. Aged mice treated with PD-1 blockade and re-challenged with HMPV fourteen months after primary infection lost less weight and had a trend towards improved $CD8^+$ T cell IFNγ production as compared to isotype control mice, but did not accumulate as many $CD8^+$ $CD69^+$ $CD103^+$ memory T cells. Taken together, these results suggest that therapeutic PD-1 blockade in the aged host may improve $CD8^+$ T cell function during respiratory viral infections.

4.3 Materials & Methods

4.3.1 Mice and viral infection

C57BL/6 (B6), congenic CD45.1, and *Rag*$^{-/-}$ mice were purchased from The Jackson Laboratory. *Pdcd1*$^{-/-}$ mice were obtained with permission from Dr. Tasuku Honjo (Kyoto University, Kyoto, Japan). All animals were bred and maintained in specific pathogen-free conditions in accordance with the University of Pittsburgh Institutional Animal Care and Use Committee. 6-7wk and 10 month old *Pdcd1*$^{-/-}$ and age-matched B6 mice were used in all experiments involving *Pdcd1*$^{-/-}$ mice. In select re-challenge experiments 70-71 week-old B6 animals were used. HMPV (strain TN/94-

49, genotype A2) was grown and titered in LLC-MK2 cells as described (160). Influenza virus strain A/34/PR/8 (PR8) was grown in MDCK cells and titered on LLC-MK2 cells (46). For all experiments, mice were anesthetized with isoflurane in a heated chamber and infected via orotracheal route with $2.0x10^6$ PFU HMPV, 500 PFU PR8, or sterile PBS in 100 μL. Mock infected mice were infected under the same conditions with sterile PBS. Viral titers were measured by plaque assay as described (160, 161).

4.3.2 Antibody treatment

On the two days prior to infection and days 1, 2, and 5 post-infection, aged and young B6 mice were injected intraperitoneally with 200 μg in sterile PBS of αPD-1 (BioXCell Cat# BE0033-2) or rat IgG2a isotype control (BioXCell Cat# BE0089) via intraperitoneal injections.

4.3.3 Bone marrow transplant

Irradiation: One day prior to transplant, an X-ray source (MultiRad 350, Precision X-Ray Irradiation) was used to condition recipient mice with 10-11 cGy total body irradiation in two split doses four hours apart. Irradiated mice were placed on an immunocompromised rack in the animal facility and given sterile food and water.

Bone marrow (BM) single cell suspension: Femur and tibia from *Rag1*$^{-/-}$ mice were harvested, tissue removed, and clean cuts made at either bone end. Using a 25G needle, marrow was flushed from the bone into a conical tube using Dulbecco's Modified Eagle Medium with 10% FBS, 1% Pen Strep antibiotics, 1% L-glutamine, 1% MEM Non-Essential Amino Acids, 0.1% 50mM β-mercaptoethanol (D-10 medium). BM was spun down at 350xg for 5 min and the cell pellet was

filtered through a 70 μm strainer, washed 2x with 5 mL sterile PBS, and counted on a BD Accuri™ cytometer.

B and T cell magnetic column selection: For B and T lymphocyte magnetic column selection, spleen and lymph nodes (inguinal, peritoneal, and submandibular) were collected from B6 and congenic CD45.1 donor mice aged either 6-7wks or 70-71wks. All lymph nodes and each spleen per mouse were passed through a 70 μm strainer, spun down at 350xg for 5 min, pooled together through a 40μm strainer, and spun down again at 350xg for 5 min. The spleen/lymph node single cell suspension from two mice were combined in 900 μL aMACs buffer, incubated with CD90.2 microbeads or CD19-biotin and biotin-labeled microbeads, and separated via an LS column (Miltenyi 130-042-401) per Miltenyi instructions. Plunge was collected from the columns, spun down at 350xg for 5 min, and cell pellet was washed with 5 mL sterile 1XPBS x2. Cells were counted on BD Accuri™ cytometer.

Tail vein injections: $1x10^7$ T, B, and *Rag1*$^{-/-}$ BM cells were resuspended per ml of sterile PBS, followed by injection of 200 μL of cells ($2x10^6$ of each cell type) into irradiated recipient mice via tail vein injection.

4.3.4 CD4$^+$ and CD8$^+$ T cell adoptive transfer

CD4 and CD8 biotinylated antibodies along with anti-biotin microbeads were used for positive selection of CD4 and CD8 subsets of T cells for use in combination experiments. $1x10^6$ CD4 and $1x10^6$ CD8 T cells were combined per mouse, with the remainder of the cell populations as outlined above.

4.3.5 Mixed Bone Marrow Chimera

BM single cell suspension was harvested as outlined above from aged CD45.2 and young CD45.1 donors. BM was injected via tail vein injection into lethally irradiated aged CD45.2 and young CD45.1 recipients in a 1:1 ratio.

4.3.6 CD45.1 IV labeling

Mice were administered 4μg of CD45.2-BUV496 (BD Cat# 741092) in 200μL sterile PBS via tail vein injection and were euthanized 3 min post-injection as previously described (154).

4.3.7 IFNγ ELISpot assay

ELISpot was performed as previously described (46, 163). In select experiments, 10μg of αPD-1 (BioXCell Cat# BE0033-2) or rat IgG2a isotype control (BioXCell Cat# BE0089) were added to ELISpot wells along with HMPV $N_{11\text{-}18}$ peptide. Influenza NP366 peptide (GenScript Peptide Sequence: ASNENMETM) served as control.

4.3.8 IgG HMPV ELISA

One μg of TN/94-49 HMPV viral stock per well was diluted in 1x ELISA coating buffer (BioLegend Cat# 421701) was plated overnight at 4^{o}C. The remainder of the ELISA was performed as in (196).

4.3.9 Flow cytometry staining

Flow cytometry staining was performed as described previously (213, 214). In brief, mice were euthanized and the right lung harvested. The lung was cut into 2 mm segments using scissors, resuspended in RPMI/10% FBS, and incubated for 1 hr at 37ºC with DNAse and collagenase. After digestion, the lung was filtered through 70 μm filters, spun at 1500 rpm for 5min, and the pellet resuspended in 2 mL ACK Lysis Buffer (Gibco A10492-01) for 1 min. 10 mL RPMI/10%FBS was added after ACK Lysis and cells were spun at 1500rpm for 5min. Cells then underwent either tetramer staining or *ex vivo* peptide stimulation.

Tetramer staining: Cells were incubated with 1:2000 100mg dasatinib in 1XPBS/1% FBS (FACS) for 30 min before adding APC conjugated $N_{11\text{-}18}$ 1:200 in FACS/dasatinib for 90 min. Cells were then spun down at 1500rpm for 3 min and washed 1x with FACS buffer.

Ex vivo peptide stimulation: 100 μL of cells were added to a flat-bottom 96-well tissue culture plate. The following was added to cells: 100 μL of 200 μM N11 HMPV peptide or NP366 for irrelevant control diluted 1:10 in RPMI/10% FBS, 6 μL CD107a-PE, and 22 μL BFA (BD Cat. #51-2301KZ)/Monensin (BD Cat. #2092KZ). In addition, 1:1000 PMA/ionomycin instead of peptide was added to one aliquot of cells as a positive control. Cells were incubated for 5hrs at 37ºC.

For both conditions: After either tetramer staining or peptide stimulation, cells were stained with Live/Dead dye 1:1000 in PBS for 12 min, washed 1x with PBS, and blocked with αCD16/32 Fc

block (Tonbo Biosciences Cat. #70-0161-M001) 1:100 in FACS buffer for 10min. For surface staining, cells were stained with surface antibody 1:100 in BD Brilliant Stain Buffer (BD Cat. #566349) buffer for 30 min at 4ºC. Cells were spun at 1500 rpm for 3min and washed 1x with FACS buffer.

Intracellular cytokine staining: Following staining for surface markers, cells were fixed for 30min with eBioscience™ Foxp3/Transcription Factor Staining Buffer Set (ThermoFisher 00-5523-00) at 4ºC, spun at 1640 rpm for 3 min, washed 1x with Foxp3 Fix/Perm Buffer, and stained with 6µL/antibody in Foxp3 Fix/Perm Buffer for 1 hr at 4ºC. Cells were spun at 1640 rpm for 3 min, washed 1x with FACS buffer, resuspended in FACS buffer, and stored in the dark at 4ºC until analysis on a Cytek® Aurora multispectral flow cytometer.

Intracellular transcription factor staining: For transcription factor staining, cells were fixed for 18 hrs in Foxp3 Fix/Perm at 4ºC. After fix/perm, cells were washed 1x with Foxp3 Fix/Perm Buffer and stained with 2.5 µL antibody in Foxp3 Fix/Perm Buffer for 1hr at 4ºC.

After intracellular staining, cells were spun down at 1640 rpm for 3min, washed 1x with FACS buffer, resuspended in FACS buffer with 100 µL BioLegend Precision Count Beads™ (BioLegend Cat. #424902) and run on the Cytek® Aurora multispectral flow cytometer. Fluorescence minus one (FMO) controls were used for all inhibitory receptors and transcription factors. For HMPV tetramer staining, influenza NP366-APC tetramers were used as irrelevant controls. Any irrelevant tetramer background staining was subtracted from the final tetramer frequency. Unstained cells from each experiment were fixed for 20 min in 2% PFA and used on the flow cytometer to

minimize autofluorescence. Data analysis was performed with FlowJo (v10.8.1). A full list of antibodies used in all experiments is shown in **Table 1** & **2**.

4.3.10 scRNAseq Data Analysis

$CD8^+$ T cell scRNAseq dataset from lungs of mice and humans was kindly shared with us from Maxim Artyomov: https://www.synapse.org/#!Synapse:syn22255433/wiki/604556 and was generated as described in (150).

4.3.11 qRT-PCR

Performed as in (46). All values were normalized to the housekeeping gene *Hprt*. Experimental WT and *Pdcd1*$^{-/-}$ lung homogenate samples were reported as relative expression to housekeeping gene (*Hprt*). Samples with Ct values less than 40 were considered positive.

4.3.12 Histopathologic score

Performed as in (213, 214). 10% formalin was injected into a section of the lower left lung lobe and stored in 10% formalin in histology cassettes (Fisher Scientific B851000WH). Tissue sections were stained with H&E by the UPMC Children's Hospital of Pittsburgh Histology Core and slides were imaged and scored at 200X magnification. Scoring criteria per field included: 0: no inflammation; 1:75% inflammation. To generate the histopathologic score, the score for each sample was added and divided by the total number of fields analyzed.

4.3.13 Study Approval

Data analysis was performed using Prism version 9.0 (GraphPad Software). Comparisons between two groups were performed using an unpaired 2-tailed Student's *t* test or Mann-Whitney as appropriate. Multiple group comparisons were performed using a 1-way or 2-way ANOVA as appropriate with correction for multiple comparisons (Dunnett test). A *P* value less than 0.05 was considered significant. Error bars in each graph represent SEM.

4.3.14 Author Contributions

OBP: conceived, designed, and performed experiments, acquired and analyzed data, and wrote manuscript. DA: contributed analytic tools, revised manuscript. TE: contributed analytic tools, revised manuscript. SW: acquired data, revised manuscript. MJ: acquired data, revised manuscript. TDO: acquire data, revised manuscript. RAG: contributed analytic tools, revised manuscript. JJE: designed experiments, interpreted data, and revised manuscript. JVW: conceived and designed experiments, interpreted data, and revised manuscript.

4.4 Results

4.4.1 Aged $CD8^+$ T cells upregulate PD-1 at baseline and during HMPV infection

PD-1 signaling regulates $CD8^+$ T cell function in young HMPV-infected mice (46, 52, 61, 62). In addition, HMPV-specific $CD8^+$ T cells from aged mice demonstrated increased PD-1 expression

(213). We hypothesized that PD-1:PD-L signaling also plays an important role in aged $CD8^+$ T cell function during HMPV infection. To test this hypothesis, we first measured PD-1 and PD-L1/L2 expression on young and aged immune cells in the lung by analyzing publicly available scRNAseq datasets (150). *Pdcd1* was significantly increased on aged lung $CD8^+$ T cells compared to young $CD8^+$ T cells (**Fig 4-1A-B**) while there was no difference in *Pdcd1* expression between age groups for $CD4^+$ T cells or B cells (**Fig 4-1C-D**). In our aged mouse HMPV model, aged mock infected $CD4^+$ T cells had increased *Pdcd1* expression compared to young $CD4^+$ T cells, but there was no difference in $CD19^+$ B cells (**Appendix Fig 14A**). We also found that upregulation of PD-1 during HMPV infection was specific to $CD8^+$ T cells, with no difference in PD-1 on $CD4^+$ T or $CD19^+$ B cells between young and aged HMPV-infected mice (**Appendix Fig 14B**). PD-1 expression robustly increased with infection in young mice but stayed elevated in aged mice in both mock and HMPV infection (**Fig 4-1E**). scRNAseq data revealed no difference in *Havcr2* (Tim-3), *Lag3*, or *Cd244* (2B4) inhibitory receptor expression on $CD8^+$ T cells (**Appendix Fig 14C-E**), which we confirmed at the protein level in mock infected mice via flow cytometry (**Appendix Fig 14F**).

We performed a series of transplants and adoptive transfers of young or aged cells into young or aged hosts to test whether elevated PD-1 expression on aged $CD8^+$ T cells is cell-intrinsic or dependent on the host environment. Mixed bone marrow (BM) chimeras of congenically marked young or aged BM transplanted in a 1:1 ratio into lethally irradiated young or aged hosts revealed that there was a significant increase of PD-1 expression in aged $CD8^+$ T cells compared to young cells in an aged host, with a similar trend for aged $CD8^+$ T cells in a young host (**Fig 4-1F**). When congenically marked bulk young or aged purified T cells were transplanted into lethally irradiated

young or aged hosts, aged $CD8^+$ T cells showed a trend toward increased PD-1 expression in a young host (**Fig 4-1G**). There was no difference in PD-1 expression between aged and young $CD8^+$ T cells in an aged host, but there was a significant increase in PD-1 in the aged $CD8^+$ T cells/aged host compared to young $CD8^+$ T cells/young host control (**Fig 4-1G**). Lastly, to confirm if this phenomenon was specific to $CD8^+$ T cells alone, we adoptively transferred young or aged $CD8^+$ T cells along with young $CD4^+$ T and B cells into *Rag1*$^{-/-}$ recipients that lack all T and B lymphocytes. Aged $CD8^+$ T cells significantly upregulated PD-1 in a young *Rag1*$^{-/-}$ host compared to young $CD8^+$ T cells (**Fig 4-1H**). Overall, these findings indicate that there are both cell-extrinsic and cell-intrinsic effects impacting PD-1 expression on aged $CD8^+$ T cells.

We next assessed expression of PD-L1 and PD-L2 in young vs. aged mice. There were no significant differences in PD-L1 or PD-L2 expression between ages in mock- or HMPV-infected groups across numerous innate immune cell types (**Fig 4-1I & Appendix Fig 14G**), with the exception of a small increase in PD-L2 expression on aged mock-infected interstitial macrophages (IMs) (**Appendix Fig 14G**). Notably, alveolar macrophages expressed very high levels of PD-L1 at baseline and under all conditions, as previously reported (43). We also found no difference between ages in gene and protein expression of *Cd274* (PD-L1) (**Fig 4-1J**) or in *Pdcd1lg2* (PD-L2) (**Appendix Fig 14H**) in the lung myeloid cell scRNAseq dataset (150).

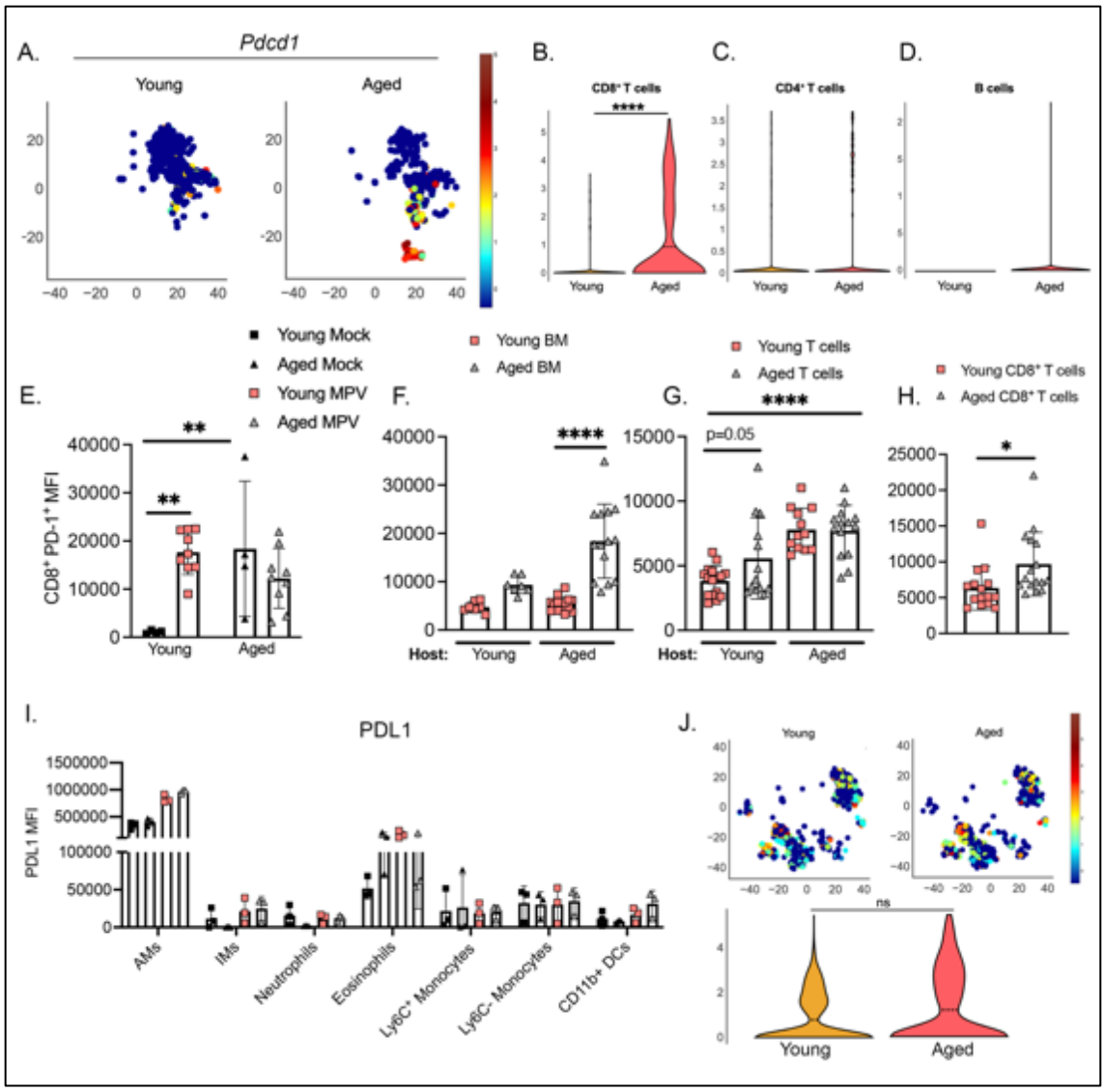

Figure 4-1. Aged CD8$^+$ T cells upregulate PD-1 at baseline and during HMPV infection.

(A) Heat map of *Pdcd1* on lung CD8$^+$ T cells from uninfected, naive aged and young mice. **(B-D)** Violin plot of *Pdcd1*$^{-/-}$ expression from uninfected, naive aged and young mice on lung CD8$^+$ T, CD4$^+$ T, and B cells, respectively. **(E)** Mean fluorescence intensity (MFI) of PD-1 expression on CD8$^+$ T cells in young and aged mock or infected mice. **(F-H)** MFI of PD-1 expression on lung CD8$^+$ T cells in day 7 post-infection (p.i.) in **(F)** aged/young mixed bone marrow (BM) chimera model, **(G)** syngeneic transplant of bulk aged or young T cells along with young B cells and *Rag1*$^{-/-}$ BM, and **(H)** adoptive transfer of aged or young CD8$^+$ T cells into young *Rag1*$^{-/-}$ recipients. **(I)** PDL1 MFI expression on lung innate immune cells at day 1 p.i. **(J)** Heat map of PDL1 (i.e. *Cd274*) expression in lung myeloid cell cluster in uninfected, naive young and aged mice (TOP) and violin plot (BOTTOM). *P<0.05; ****P<0.0001, unpaired t-test

or one-way ANOVA. Each data point represents one individual mouse. Data in (E) represent three experimental replicates, 1 mouse/group. Data in (F) represents two experimental replicates, 3-7 mice/group. Data in (G) represent four experimental replicates, 3-5 mice/group. Data in (H) represent two experimental replicates, 6-7 mice/group. Data in (I) represent 1 experimental replicate, 3 mice/group. BM: bone marrow, MFI: mean fluorescence intensity, AM: alveolar macrophages, IM: interstitial macrophages, DC: dendritic cells

4.4.2 Proportion of granzyme B expressing CD8$^+$ T cells increases after PD-1 blockade

Given the increased PD-1 expression on aged CD8$^+$ T cells, we tested whether *in vivo* PD-1 blockade would rejuvenate Tcf1$^-$ Tox$^+$ Eomes$^+$ exhausted (T_{EX}) CD8$^+$ T cells in aged mice. Studies have previously shown PD-1 blockade improves CD8$^+$ T cell function in chronic viral infection and cancer models (177, 180). We treated aged mice with isotype control or PD-1 blocking antibody on the two days prior to HMPV infection and days 1, 2, and 5 p.i. (**Fig 4-2A**). We found no significant difference in weight loss (**Fig 4-2B**) or viral burden in isotype control vs. anti-PD-1 treated mice (**Fig 4-2C**). PD-1 blockade had no significant impact on the production of HMPV-specific lung CD8$^+$ T cells based on tetramer staining with the HMPV viral epitope H2-D/K^b N_{11-18} (N11) (**Fig 4-2D-E**), nor did it impact the T_{EX} CD8$^+$ T cells that expressed Tox and Eomes (**Fig 4-2F-G; Appendix Fig 14I-K**). However, *in vivo* PD-1 blockade in aged mice resulted in a striking increase in granzyme B production in CD44$^+$ CD62L$^-$ CD8$^+$ T cells (**Fig 4-2H-I**), which was even more pronounced for HMPV-specific (or N11 tetramer$^+$) CD8$^+$ CD44$^+$ Tcf1$^-$ cells (**Fig 4-2J**). IFNγ production did not significantly increase in aged mice treated with PD-1 blockade (**Fig 4-2K-M**). Thus, PD-1 blockade alone appeared to have a favorable impact on HMPV-specific CD8$^+$T cell granzyme B production.

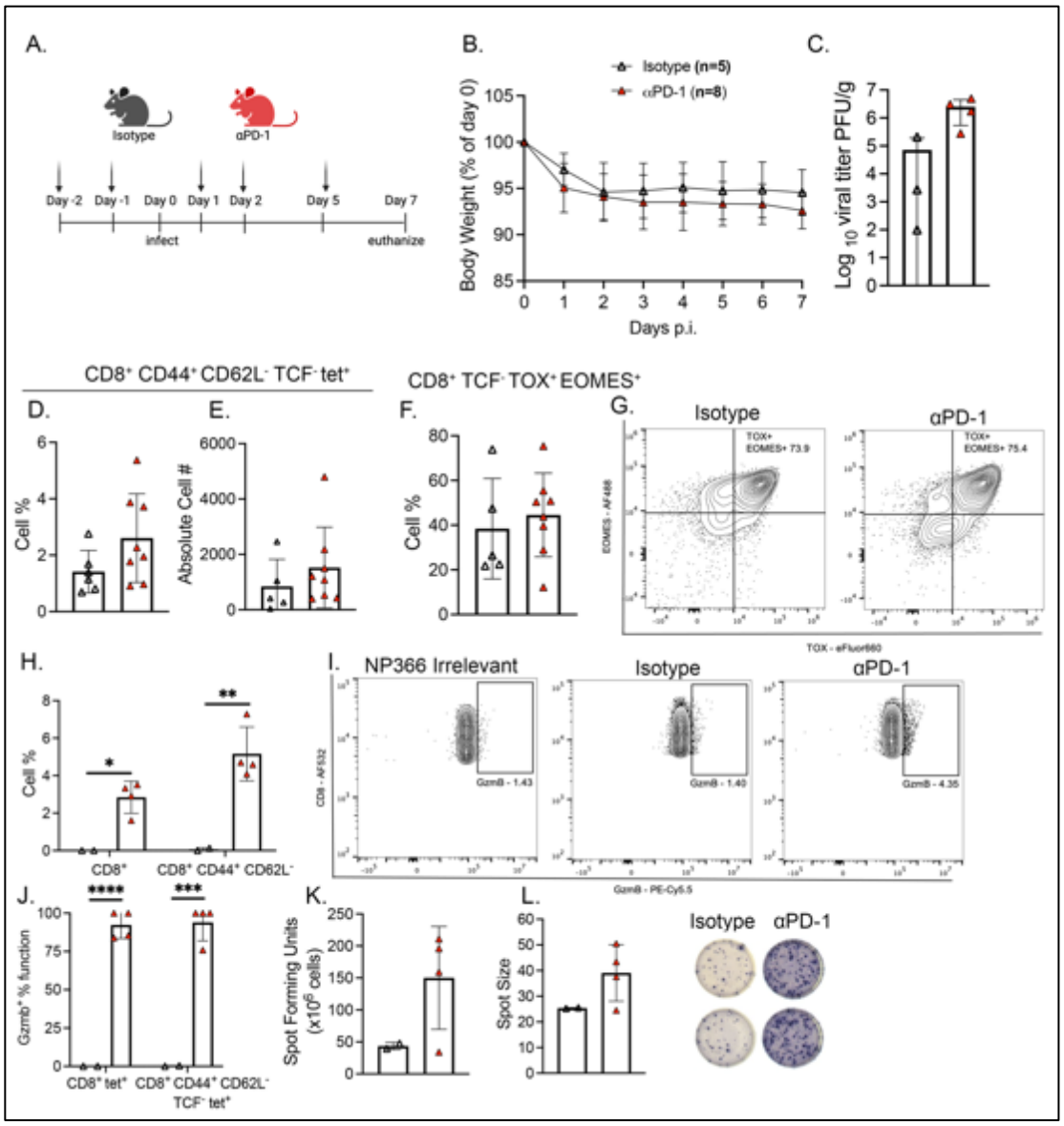

Figure 4-2. Proportion of granzyme B expressing CD8$^+$ T cells increases after PD-1 blockade.

(A) Aged mice were treated with 200g/200L PD-1 or rat isotype control via intraperitoneal injection two days prior to infection and days 1, 2, and 5 post-infection. **(B)** Weight loss during infection. **(C)** Viral titer in PFU/g between aged mice treated with isotype control of PD-1 blockade. **(D-E)** Cell percent and absolute cell number of lung CD44$^+$ CD62L$^-$ TCF$^-$ tet$^+$ CD8$^+$ T cells. **(F)** TCF$^-$ TOX$^+$ EOMES$^+$ lung CD8$^+$ T cells in aged mice treated with isotype or PD-1 blockade. **(G)** Representative flow plots of TOX and EOMES staining. **(H)** Bulk lung CD8$^+$ and CD44$^+$ CD62L$^-$ Gzmb$^+$ cell percent. **(I)** Representative flow plots of Gzmb staining on lung CD8$^+$ CD44$^+$ CD62L$^-$ T cells. **(J)** GzmB percent function of lung CD8$^+$ tet$^+$ and CD8$^+$ CD44$^+$ CD62L$^-$ TCF$^-$ tet$^+$ in both groups. **(K)** Spot number from *ex vivo*

peptide stimulation IFNγ ELISpot of lung lymphocytes from aged isotype or PD-1 blockade treated mice and **(L)** spot size. **(M)** Representative images of ELISpot wells. *P<0.05, **P<0.01, ***P<0.001, ****P<0.0001. Absolute cell number calculation by Biolegend Precision Counting Beads. Each data point represents one individual mouse. Data in (B-G) represent three experimental replicates 2-4 mice/group. Data in (H-J) represent two experimental replicates, 2-3 mice/group. Data in (K-M) represent one experimental replicate 2-4 mice/group.

4.4.3 Aged *Pdcd1*$^{-/-}$ mice have improved CD8$^+$ T cell granzyme B production during HMPV infection

As a complementary approach to antibody blockade, we utilized *Pdcd1*$^{-/-}$ mice, which exhibited increased CD8$^+$ T cell function during HMPV infection in young 6-8-week-old mice (46). We therefore infected aged *Pdcd1*$^{-/-}$ mice and age-matched WT mice, and evaluated the antiviral CD8$^+$ T cell response at day seven post-infection. Of note, these age-matched *Pdcd1*$^{-/-}$ and WT mice were not littermates. In addition, *Pdcd1*$^{-/-}$ mice develop severe autoimmune disease by 9-10 months, and thus these experiments used knockout mice that were at most ten months of age. We confirmed PD-1 expression was absent on *Pdcd1*$^{-/-}$ CD8$^+$ T cells (**Appendix Fig 15A**). Aged *Pdcd1*$^{-/-}$ mice infected with HMPV had no difference in CD8$^+$ N11-specific T cells at day seven p.i. (**Fig 4-3A-C**) but exhibited a trend towards increased CD8$^+$ CD44$^+$ CD62L$^-$ Tcf1$^-$ N11-specific T cells (**Fig 4-3D-F**). There was no significant difference in weight loss (**Appendix Fig 15B**) or viral titer (**Appendix Fig 15C**) in aged mice. We have previously shown that blocking the PD-1/L pathway in young mice improves viral clearance (46). No difference was seen in Tim-3 expression between aged *Pdcd1*$^{-/-}$ and WT mice (**Appendix Fig 15D-E**). However, LAG-3 expression was increased (**Appendix Fig 15F-G**) on *Pdcd1*$^{-/-}$ CD8$^+$ tet$^+$ T cells. PD-1 absence did not significantly affect the expression levels or absolute cell numbers of CD44 and CD62L on CD8$^+$ T cells (**Appendix Fig 15H & K**). We also assessed whether the absence of PD-1 affected the terminal

differentiation of $CD4^+$ T cell subsets. We found no significant differences in the frequencies or absolute cell number of $CD4^+$ $Foxp3^+$, $T\text{-}bet^+$, $GATA3^+$, (**Appendix Fig 15I & L**) or Th1:Th2 ratio between genotypes (**Appendix Fig 15J**). We also found no difference in accumulation of inflammatory infiltrates in the lung as measured by histopathology score (**Fig 4-3L-N**).

Considering the minimal differences in clinical disease, $CD8^+$ tetramer production, and $CD8^+$ differentiation to effector ($CD44^+$ $CD62L^-$) and memory ($CD44^-$ $CD62L^+$; $CD44^+$ $CD62L^+$) subsets, we next assessed $CD8^+$ T cell antiviral function in the presence and absence of PD-1. There was a trend toward increased granzyme B expression in bulk *Pdcd1*$^{-/-}$ $CD8^+$ T cells and significant increase in granzyme B production in $CD44^+$ $CD62^-$ $CD8^+$ T cells (**Fig 4-3G**). There was also a striking increase in the percentage of $CD44^+$ $CD62L^+$ $Tcf1^-$ tet^+ cells making granzyme B in aged *Pdcd1*$^{-/-}$ mice (**Fig 4-3H**).

We next assessed whether this increase in $CD8^+$ T cell function was comparable to the increase in function we observed in young *Pdcd1*$^{-/-}$ T cells compared to young WT T cells (**Appendix Fig 15M**) (46, 52, 61, 62). Comparing *Pdcd1*$^{-/-}$ and WT $Gzmb^+$ $CD8^+$ T cells for both age groups revealed a similar increase in granzyme B production by cells lacking expression of PD-1 (**Fig 4-3I**). This finding indicates that granzyme B production of $CD8^+$ T cells is improved in the absence of PD-1 signaling to a similar degree regardless of age. There was no significant increase in IFNγ production in aged *Pdcd1*$^{-/-}$ $CD8^+$ T cells, suggesting that PD-1 signaling effects were specific to granzyme B production (**Fig 4-3J-K**).

We did investigate the baseline characteristics of $CD4^+$ and $CD8^+$ T lymphocytes in mock-infected aged B6 and *Pdcd1*$^{-/-}$ mice. Interestingly, aged *Pdcd1*$^{-/-}$ mock-infected mice had an increased in the absolute number of $CD4^+$ and $CD8^+$ T lymphocytes in lung, in the absence of infection (**Fig 4-3O**). Aged *Pdcd1*$^{-/-}$ mice also had more $CD4^+$ $Foxp3^+$ T lymphocytes (**Fig 4-3P**). Lastly, aged *Pdcd1*$^{-/-}$ mice accumulated more $CD44^-$ $CD62L^-$, $CD44^-$ $CD62L^+$, and $CD44^+$ $CD62L^-$ $CD8^+$ T lymphocytes at baseline (**Fig 4-3Q**).

Overall, these results indicate that the absence of PD-1 in aged mice has a specific effect on improving granzyme B production in $CD8^+$ T cells during HMPV infection, but no discernable clinical effect on the outcome of viral infection.

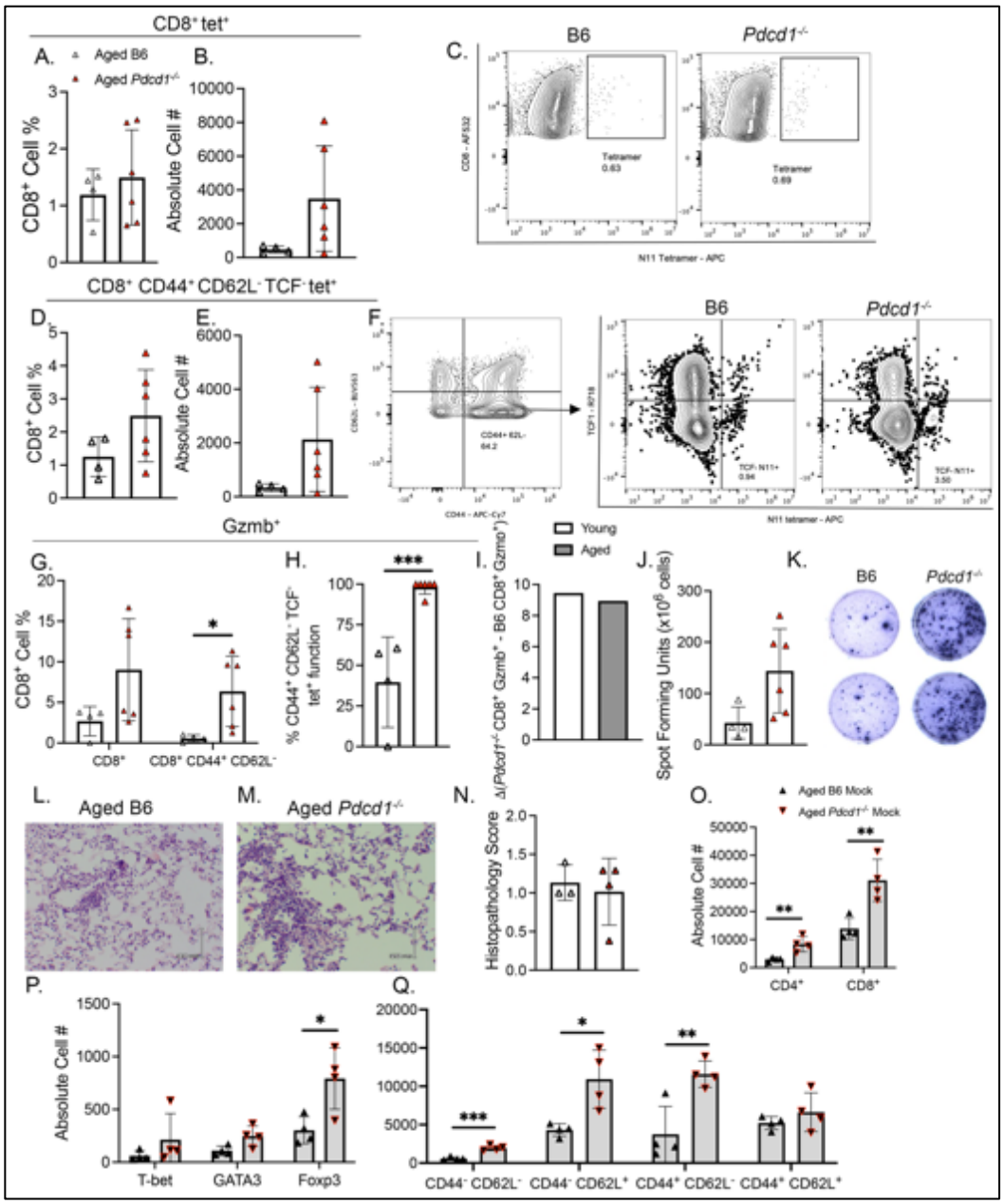

Figure 4-3. Aged *Pdcd1*$^{-/-}$ mice have improved CD8^{+} T cell granzyme B production during HMPV infection.

(A-B) Cell percent (LEFT) and absolute cell number (RIGHT) of lung CD8^{+} tet^{+} T cells in B6 and *Pdcd1*$^{-/-}$ mice at day 7 p.i. **(C)** Representative flow plots of tetramer staining. **(D-E)** Cell percent (LEFT) and absolute cell number (RIGHT) of lung CD8^{+} CD44^{+} CD62L^{-} TCF^{-} tet^{+} cells in aged B6 and *Pdcd1*$^{-/-}$ mice at day 7 p.i. **(F)** Representative flow plots of TCF^{-} tetramer staining. (G) Granzyme B^{+} bulk CD8^{+} and CD44^{+} CD62L^{-} CD8^{+} T cells. **(H)** Percent function of granzyme B^{+} CD44^{+} CD62L^{-} TCF^{-} tet^{+} lung CD8^{+} T cells. **(I)** Delta change of *Pdcd1*$^{-/-}$ CD8^{+} Gzmb^{+} T cells minus B6 CD8^{+} Gzmb^{+} T cells in young and aged HMPV infected mice at day 7 p.i. **(J)** ELISpot *ex vivo* peptide

stimulation IFNγ production from B6 or *Pdcd1*$^{-/-}$ lung lymphocytes. **(K)** Representative ELISpot well images. **(L-M)** H&E images of aged B6 and *Pdcd1*$^{-/-}$ lungs on day 7 p.i. **(N)** Histopathology score from both groups of mice. **(O)** Absolute cell number of CD4^{+} and CD8^{+} T lymphocytes, **(P)** T-bet, GATA3, Foxp3^{+} CD4^{+} T lymphocytes, and **(Q)** CD44, CD62L expression on CD8^{+} T lymphocytes in aged B6 of *Pdcd1*$^{-/-}$ mock infected mice. Absolute cell number calculation by BiolegendPrecision Counting Beads. The histopathology score: average score per section field by a group-blinded experienced lung pathologist. 0 = no inflammation. 1 = <25% inflammation, 2 = 25-50% inflammation, 3 = 50-75% inflammation, and 4 = >75% inflammation. *P<0.05, ***P<0.001; upaired t-test or one-way ANOVA. Each data point represents one individual mouse. Data (A-K) represent two experimental replicates, 2-3 mice/group. Data (L-M) represent one experimental replicate 3-4 mice/group.

4.4.4 Aged *Pdcd1*$^{-/-}$ influenza-infected mice also exhibited improved CD8^{+} T cell granzyme B production

To test whether these findings were generalizable to other respiratory viruses, aged B6 or *Pdcd1*$^{-/-}$ mice were infected with influenza strain PR8 and euthanized on day seven post-infection to assess the CD8^{+} T cell response. There was no significant difference in weight loss between the two groups (**Fig 4A**). We again observed no difference in bulk CD8^{+} tet^{+} cell frequency or absolute cell number (**Fig 4B-C**). There was also no difference in CD44^{+} CD62L^{-} Tcf1^{-} tet^{+} T cells in *Pdcd1*$^{-/-}$ mice (**Fig 4D-E**). Similar to aged *Pdcd1*$^{-/-}$ HMPV-infected mice, aged *Pdcd1*$^{-/-}$ CD8^{+} T cells had significantly improved granzyme B production during PR8 influenza infection (**Fig 4F-G**) with no significant difference in IFNγ production (**Fig 4J-K**). Comparing granzyme B production (**Fig 4H**) between *Pdcd1*$^{-/-}$ and WT CD8^{+} T cells revealed that aged *Pdcd1*$^{-/-}$ CD8^{+} T cells had a robust increase in granzyme B function, surpassing even that of young *Pdcd1*$^{-/-}$ CD8^{+} T cells (**Fig 4I**). In addition, there was no difference in influenza titer in the lung between the two groups (**Fig 4L**). These findings suggest that the absence of PD-1 in aged mice selectively improves CD8^{+} T

granzyme B production, but not other measures of CTL function, similar to or exceeding that of young mice, against multiple respiratory viruses.

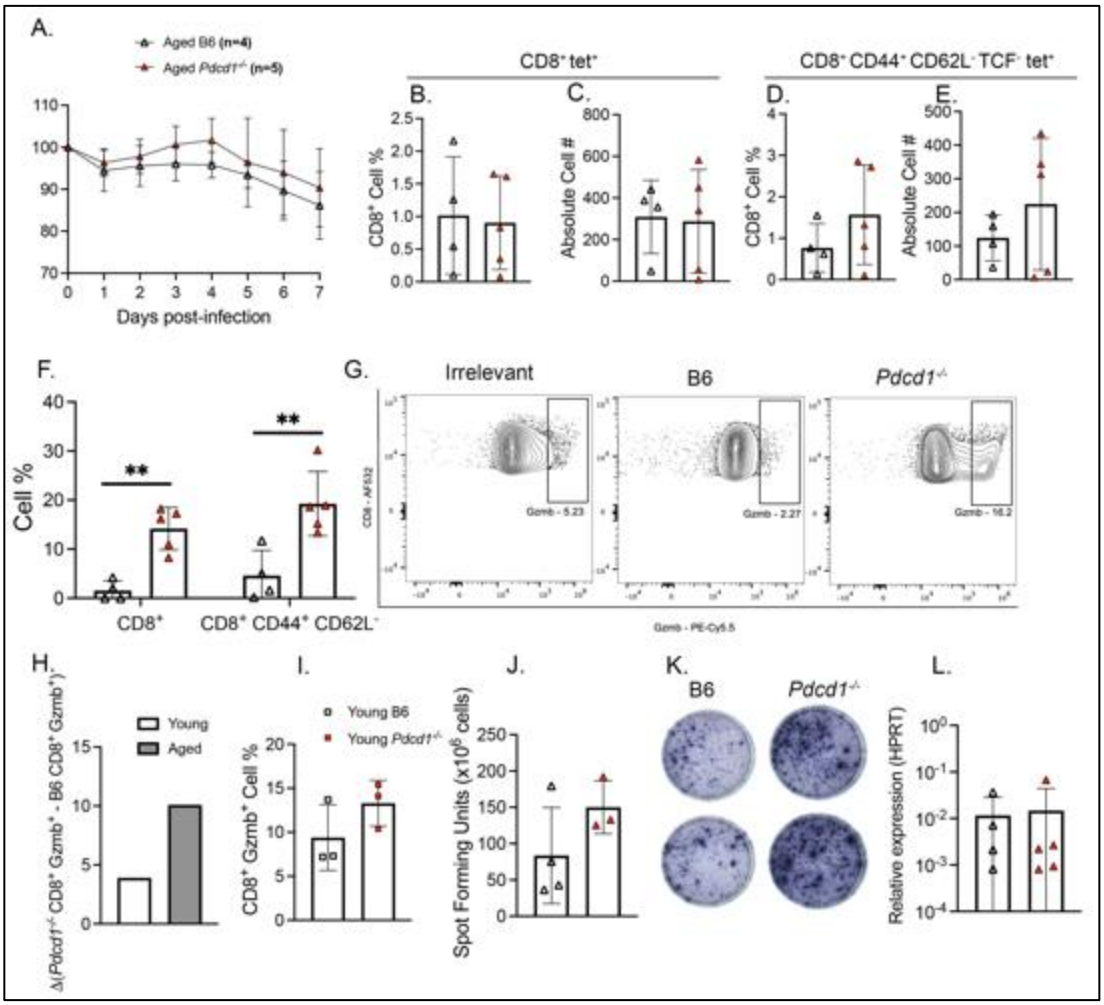

Figure 4-4. Aged *Pdcd1*$^{-/-}$ influenza-infected mice also exhibited improved CD8$^+$ T cell granzyme B production.

(A) Weight loss of aged B6 and *Pdcd1*$^{-/-}$ mice during influenza PR8 infection. **(B-C)** Bulk lung CD8$^+$ tet$^+$ cell percent and absolute cell number. **(D-E)** Terminally differentiated lung CD8$^+$ CD44$^+$ CD62L$^-$ TCF$^-$ tet$^+$ cell percent and absolute cell number. **(F)** Bulk lung CD8$^+$ T cell and CD8$^+$ CD44$^+$ CD62L$^-$ granzyme B production. **(G)** Representative flow plots of granzyme B staining. **(H)** Delta change of *Pdcd1*$^{-/-}$ CD8$^+$ Gzmb$^+$ T cells minus B6 CD8$^+$ Gzmb$^+$ in lungs of young and aged PR8 infected mice. **(I)** Lung CD8$^+$ granzyme B$^+$ cell percent in young B6 or *Pdcd1*$^{-/-}$ mice. **(J)** Spot forming units from IFNγ ELISpot *ex vivo* Class I peptide stimulation from aged B6 and *Pdcd1*$^{-/-}$ lung lymphocytes. **(K)** Representative images of wells from IFNγ ELISpot. **(L)** qRT-PCR relative expression to

housekeeping gene (HPRT) or Influenza A transcripts in lung homogenate. Absolute cell number calculation by Biolegend Precision Counting Beads. **P<0.05; ***P<0.001. unpaired t-test or two-way ANOVA. Each data point represents one individual mouse. Data (A-G; I) represent two experimental replicates, 2-3 mice/group. Data in H represents one experimental replicate 3 mice per group. Data in (J-L) represent one experimental replicate 3-4 mice/group.

4.4.5 Aged *Pdcd1*$^{-/-}$ CD8^{+} T cells transplanted into young mice had increased granzyme B production

To test whether increased CD8^{+} T cell granzyme B production in the absence of PD-1 was cell-intrinsic, young or aged WT or *Pdcd1*$^{-/-}$ T cells were transplanted into lethally irradiated young CD45.1 mice along with young CD45.1 B cells and *Rag1*$^{-/-}$ BM to reconstitute the myeloid compartment (**Fig 4-5A**). Six weeks post-transplant, recipient mice were infected with HMPV and euthanized at day seven p.i. We confirmed the identity of transplanted T cells by assessing PD-1 expression on CD45.2^{+} CD8^{+} T cells (**Appendix Fig 16A**). There was no difference in weight loss or viral burden between the four groups (**Appendix Fig 16B-C**). We also assessed engraftment of recipient (CD45.1) and donor (CD45.2) total CD3^{+} lymphocytes, CD4^{+}, and CD8^{+} T cells (**Appendix Fig 16D**). *Pdcd1*$^{-/-}$ lymphocytes engrafted better compared to B6 lymphocytes (**Appendix Fig 16D-G**) especially in bulk CD3^{+} (**Appendix Fig 16E**) and CD8^{+} T lymphocytes (**Appendix Fig 16G**), as previously observed (62).

There were no significant differences in the absolute number or percentage of CD8^{+} CD44^{+} CD62L^{-} Tcf1^{-} tet^{+} cells between mice that received aged WT or aged *Pdcd1*$^{-/-}$ T cells, with aged *Pdcd1*$^{-/-}$ T cells producing more Tcf1^{-} tet^{+} CD8^{+} T cells (**Fig 4-5B-C**). However, there was a significant increase in stem-cell like CD8^{+} T-bet^{low} TCF^{+} T cells previously described in (215) in

aged *Pdcd1*$^{-/-}$ compared to aged B6 mice, which could indicate a shift in the bulk CD8$^+$ T cell repertoire toward more stem-cell like CD8$^+$ T cells (**Fig 4-5D**). Most notably, there was a significant increase in granzyme B production (**Fig. 4-5E; 5I**) and a marker of degranulation (CD107a$^+$) (**Fig 4-5F**), with a trend toward increased IFNγ production (**Fig 4-5G**), in aged *Pdcd1*$^{-/-}$ CD8$^+$ T cells compared with aged WT CD8$^+$ T cells transplanted into young recipients. In addition, we assessed if the absence of PD-1 improved the function of aged CD8$^+$ T cells relative to young CD8$^+$ T cells. Aged *Pdcd1*$^{-/-}$ CD8$^+$ T cells exhibited improved function by all three measures to a similar extent as young *Pdcd1*$^{-/-}$ cells, when comparing to age-matched B6 CD8$^+$ T cells (**Fig 4-5H**).

To remove irradiation as a confounding variable, we performed adoptive transfer of young or aged *Pdcd1*$^{-/-}$ CD8$^+$ T cells into young *Rag1*$^{-/-}$ recipients along with young WT CD4$^+$ T cells and B cells (**Appendix Fig 17A**). When we compared the function of young and aged *Pdcd1*$^{-/-}$ CD8$^+$ T cells in this model, we observed that young *Pdcd1*$^{-/-}$ CD8$^+$ T cells were still more functional in granzyme B and IFNγ production compared to aged *Pdcd1*$^{-/-}$ CD8$^+$ T cells (**Appendix Fig 17B-D**).

Taken together, these data indicate that the absence of PD-1 improves engraftment of not just CD8$^+$ T cells but CD4$^+$ T cells as well. We hypothesize that the increased granzyme B production in aged *Pdcd1*$^{-/-}$ CD8$^+$ T cells may be a result of a cell-intrinsic effect caused by the absence of PD-1 signaling or simply a difference in the homeostatic expansion based on the improved engraftment ability of *Pdcd1*$^{-/-}$ lymphocytes.

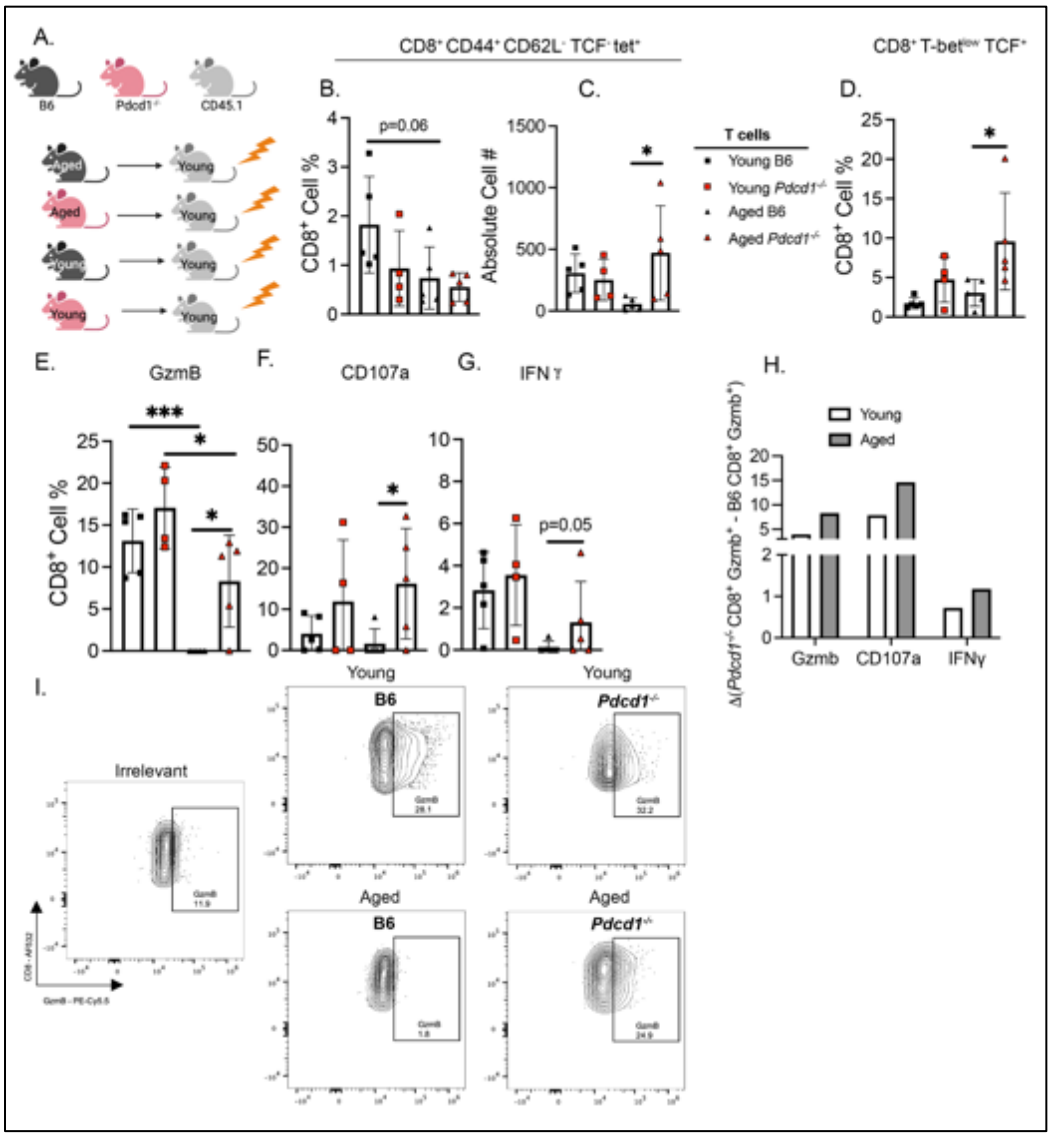

Figure 4-5. Aged *Pdcd1*$^{-/-}$ CD8^{+} T cells transplanted into young mice had increased granzyme B production.

(A) Experimental schematic - aged or young B6 or *Pdcd1*$^{-/-}$ T cells, young B6 CD19^{+} B cells, and young *Rag1*$^{-/-}$ BM were transplanted into lethally irradiated CD45.1 young recipients. 6 wks post-transplant, mice were infected with HMPV and CD8^{+} T cell response assessed on day 7 p.i. **(B-C)** TCF^{-} tet^{+} lung CD8^{+} cell percent and absolute cell number in all four groups. **(D)** Cell percent of stem-cell like T-bet^{low} TCF^{+} lung CD8^{+} T cells. **(E-G)** lung CD8^{+} T cells positive for granzyme B, CD107a, and IFNγ, respectively. **(H)** Delta change of donor *Pdcd1*$^{-/-}$ CD8^{+} Gzmb^{+} T cells minus B6 CD8^{+} Gzmb^{+} T cells in young HMPV-infected recipient. **(I)** Representative flow plots of granzyme B staining. *P<0.05; ***P<0.001; one-way ANOVA. Each data point represents one individual mouse. Data represent one experimental replicate, 4-5 mice/group.

4.4.6 Aged *Pdcd1*$^{-/-}$ had fewer resident memory T cells 40 days p.i.

Since nearly all children are seropositive for HMPV by five years of age, adult infections are considered to represent reinfections (1). While adult serum antibody titer affects susceptibility to HMPV reinfection and disease (193), little is known about T cell memory and adult HMPV reinfection. Thus, we tested how PD-1 signaling affected CD8$^+$ T cell memory formation in young and aged mice. At day 40 p.i., aged or young B6 or *Pdcd1*$^{-/-}$ mice were injected with CD45.2 antibody to label blood (CD45$^+$) vs. tissue (CD45$^-$) cells and then immediately euthanized (**Fig 4-6A**). Young WT and *Pdcd1*$^{-/-}$ mice were included in this study to assess whether any differences we observed in the aged *Pdcd1*$^{-/-}$ was due to the absence of PD-1 signaling irrespective of age. As shown previously (214), aged B6 mice accumulated significantly more CD8$^+$ CD45.2$^-$ T cells in the lungs compared to young B6 mice (**Fig 4-6B-C**). However, aged *Pdcd1*$^{-/-}$ mice had significantly fewer lung CD8$^+$ CD45.2$^-$ T cells than aged WT B6 (**Fig 4-6B-C**). This decrease in CD8$^+$ CD45.2$^-$ T cells was specific to aged mice as this difference was not observed in young mice (**Fig 4-6B-C**). In addition, aged *Pdcd1*$^{-/-}$ mice also had significantly fewer CD8$^+$ CD45.2$^-$ CD44$^+$ CD62L$^-$ CD69$^+$ CD103$^+$ tissue-resident memory T cells in the lung (**Fig 4-6D-F**) compared to aged WT mice, by both percentage (**Fig 4-6E**) and absolute number (**Fig 4-6F**). There was no significant difference in CD8$^+$ CD45.2$^-$ CD44$^+$ CD62L$^-$ CD69$^+$ CD103$^+$ tissue-resident memory T cell production in young mice of either genotype (**Fig 4-6E-F**), indicating that this difference in CD8$^+$ T cell memory formation was specific to aged mice. Aged *Pdcd1*$^{-/-}$ mice also had fewer HMPV-specific CD8$^+$ CD45.2$^+$ N11 tet$^+$ and CD44$^+$ CD62L$^-$ CD69$^+$ CD103$^+$ N11 tet$^+$ T cells in the lung than aged WT mice (**Fig 4-6G-H**). Lastly, there was minimal IFNγ production in young WT and *Pdcd1*$^{-/-}$ mice at day 40 p.i. (**Fig 4-6I-J**). However, there was robust IFNγ production from aged WT T cells, as previously shown (214), which was significantly diminished in *Pdcd1*$^{-/-}$ aged mice

(**Fig 4-6I-J**). These findings suggest that there is an age-associated, PD-1 dependent, increase in lung tissue resident memory CD8$^+$ T cells.

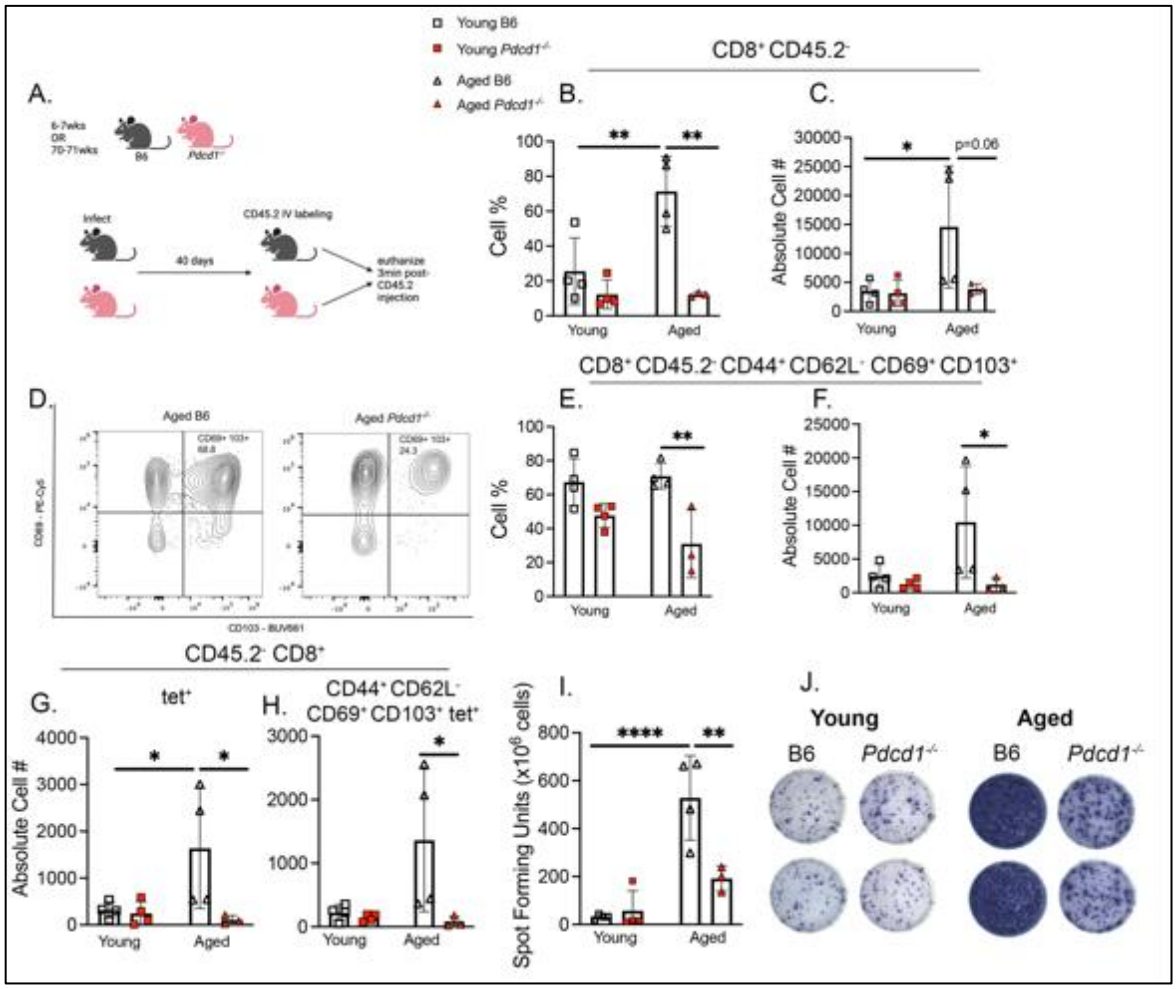

Figure 4-6. Aged *Pdcd1*$^{-/-}$ mice had fewer resident memory T cells 40 days p.i

(A) Experimental schematic. **(B-C)** CD8$^+$ CD45.2$^-$ cell percent and absolute cell number in lungs of young and aged B6 and *Pdcd1*$^{-/-}$ mice. **(D)** Representative flow plots of CD69 and CD103 staining. **(E-F)** Cell percent and absolute cell number of CD8$^+$ CD45.2$^-$ CD44$^+$ CD62L$^-$ CD69$^+$ CD103$^+$ in all four groups. **(G-H)** Absolute cell number of bulk lung CD45.2$^-$ CD8$^+$ tet$^+$ and memory CD44$^+$ CD62L$^-$ CD69$^+$ CD103$^+$ T cells in all four groups. **(I)** Spot forming units from IFNγ ELISpot *ex vivo* Class I peptide stimulation from lung lymphocytes. **(J)** Representative images from IFNγ ELISpot wells. Absolute cell number calculated using BioLegend Precision Counting Beards. *P<0.05; **P<0.01; ****P<0.0001, one-way ANOVA. Each data point represents one individual mouse. Data represent one experimental replicate 3-4 mice/group.

4.4.7 PD-1 blockade improves weight loss during reinfection of aged mice

To model reinfection of aged adults, B6 mice were infected with HMPV at 6-7 weeks of age, aged in house, and re-challenged fourteen months p.i. (214). Two days prior to re-challenge, and on days 1, 2, and 5 following re-challenge, aged mice were treated with either PD-1 blocking antibody or isotype control (**Fig 4-7A**). PD-1 blockade prevented weight loss in re-challenged aged mice compared with isotype treated controls (**Fig 4-7B**), but both groups had no detectable viral titer by day seven post re-challenge (**Appendix Fig 17E**). Viral replication may have been limited in this re-challenge by anti-HMPV antibody responses in all groups (**Appendix Fig 17F**). Aged αPD-1 mice produced fewer terminally differentiated Tcf1$^-$ tet$^+$ CD8$^+$ T cells (**Fig 4-7C**), bulk CD45.2$^-$ CD69$^+$ CD103$^+$ (T_{RM}) CD8$^+$ T cells (**Fig 4-7D**), and tetramer specific CD45.2$^-$ T_{RM}s (**Fig 4-7E**). Representative flow plots of T_{RM} gating are shown in **Fig 4-7F**. Despite this decrease in production of T_{RM}, in aged mice, PD-1 blockade slightly increased bulk IFNγ CD8$^+$ T cell function (**Fig 4-7G; 7J**) and IFNγ production in CD44$^+$ CD62L$^-$ CD8$^+$ T cells (**Fig 4-7H**). In addition, the percentage of IFNγ-producing T_{RM} also tended to increase with PD-1 blockade (**Fig 4-7I**). Overall, these data suggest that PD-1 blockade does impact CD8$^+$ T_{RM} memory T cell production and weight loss in aged mice after re-challenge.

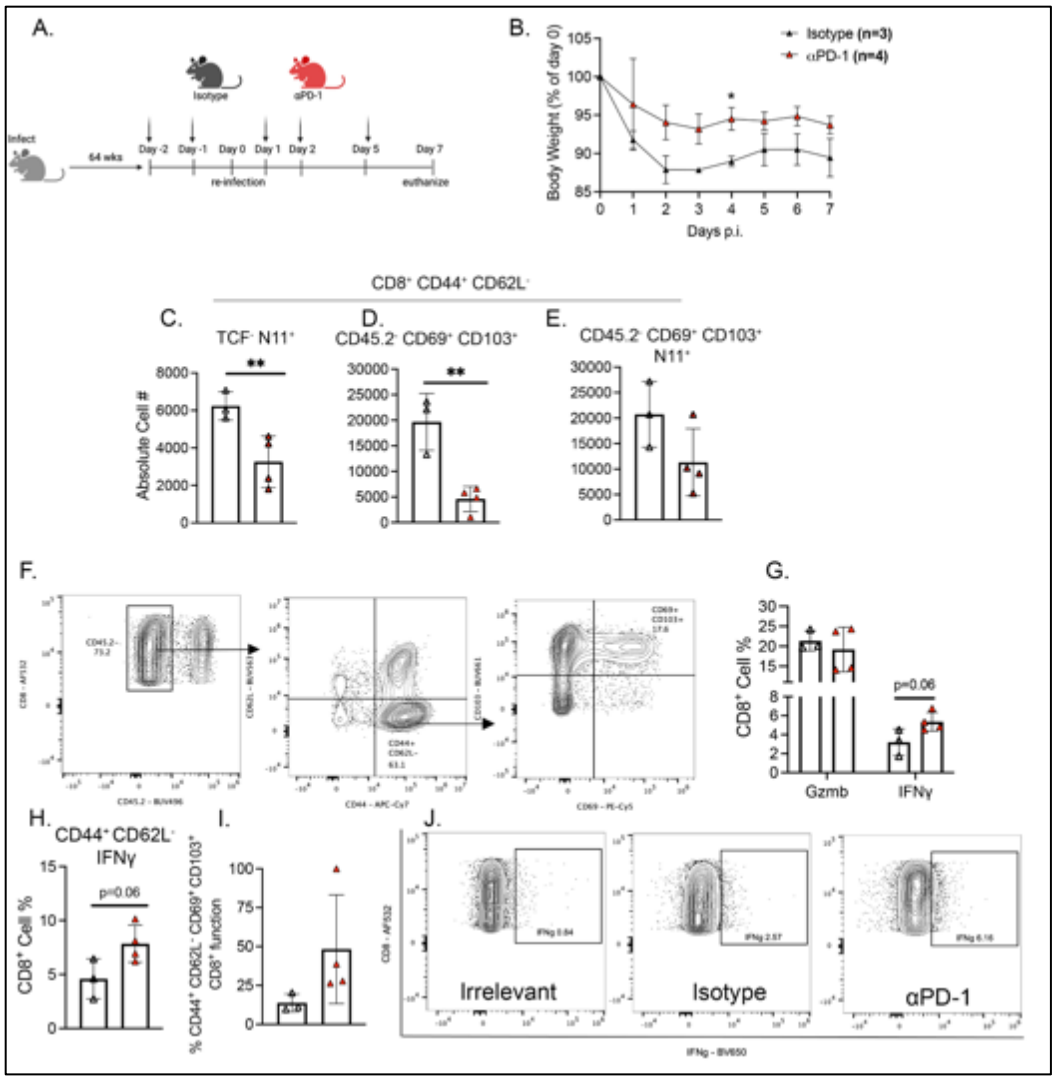

Figure 4-7. PD-1 blockade improves weight loss and memory CD8$^+$ T cell function during reinfection of aged mice.

(A) Experimental schematic. **(B)** Weight loss post re-challenge. **(C-E)** Absolute cell number of lung CD8$^+$ CD44$^+$ CD62L$^-$ **(F)** Representative flow plots of CD69 and CD103 staining. **(G)** Percentage of lung CD8$^+$ Gzmb$^+$ and IFNγ^+ cells in both groups. **(H)** Percentage of CD8$^+$ CD44$^+$ CD62L$^-$ IFNγ^+ cells in lung. **(I)** Percentage of memory CD8$^+$ T cells expresisng IFNγ in lung. **(J)** Representative flow plots of IFNγ staining. Absolue cell number calculation by BioLegend Precision Counting Beads *P<0.05; **P<0.01; unpaired t-test or two-way ANOVA. Each data point represents one individual mouse. Data represent one experimental replication with 3-4 mice/group.

4.5 Discussion

In this study, we investigated the role of PD-1 signaling in an aged mouse HMPV model. We found: (1) PD-1 expression was increased on aged $CD8^+$ T cells; (2) PD-1 signaling significantly impaired granzyme B production of aged $CD8^+$ T cells against two respiratory viruses; (3) this improved function was primarily cell-intrinsic or due to homeostatic differences in *Pdcd1*$^{-/-}$ $CD8^+$ T cells, as aged B6 $CD8^+$ T cells failed to improve cytokine production when transplanted into young hosts; and (4) removal of PD-1 signaling resulted in accumulation of fewer cytotoxic $CD8^+$ T_{RM} in aged mice.

Consistent with our data, we found that PD-1 was upregulated in aged mice in publicly available scRNAseq datasets (150). Our data in mock-infected aged mice corroborated these findings and further showed that PD-1 expression persisted on aged $CD8^+$ T cells during HMPV infection despite transfer into a young host. In a mixed bone marrow chimera transplant model, we observed this same phenomenon during HMPV infection. However, there was no difference in PD-1 expression on young or aged $CD8^+$ T cells in aged hosts in the bulk T cell syngeneic transplant model. Aging is multifactorial and the aged microenvironment and well-known inflammaging hypothesis (117, 130) as well as epigenetic changes in aged $CD4^+$ T cells (153) could be possible explanations for these findings. For example, there is known to be an accumulation of inflammatory monocytes in aged mice (221, 222), which could propagate an inflammaging phenotype. Our own scRNAseq analysis of whole lung cells from young and aged HMPV-infected mice corroborate published data (221, 222), identifying a unique inflammatory monocyte population present in uninfected aged mice that significantly expands following HMPV infection (unpublished data). We hypothesize that these age-related changes in other immune cells

significantly impacts PD-1 expression on $CD8^+$ T cells in the aged host, which could explain the findings in **Fig. 1**. Future investigations will elucidate the contribution of the aged microenvironment and somatic cells on $CD8^+$ T cell function and epigenetic changes associated with increased age.

PD-1 blockade did not affect the population of T_{EX} $CD8^+$ T cells that expressed TOX and EOMES, which are markers of terminal exhaustion (150, 153). This suggests that PD-1 signaling does not propagate or affect the expression of these markers in aged $CD8^+$ T cells. This finding is consistent with reports that $CD8^+$ T cell exhaustion can occur in the genetic absence of PD-1 (223); in that context, PD-1 signaling promoted excessive expansion and differentiation of cytotoxic $CD8^+$ T cells (223) leading to more exhausted $CD8^+$ T cells. In our model, *Pdcd1*$^{-/-}$ aged mice tended to accumulate terminally differentiated $CD8^+$ tet^+ T cells. Importantly, at baseline aged *Pdcd1*$^{-/-}$ mice did have increased bulk $CD4^+$ and $CD8^+$ T lymphocytes with an increase in $CD4^+$ $Foxp3^+$ T lymphocytes and an increase in naïve ($CD44^-$ $CD62L^+$) and effector ($CD44^+$ $CD62L^-$) $CD8^+$ T lymphocytes. This does indicate that there are baseline differences between B6 and *Pdcd1*$^{-/-}$ aged mice which could contribute to how aged *Pdcd1*$^{-/-}$ respond to HMPV infection.

In addition, the absence of PD-1 signaling did not have an impact on the clinical outcome in aged mice (i.e. weight loss and viral titer). We hypothesize that this is due to the multifactorial nature of the immune response to HMPV, especially in the aged host. We have previously shown that $CD8^+$ T cells are not the only cell type responsible for viral clearance since $CD8^+$ depletion in either aged or young mice had minimal effect on weight loss or viral clearance during HMPV infection (213). Another study on HMPV infection also supports these findings, indicating the dual role of

both CD4+ and CD8+ T cells in affecting the clinical outcome in mice infected with respiratory viruses (51).

Notably, the absence of PD-1 signaling had a predominant effect on $CD8^+$ T cell granzyme B production. It is well known that PD-1 blockade has a profound effect on activation of $CD8^+$ effector T cells during acute viral infection (224). In the current study in both HMPV and influenza infection, aged *Pdcd1*$^{-/-}$ $CD8^+$ T cells exhibited increased granzyme B production, which was recapitulated in the transplant experiments. However, the impaired granzyme B production still present in the adoptive transfer of aged *Pdcd1*$^{-/-}$$CD8^+$ T cells compared to young *Pdcd1*$^{-/-}$ $CD8^+$ T cells indicates that aged $CD8^+$ T cells have other age-related cell intrinsic deficits that inhibit $CD8^+$ antiviral T cell function (213). These findings also suggest that aged $CD8^+$ T cells may require help from $CD4^+$ T cells and B cells that are unrestrained by PD-1 signaling. Furthermore, blockade of other inhibitory receptors including Tim-3 failed to improve $CD8^+$ T cell function during HMPV infection to the same degree as PD-1 blockade (62). LAG-3 blockade has been shown to enhance $CD8^+$ T cell function against HMPV, but it also enhanced lung pathology, indicating that LAG-3 may play a role in limiting lung damage during infection (62).

Importantly, antibody blockade and PD1-deficient mouse approaches globally block or remove PD-1 signaling from all cells. Thus, we cannot fully exclude the effect of other cells. PD-1 is known to play an important role in the function of $CD4^+$ T lymphocytes, especially $Foxp3^+$ $CD4^+$ regulatory T cells (Tregs) (225, 226). We saw some differences at baseline in expression of $CD4^+$ T cell transcription factors with increased absolute numbers of *Foxp3*$^+$ $CD4^+$ T cells. This indicates that, at least at the transcriptional level, removal of PD-1 signaling does have an effect on $CD4^+$ T

cell differentiation, which could contribute to our findings in this study. We previously showed that Tregs play an integral role early during HMPV infection (63). However, we focused the current studies on the effects of PD-1 on $CD8^+$ T cells for a number of reasons, including: the preferential increase in PD-1 expression on aged $CD8^+$ T cells but not $CD4^+$ T cells; the central role of $CD8^+$ T cells in controlling HMPV (46, 52, 61, 62); and cell-intrinsic, age-associated, $CD8^+$ T cell functional impairment (213).

Aged *Pdcd1*$^{-/-}$ $CD8^+$ T cells had improved granzyme B production compared to aged WT $CD8^+$ T cells even when transplanted into a young host. We previously showed in a transplant model that aged WT $CD8^+$ T cells exhibited cell-intrinsic impairment of granzyme B production that was not restored by a young microenvironment (213). In this study, we further show that in the absence of PD-1, aged *Pdcd1*$^{-/-}$ $CD8^+$ T cells have a cell-intrinsic increase in granzyme B production. The significant increase in engraftment of *Pdcd1*$^{-/-}$ lymphocytes was also observed in a prior mixed BM chimera model (62). Others have found that the absence of PD-1 can cause an increase in activation and proliferation of T lymphocytes (220, 223), which could provide one explanation for this finding. We report the absolute cell numbers for these transplant results to try and account for the differences in engraftment. However, considering these findings, we cannot rule out the possibility that the improved granzyme B production in aged *Pdcd1*$^{-/-}$ $CD8^+$ T cells could be due to homeostatic or cell-intrinsic differences. Future studies can analyze this further investigating proliferation capacity and metabolism potential of *Pdcd1*$^{-/-}$ $CD8^+$ T cells. This increase in engraftment, coupled with the increase in activation and terminal differentiation of *Pdcd1*$^{-/-}$ $CD8^+$ T cells, suggest possible avenues for PD-1 blockade therapy to be used in conjunction with CAR-

T cells. Furthermore, studies have found a synergistic effect in mice against tumors when CAR-T cells are genetically modified to express PD-1 blocking antibodies (227, 228).

It is not fully clear why older adults are more likely to experience severe respiratory disease upon HMPV re-infection. HMPV and RSV re-infections in aged humans and mice occur despite the presence of neutralizing antibodies (94, 193, 194). Importantly, mice are semi-permissive hosts for HMPV, and thus are a limited model for re-infection. These findings together could explain why aged mice had undetectable viral titer at day seven after re-challenge. Our previous studies suggest that aged $CD8^+$ T cell dysfunction contributes to severe HMPV disease in older individuals (213, 214). We and others have also previously found that $CD8^+$ T_{RM} accumulate in aged mice and can contribute to increased disease severity and lung pathogenesis in HMPV (214) and influenza (189). This $CD8^+$ T_{RM} accumulation was impaired in aged *Pdcd1*$^{-/-}$ mice, which leads to the hypothesis that PD-1 signaling may be impacting the formation and accumulation of this $CD8^+$ memory T cell population in the aged host. PD-1 signaling is required for optimal $CD8^+$ memory T cell formation (220, 229). These studies reported that the timing of PD-1 blockade was important to optimize effector $CD8^+$ T cell function without severely limiting memory formation (220, 224). Further supporting this, one study found that PD-1 signaling serves as a mediator to limit $CD8^+$ T_{RM} activity in the lung during influenza infection, which helped prevent lung fibrosis (230). Since $CD8^+$ T cells develop age-associated functional impairment and accumulate cytotoxic memory cells that contribute to severe disease in older adults infected with respiratory viruses (155, 157, 170), this opens up the possibility of using αPD-1 therapy in elderly individuals during a window of time shortly after they are infected with a respiratory virus.

Mice receiving PD-1 blockade upon re-challenge fourteen months after primary infection were clinically better (i.e. less weight loss), had fewer $CD8^+$ T_{RM}, but with borderline more function. We suspect that PD-1 blockade performed on mice aged in-house fourteen months after primary infection was only semi-effective because the cytotoxic $CD8^+$ T_{RM} population may have already formed. Therefore, PD-1 blockade two days prior to re-challenge and subsequent boosting post-re-challenge may not have been sufficient to affect the $CD8^+$ T_{RM} function to the same degree as other models in this study. *Pdcd1*$^{-/-}$ mice have never expressed PD-1, which may have profound effects on $CD8^+$ T_{RM} formation that are not observed when giving PD-1 blockade to WT aged mice. However, we are actively investigating the mechanism behind PD-1 blockade in fourteen month re-challenged mice. While $CD8^+$ T cells contribute to pathogenesis, other immune cells may have been affected by PD-1 blockade, leading to diminished inflammation and thus reduced weight loss. Future experiments and conditional knockout mice are needed to define the role of PD-1 on select immune cell subsets.

In summary, in this study we identified preferentially increased PD-1 expression on aged $CD8^+$ T cells that persisted even when these cells were transplanted into young hosts. We also show that removal of PD-1 signaling has a positive effect on granzyme B production by aged $CD8^+$ T cells during multiple types of respiratory viral infection. We further demonstrated that *Pdcd1*$^{-/-}$ aged mice did not develop a cytotoxic $CD8^+$ T_{RM} population in the lung 40 days p.i. These results indicate a temporal role of PD-1 signaling in both the initial antiviral response to improve granzyme B production, as well as during the resolution phase of infection when the memory $CD8^+$ T cell compartment is formed. Lastly, using an aged re-challenge model we show that aged mice receiving PD-1 blockade lost less weight and produced fewer $CD8^+$ T_{RM}. These findings can

inform future studies interrogating the therapeutic potential of PD-1 blockade in aged humans infected with respiratory viruses.

4.6 Acknowledgements

We thank the University of Pittsburgh Unified Flow Core for help with flow cytometry. We thank the NIH Tetramer Core Facility (contract number 75N93020D00005) for providing tetramers. We also thank Maxim Artyomov, PhD for the use of his publicly available scRNAseq dataset.

5.0 A Method for Staining Class I and II Tetramers

Olivia B. Parks*[1], Jie Lan*[1], Justin Tometich[1], Timothy Hand[1], John V. Williams[1,2,#]

[1]Department of Pediatrics, Division of Infectious Diseases, University of Pittsburgh School of Medicine, Pittsburgh, PA, USA

[2]Institute for Infection, Inflammation, and Immunity in Children (i4Kids), Pittsburgh, PA, USA

*denotes co-first authorship

 # Corresponding Author:

John V. Williams, MD

University of Pittsburgh

Rangos Research Building

4401 Penn Avenue

Pittsburgh, PA 15224

Phone: 412-692-8298

Email: jvw@chp.edu

Competing Interest Statement: JVW serves on the Scientific Advisory Board of Quidel and an Independent Data Monitoring Committee for GlaxoSmithKline, neither involved in the present work. All other authors declare no conflicts of interest.

Keywords: Respiratory viral infection, class I tetramer, class II tetramer, viral immunology

In preparation for publication in *Journal of Immunological Methods*

5.1 Introduction: $CD4^+$ and $CD8^+$ T cell coordinated response

The most important functions of an adaptive immune are to destroy invading pathogens and provide long-lasting antigen-specific protection. T cells and B cells are the main components of adaptive immunity. CD4 and CD8 T cells contribute to host defenses during acute and chronic infection with viruses, intracellular bacteria, and other pathogens.

One of the roles for $CD4^+$ T cells is helping $CD8^+$ T cell responses. Decades of studies have shown that $CD8^+$ T cell expansion depends on IL-2 secretion from $CD4^+$ T cells engage antigen presenting cells such as macrophages and dendritic cells (231-233). However, other studies have challenged this $CD4^-CD8$ T cell cooperation model, finding that $CD4^+$ T cells were dispensable for the clonal expansion of effector $CD8^+$ T cells during viral infection (234-239). Furthermore, studies using LCMV infection revealed that $CD4^+$ T cells primarily sustained, rather than initiated, $CD8^+$ effector responses (240-243). Thus, whether $CD4^+$ T cells are truly indispensable during the $CD8^+$ T cell effector response is likely context dependent.

Antigen presentation via major histocompatibility complex (MHC) proteins is essential for initiating the adaptive immune response. Peptide-MHC class I complexes presented on all nucleated cells can be recognized by $CD8^+$ T cells (244). In contrast, the presentation of peptides by MHC class II, which is mediated only by specialized antigen-presenting cells, activates $CD4^+$ T cells, leading to the coordination and regulation of $CD8^+$ T cells (245). Peptide-major histocompatibility complex (pMHC) multimers conjugated to fluorochromes make identification, enumeration, and phenotypic characterization of antigen-specific T cells much more approachable. Little is published on methods for staining epitope-specific $CD4^+$ and $CD8^+$ T cells together. To

address this gap in knowledge, we sought to establish a method to co-stain MHC-I and MHC-II tetramers (Class I and Class II tetramers, respectively) within the same panel. We referenced protocols previously published on optimal staining conditions for individual tetramers to determine the optimal Class I and Class II co-staining conditions. Additionally, we used two sets of Class I and Class II tetramers (HMPV and flu to establish a co-staining method that is generalizable across pathogens. We incorporated this co-staining method into a multispectral Aurora flow panel which provides a powerful method to comprehensively assess $CD4^+$ and $CD8^+$ lineage transcription factors, memory markers, and virus-specific T cell responses within the same sample?.

5.2 Materials & Methods

5.2.1 Mice and viral infection

C57BL/6 mice (catalog number: 000664) were purchased from The Jackson Laboratory. All animals were bred and maintained in specific pathogen-free conditions in accordance with the University of Pittsburgh Institutional Animal Care and Use Committee. Mice 6-7wk old of age were used in all experiments. HMPV (pathogenic clinical strain TN/94-49, genotype A2) was grown and titered in LLC-MK2 cells as previously described (160). Influenza virus strain A/34/PR/8 (PR8 H1N1) was obtained from ATCC, grown in MDCK cells, and titered on LLC-MK2 cells as previously described (46). For all experiments, mice were anesthetized with isoflurane and infected intratracheally with $2.0x10^6$ PFU HMPV or 500PFU PR8 H1N1 in 100 μL volume. All animals were handled according to protocols approved by the University of Pittsburgh IACUC.

5.2.2 Flow cytometry staining

Lung tissue was harvested, physically disrupted with scissors and incubated for one hour with collagenase and DNase at 37ºC. Following digestion, lung tissue was strained through a 70um strainer, treated with 2 mL ACK Lysis Buffer (Gibco A10492-01) for 1 minute, and resuspended in RPMI+10%FBS. Cells were counted on the hemacytometer and $2x10^6$ single cell suspension was used for flow cytometry staining. For tetramer staining, cells were incubated for 30mins at RT in 1:2000 100mg dasatinib in 1XPBS/1% FBS (FACS) and stained with 1:100 of MPV (APC conjugated 1.4mg/mL, BV421 conjugated 1.2mg/mL) or Flu tetramer as appropriate. MPV and Class I flu tetramers were generated at the NIH tetramer core. Class II flu tet was generated in house. Cells were incubated with Class I, II, at either room temperature (RT) or 37C for 90 min or 3 hrs depending on the conditions tested. A full list of the conditions tested is shown in **Table 3**.

Table 3. Class I and II tetramer co-staining conditions tested

Tetramer	Temperature	Incubation Time (min)
Class I	RT	90
Class II	37ºC	180
1. Class I 2. Class II	RT 37ºC	90 180
1. Class II 2. Class I	37ºC RT	180 90
Class I and II	37ºC	180

Cells were then washed twice in FACS buffer, stained with 1:1000 Live/Dead in PBS for 10min at RT, 1:100 anti-CD16/32 Fc block (Tonbo Biosciences Cat. #70-0161-M001) in FACS buffer

for 10 min at RT, 1:100 surface antibodies in BV Buffer (BD Cat. #566349) for 30min at 4ºC, and fixed for 20 min at 4ºC in 2% PFA. Cells were washed x2 with FACS after each staining step. After fixation, cells were resuspended in 200 μL FACS and run on either the Fortessa flow cytometer or Cytek® Aurora multispectral flow cytometer. For experiments staining for intracellular transcription factors, cells were incubated for 18hrs at 4ºC in eBioscience™ Foxp3/Transcription Factor Staining Buffer Set (ThermoFisher 00-5523-00), washed 2x in Foxp3 Fix/Perm Buffer, and then stained 1:50 in Foxp3 Fix/Perm Buffer/5% rat serum for 1 hr at 4ºC. A full list of antibodies used in all experiments is shown in **Tables 4-6**. Fluorescence minus one (FMO) controls were used for all inhibitory receptors and transcription factors. For MPV tetramer staining, Flu tetramer was used as the irrelevant control and vice versa for Flu tetramer staining. Any irrelevant tetramer background staining was subtracted from the final tetramer frequency. Unstained cells from each experiment were fixed for 20 min in 2% PFA and utilized on the flow cytometer to minimize autofluorescence. Data analysis was performed with Flowjo (v10.8.1).

Table 4. HMPV tetramer co-staining conditions flow cytometry panel

Marker	Fluorochrome	Host	Catalog	Clone
Live/Dead	Fixable Aqua	--	L34957	--
CD19	BV785	rat	115543	6D5
NK1.1	BV785	mouse	108749	PK136
CD3e	PE	hamster	553064	145-2C11
CD4	PE-Cy7	rat	552775	RM4-5
CD8a	AF700	rat	100730	53-6.7
HMPV M94 Class I	BV421	--	NA	--
HMPV N37 Class II	APC	--	NA	--

Table 5. Influenza tetramer co-staining conditions flow cytometry panel

Marker	Fluorochrome	Host	Catalog	Clone
Live/Dead	Fixable Aqua	--	L34957	--
CD19	BV421	rat	115538	6D5
NK1.1	BV421	mouse	562921	PK136
CD3e	FITC	hamster	100306	145-2C11
CD4	PE-Cy7	rat	552775	RM4-5
CD8a	AF700	rat	100730	53-6.7
Flu NP366 Class I	APC	--	NA	--
Flu NP311 Class II	PE	--	NA	--

Table 6. Aurora multispectral flow cytometry panel for tetramer co-staining

Marker	Fluorochrome	Host	Catalog	Clone
Live/Dead	Fixable Violet	--	L23105	--
CD19	BV421	rat	115538	6D5
CD3e	FITC	hamster	100306	145-2C11
CD4	BUV395	rat	740208	RM4-5
CD8a	AF700	rat	100730	53-6.7
CD44	APC-Cy7	rat	560568	IM7
CD69	BUV496	hamster	741063	H1.2F3
CD103	BUV661	rat	741504	M290
Foxp3	PerCP-Cy5.5	rat	45-4773-82	FJK-16s

T-bet	AF594	mouse	644834	4B10
GATA-3	BV711	mouse	565449	L50-823
Rorγt	AF647	mouse	562682	Q31-378
PD-1	PE-Cy7	rat	109110	RMP1-30
TIM-3	BV605	rat	119721	RMT3-23
LAG-3	BUV805	rat	748540	C9B7W
2B4	BUV737	rat	749155	C9.1
Flu NP366 Class I	APC	--	NA	--
Flu NP311 Class II	PE	--	NA	--

5.2.3 Statistical Analysis

Data analysis was performed using Prism version 9.0 (GraphPad Software). Comparisons between 2 groups were performed using an unpaired 2-tailed Student's *t* test or Mann-Whitney as appropriate. Multiple group comparisons were performed using a 1-way or 2-way ANOVA as appropriate. A *P* value less than 0.05 was considered significant. Error bars in each graph represent SEM.

5.2.4 Study Approval

All animals were maintained in accordance with *Guide for the Care and Use of Laboratory Animals* (NIH publication no. 85-23. Revised 1985) and were handled according to protocols approved by the University of Pittsburgh Subcommittee on Animal Care (IACUC).

5.2.5 Author Contributions

JL: conceived, designed, and performed experiments, acquired and analyzed data, and wrote manuscript. OBP: conceived, designed, and performed experiments, acquired and analyzed data, and wrote manuscript. JT: contributed analytic tools, revised manuscript. TH: contributed analytic tools, revised manuscript. JVW: conceived and designed experiments, interpreted data, and revised manuscript.

5.2.6 Acknowledgements

Supported by NIH AI085062 (JVW), F30HL159915 (OBP), T32 GM008208 (OBP), and the Henry L. Hillman Foundation (JVW). We thank the University of Pittsburgh Unified Flow Core for helping with flow cytometry. We thank the NIH Tetramer Core Facility (contract number 75N93020D00005) for providing tetramers. The authors have no additional financial interests.

5.3 Results

5.3.1 HMPV Class I & II tetramers can be stained together for 3 hrs at 37C.

To establish optimal Class I and II tetramer co-staining conditions, we developed four different staining conditions (**Table 3**). We used previously established incubations and temperature conditions for Class I (46, 52) and II tetramers (unpublished data). NP366 and NP311 influenza tetramers were used for irrelevant Class I and II tetramer staining, respectively (**Fig 5-1A**). A full

list of antibodies used in this experiment found in **Table 4**. There were no significant differences in background staining with NP366 at room temperature (RT) for 90min or 37°C for 3 hrs (**Fig 5-1A**). However, NP311 had significant background compared to the fluorescence minus one (FMO) control (**Fig 5-1A**). To establish baseline tetramer staining at the optimal conditions previously reported (46, 52), we tested Class I staining alone at RT for 90 min and Class II staining alone at 37°C for 3 hrs (**Fig 5-1B**). Class I and Class II staining was unchanged whether Class I was added before or after Class II (**Fig 5-1C & 5-1D**). Class I and II cell frequencies were similar to individual staining (**Fig 5-1B**) when both tetramers were stained together at 37°C for 3 hrs (**Fig 5-1E**). These results indicate that staining Class I and II tetramers together at 37°C for 3 hrs yields frequencies similar to staining Class I and Class II tetramer alone.

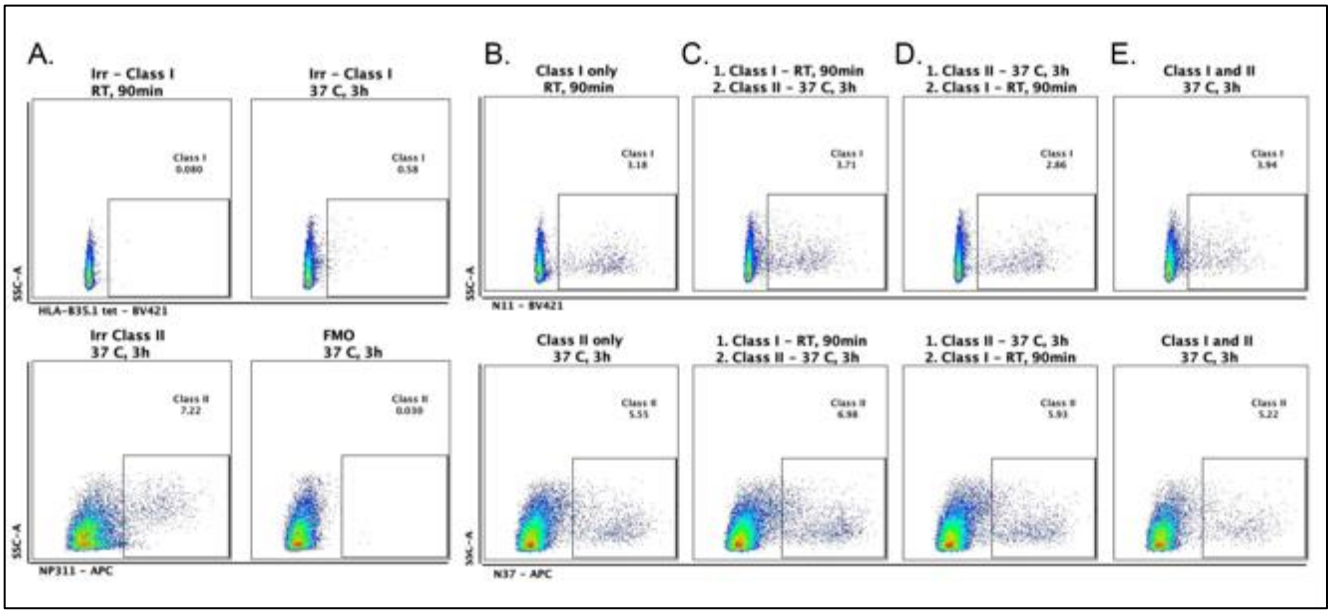

Figure 5-1. HMPV Class I & II tetramers can be stained together for 3hrs at 37C

Top panels show $CD8^+$ $tetramer^+$ T cells (Class I) while bottom panels show $CD4^+$ $tetramer^+$ (Class II) T cells. **(A)** Irrelevant Class I, Class II, and Class II FMO staining at RT for 90min or 37°C for 3hrs. **(B)** Class I and Class II only tetramer staining at RT for 90min for 3hrs, respectively. **(C)** Class I staining at RT for 90min following by a washing step, then Class II staining at 37°C for 3hrs. **(D)** Class II staining at 37°C for 3hrs, wash cells, then Class I staining at RT for 90min. **(E)** Class I and II tetramer staining together at 37°C for 3hrs.

5.3.2 Optimal tetramer co-staining conditions confirmed using influenza tetramers.

To confirm that these co-staining conditions were generalizable to other tetramers, we tested these conditions in influenza infected mice. In this experiment, NP366 and NP311 were used to identify flu-specific T cells. A full list of antibodies used in this experiment found in **Table 5**. Based on previous studies (246, 247), the condition for MHC-I tetramer NP366 binding on CD8 T cells was performed on 4°C for 30 minutes (**Appendix Fig 12**). To find the best staining condition for MHC-II tetramer NP311, we tested different staining conditions (248-252). We found the highest number of $NP311^+$ $CD8^+$ T cells with the lowest amount of background when staining at 37°C for 1h (**Appendix Fig 13**). There was minimal background staining using an irrelevant Class I tetramer at either 4°C for 30 min or 37°C for 1 hr (**Fig 5-2A**). Similarly, minimal background staining was found with Class II irrelevant staining or FMO staining at 37°C for 1 hr (**Fig 5-2A**). Class I tetramer frequency was slightly diminished when stained sequentially either before or after Class II (**Fig 5-2C-2D**). Class II staining remained unchanged with either condition (**Fig 5-2C-2D**). Class I and II tetramers were stained together at 37°C for 1 hr resulted in optimal tetramer frequencies (**Fig 5-2E**) most similar to Class I and II tetramer staining alone (**Fig 5-2A**). Taken together, these results suggest that MHC-I and MHC-II tetramer can be stained at the same time under the specific conditions required for MHC-II tetramer staining. This staining condition does not affect MHC-I tetramer staining.

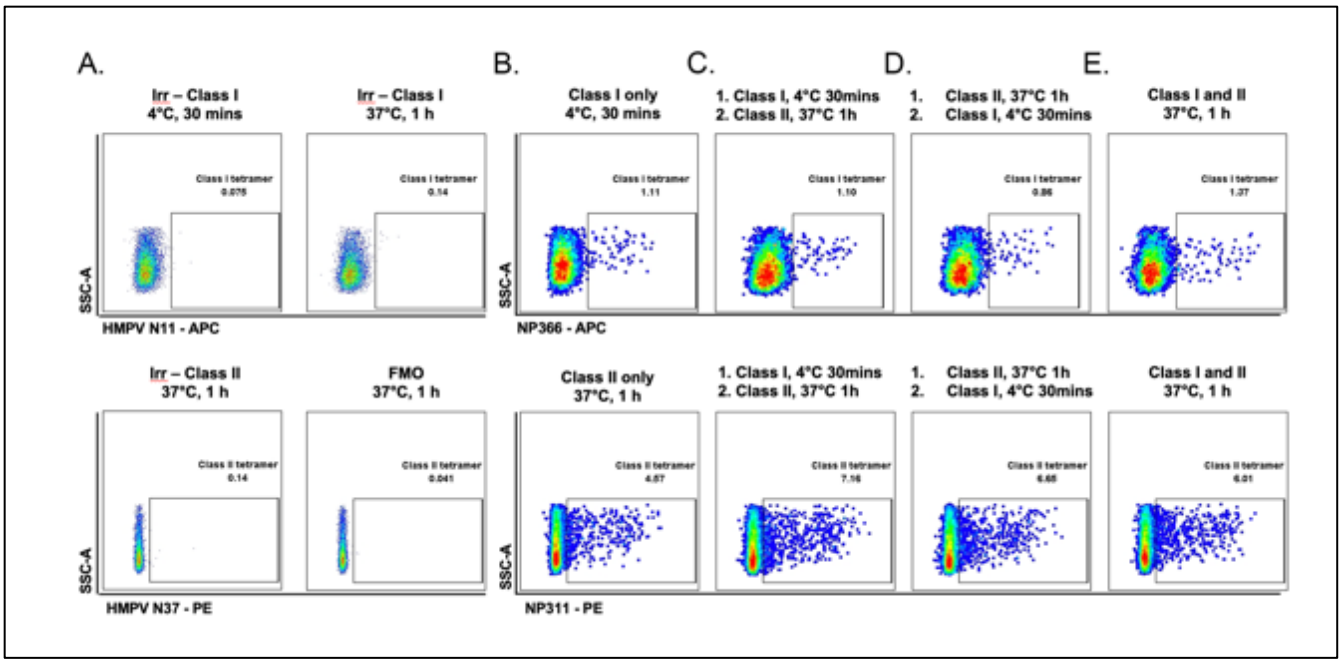

Figure 5-2. Optimal tetramer co-staining conditions confirmed using influenza tetramers.

Top panels show CD8$^+$ tetramer$^+$ T cells (Class I) while bottom panels show CD4$^+$ tetramer$^+$ (Class II) T cells. **(A)** Irrelevant Class I, Class II, and Class II FMO staining at 4°C for 30min or 37°C for 1hr. **(B)** Class I and II only at 4°C for 30min or 37°C for 1hr, respectively. **(C)** Class I staining at 4°C for 30min, followed by a washing step, then Class II staining at 37°C for 1hr. **(D)** Class II staining at 37°C for 1hr, wash cells, then Class I staining at 4°C for 30min. **(E)** Class I and II tetramer staining together at 37°C for 3hrs.

5.3.3 Tetramer co-staining conditions can be used in multispectral flow panel.

Now that we had established optimal staining conditions for Class I and II tetramers that are generalizable across multiple respiratory viral pathogens, we next wanted to test these conditions using our 19-color multispectral flow panel (**Table 6**). Using this panel, live, lymphocyte, single cells CD44$^+$ CD3$^+$ CD19$^-$ (**Fig 5-3A**) can be isolated by CD8$^+$ tetramer$^+$ T cells (**Fig 5-3B**) and CD4$^+$ tetramer$^+$ T cells (**Fig 5-3C**). Lineage specific CD4$^+$ T cells can also be identified by expression of canonical transcription factors *T-bet*, *GATA-3*, *Foxp3*, *Rorγt* (**Fig 5-3D**). In addition,

$CD8^+$ memory T cell subsets can also be identified using CD69 and CD103 staining (**Fig 5-3E**). Lastly, an integral part of respiratory viral infection is assessing $tetramer^+$ T cell impairment (46, 52, 61, 62). This can, in part, be evaluated by looking at inhibitory receptor (i.e. PD-1, TIM-3, LAG-3, 2B4) expression on $tetramer^+$ T cells (**Fig 5-3F**). Overall, combining this co-staining protocol with our multispectral panel introduces a powerful modality in immunology research which provides a comprehensive look at the immune landscape of both $CD8^+$ and $CD4^+$ virus-specific T cells within the same mouse.

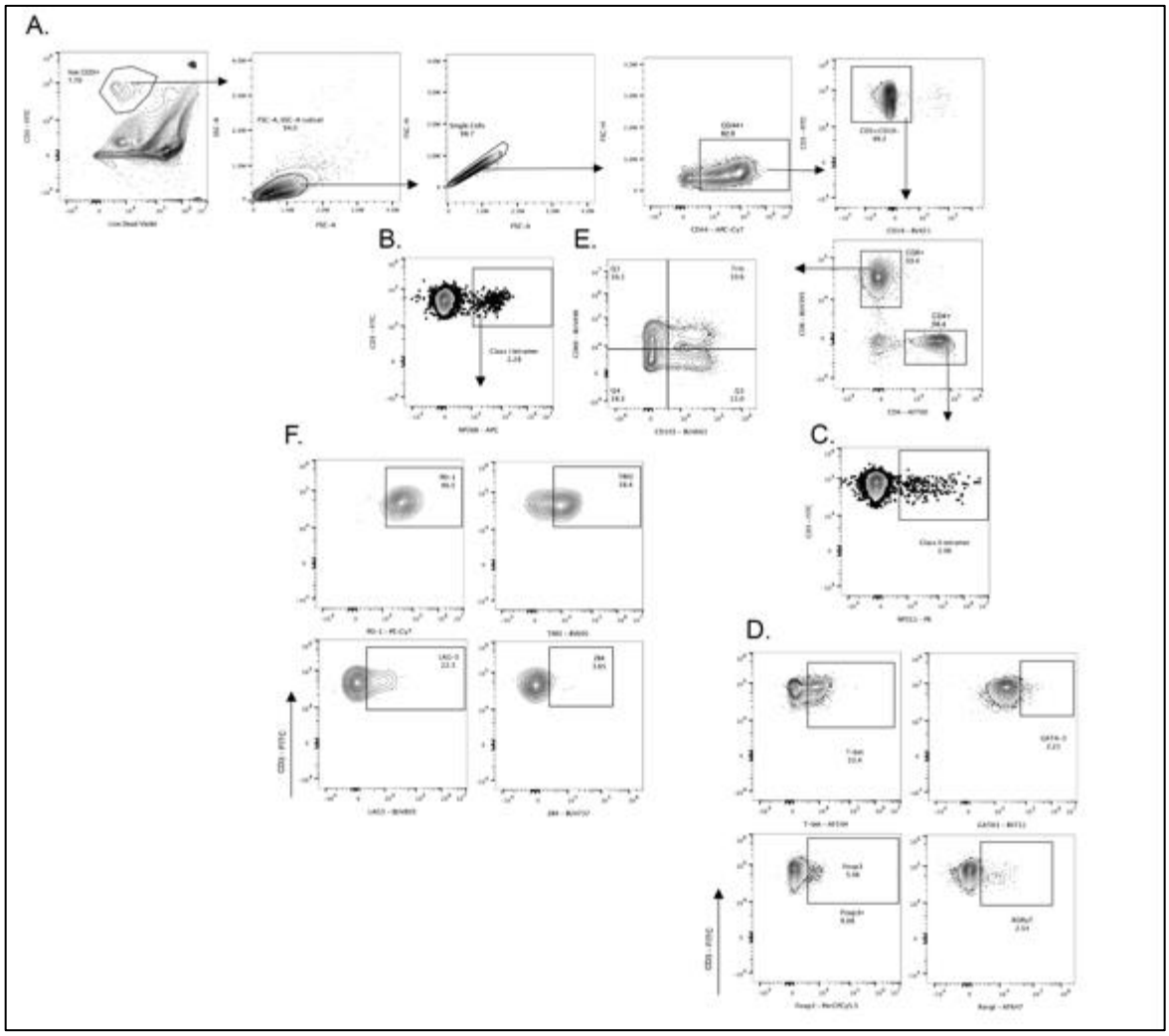

Figure 5-3. Gating strategy for Aurora Cytek multispectral flow panel with tetramer co-staining.

(A) Gating strategy to isolate live, single cell lymphocytes that are $CD44^+$ $CD3^+$ $CD19^-$. **(B & C)** Class I and Class II tetramer staining, respectively. **(D)** $CD4^+$ T cell lineage specific transcription factors: *T-bet, GATA3, Foxp3,* and *Ror*γt. **(E)** $CD8^+$ T cell memory markers, CD69 and CD103 staining. **(F)** Inhibitory receptor expression off of $CD8^+$ $tetramer^+$ T cells including PD-1, Tim-3, LAG-3, and 2B4.

5.4 Discussion

An integral part of studying the cellular immune response to viral pathogens involves assessing the epitope specific T cell repertoire. Both $CD4^+$ and $CD8^+$ T lymphocytes are involved and often have a coordinated response to viral clearance and the immune response (51). The interplay between $CD4^+$ and $CD8^+$ T cells has also been observed in cancer models and controlling tumor growth (253).

Respiratory viruses such as human metapneumovirus (HMPV), respiratory syncytial virus (RSV), influenza, and SARS-CoV2 are leading causes of morbidity and mortality in children less than 5 years old, adults over 65 years old, and the immunocompromised (1, 181). Considering the public health burden of respiratory viruses, it is imperative to elucidate the $CD4^+$ and $CD8^+$ T cell coordinated immune response to optimize treatments and vaccine strategies.

Here, we establish a method for co-staining class I and II tetramers in two different respiratory viral models – HMPV and influenza. We have developed a 19-color multispectral flow cytometry panel which identifies $CD4^+$ and $CD8^+$ antigen-specific T cells as well as lineage specific transcription factors (i.e. *T-bet, GATA3, Foxp3,* etc) and memory markers. This panel and co-

staining protocol collectively provides a comprehensive landscape of the T cell immune response within the same mouse. Other studies, such as (254), have developed multispectral flow panels to assess multiple $CD4^+$ and $CD8^+$ T cell subsets, but they have not also identified virus-specific $CD4^+$ and $CD8^+$ T cells within the same panel, underscoring a unique aspect of this study.

Furthermore, we have validated that the Class I and Class II tetramer staining is specific to $CD8^+$ and $CD4^+$ T cells, respectively. There was an absence of any non-specific binding of Class I tetramer on $CD4^+$ T cells or Class II tetramer on $CD8^+$ T cells (**Fig 5-1 & 5-2**). This emphasizes that our staining protocol is specific towards Class I and Class II tetramer-specific T cells without any cross-reactivity. There was some additional background in the Class II irrelevant tetramer staining under 37°C for 3 hrs (**Fig 5-1**). Considering that this background staining was absent in Class II irrelevant tetramer at 37°C for 1 hr (**Fig 5-2**), we hypothesize that the extended incubation time to 3 hrs contributed to the background staining. In future HMPV studies, we may consider shortening the incubation time to avoid this issue.

One constraint of this protocol is the inability to perform Class I/II tetramer staining and *ex vivo* peptide stimulation intracellular staining in the same panel. Our lab has previously shown that tetramer staining frequency decreases significantly when tetramer and *ex vivo* peptide stimulation are performed in the same panel (46, 52) as tetramer begins to lose its affinity for peptide on the surface of T lymphocytes during the *ex vivo* peptide stimulation. In our approach we separate aliquots of cells for tetramer co-staining and *ex vivo* peptide stimulation to assess functional cytokine production. In this way, we can determine the functionality of the $tetramer^+$ $CD4^+$ or $CD8^+$ T cells by dividing the percent positive for a cytokine (i.e. IFNγ) by the tetramer frequency.

Therefore, our approach still enables us to analyze both the tetramer response and functionality of $CD4^+$ and $CD8^+$ T cells from the same mouse in a single experiment.

Additionally, our staining protocol and panel does not include myeloid lineage cells or B cells. We have previously shown that interferon gamma (IFNγ) signaling and dendritic cells play integral roles in the innate immune response to HMPV (43). Others have reported that re-infections of RSV and HMPV can still occur despite a high neutralizing titer, indicating that the humoral immune response is not always sufficient to protect against re-infection (193). Furthermore, our lab has shown that HMPV viral clearance and establishment of immune memory are dictated by the cell-mediated adaptive immune response (46, 52, 61, 62). Based on these findings, we developed this protocol and multispectral panel focused on T lymphocytes and the adaptive immune response due to their predominant effect on the immune response to HMPV.

This tetramer co-staining protocol has only been tested and validated in C57BL/6 mice. So another drawback of this study is these conditions may not be suitable for mice with a genetic background other than C57BL/6. A possible future direction to make this protocol even more widely applicable would be to develop a multispectral panel, generate tetramers specific to the MHC repertoire, and test co-staining conditions on other mice, such as BALB/c.

Taken together, this Class I/II tetramer co-staining protocol is generalizable to at least two different respiratory viruses, has no cross-reactivity between the two tetramers, and provides a comprehensive immune landscape of key surface and transcription markers canonical to $CD4^+$ and $CD8^+$ T cells through this multispectral panel. Future directions will apply this co-staining protocol

and multispectral panel using HMPV and influenza mouse models to elucidate key lymphocyte populations driving the immune response and vaccine candidate effectiveness.

6.0 C1q and $CD8^+$ T cell function

6.1 Introduction: C1q Complement Protein

The three complement pathways – classical, lectin, and alternative – have numerous critical roles in both innate and adaptive immunity. The primary functions of these pathways are to recognize and opsonize pathogens and cells, trigger enzymatic cascades for clearance of microbes and infected or apoptotic cells, and activate inflammatory cascades that recruit immune cells (255). Recent studies have implicated the initiating component of the classical pathway – C1q – as serving dual roles in both the complement system and in regulating $CD8^+$ T cell function (256-259).

The C1 complex is composed of three C1q subunits, C1qa, C1qb, C1qc. To form the C1 complex, the three C1q subunits assemble via disulfide bonds (**Fig 6-1A & B**) and form the C1q helical polypeptide structure (**Fig 6-1C**) (255). The C1q polypeptide associates with two subunits each of C1r and C1s (i.e. $C1r_2C1s_2$) to form the functional C1 complex (**Fig 6-1D**) (255). The majority of complement proteins are produced by the liver (260) with the exception of C1q, which is produced mostly by macrophages (261). Bone marrow (BM) transplant of wild-type BM into a $C1q^{-/-}$ mouse leads to normal serum levels of C1q, indicating that C1q production is primarily myeloid derived (261).

The C1 complex and the complement classical pathway comprise an integral part of innate host-defense against pathogens (255). The C1 complex binds to antigens displayed on infected or

apoptotic cells as well as pathogen associated molecular patterns (PAMPs) (260). After binding, the C1r and C1s enzymes are activated and cleave the C4 and C2 proteins (260). The product of cleaving these proteins forms the C3 convertase enzyme (260). The formation of C3 convertase initiates the downstream cascade of protein cleaving to form a membrane attack complex and protein fragments that opsonize additional pathogens and infected cells (**Fig 6-2**) (260).

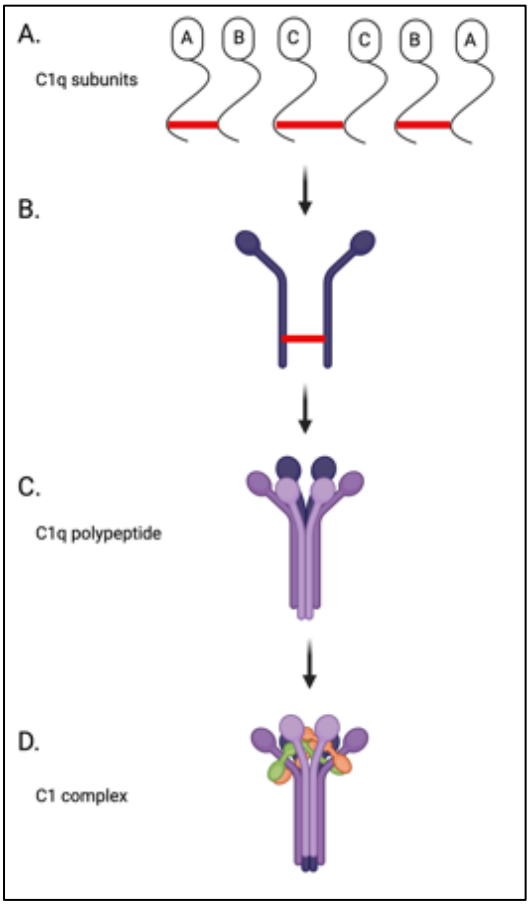

Figure 6-1. C1q complex structure

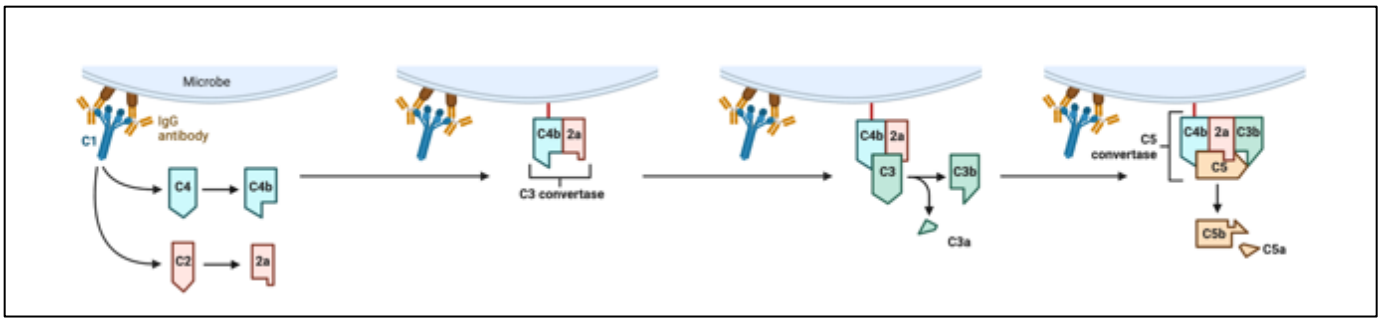

Figure 6-2. Classical complement pathway

Another well-defined role for the C1 complex is protection against autoimmune diseases. Individuals deficient in C1q have a strong risk for developing systemic lupus erythematosus (SLE) and rheumatoid arthritis (RA) (262). The C1 complex does not just remove pathogens, but also apoptotic cells (262). When C1q is absent and the C1 complex cannot form, cells undergoing apoptosis accumulate (262). Dying cells undergo lysis and their intracellular contents are exposed. This initiates an immune response that recognizes the released intracellular antigens as "non-self", thus perpetuating the development of autoimmune diseases (262). Low or absent levels of C1q can also cause hereditary angioedema (HAE) (263). Specifically, HAE is caused by genetic defects in the C1 esterase inhibitor (C-Inh) which results in the uncontrolled production of bradykinin (263). This can have life-threatening consequences, as patients with HAE can suffer from angioedema attacks which target the upper airway, face, and abdomen (263). In addition, idiopathic nonhistaminergic acquired angioedema (AAE) is a condition with spontaneous episodes of urticaria in which the patient has normal C1q esterase inhibitor levels but low C1q levels with anti-C1q antibodies present (264, 265).

Most importantly for the context of this discussion is the role of C1q role in regulating T cell function. Previous studies in cancer and autoimmunity have found a unique population of produce

C1q-producing inflammatory monocytes, which play a distinct role in disease pathogenesis separate from the complement pathway (256-259).

There are several potential mechanisms by which complement can act on $CD8^+$ T cells. First, the enzymatic cleavage of products followed by the convergence of the classical complement pathway on C3 and membrane attack complex formation leads to multiple extracellular signals capable of influencing $CD8^+$ T cell responses. C1q can also directly interact with cells through membrane bound receptors, such as high molecular weight kininogen (HK), Factor XII (Hageman factor), fibrinogen, thrombin, calreticulin, and multimeric vitronectin (266, 267). Calreticulin in particular is most abundantly expressed on dying cells, facilitating the clearance of apoptotic debris as described above. C1Q binding protein, aka gC1qR, is a membrane-bound protein that binds specifically to the globular heads of a fully assembled C1q and became a large focus of this study. During viral infection gC1qR is upregulated on rapidly dividing cells (268). Complete knockdown of gC1qR was incompatible with T cell survival (269). A partial gC1qR knockdown in CAR-T cells exacerbated exhaustion of tumor-infiltrating T lymphocytes (TILs) and impaired the anti-apoptotic capacity of T cells in cancer models (269).

In this study, we identify a novel role for C1q-producing inflammatory monocytes during respiratory viral infection. In a murine model of HMPV, C1q was required for optimal $CD8^+$ T cell effector function, which express the complement receptor gC1qR. In human samples, the C1q/gC1qR axis was present on $CD8^+$ T cells following severe respiratory viral infection.

6.2 Monocyte and macrophage production of C1q potentiates CD8$^+$ T cell effector function following respiratory viral infection

Taylor Eddens*[1], Olivia B. Parks*[2,7], Dequan Lou[3], Li Fan[3], Jorna Sojati[2,7], Manda Jo Ramsey[4], Lori Schmitt[5], Claudia M. Salgado[5], Miguel Reyes-Mugica[5], Alysa Evans[6], Henry M. Zou[3], Tim D. Oury[5], Craig Byersdorfer[4], Kong Chen[3], John V. Williams[7,8,#]

* denotes co-first authorship

Affiliations:

[1]Division of Allergy/Immunology, Department of Pediatrics, University of Pittsburgh School of Medicine, Pittsburgh, PA, USA

[2]University of Pittsburgh Medical Scientist Training Program, Pittsburgh, PA, USA

[3]Division of Pulmonary, Allergy and Critical Care Medicine, Department of Medicine, University of Pittsburgh School of Medicine, Pittsburgh, PA, USA

[4]Division of Blood and Marrow Transplant and Cellular Therapies, Department of Pediatrics, University of Pittsburgh School of Medicine, Pittsburgh, PA, USA

[5]Department of Pathology, University of Pittsburgh School of Medicine, Pittsburgh, PA, USA

[6]Program in Microbiology and Immunology, University of Pittsburgh School of Medicine, Pittsburgh, PA, USA

[7]Division of Infectious Diseases, Department of Pediatrics, University of Pittsburgh School of Medicine, Pittsburgh, PA, USA

[8]Institute for Infection, Inflammation, and Immunity in Children (i4Kids), Pittsburgh, PA, USA

 # Corresponding Author:

John V. Williams, MD

University of Pittsburgh

Rangos Research Building

4401 Penn Avenue

Pittsburgh, PA 15224

Phone: 412-692-8298

Email: jvw@chp.edu

Under review at *AJRCMB*

6.3 Summary

Respiratory viral infections remain a leading cause of morbidity and mortality. Using a murine model of human metapneumovirus (HMPV), we identified lung recruitment of a C1q-producing inflammatory monocyte population concomitant with viral clearance by adaptive immune cells. Genetic ablation of C1q led to reduced $CD8^+$ T cell function. Production of C1q by a myeloid lineage was sufficient to enhance $CD8^+$ T cell function. Activated and dividing $CD8^+$ T cells expressed a C1q receptor, gC1qR. Perturbation of gC1qR signaling led to altered $CD8^+$ T cell IFN-γ production, metabolic capacity, and cell division. Autopsy specimens from fatal respiratory viral infections in children demonstrated diffuse production of C1q by an interstitial population. Humans with severe COVID-19 infection also demonstrated upregulation of gC1qR on activated and rapidly dividing $CD8^+$ T cells. Collectively, these studies implicate C1q production from monocytes as a critical regulator of $CD8^+$ T cell function following respiratory viral infection.

6.4 Materials & Methods

6.4.1 Experimental model and study participant details

Mice and virus stocks

C57BL/6 (strain 664), 6(Cg)-C1qa$^{tm1d(EUCOMM)Wtsi}$/TennJ (strain 31675, referred to as *C1qa*$^{-/-}$), B6.129S4-C3^{tm1Crr}//J (strain 29661, referred to as C3$^{-/-}$), *Rag1*$^{-/-}$ (strain 2216) and B6.SJL-*Ptprc*^{a} *Pepc*^{b}*/BoyJ* (strain 2014, referred to as CD45.1) mice were purchased from the Jackson Laboratory. Six-to-eight-week old mice were anesthetized with 3% isoflurane and infected with

$2.0x10^6$ PFU of HMPV strain TN/94-49 (genotype A2) in 100 μL sterile PBS. HMPV was grown in LLC-MK2 cells and purified as previously described (160). Mice were treated with a mock-infected LLC-MK2 lysate as a negative control. In select experiments, mice were infected with $1.0x10^5$ PFU of clinical isolate C2-202 (genotype B1) (freeze/thawed a maximum of three times) (20). Clinical scoring was performed with 1 point added for each of the following variables: hunched, ruffled fur, rapid breathing, decreased activity. All animals were handled according to protocols approved by the University of Pittsburgh Institutional Animal Care and Use Committee.

Human lung tissue staining

Lung samples from children who died from respiratory viral infections (autopsy cases) were selected on retrospective review of specimens from the Department of Pathology, UPMC Children's Hospital of Pittsburgh. Normal lung tissues resected as perilesional lung in patients with pleural blebs were used as normal control. Use of cadaveric and normal control tissue was approved by the University of Pittsburgh Committee for Oversight of Research and Clinical Training Involving Decedents (CORID).

6.4.2 Single cell RNA sequencing

The lungs were removed from HMPV-infected or mock-infected mice on day 7 post-infection. The lungs were then minced via scissors, digested with DNAse/collagenase at 37°C for 1 hour, passed through a 70μm strainer, and treated with RBC lysis buffer (ACK, Gibco, Cat:A1049210) to generate a single cell suspension. Cells were then stained with cell hashing antibody from Biolegend following the CITE-seq protocol (https://cite-seq.com/protocols, Cell_hashing_protocol_190213). After the final wash, cells were passed through a 40 uM cell

strainer and enumerated by Cellometer2000 before loading onto 10x Chromium controller for cell capture using 5' V2 kits. Libraries for gene expression and hash tag oligos were constructed following protocols from 10x Genomics and the New York Genome Center. Final libraries were QCed by Agilent TapeStation then sequenced on an Illumina Novaseq 6000 targeting 50,000 reads per cells. Sequencing data were processed with Cellranger 7.0 before downstream analysis using Seurat.

6.4.3 Single Cell RNA-Seq data processing

Single cell RNA sequencing analysis was performed using Seurat 4.0 with R (version 4.1.1). QC metrics included nFeature_RNA>200, nFeature_RNA<5000, and percent.mt<20 followed by normalization. Samples were then demultiplexed by hash-tag-oligos (HTOs) and doublets identified by HTOs were removed before downstream analysis. QC metrics were assessed for each HTO after demultiplexing (**Appendix Fig 28**) and analysis was continued with QC cutoffs above. Poor-quality droplets were excluded from subsequent analysis if a deficient number of genes or high percentage of mitochondrial genes were detected. Quality control of the QC cutoffs was performed on RNA (**Appendix Fig 29**). For human single-cell RNA sequencing analysis, the following publicly available dataset was mined: GSE145926 (270).

6.4.4 C1q ELISA

Bronchoalveolar lavage fluid was obtained by cannulating the trachea of a euthanized animal and insufflating the lungs with PBS as previously described (213). Quantification of C1q on lung

homogenate and bronchoalveolar lavage fluid (BAL) was performed via ELISA following manufacturer's instructions (Abcam, cat# 291069).

6.4.5 Viral burden titration

Viral titers were measured via plaque titration as described previously (160, 161). Briefly, lung homogenates were serially diluted 1:10 in Opti-MEM media containing 1:2000 trypsin and adsorbed to a monolayer of LLC-MK2 cells in a 24-well tissue culture dish for one hour at room temperature. Methylcellulose-containing overlay media with 1:500 trypsin was added, followed by a five-day incubation at 37°C. Plates were then fixed with formalin, blocked with PBST containing 5% nonfat dried milk, stained using 1:1000 guinea pig anti-HMPV primary antibody and 1:1000 anti-guinea pig-HRP secondary antibody, and developed using TrueBlue^{TM} substrate (KPL, Cat #5510-0050).

6.4.6 Histology

Following dissection and isolation, the lower half of the left lung lobe was insufflated with 10% formalin, embedded in paraffin, sectioned, and stained with H&E. Histologic scoring was performed by a pathologist in a blinded fashion.

6.4.7 Flow cytometry/ImageStream

Following generation of a single cell suspension from lung as above, cells were then plated for *ex vivo* peptide stimulation or tetramer staining in parallel, as described previously (46). Full gating

strategies can be found in prior publication (214). For peptide stimulation, cells were stimulated with 10 μM N11 peptide or irrelevant control peptide in the presence of BFA/monensin and CD107-PE antibody for 5 hours at 37°C. Cells were then stained with live/dead violet (1:1000 in PBS, Invitrogen, Cat:L34964A), washed x2 in FACS, treated with Fc blockade (1:100 in FACS buffer, Tonbo™, Cat:70-0161-M001), and stained for surface markers for 45 mins at 4°C (1.5μL antibody/sample in BD Horizon™ Buffer, cat:566349, **Table 7**). Cells were then fixed with FOXP3 fix/permeabilization buffer for 20 minutes (Invitrogen, Cat:50-112-8857), washed x1 in permeabilization buffer, and stained for intracellular markers for 30 minutes at 4°C(4.5μL antibody/sample in 1:1 mixture of BD buffer and fix/perm buffer, **Table 7**). Cells were resuspended in FACS buffer. For tetramer staining, cells were incubated for 30mins at RT in FACS buffer containing 1:2000 100mg dasatinib, followed by 1:100 N11 class I tetramer or an irrelevant tetramer for 90 minutes at RT in the dark. After live/dead, Fc block, and surface staining as above, cells were fixed for 18 hours with FOXP3 fix/permeabilization buffer. Cells were then washed in fix/perm buffer x2 and resuspended in FACS buffer. Cells were then stained for transcription factors (2.5μL antibody/sample in 1:1 mixture of BD buffer and fix/perm buffer, **Table 7**). Following two washes, the cells were resuspended in FACS buffer with 100μL of Biolegend Counting Beads. Fluorescence minus one (FMO) controls were used for all inhibitory receptor and transcription factor gating. For macrophage staining, cells were stained for live/dead, Fc blockade, and surface markers as above (**Table 7**). Cells were then fixed in FOXP3 fix/perm buffer for 40 minutes, stained with 1.5μL anti-C1q-FITC for 1 hour at 4°C, washed, and subsequently resuspended in FACS buffer. For all conditions, samples were strained through nylon filters and run on a Cytek® Aurora multispectral flow cytometer. Unstained cells from each experiment were generated using 2% PFA and used to minimize autofluorescence. Data analysis was performed

with Flowjo(v10.8.1). For ImageStream visualization, the same flow cytometry protocol was used as described above with the exception that CD68-APC-Cy7, CD3-BV605, and C1q-PE concentrations were doubled to account for compensation on the ImageStream® software. ImageStream® data analysis was performed on IDEAS® Image Analysis Software.

Table 7. Key resources table for C1q studies

Adaptive panels	Fluorochrome	Host	Catalog	Clone
CD19	BV785	rat	115543	6D5
CD3e	BUV395	hamster	565992	145-2C11
CD4	AF700	rat	100536	RM4-5
CD8a	AF532	rat	58-0081-80	53-6.7
CD44	APC-Cy7	rat	560568	IM7
CD62L	BUV563	rat	741230	MEL-14
Tetramer plate				
Foxp3	PerCP-Cy5.5	rat	45-4773-82	FJK-16s
T-bet	PE	mouse	644809	4B10
GATA-3	BV711	mouse	565449	L50-823
Rorγt	AF647	mouse	562682	Q31-378
PD-1	PE-Cy7	rat	109110	RMP1-30
TIM-3	BV605	rat	119721	RMT3-23
LAG-3	BUV805	rat	748540	C9B7W
2B4	BUV737	rat	749155	C9.1
HMPV N11 Class I tetramer	APC	--	--	--

Influenza NP366 Class I tetramer	APC	--	--	--
Peptide stimulation plate				
Perforin	FITC	rat	11-9392-82	eBioOMAK-D
GzmB	PE-Cy5.5	rat	35-8898-80	NGZB
TNF	BUV661	rat	750025	MIH44
IFNγ	BV650	rat	505831	XMG1.2
CD107a (LAMP1)	PE	rat	121611	1D4B
Monocyte panel	**Fluorochrome**	**Host**	**Catalog**	**Clone**
CD45.2	BUV496	mouse	741092	UV7
Ly-6G	APC-Cy7	rat	127624	1A8
Ly-6C	AF700	rat	128024	Hk1.4
CD64	BV711	mouse	139311	X54-5/7.1
CD103	BV785	rat	121439	10F.9G2
CD11b	APC	rat	101211	MI/70
CD11c	BUV805	hamster	749090	HL3
F4/80	BV421	rat	123131	BM8
SiglecF (CD170)	AF647	rat	155519	S17007L
CD68	PE-Cy7	rat	137015	FA-11
C1q	FITC	mouse	MA1-403131	JL-1
ImageStream panel	**Fluorochrome**	**Host**	**Catalog**	**Clone**
C1q	PE	rat	569965	RmC7H8
SiglecF (CD170)	PE-Cy7	rat	155527	155519

CD8a	BV510	rat	100751	53-6.7
CD3e	BV605	hamster	100351	145-2C11
CD68	APC-Cy7	rat	137023	FA-11
Immunofluorescence staining reagents	**Fluorochrome**	**Host**	**Catalog**	**Clone**
Anti-C1q antibody (diluted 1:1000)	Unconjugated	rat	HM1044	7H8
Anti-CD68 antibody (diluted 1:1000)	Unconjugated	rabbit	PA5-78996	--
Donkey anti-rat IgG (diluted 1:1000)	AF488	donkey	A-21208	--
Donkey anti-rabbit IgG (2 drops/1mL)	AF594	donkey	R37119	--

6.4.8 Immunofluorescent staining

Mice were infected as above and lung tissue was removed and insufflated with 4% paraformaldehyde and incubated at 4°C for 2 hours. Specimens were washed three times with PBS (10 mins/wash), then transferred to a 15% sucrose solution until tissue sank. Specimens were moved until 30% sucrose solution. Lungs were then embedded in OCT, frozen, and cryosectioned. Tissue was then fixed to the slide with 4% paraformaldehyde, blocked with 1% bovine serum albumin in PBS, and stained (**Table 7**) per prior protocol (271). Cells were mounted with DAPI-containing mounting media and imaged using a Leica Stellaris 5 confocal microscope (272).

6.4.9 Bone marrow transplantation and adoptive transfer models

For bone marrow transplantation, CD45.1 or C1qa$^{-/-}$ recipients were irradiated with two doses of 5.5 Gy 5 hours apart (MultiRad 350, Precision X-Ray Irradiation). Twenty-four hours later, bone marrow from either CD45.2 B6 or *C1qa*$^{-/-}$ mice was isolated by flushing the femur/tibia with D-10 media. Irradiated mice then received 2.0x10^{6} cells in 200µL sterile PBS via tail vein injection. Following a 6-week engraftment period, mice were infected with HMPV and analyzed for CD8 function as above. For adoptive transfer, CD19^{+} cells, CD8^{+} T cells, and CD4^{+} T cells were purified from donor lymph nodes/spleen via magnetic separation. Briefly, CD45.1 B6, CD45.2 B6 or *C1qa*$^{-/-}$ lymph nodes and spleens were processed sequentially through 70µm and 40µm filters. For CD4^{+} and CD8^{+} negative selection, cells were incubated for 5 minutes with selection antibody cocktail (Miltenyi Biotec, cat # 130-104-454, 130-104-075) followed by a 10 minute incubation with anti-biotin magnetic beads (cat# 130-090-485). CD19^{+} cells were isolated via positive selection by incubating cells with anti-CD19 biotin conjugated antibody (Invitrogen cat # 13-0193-82), followed by incubation with anti-biotin beads. Labeled cells were then applied to primed LS columns (Miltenyi Biotec cat # 130-042-401) and collected following two washes. Cells were then washed with PBS and counted on a BD Accuri^{TM} cytometer. A mixture of 2.0x10^{6} B6 CD19^{+}, 2.0x10^{6} B6 CD4$_{+}$, and a 1:1 mixture CD45.1:*C1qa*$^{-/-}$ of 2.0x10^{6} total CD8^{+} T cells was then administered to *Rag1*$^{-/-}$ recipients via tail vein injection. Following a 3-week reconstitution period, mice were then infected with HMPV and analyzed as above.

6.4.10 Monocyte-T cell Co-Culture

B6 or *C1qa*$^{-/-}$ mice were infected with 1x10^6 PFU/100µL TN/94-49 HMPV. On day 7 p.i., mice were euthanized and both right and left lungs were harvested. Lungs were enzymatically digested, run through 70µm and 40µm filters, and treated with ACK lysis buffer, as described above. The single cell suspension was incubated with CD11b positive selection beads (Miltenyi Biotec cat# 130-126-725) for 10min and run through primed LS columns (Miltenyi Biotec cat # 130-042-401) as described above. The unlabeled cells in the flow-through were incubated with CD8 negative selection beads (Miltenyi Biotec cat# 130-104-075) as described above. The CD11b and CD8 selected cells were washed with PBS and counted on a BD Accuri^{TM} cytometer. 0.2x10^6 CD11b selected cells and 0.2x10^6 CD8 selected cells were resuspended in complete RPMI with 1:1000 10U of recombinant IL-2 (Cat# 200-02) and plated in a 48-well flat bottom plate. 200 µM N11, M94, and F528 HMPV peptides were diluted 1:10 in complete RPMI and added to each co-culture condition. In select wells, 10µg anti-gC1qR (clone 74.5.2, Santa Cruz cat# sc-23884-L), 10 µg of recombinant C1q (M099, ComplementTech), or both were added. Plate was incubated at 37ºC for 48 hrs. After incubation, cells were harvested from supernatant and from the well surface via 5 mM EDTA+PBS for 30 min on ice. Once isolated, cells were spun down, washed with 200uL PBS, and proceeded with flow cytometry staining.

6.4.11 IFN-γ ELISpot

Following generation of a single cell suspension from lung, 50,000 cells were plated per well in triplicate on an IFN-γ ELISpot plate (R&D systems, cat# EL485), with 10µM of irrelevant (LCMV gp66-77 peptide) or a MHC class I restricted immunodominant HMPV epitope (N11). Antibody

blockade was performed with 10 μg/mL anti-gC1qR (clone 74.5.2, Santa Cruz cat# sc-23884-L) or anti-PD-L1 (clone 10F.9G2, BioXcell cat# BE0101). The plate was incubated for 48 hours at 37°C and developed per manufacturer's instructions.

6.4.12 gC1qR blockade *in vivo*

On days 5 and 6 post-infection, 50 μg of anti-gC1qR or isotype control antibody was administered to anesthetized mice via the oropharyngeal route. Equal volume PBS was used as control. CD8 endpoints were assessed as above.

6.4.13 Metabolic profiling

A single lung cell suspension was generated as above, followed by further enrichment of $CD8^+$ T cells by magnetic bead separation (Miltenyi Biotec, cat# 130-104-075) per manufacturer's instructions. $CD8^+$ T cells were then counted using a BD Accuri™ cytometer and plated with 200,000 cells/well with 10 μg/mL anti-gC1qR. Metabolic status was assessed using Agilent Seahorse XF Cell Mito Stress Test Kit (cat# 103010-100) per manufacturer's instructions on the Agilent Seahorse XFe96 analyzer.

6.4.14 Quantification and Statistical Analysis

All data displayed as mean ±SEM. Analyses with two groups were analyzed using unpaired student's t tests, while analyses with three or more groups were analyzed using a one-way ANOVA test with Tukey's multiple comparisons. Analyses with two time points (e.g., day 1 and day 7)

were analyzed using a two-way ANOVA with Holm-Sidak multiple comparisons. Significance was defined as $p<0.05$ for all analyses. All statistical analyses for mouse experiments were performed using GraphPad Prism (v.9.3.0). For single cell RNA sequencing analysis, differential gene expression by assessing log_2FC with an adjusted p-value of <0.05 using non-parametric Wilcoxon rank sum test with Bonferroni correction for multiple comparisons. Permutation tests were used for assessing differences in cell abundance and have been included as supplemental figures. Global differential gene assessment was performed via pseudobulk analysis between mock vs. HMPV infected animals. All single cell analysis was performed using the Seurat pipeline in R studio.

6.5 Results

6.5.1 C1q is produced by an inflammatory macrophage population in the lungs of mice infected with human metapneumovirus.

Single cell RNA sequencing using the 10x Genomics platform was performed on lung tissue from mock-infected vs HMPV-infected mice on day seven post-infection, by which time at viral burden is rapidly cleared due to adaptive immunity. An average of 5,730 cells were captured/sequenced per sample, with an average of 24,964 reads per cell. Using clustering analysis, nine unique cellular populations were identified: T cells, B cells, inflammatory monocytes, endothelial cells, monocytes, fibroblasts, macrophages, NK cells, and neutrophils (**Fig 6-3A**). These clusters were manually annotated based on expression of canonical markers (**Fig 6-3B**). Notably, the inflammatory monocyte population shared expression of several genes associated with monocytes,

but were differentiated by expression of C1qa, C1qb, and C1qc (**Fig 6-3A-B**). These clusters were then visualized via UMAP non-linear dimensional reduction, with cells from every cluster observed in both mock and HMPV-infected animals (**Fig 6-3C**). However, HMPV-infected mice had a statistically significant expansion of the T cell and inflammatory monocyte compartments compared to mock infected animals (**Fig 6-3D**, **Appendix Fig 18A**).

For the T cell compartment, this expansion was partially comprised of $CD8^+$ cells that expressed granzyme B (*Gzmb*), PD-1 (*Pdcd1*) and IFNγ (*Ifng*) (**Appendix Fig 18B-C**), consistent with prior reports (46, 62). As PD-1 is prominently upregulated in this model, we next sought to characterize signaling pathways and downstream targets in an unbiased manner using NicheNet (273). This predictive package identified eighteen prioritized ligands, including PD-L1 (i.e., *Cd274*), the ligand for PD-1 (**Appendix Fig 18D**). Further corroborating prior studies, PD-L1 was predicted to regulate several target genes, including *Ifng* (**Appendix Fig 18D**). These data demonstrate that the single cell RNA sequencing methodology and subsequent unbiased pathway analysis adequately captured biologic processes consistent with our prior work, validating use of this dataset for discovery purposes. As described above, the inflammatory monocyte (iMono) population was noted to have marked expression of C1qa, C1qb, and C1qc (**Fig 6-3E**) not observed in other populations. Using differential expression analysis, C1qa, C1qb, and C1qc were significantly upregulated in iMonos compared to Monos/Macs. As an alternative statistical approach, global differential gene expression was also calculated between HMPV-infected animals and mock-infected animals. In this analysis, C1qa, C1qb, and C1qc were significantly upregulated in HMPV-infected lungs ($p<1x10^{-50}$).

Given the interesting expansion of both $C1q^+$ inflammatory monocytes and T cells, we next sought to analyze cell-to-cell communication with an emphasis on these two populations. To model this, we used CellChat, a package that quantitatively infers connections and signaling pathways between scRNAseq cell clusters (274). HMPV-infected animals had an increased number of interactions as well as increased interaction strength (**Fig 6-3F**). CellChat pathway analysis also revealed a strong complement signature in HMPV-infected animals (**Fig 6-3G**). In the HMPV-infected lung, inflammatory monocytes were the largest contributors of outgoing signals by number, followed closely by macrophages and fibroblasts (**Appendix Fig 19A-B**). As for receiving signals, T cells had the most incoming signals from inflammatory monocytes. Inflammatory monocytes had several methods of communicating to T cells when analyzed at a ligand:receptor level, including through chemotactic mechanisms (**Appendix Fig 19C).** Collectively, these single cell RNA sequencing data demonstrate that HMPV-infected mice have evidence of a C1q-producing inflammatory monocyte population and expansion of $CD8^+$ effector T cells, with predicted cell-to-cell communication occurring between the two cell types.

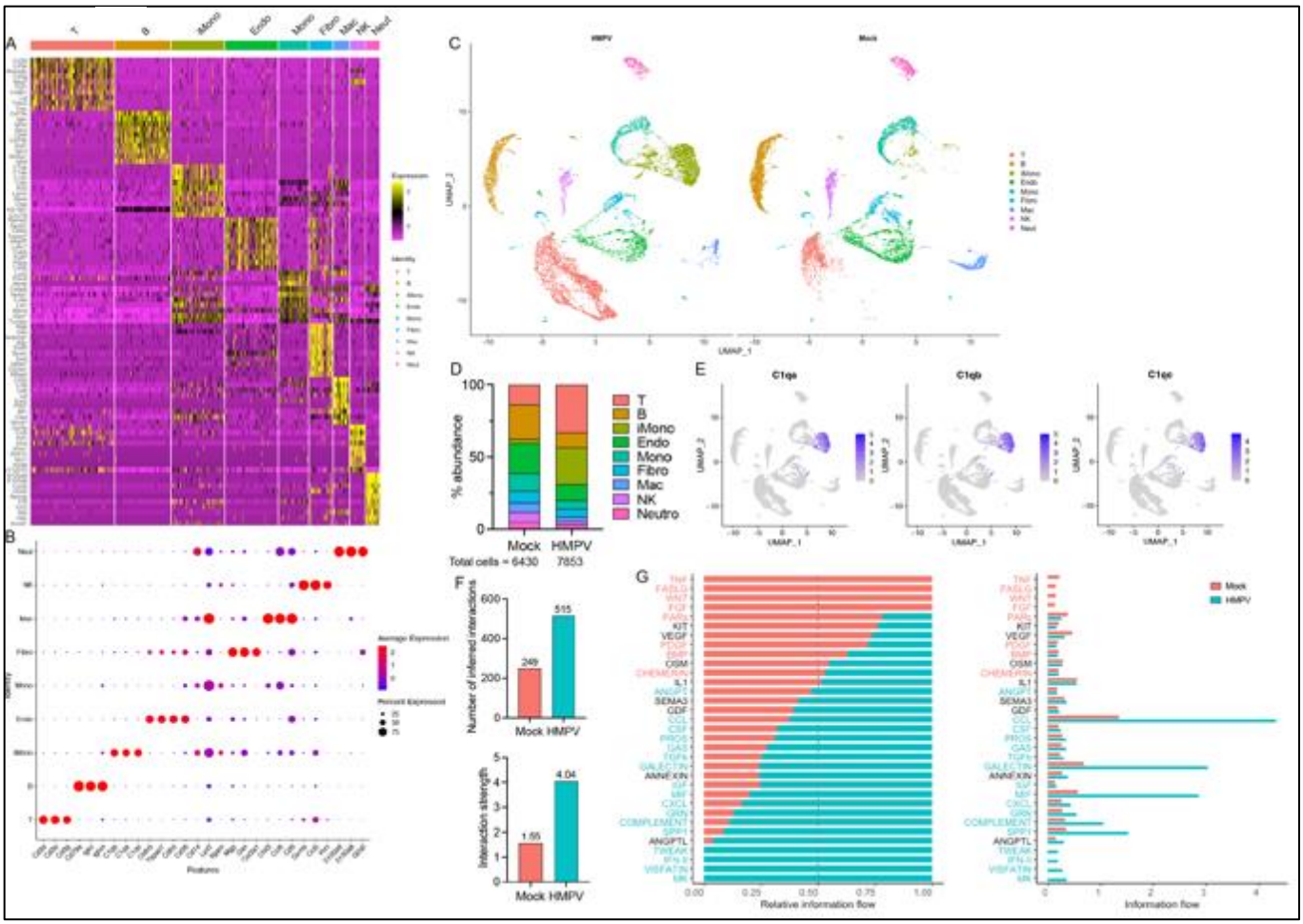

Figure 6-3. Identification of a C1q signature on day 7 after HMPV infection.

(A) Heat map demonstrating clustering of 9 different cell populations after single cell RNA sequencing. **(B)** Dotplot with expression of marker genes used for manual annotation for individual clusters. **(C)** Uniform Manifold Approximation and Projection (UMAP) representation of cell populations in mock infected vs. HMPV-infected animals demonstrating an increased inflammatory monocyte (iMono) and T cell population post-infection. **(D)** Percent abundance of cell populations by cluster in both mock and HMPV infected animals. **(E)** Feature plot of C1qa, C1qb, and C1qc shown as UMAPs, demonstrating production in iMonos. **(F)** CellChat analysis showing number of inferred interactions (top) and interaction strength (bottom) in mock and HMPV infected animals. **(G)** Pathway analysis of information flow using CellChat. Single cell RNA sequencing was performed as single replicate with two mice in each group.

To validate these single cell RNA sequencing findings, we next assessed C1q production at the protein level. C1q was upregulated in bronchoalveolar lavage fluid over the course of HMPV infection, peaking at day seven post-infection (**Fig 6-4A**). Additionally, using validated surface markers for various monocyte/macrophage populations, we next identified the inflammatory monocyte population via flow cytometry (**Fig 6-4B**, **Appendix Fig 20A-B**). The number of iMonos was significantly increased in HMPV-infected mice at day seven post-infection (**Fig 6-4B**, **Appendix Fig 20C**). Similarly, there was a significant increase in C1q-expressing inflammatory monocytes at day seven post-infection (**Fig. 6-4B**, **Appendix Fig 20D**). C1q production was not seen in other myeloid cells, such as neutrophils (**Appendix Fig 20E**). Additionally, if staining for C1q was performed prior to permeabilization, the signal in the inflammatory monocyte population was absent, suggesting that the C1q detected was intracellular (**Appendix Fig 20F**). To further assess production of C1q, we used ImageStream imaging flow cytometry technology to capture high-resolution images of individual cells from the single cell suspensions of either mock and HMPV-infected mice. Inflammatory monocytes from HMPV-infected mice had a robust C1q intracellular signal (**Fig. 6-4C, top**), and C1q staining was not observed in $CD3^+$ $CD8^+$ T cells (**Fig. 6-4C, bottom**). Minimal C1q production was noted in mock infected animals in either cell type (**Fig. 6-4C**). Further assessing co-localization, immunofluorescent staining on fixed lung specimens demonstrated C1q and CD68 overlap in the B6 HMPV specimen, but not B6 mock or C1q deficient mice (**Fig. 6-4D**, **Appendix Fig 21**). Collectively, these data demonstrate that HMPV-infected animals have a robust C1q-producing inflammatory monocyte population in the latter stages of infection, coincident with adaptive immunity.

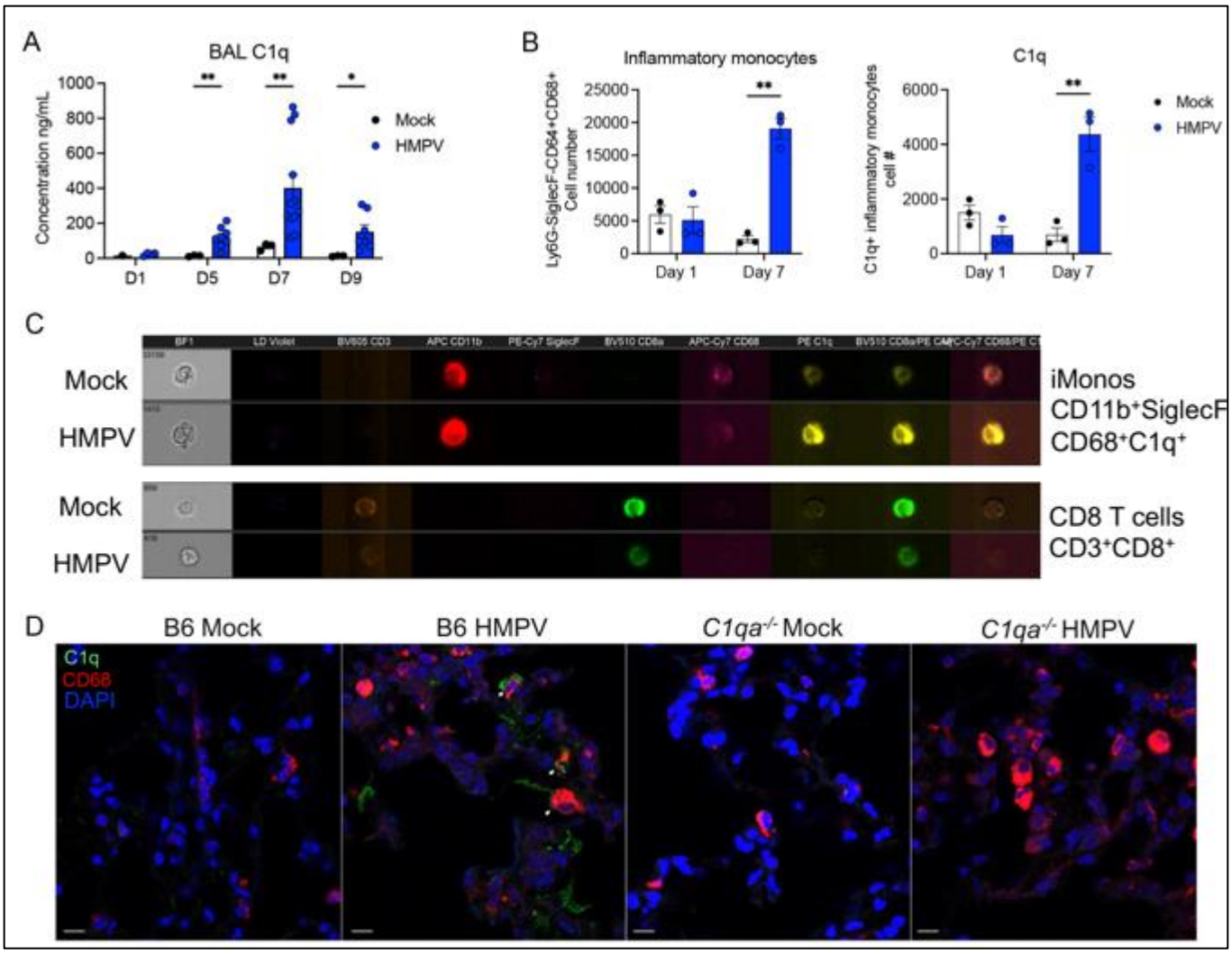

Figure 6-4. Validation of C1q production by inflammatory monocytes in HMPV infection.

(A) C1q protein quantity in bronchoalveolar lavage (BAL) specimens from mock or HMPV infected animals at various time points. * $p<0.05$, ** $p<0.01$ by two-way ANOVA with multiple comparisons, n=1-3 for mock groups, n=4-12 for infected groups. **(B)** Enumeration of inflammatory monocytes (left) and C1q-producing inflammatory monocytes (right) by flow cytometry isolated from the lung at day 7 post-infection. ** $p<0.01$ by two-way ANOVA with multiple comparisons, n=3/group, representative of single replicate. **(C)** ImageStream analysis of C1q production in inflammatory monocytes (top) vs. CD8 T cells (bottom). **(D)** Immunofluorescent staining of C1q, CD68, and DAPI showing co-localization of C1q with CD68 in the B6 HMPV infected group alone (white arrow heads). Scale bars represent 10 μm.

6.5.2 C1q is required for optimal CD8 effector function.

We next assessed $CD8^+$ T cell responses in the absence of C1q using 6(Cg)C1qa$^{tm1d(EUCOMM)Wts}$ /TennJ (referred to as *C1qa*$^{-/-}$) mice following infection with HMPV (TN/94-49), a well-characterized strain of the virus that causes mild disease in adult B6 mice (46). Lack of C1q induction was confirmed in *C1qa*$^{-/-}$ mice via ELISA (**Appendix Fig 22A**). There was no difference in weight loss or viral titer between *C1qa*$^{-/-}$ and B6 mice (**Appendix Fig 22B-C**). At day seven post-infection, there was also no difference in the frequency or absolute number of epitope-specific $CD8^+$ T cells recognizing the immunodominant HMPV epitope N_{11-18} (**Fig 6-5A**). Similarly, inhibitory receptors (i.e. PD-1, Tim-3, LAG-3, and 2B4), activation markers (CD44, CD62L), and transcription factors (i.e. T-bet, Gata3, Foxp3, Eomes, Tox, and Tcf1) on virus-specific $CD8_+$ T cells were unchanged between the two groups (**Appendix Fig 22D-F**). B6 and *C1qa*$^{-/-}$ mice displayed similar extents of immunopathology following TN/94-49 infection. (**Appendix Fig 22G-H**). However, $CD8^+$ T cells from *C1qa*$^{-/-}$ mice exhibited a striking decrease in function, producing significantly less granzyme B, IL-2, and IFNγ (**Fig 6-5B**). Combinatorial analysis assessing CD107a, IFNγ, granzyme B, IL-2, and perforin production revealed that *C1qa*$^{-/-}$ $CD8^+$ T cells were less polyfunctional compared to $CD8^+$ T cells from B6 mice (**Fig 6-5C**). To determine the effects of C1q signaling to $CD8^+$ T cells during severe HMPV infection, we used a clinical isolate of HMPV, C-202, known to cause severe disease in young adult mice (manuscript submitted). *C1qa*$^{-/-}$ mice were able to clear the virus, but lost significantly more weight (**Appendix Fig 23A**) and had higher clinical scores compared to B6 mice (**Appendix Fig 23B**). *C1qa*$^{-/-}$ mice also had enhanced histopathology following C-202 infection when compared to B6 mice (**Appendix Fig 23C-D**). These data indicate that the absence of C1q signaling has detrimental effects to $CD8^+$ T cell function and lung pathology during severe respiratory disease.

To determine if this $CD8^+$ T cell phenotype required the complement pathway downstream of C1q, we used *C3*$^{-/-}$ mice which lack C3, a common protein utilized by all three complement pathways (**Appendix Fig 24A**). There was no difference in weight loss (**Appendix Fig 24B**). In contrast to WT B6 mice, *C3*$^{-/-}$ mice had detectable viral titers at day seven post-infection (**Appendix Fig 24C**). However, there were no differences in epitope-specific $CD8^+$ T cell frequency in *C3*$^{-/-}$ mice (**Appendix Fig 24D**). There was also no difference in inhibitory receptor (**Appendix Fig 24E**), transcription factor expression (**Appendix Fig 24E**), or polyfunctionality of $CD8^+$ T cells (**Appendix Fig 24F-G**) between *C3*$^{-/-}$ and B6 mice, suggesting the alternative complement activation and shared membrane attack complex formation pathway is not involved in the CD8 dysfunction.

To assess if myeloid-derived C1q was required for enhanced $CD8^+$ T cell function, we utilized a four-way reciprocal bone marrow (BM) chimera approach. First, *C1qa*$^{-/-}$ or B6 BM was transplanted into lethally irradiated CD45.1 recipients or the reciprocal where CD45.1 BM was transplanted into lethally irradiated *C1qa*$^{-/-}$ and B6 recipients (**Fig 6-5D**). For clarity, the experimental groups are referred to as: BM → host (i.e. *C1qa*$^{-/-}$ BM into CD45.1 recipient = *C1qa*$^{-/-}$ $_{BM}$ → $CD45.1_H$) There was no difference in viral titer between transplant groups. There were equal numbers of inflammatory monocytes in *C1qa*$^{-/-}$$_{BM}$ → $CD45.1_H$ and $B6_{BM}$ → $CD45.1_H$ groups (**Fig 6-5E**), but *C1qa*$^{-/-}$$_{BM}$ → $CD45.1_H$ had negligible $C1q_+$ inflammatory macrophages compared to $B6_{BM}$ → $CD45.1_H$ (**Fig 6-5F**). This was also reflected in the C1q protein level in whole lung homogenate, with *C1qa*$^{-/-}$$_{BM}$ → $CD45.1_H$ mice having minimal C1q detection (**Appendix Fig 25A**). Compared to $B6_{BM}$ → $CD45.1_H$, $CD8^+$ T cells from the *C1qa*$^{-/-}$$_{BM}$ → $CD45.1_H$ group tended to

produce less granzyme B (**Fig 6-5G**), while there was no difference in $CD8^+$ production of IL-2 or IFN-γ in either group (**Appendix Fig 25B**).

To demonstrate *C1qa*$^{-/-}$ $CD8^+$ T cells were not intrinsically defective, a competitive adoptive transfer experiment of congenically labeled CD45.1 B6 vs CD45.2 *C1qa*$^{-/-}$ $CD8^+$ T cells into the same *Rag1*$^{-/-}$ recipient with reconstituted with CD45.1 $CD4^+$ T and B lymphocytes was performed (**Appendix Fig 25C**). No difference was observed in granzyme B or IFN-γ production in B6 vs *C1qa*$^{-/-}$ $CD8^+$ T cells in this model (**Appendix Fig 25D**).

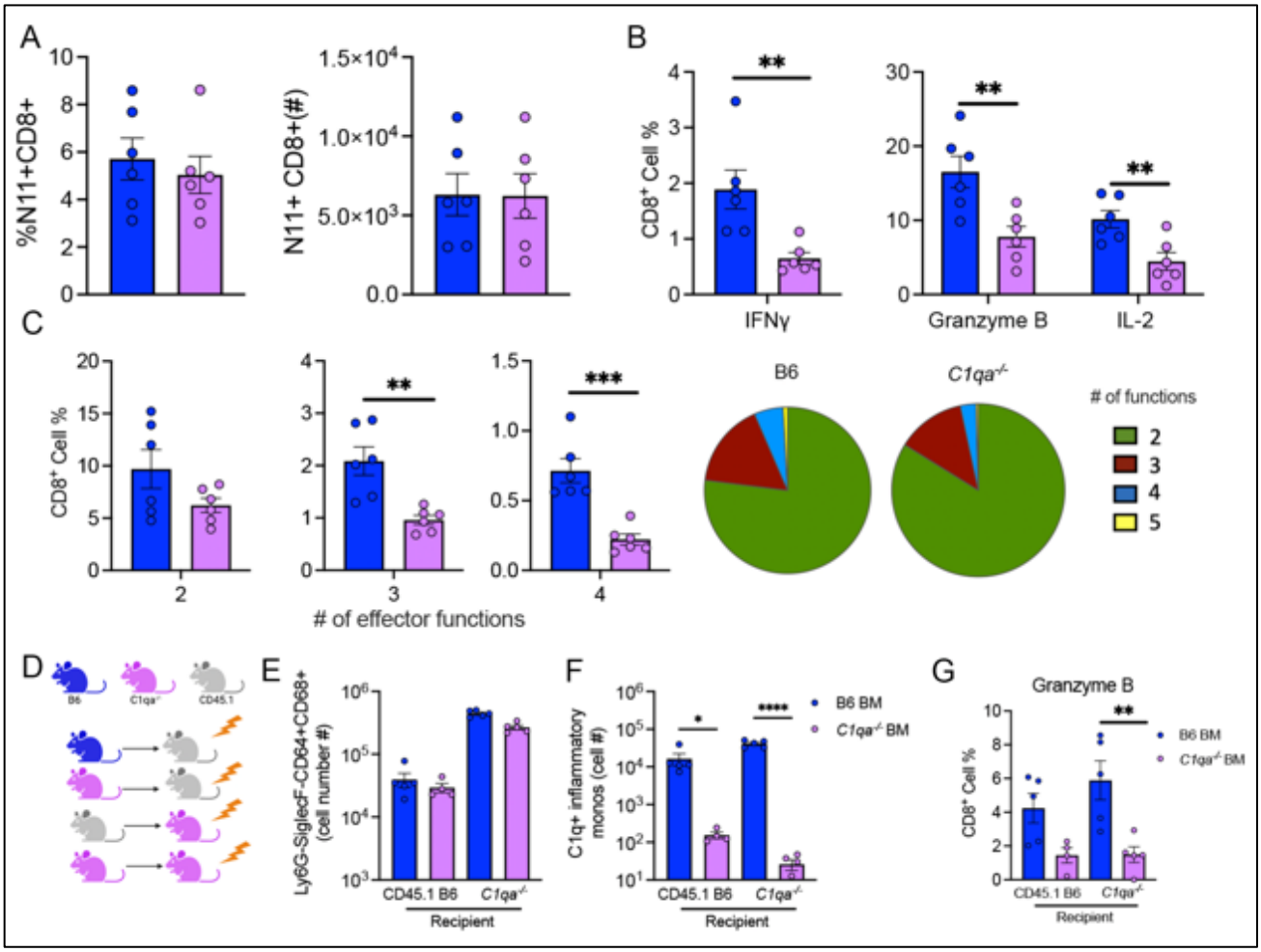

Figure 6-5. Absence of C1q leads to less functional $CD8^+$ T cells.

(A) Similar N11$^+$ CD8$^+$ T cells/CD3$^+$CD8$^+$ leukocytes in the lung between B6 and *C1qa*$^{-/-}$ in cell percent and absolute cell number. **(B)** CD8$^+$ T cells in *C1qa*$^{-/-}$ mice had impaired production of effector cytokines, granzyme B, IL-2, and IFN-γ. **(C)** Combinatorial analysis of functional markers revealed that CD8$^+$ T cells from *C1q*$^{-/-}$ mice produced significantly less 3 or 4 markers. Bar graphs (left) show raw data, pie charts (right) reflect summary of raw data. **(D)** Experimental schematic for fourway transplant. **(E)** Inflammatory monocyte cell number isolated from the lungs at day 7 postinfection in transplant model. **(F)** The recipients that received B6 BM had significantly more C1q producing inflammatory monocytes compared to recipients that received *C1qa*$^{-/-}$ BM. **(G)** Recipient mice that received *C1qa*$^{-/-}$ BM had CD8$^+$ T cells that produced less granzyme B compared to mice that received B6 BM. *p<0.05, ** p<0.01, *** p<0.005, **** p<0.001 by two way ANOVA with multiple comparisons. Data in A-C represents two experimental replicates, 3 mice/group/replicate. Data in D-G represents one experimental replicate 3-5 mice/group.

6.5.3 Blockade of gC1qR leads to reduced CD8 effector function.

As mice lacking myeloid-derived C1q had reduced CD8$^+$ T cell function following HMPV infection, we next assessed if C1q was directly acting on CD8$^+$ T cells. Recombinant C1q bound strongly to purified lung CD8$^+$ T cells from day seven post-HMPV infected *C1qa*$^{-/-}$ animals (**Fig 6-6A**). To assess possible receptors for C1q on CD8$^+$ T cells, we further analyzed the T cell compartment from the single cell RNA sequencing dataset, identifying naïve, effector, dividing, and nonspecific subsets (**Fig 6-6B**). One extracellular receptor for C1q, gC1qR (i.e. C1qbp), was expressed on a subset of dividing, cytotoxic CD8$^+$ T cells with increased expression of *Mki67* and on *Gzmb* CD8$^+$ T cells (**Figs 6-6C**, **Appendix Fig 26A**) (275). Both the dividing and non-dividing CD8$^+$ T cell effector populations were significantly expanded in HMPV infected animals by permutation testing (**Fig 6-6D, Appendix Fig 26B**). Additional C1q receptors were also assessed, with calreticulin (*Calr*) representing the only other notable receptor expressed within T cells (**Appendix Fig 26A**). Calreticulin is primarily surface bound on apoptotic cells and plays a critical

role in complement-mediated clearance of cell debris (276, 277). Since these analyses suggested gC1qR as a surface bound C1q receptor on $CD8^+$ T cells, we subsequently utilized a blocking antibody on *ex vivo* stimulated lung cells from mice infected with HMPV. Production of IFN-γ was abrogated in cells treated with N11 HMPV peptide (a dominant MHC class I peptide) and α-gC1qR antibody (**Fig 6-6E**). As described previously, IFN-γ production was enhanced following blockade of PD-L1 (**Fig 6-6E**) (61). However, αgC1qR treatment reduced IFN-γ production even in the presence of PD-L1 blockade, suggesting two distinct pathways of IFN-γ regulation in $CD8^+$ T cells (**Fig 6-6E**). IL-2, IFN-γ, and downstream IFN response genes *Cxcl10* and *Cxc9* protein levels were also decreased when cells were treated with αgC1qR and combination treatment; again, αgC1qR blockade reduced production of these cytokines despite the presence of PD-L1 blockade (**Appendix Fig 27**). Moreover, cells treated with recombinant C1q also demonstrated an upregulation of IFN-γ production, which was again blunted by αgC1qR blockade (**Fig 6-6E**).

C1q has previously been shown to regulate $CD8^+$ T cell metabolism and function in a chronic viral infection model (257). To that end, purified $CD8^+$ T cells isolated from the lungs at day seven post-HMPV infection showed a diminished spare respiratory capacity (SRC) when treated with αgC1qR antibody (**Fig 6-6F**). Given the expression of gC1qR on rapidly dividing $CD8^+$ T cells, proliferation was next assessed using an *ex vivo* co-culture model whereby B6 $CD8^+$ T cells isolated from HMPV infected mice were stimulated with peptide for 48 hours in the presence of *C1qa*$^{-/-}$ monocytes (**Fig 6-6G**). Recombinant C1q administration led to increased Ki67MKI67 expression within $CD8^+$ T cells (**Fig 6-6G**). Treatment with αgC1qR had no effect on cell division in the absence of C1q, but blunted the C1q-induced MKI67 expression (**Fig 6-6G**). Furthermore, administration of anti-gC1qR Ab *in vivo* significantly reduced granzyme B production in CD8 T

cells during HMPV infection, with a trend in reduced IFNγ as well (**Fig 6-6H**). Collectively, these data demonstrate a critical role for gC1qR receptor in maintaining optimal CD8$^+$ T cell effector function and metabolic capacity that functions independently of PDL1 signaling.

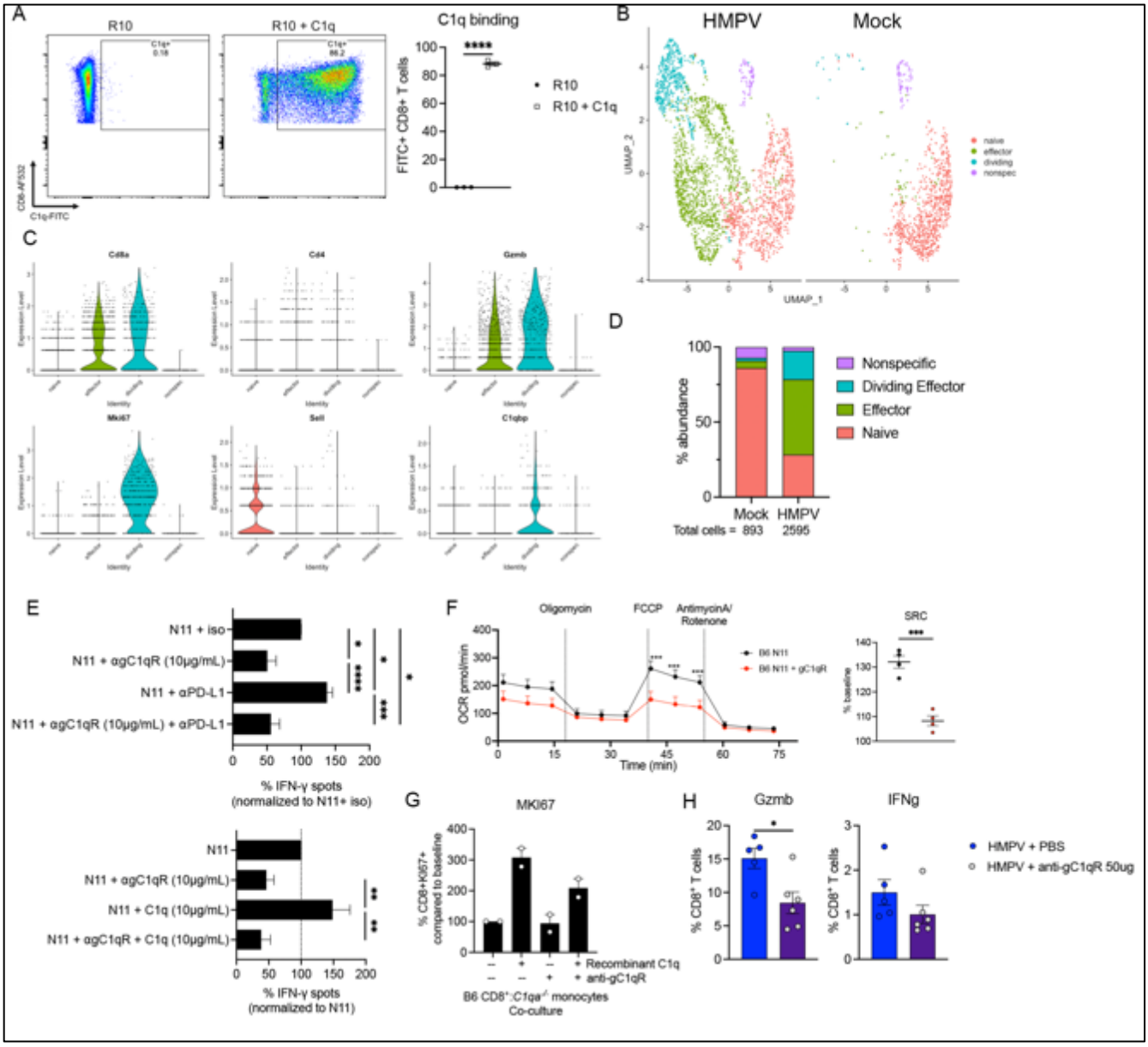

Figure 6-6. gC1qR blockade leads to reduced CD8$^+$ T cell function.

(A) C1q bound to cultured murine CD8$^+$ T cells. Representative flow plots (left), quantification of C1q-FITC$^+$ CD8$^+$ T cells (right). Data shown of one replicate, n=3 **(B)** UMAP visualization of T cells by single cell RNA sequencing split by infection status. **(C)** Violin plots showing expression of C1QBP (i.e gC1qR), CD8, SELL,

CD4, GZMB, and MKI67. **(D)** Abundance plots of T cell subsets. **(E)** ELISpot of IFN-γ in murine lung lymphocytes undergoing ex vivo Class I peptide stimulation on day 7 p.i. +/- αgC1qR treatment. Additionally, PDL1 blockade increased IFN-γ production, combination treatment resulted in decreased IFN-γ production (top). Bottom panel shows IFN-γ ELISpot with addition of recombinant C1q +/- αgC1qR. Two replicates, n=3/group/replicate, performed in triplicate. **(F)** Purified $CD8^+$ T cells on day 7 p.i. had diminished spare respiratory capacity (SRC) when treated with αgC1qR. *p<0.05, ** p<0.01, *** p<0.005, **** p<0.001 by unpaired t-test or two-way ANOVA with multiple comparisons. **(G)** Co-culture of 50,000 B6 $CD8^+$ T cells and 50,000 *C1qa*$^{-/-}$ monocytes isolated from mice at day 7 post-infection, followed by 48-hour stimulation with HMPV peptides plus 10 μg of C1q and/or 10 μg αgC1qR. Cells were then stained for Ki67 via flow cytometry to assess cell division. N=2, one replicate, normalized to untreated stimulated condition. **(H)** Administration of αgC1qR oropharyngeally in vivo on day 5 and 6 post-infection reduces CD8 T cell effector function. Two replicates, n=2-3/group/replicate, *p<0.05 by student's t-test.

6.5.4 C1q in human respiratory viral infection.

The production of C1q by myeloid populations is one of myriad differences between murine and human immunology. Human alveolar macrophages produce C1q at steady state, while C1q production in mice is often limited to interstitial macrophages and recruited alveolar macrophages post-inflammatory stimulus (278-280). However, we tested whether respiratory viral infection altered C1q production in the lung by using immunofluorescent staining on archived pediatric lung specimens. In a child who had a partial lung resection due to pleural blebs, C1q was visualized in the alveolar spaces (**Fig 6-7A, top**). In a case of fatal HMPV infection, the location of $C1q^+$ cells markedly shifted to the interstitial and perivascular spaces (**Fig 6-7A, middle**). Likewise, staining from a fatal case of mixed rhinovirus/parainfluenza virus pneumonia showed numerous interstitial and perivascular inflammatory cells producing C1q (**Fig 6-7A, bottom**).

We next queried publicly available single-cell RNA sequencing data from bronchoalveolar immune cells in humans with COVID-19 infection (270). Healthy control participants and moderate COVID-19 patients had high levels of C1q production at baseline in BAL specimens, while severe COVID-19 patients had a loss of C1q expression (**Fig 6-7B**). Evaluation of the T cell compartment in this data set demonstrated an increase in both dividing $CD8^+$ and $CD4^+$ T cell populations in moderate and severe COVID-19 disease (**Fig 6-7C-D, Appendix Fig 28A**). Notably, gC1qR (gene:*C1QBP*) expression could be noted on all T cell populations, but was most abundantly expressed on the rapidly dividing $CD8^+$ T cell population (**Appendix Fig 28B**). Using differential gene expression analysis, *C1QBP* expression was significantly upregulated in dividing CD8s in severe COVID-19 disease compared to moderate disease (**Appendix Fig 28C**). Similar to the animal model of HMPV, *C1QBP* and *MKI67* expression largely co-localized to the rapidly dividing CD8 cluster (**Fig 6-7E**). Collectively, these data demonstrate altered C1q production in the human lung following respiratory viral infection and the presence of a known receptor for globular C1q on $CD8^+$ T cells.

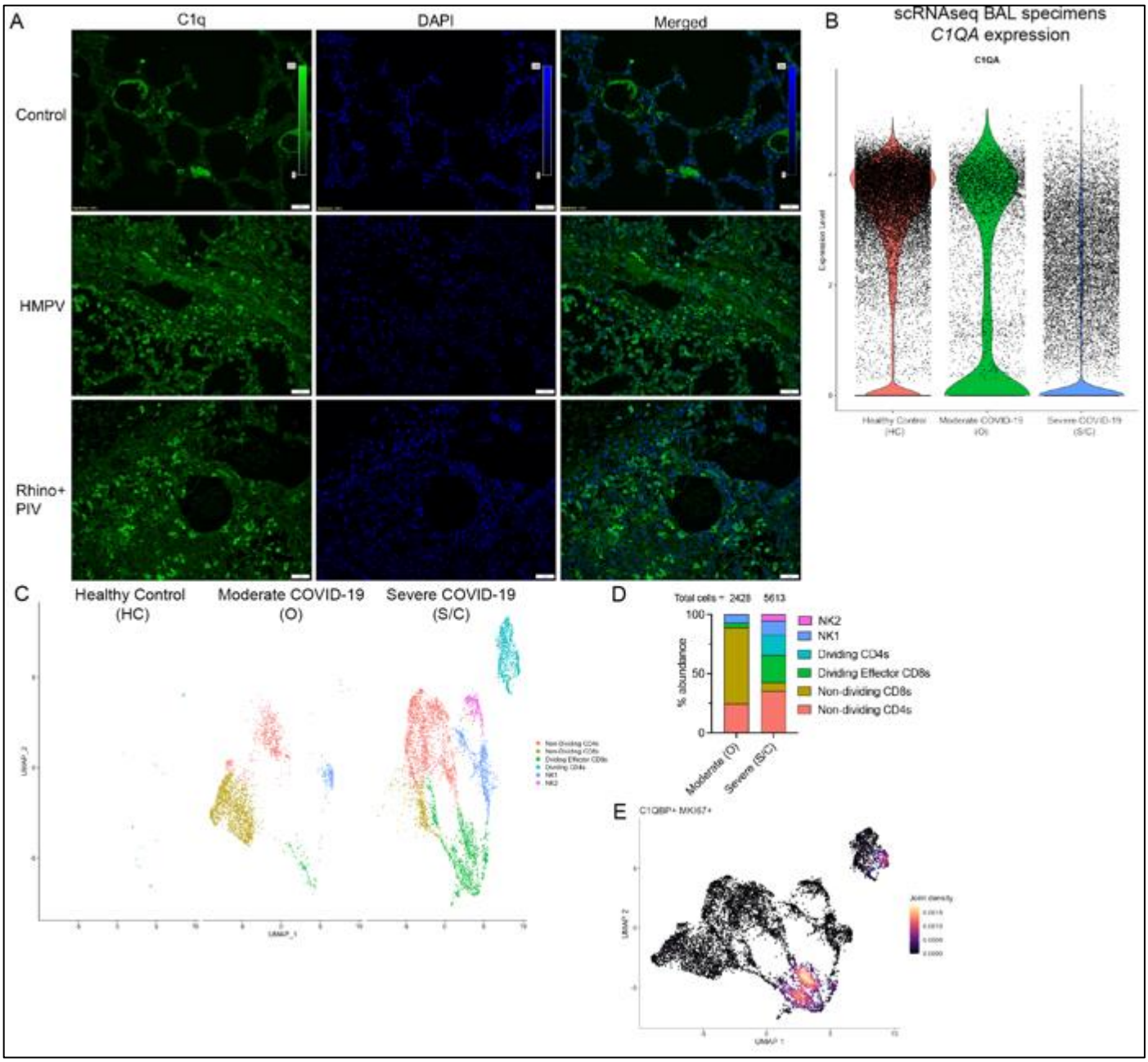

Figure 6-7. Evidence of C1q:gC1qR axis in humans with respiratory viral infections.

(A) Immunofluorescent staining of human lung tissue (top: resection from child with pleural blebs, middle: autopsy specimen from a child who succumbed to HMPV, bottom: autopsy specimen from a child who succumbed to rhinovirus/parainfluenza (PIV) infection). C1q (green) is present in alveolar spaces in healthy child with re-distribution to interstitial spaces in infectious conditions. **(B)** C1QA expression (left) is reduced in severe COVID-19 (S/C) infection compared to healthy controls (HC) or moderate cases (O). **(C)** UMAPs of the subset of T cells from overall dataset separated by disease state. **(D)** Abundance plots of various subsets

in moderate vs. severe COVID-19 disease showing. **(E)** Co-expression of MKI67 (marker of rapid division) and C1QBP is largely confined to rapidly dividing CD8 cluster.

6.6 Discussion

Taken together, our data identify an integral role for C1q signaling in respiratory viral infection. Three key findings from this study include: (1) there is a novel inflammatory monocyte population that produces C1q concomitant with adaptive immune-mediated clearance of virus; (2) C1q directly impacts $CD8^+$ T cell function in our murine model; and (3) the C1q/gC1qR axis presents a possible mechanism as to how monocyte-derived C1q regulates $CD8^+$ T cell function in both mice and humans across multiple respiratory viral pathogens.

C1q is canonically thought of as the initiator of the classical complement pathway in the innate immune response (255). However, C1q has also been implicated in both homeostasis and inflammation, including clearance of apoptotic debris and recognition of damage/pathogen associated molecular patterns with resultant phagocytosis of extracellular pathogens (281). Previous studies in cancer and autoimmunity models in mice identified inflammatory monocytes and macrophages as key producers of C1q, which facilitates a unique role of C1q independent of the complement cascade (256-259).

Here, we demonstrate a novel role of a C1q-producing myeloid population that promotes $CD8^+$T cell function following respiratory viral infection in our murine model. During HMPV infection, the absence of C1q resulted in diminished effector $CD8^+$ T cell polyfunctionality and severe

clinical disease when infected with a virulent strain of HMPV. In contrast to our data, in chronic LCMV infection in *C1qa*$^{-/-}$ mice, CD8^{+} T cells differentiated into short-lived effector cells with diminished metabolic capacity but more potent effector activity (257). These data suggest that the duration of infection/exposure to antigen may play a role in this regulatory pathway on CD8^{+} T cells, as pathogen-specific antibody and/or immune complex formation may alter the effects of C1q on CD8^{+} T cells.

There are differences between murine and human C1q production in the lung. In the human lung, alveolar macrophages produce C1q at baseline, while mice have negligible C1q production in the absence of infection (278-280). In staining of human lung tissue, C1q could be distinctly seen in the alveolar spaces of a lung section from an uninfected child; this distribution changed dramatically to an interstitial population in the setting of lethal respiratory viral infection, consistent with our animal model. Additionally, single cell sequencing of the myeloid compartment in humans infected with COVID-19 revealed C1q as a differentially expressed gene in alveolar macrophages, although some expression was observed in monocyte-derived macrophages (282). Interestingly, C1q transcript was lost in the cells isolated from bronchoalveolar lavage fluid from patients with severe COVID. These data, coupled with the immunofluorescent images shown in our study, suggest that the cell type and location of C1q production shifts during acute respiratory viral infection in humans.

The next question we addressed is how communication between C1q and CD8^{+} T cells is mediated. C1q has previously been shown to bind to human CD8^{+} T cells, with increased binding following in vitro stimulation (283). Similarly, our data show that following HMPV infection murine CD8^{+}

T cells readily bound C1q. This is of note because C1q can bind to apoptotic cells to promote phagocytosis, and to the Fc receptor of IgG antibodies to initiate the classical complement pathway (284). However, the most notable receptor for C1q in the context of the immune response, gC1qR (i.e. C1q binding protein, C1qBP), recognizes the globular head of the C1q polypeptide and has been shown to play a critical role in mitochondrial fitness (269, 275, 285). In addition to C1q, gC1qR has numerous ligands, including high molecular weight kininogen (HK), Factor XII (Hageman factor), fibrinogen, thrombin, calreticulin, and multimeric vitronectin (266, 267). However, we show a unique role of gC1qR where rapidly dividing $CD8^+$ T cells during HMPV infection upregulated gC1qR expression in our murine model and in patients with severe COVID-19. These findings are consistent with a prior study which demonstrated that gC1qR is abundantly expressed on human $CD8^+$ T cells in the setting of chronic hepatitis C infection (268). Subsequent *in vitro* blockade of gC1qR led to reduced effector function and cell division in our model. Blocking gC1qR signaling in $CD8^+$ T cells from the murine lung following HMPV infection also led to reduced metabolic capacity, similar to a prior study assessing the metabolomics of *C1qa*$^{-/-}$ $CD8^+$ T cells in the LCMV chronic model (257). Collectively, these data identify gC1qR as at least one of the critical C1q receptors required for optimal $CD8^+$ T cell function in multiple respiratory viral models.

There are limitations and possible future directions from the current study. First, *C1qa*$^{-/-}$ mice cleared HMPV comparably to wild type mice, despite the diminished $CD8^+$ T cell effector function. However, in our C-202 model and in prior LCMV models, *C1qa*$^{-/-}$ mice have increased pathology (257). These findings may suggest effective, but pathologic, alternative mechanisms of clearance in the absence of C1q, which would warrant further study of other anti-viral cell types

such as NK cells. Second, restoration of $CD8^+$ T cell functionality following B6 hematopoietic stem cell transplantation was noted with granzyme B production, but not other effector functions. These data support a role for C1q in $CD8^+$ T cell responses, but the effects may be limited by the negative effects of whole body radiation in the absence of C1q (286). The interplay between C1q, $CD8^+$ T cell function, and pathogen-specific antibody could also be explored mechanistically by passive convalescent serum transfer in *C1qa*$^{-/-}$ mice and/or rechallenge experiments. The latter would also be fascinating in the context of $CD8^+$ T cell memory formation in the absence of C1q. Further evaluation of the C1q/gC1qR axis in both mouse models and human samples are warranted. gC1qR loss of function is poorly tolerated in T cells, with an *in vitro* knockdown approach in mice resulting in diminished proliferative capacity, increased mitochondrial membrane permeability, and ultimately increased apoptotic cell death (269). This makes it technically challenging to completely knock out the gC1qR receptor on $CD8^+$ T cells, as this will have detrimental effects to the survival of $CD8^+$ T cells, but also underscores the importance of this receptor in $CD8^+$ T cell fitness. In a chimeric antigen receptor (CAR) T cell system, heterozygosity of gC1qR lead to reduced $CD8^+$ T cell effector function and increased tumor burden (269), which supports our hypothesis that gC1qR signaling on $CD8^+$ T cells is crucial to their function. One future study could assess serum C1q levels in acute disease or *ex vivo* manipulation of gC1qR from cells isolated from infected patients which could provide insights into the potential diagnostic and/or therapeutic potential of this pathway.

Collectively, the current study identifies a novel C1q-producing monocyte population and elucidates a potential mechanism of how C1q signaling via gC1qR on $CD8^+$ T cells can regulate optimal $CD8^+$ cytotoxic antiviral effector function during respiratory viral infections.

7.0 Overall Discussion & Future Directions

This thesis has examined the aged $CD8^+$ T cell response and the role of the complement protein, C1q, in regulating $CD8^+$ T cell function during HMPV infection. There are several key conclusions from these studies: (1) we developed an aged mouse model of severe HMPV disease for both primary infection and re-challenge; (2) the functional deficits in aged $CD8^+$ T cells are primarily cell intrinsic; (3) an exhausted $CD8^+$ T cell population accumulated in the aged lung independent from HMPV infection; (4) PD-1 blockade selectively increased granzyme B production in aged $CD8^+$ T cells; (5) our vaccination strategies were unsuccessful in aged mice; and (6) we identified a novel role for C1q-producing inflammatory monocytes in regulating optimal $CD8^+$ T cell antiviral function.

We developed an aged mouse model of severe HMPV disease for both primary infection and re-challenge. Using this mouse model for primary infection experiments, 6-7wk and 70-71wk old mice were infected with HMPV and euthanized on day seven post-infection with weights and clinical scores taken daily. Only one prior study investigated the aged immune response to HMPV using mice (169). This study used 18-month-old BALB/c mice and only assessed bulk CD8, CD4, and B cells, but not the viral specific T cell response (169). Our aged mouse model, transplant model, and the HMPV tetramer tools available in our lab allowed us to quantitate and characterize the antigen-specific $CD8^+$ T cell response (**Fig 2-2)** as well as the intrinsic and extrinsic factors affecting aged $CD8^+$ T cell function (**Fig 2-4 & 2-5**). We found, through depletion studies, that $CD8^+$ T cells were not solely responsible for weight loss and viral clearance (**Appendix Fig 1**). Both aged and young HMPV-infected mice still cleared virus and aged mice still lost weight during

infection (**Appendix Fig 1**). These findings are consistent with previous reports showing the dual role of both $CD4^+$ and $CD8^+$ T cells in controlling weight loss and viral clearance (51). $CD4^+$ T cells also undergo epigenetic changes with increased age and exhibit dysfunction during infection (287). Future work could assess the HMPV-specific $CD4^+$ T cell response in our aged mouse model as this may further inform what was observed in aged $CD8^+$ T cells and overall clinical disease.

Considering that the majority of children are seropositive for HMPV by five years of age (1), it is likely that elderly humans with severe HMPV disease are actually experiencing re-infections. Therefore, we developed a more physiologic aged mouse model where B6 mice were infected at 6-7wks, aged-in-house until 70-71wks, and re-infected. Aged re-challenged mice accumulated cytotoxic $CD69^+$ $CD103^+$ tissue resident memory $CD8^+$ T cells (T_{RM}) (**Fig 3-2**). Upon re-challenge, aged mice lost weight similar to aged primary infected mice, but had no detectable virus in lungs (**Fig 3-1B & C**). This was most likely due to either enhanced viral clearance by memory $CD8^+$ and $CD4^+$ T cells or due to the fact that HMPV is semi-permissive in mice and antibodies neutralized the virus. Aged re-challenge mice did have a robust IgG HMPV response, which could indicate that the virus was neutralized upon re-infection (**Fig 3-1D**). Dysfunction in the humoral response has been implicated in vaccine ineffectiveness in the elderly (190). Furthermore, studies in both HMPV (193) and RSV (94, 194) have shown that re-infections can still occur despite a high neutralizing titer, which indicates the crucial role in the cell-mediated memory response in controlling infection. Future directions should investigate the contribution of B cells in impairing the $CD8^+$ memory T cell response and assess the neutralizing or other functional capacity of antibodies in both our aged mouse model and patient samples from elderly humans.

The functional deficits in aged $CD8^+$ T cells are primarily cell intrinsic. In our aged mouse model, $CD8^+$ T cells co-expressed more inhibitory receptors (**Fig 2-3A & B**) and produced less granzyme B (**Fig 2-3D & E)**, which has been observed in both mice (150) and elderly humans infected with COVID-19 (170). When we performed syngeneic transplants and adoptive transfers with congenically marked cells, we found that the aged $CD8^+$ T cell phenotype and clinical disease was partially recapitulated (**Fig 2-4 & 2-5**). Since aging affects multiple immune cells including somatic cells (117, 130), we suspect that other cell types are involved in $CD8^+$ T cell function and clinical disease during infection. Future studies should examine aged myeloid cells as this population plays a significant role in raising the basal secretion of pro-inflammatory cytokines (i.e. inflammaging) (117, 130). Parabiosis between aged and young mice would also be a useful way to assess the role of secreted pro-inflammatory factors from somatic cells. Parabiotic studies have found that exposing aged mice to a young circulation improves endothelial cell function (288) and reactivated aged skeletal stem cells, which ameliorated the pro-inflammatory microenvironment (289)

Having identified an aged $CD8^+$ T cell phenotype during HMPV infection, we wanted to further characterize these $CD8^+$ T cells. With increasing age, the naïve T cell compartment diminishes as chronic antigen stimulation leads to the accumulation of memory T cells (290). During other sustained antigen simulation states such as chronic viral infection (57) and cancer (56),, $CD8^+$ T cells develop an exhausted phenotype where they lose expression of TCF1/7 – a stem-cell transcription factor – and become positive for the exhaustion transcription factors, thymocyte selection associated high mobility group box (TOX) and eomesodermin (EOMES). In our model, we found exhausted $CD8^+$ T cells accumulated in the aged lung independent from HMPV infection

(**Fig 2-6A & B**). CD4 depletion studies revealed that this $CD8^+$ T cell phenotype represented canonical exhaustion, as there was no difference in the frequency of this population between isotype and αCD4-treated aged mice (**Fig 2-6C**).

Next we asked whether there was a way to reverse and rejuvenate exhausted aged $CD8^+$ T cells. Terminal exhaustion in chronic viral infection has been indirectly targeted by using PD-1 blockade, which expands a $TCF1/7^+$ $CD8^+$ T cell population (179). In addition, in cancer models, either PD-1 blockade or 4-1BB agonism was successful in reversing tumor-infiltrating lymphocyte (TIL) exhaustion (167, 180). *In vitro* treatment with Abs to PD-1, 4-1BB, or a combination failed to improve the function of aged $CD8^+$ T cells in our model (**Appendix Fig 7**). We further examined the effect of PD-1 signaling using *in vivo* PD-1 blockade and found no difference in the accumulation of $Tcf1/7^-$ Tox^+ $Eomes^+$ $CD8^+$ T cells in either model (**Appendix Fig 14I-K**). Future studies should focus on other modalities to rejuvenate exhausted $CD8^+$ T cells and the effects of somatic and immune cell senescence on the exhausted $CD8^+$ T cell phenotype.

Senescence refers to the inability to repair DNA damage and replication errors, which leads to apoptotic cells, build up of cellular debris, development of autoreactive T cells, and chronic antigen stimulation, promoting T cell exhaustion (291). Rapamycin, an mTOR inhibitor, has shown promising results in reducing senescence in immune cells, leading to an improved immune response (291, 292). In addition, anti-senescence drugs, such as dasatinib and quercetin, have been shown to ameliorate senescence in the intestine of aged mice and improve gut microbiome homeostasis (293). Lastly, studies have recently developed CAR T cells that target the ligand natural killer group 2 member D (NKG2D) (294) or the cell-surface protein, uPAR (295), which

are heavily expressed on senescent cells (295). Future studies investigating these potential treatments in our model could improve the immune response to HMPV in elderly humans.

Although PD-1 blockade did not change the proportion of $Tcf1^{-}$ Tox^{+} $Eomes^{+}$ exhausted $CD8^{+}$ T cells, in the absence of PD-1 signaling, $CD44^{+}$ $CD62L^{-}$ $CD8^{+}$ effector T cells did have improved granzyme B production (**Fig 4-2H; 4-3G**). This finding suggests a nexus between PD-1 and granzyme B. One study used granzyme B production from human PBMCs as a determinant and predictive biomarker of successful PD-1/PD-L1 immunotherapy blockade (296). Another study found that $CD8^{+}$ T cell exhaustion can still occur in the absence of PD-1 signaling (223). Rather, blocking PD-1 resulted in the accumulation of more cytotoxic, differentiated $CD8^{+}$ T cells (223), which could explain our findings of the selective increase in granzyme B production. Future directions should focus on combining PD-1 blockade with a senolytic, anti-senescence drug to promote both rejuvenated and cytotoxic $CD8^{+}$ T cell proliferation in elderly humans infected with HMPV.

Currently there are no available vaccines for HMPV. Re-infections occur throughout life, indicating that immunity to HMPV is incomplete (1). Therefore, developing an effective vaccine against HMPV is imperative. Older adults often have a poor memory response to vaccines and require higher vaccine doses or adjuvanted vaccines (190-192). Our lab and others have previously tested several vaccine strategies in rodents (52, 202, 204), nonhuman primates (205, 206), and humans (207, 208). We tested two vaccination strategies in our aged mouse model: LPS adjuvanted HMPV cognate peptide (**Fig 3-5 & 3-6**) and UV-inactivated virus (**Fig 3-7**). Both vaccination strategies were unsuccessful in aged mice. Aged mice mounted a poor $CD8^{+}$ T_{RM}

response (**Fig 3-5C & 5D; 3-6G & H**), co-expressed more inhibitory receptors (**Fig 3-5F; Appendix 11G & H**), and produced less IFNγ (**Fig 3-5G & H; 3-6K & L**). Phase I clinical trials have been completed for an mRNA-based HMPV vaccine and have yielded promising results (297). However, this study only assessed vaccine efficacy in adults 18-49 years old (297). Future studies should investigate the efficacy of this mRNA vaccine in older adults, who are at greater risk from HMPV.

Lastly, this thesis identified a novel role for C1q-producing inflammatory monocytes. Monocytes producing C1q promoted optimal $CD8^+$ T cell antiviral function. C1q signaling via gC1qR expressed on $CD8^+$ T cells, improved $CD8^+$ T cell function during HMPV infection in mice (**Fig 6-6**) and may be an integral part of the immune response to multiple respiratory infections in humans (**Fig 6-7**). These findings indicate that the PD-L/PD-1 signaling axis is not the only regulator of antiviral $CD8^+$ T cells during HMPV infection, which is a novel finding. A previous study in mice infected with LCMV also identified a nexus between C1q and $CD8^+$ T cell function (257). However, this study found that in the absence of C1q, $CD8^+$ T cells had reduced metabolic capacity and differentiated into short-lived effector cells (257). These findings suggest that the effects of C1q on $CD8^+$ T cell function depend on whether the infection is acute or chronic. Future studies should focus on the mechanism behind gC1qR signaling in $CD8^+$ T cells by using a CAR T cell model that ablates 50% of gC1qR expression from $CD8^+$ T cells (269). This leads to impaired $CD8^+$ CAR T cell function against tumors, indicating a vital role of gC1qR in $CD8^+$ T cell function. In addition, the C1q/gC1qR signaling axis should be examined in our aged mouse model to further elucidate how C1q impacts aged $CD8^+$ T cell function.

Taken together, the work described in this thesis has uncovered novel findings regarding the role of age and C1q on $CD8^+$ T cell function during HMPV infection. We developed several mouse models to study the antiviral $CD8^+$ T cell response and generated data that serve as a foundation for future research, which will prompt further studies of treatment modalities and vaccine development to prevent severe clinical disease in vulnerable populations.

8.0 Discussion: Relation to Health and Disease

This project has implications for future research and potential clinical trials to develop novel vaccine and treatments for elderly patients infected with respiratory viruses. Aging is multifactorial and affects virtually every somatic cell, including immune cells, which can make it difficult to pinpoint one signaling pathway or cell type that is driving severe respiratory disease. However, our mouse models provided valuable tools to elucidate the aged $CD8^+$ T cell response and assess how much of the clinical severity we observed was due to cell-intrinsic $CD8^+$ T cell dysfunction versus extrinsic factors (i.e. inflammaging, myeloid cells, or $CD4^+$ T cells).

From these studies, it isis clear that $CD8^+$ T cells play an important role in facilitating severe HMPV disease, but our transplant models revealed that the aged microenvironment and other cells types are likely involved as well. In addition, our scRNAseq and studies in *C1qa*$^{-/-}$ mice revealed that PD-1 signaling is not the only pathway directly influencing $CD8^+$ T cell antiviral function.

Currently, there is no available licensed vaccine for HMPV. Since cell-mediated memory wanes in aged individuals, including in response to vaccines, successful vaccine development would involve developing a multivalent vaccine to several HMPV epitopes that includes an adjuvant that would activate the aged immune response to mount a sufficient memory T cell response.

The most promising avenues to explore in future research in addition to vaccine development would involve anti-senolytic agents (i.e. dasatinib), mTOR inhibitors (rapamycin), immunotherapy (PD-1 blockade), or administering recombinant C1q. A combination of these

therapies might yield synergistic effects and eventually be valuable in clinical settings to improve the antiviral immune response and ameliorate clinical disease.

Appendix A Appendices and Supplemental Content

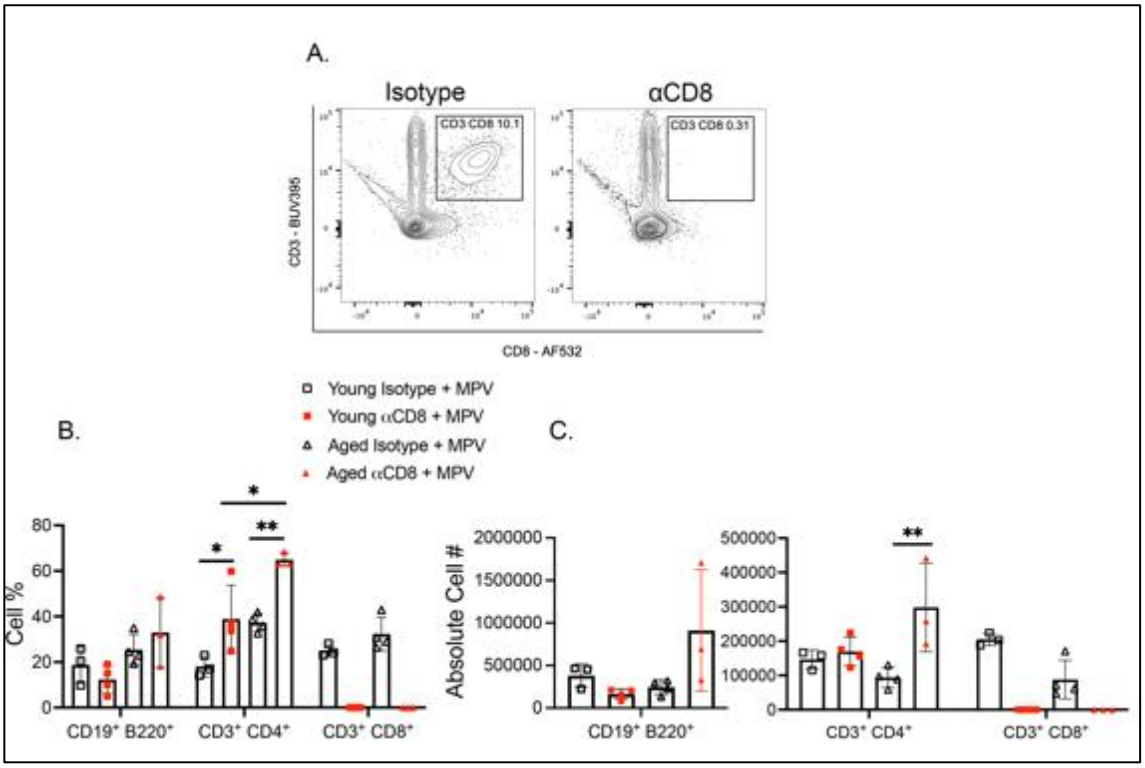

Appendix Figure 1. There was an increase in $CD4^+$ T cells with $CD8^+$ depletion

(A) Aged and young mice were treated with 300 μg CD8 or rat isotype control Ab one day prior to infection and 150 μg every other day post-infection via intraperitoneal injection. Representative flow plots from isotype control and CD8 treated on day 5 p.i. **(B & C)** There was an increase in $CD4^+$ T cells by cell percent in both age groups at day 7 p.i. and an increase in $CD4^+$ absolute cell number in aged $CD8^+$ depleted mice. *P<0.05, **P<0.01, one-way ANOVA.

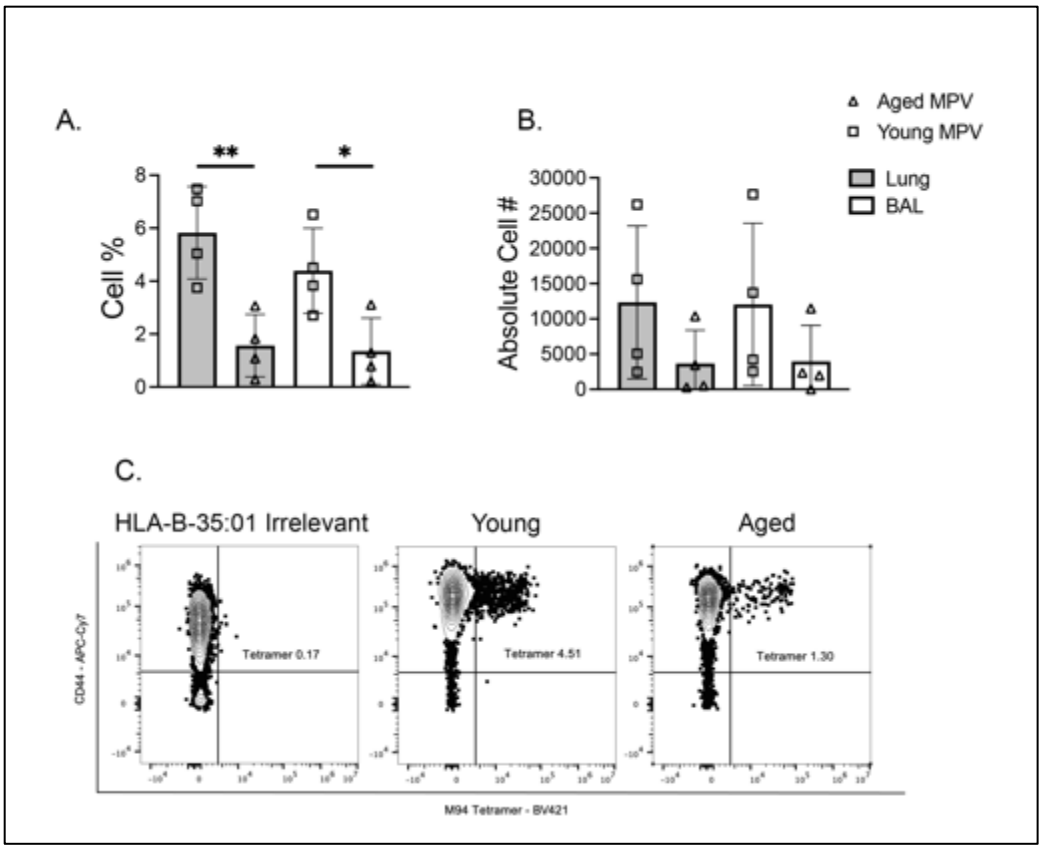

Appendix Figure 2. The impaired tetramer response in aged mice was no epitope specific.

(A) Aged infected mice had decreased $CD8^+$ M94 $tetramer^+$ cells in lung (shaded bars) and BAL (open bars) compared to young infected mice at day 7 p.i.. **(B)** Absolute cell number of $M94^+$ $CD8^+$ T cells. **(C)** Representative flow plots of tetramer staining on activated $CD44^+$ $CD8^+$ T cells. *P<0.05, unpaired t-test.

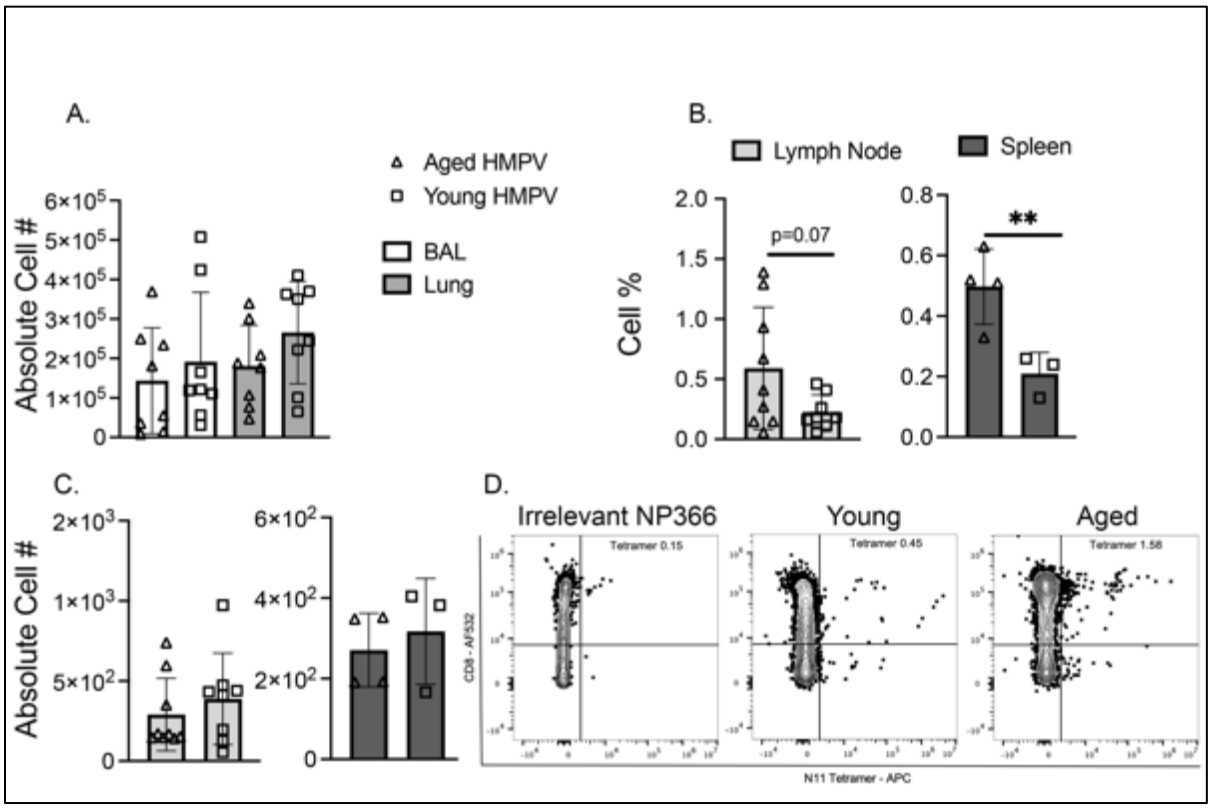

Appendix Figure 3. Similar CD8$^+$ counts and minimal tet$^+$ cells in secondary lymphoid organs.

(A) There was no difference between age groups in total CD8$^+$ T cells in either lung or BAL at day 7 p.i. **(B & C)** Aged mice tended to have more HMPV-specific CD8$^+$ T cells by cell percent in the draining lymph nodes and spleen, but there was no difference between the two age groups in absolute cell number. **(D)** Representative flow plots of aged and young infected lymph nodes on day 7 p.i. with influenza NP366 irrelevant tetramer as a control.

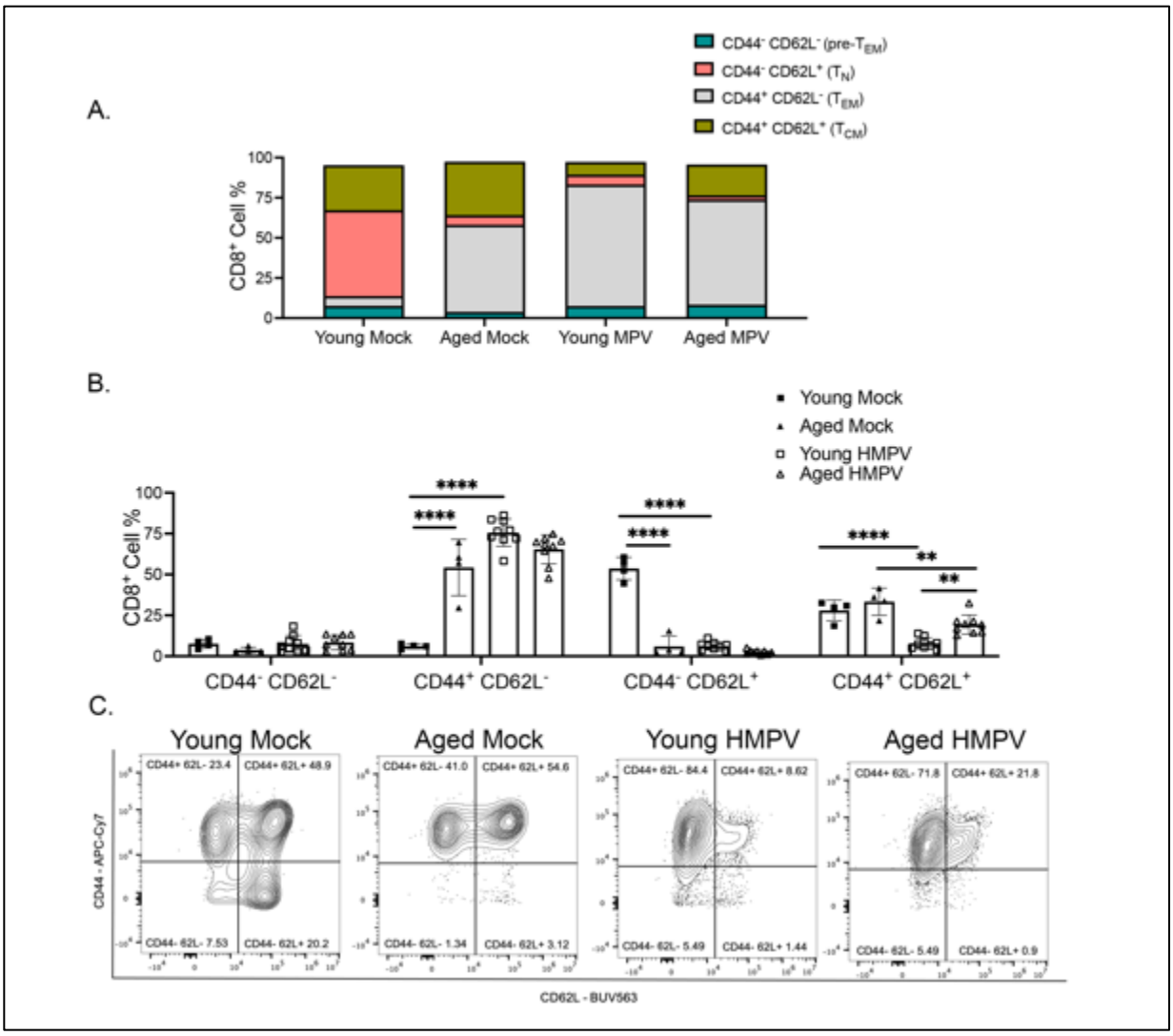

Appendix Figure 4. Aged mice had fewer CD44$^-$ CD62L$^+$ CD8$^+$ T cells in the lung.

(A & B) Uninfected aged mice at baseline had significantly fewer naïve CD8$^+$ CD44$^-$ CD62L$^+$ T cells (T_N) in the lung compared to uninfected young mice. Upon infection, young mice had a robust increase in CD8$^+$ CD44$^+$ CD62L$^-$ effector memory cells (T_{EM}) while aged mice had only a modest increase. Bar graphs showing the composition of CD44 and CD62L expression in CD8$^+$ T cells shown in **A** with raw data points shown in **B**. **(C)** Representative flow plots of CD44 and CD62L expression shown for each age group and infection status.

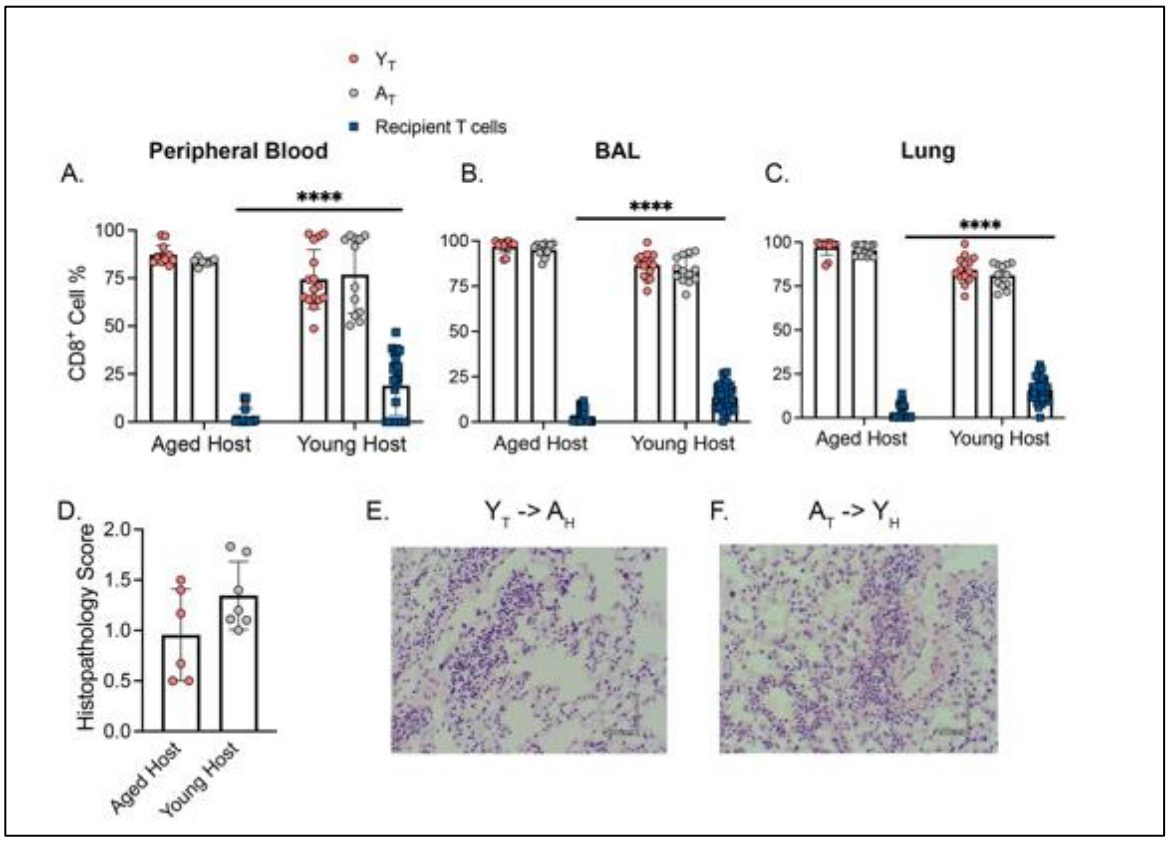

Appendix Figure 5. No significant differences in donor T cell engraftment in transplant models.

(A-C) Mice were bled by submandibular venipuncture 5 weeks post-irradiation and transplant. Lymphocytes were stained with congenic markers CD45.1 and CD45.2 to determine donor cell engraftment. Graph shows the relative frequencies of donor and recipient $CD8^+$ T lymphocytes from peripheral blood, BAL, and lung, respectively. There was a difference in recipient cells remaining in aged and young hosts, but no significant differences in donor T cell engraftment. **(D)** A_T -> Y_H tended to have a higher histopathology score compared to Y_T -> A_H at day 7 p.i.. **(E & F)** Representative histology shown. ****P<0.0001, unpaired t-test.

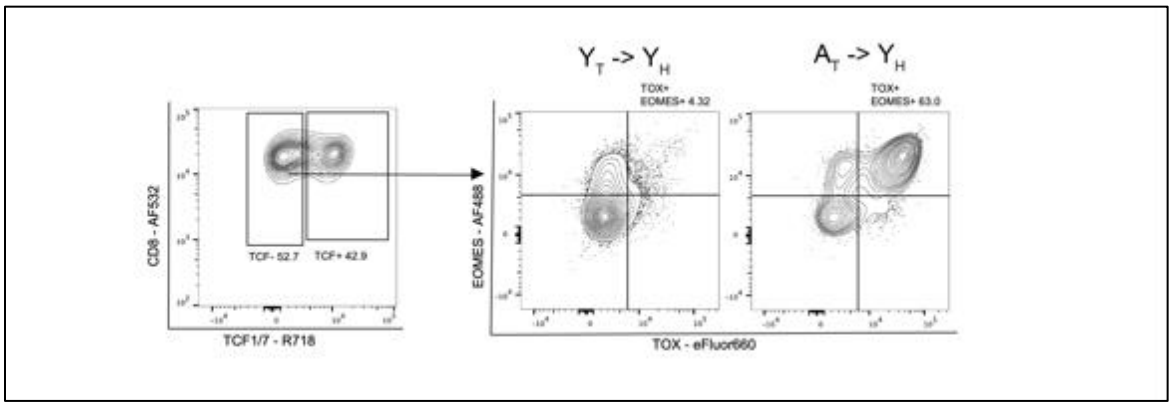

Appendix Figure 6. Representative flow plots of T_{EX} $CD8^+$ T cells

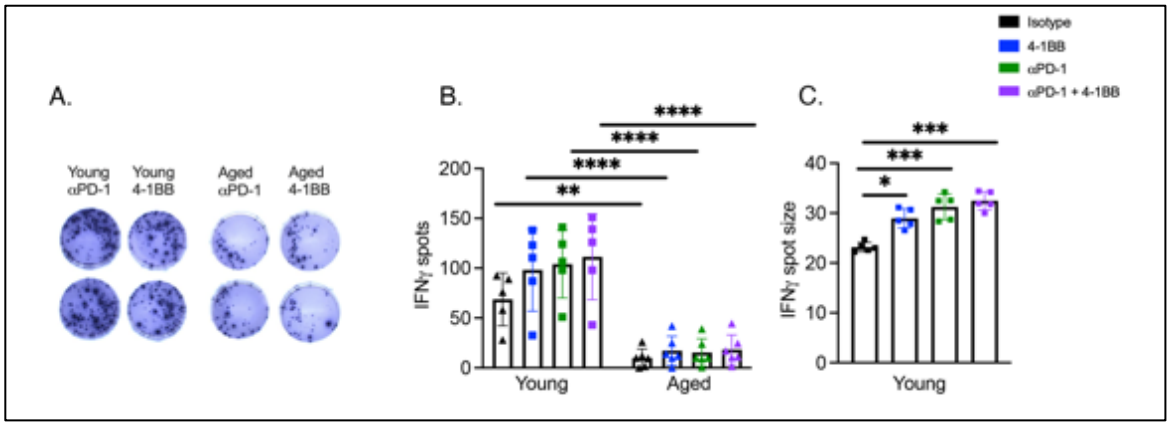

Appendix Figure 7. PD-1 blockade, 4-1BB treatment does not improve aged $CD8^+$ T cell function.

Ex vivo peptide stimulation of aged or young lung lymphocytes were isolated day 7 p.i. and were treated with isotype control antibody, PD-1 blockade, 4-1BB costimulation, or a combination. **(A-C)** IFNγ spot number was increase and spot size significantly increased in young T lymphocytes treated with 4-1BB, PD-1, and a combination while aged T lymphocytes did not show an improvement in function with any treatment. *P<0.05, ***P<0.001, ****P<0.0001, one-way ANOVA.

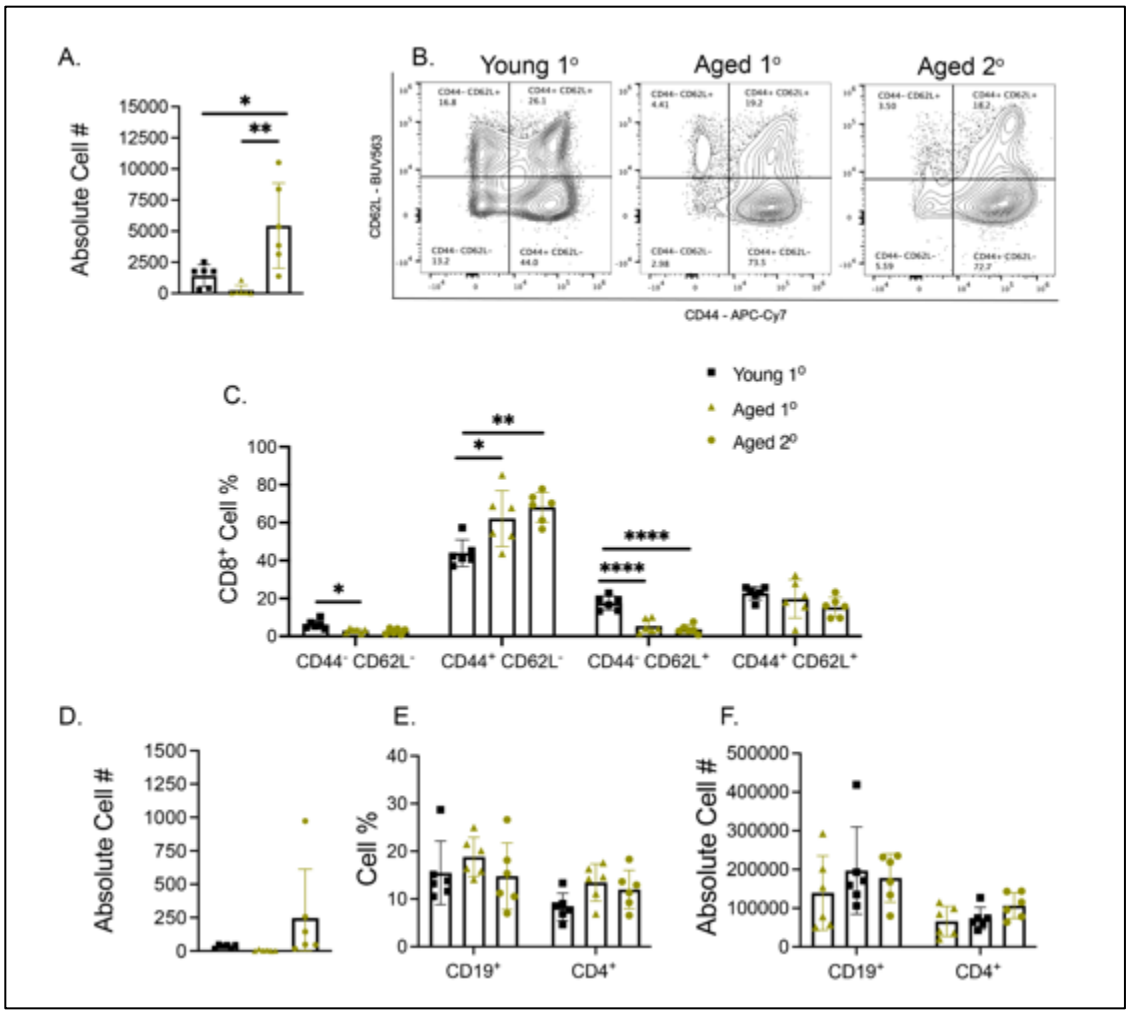

Appendix Figure 8. Aged re-challenged mice have fewer naïve CD8$^+$ CD44$^-$ CD62L$^+$ T cells but no difference in CD19$^+$ or CD4$^+$ T cells

(A) Aged re-challenged mice had increased absolute cell number of tet$^+$ CD8$^+$ T cells. **(B)** Representative flow plots showing CD44 and CD62L expression on CD8$^+$ T cells. **(C)** Aged re-challenged mice had fewer CD8$^+$ CD44$^-$ CD62L$^+$ T cells and increased CD8$^+$ T cells expressing CD44$^+$ CD62L$^-$. **(D)** Aged re-challenged mice had a modest increase in absolute cell number of tet$^+$ CD8$^+$ memory T cells. **(E-F**) There was no difference in cell percent or absolute cell number of CD19$^+$ or CD4$^+$ cells between the groups. Data represet 3 independent experiments with 5-6 mice per experiment. *P<0.05, **P<0.01, ****P<0.0001, one-way ANOVA.

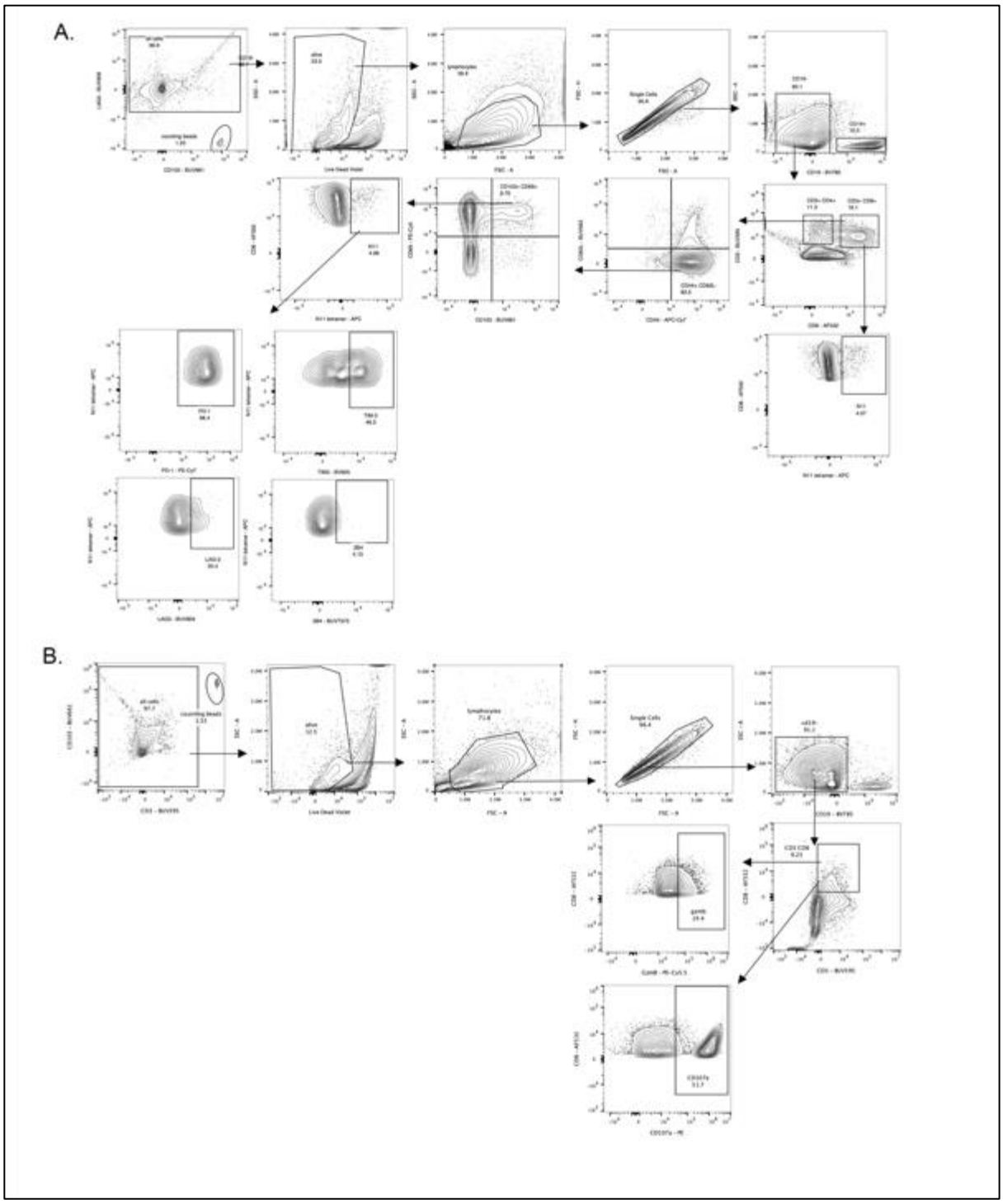

Appendix Figure 9. CD8$^+$ memory T cell and *ex vivo* peptide stimulation gating strategies

(A) CD8$^+$ memory T cell gating strategy. **(B)** *Ex vivo* peptide stimulation gating strategy.

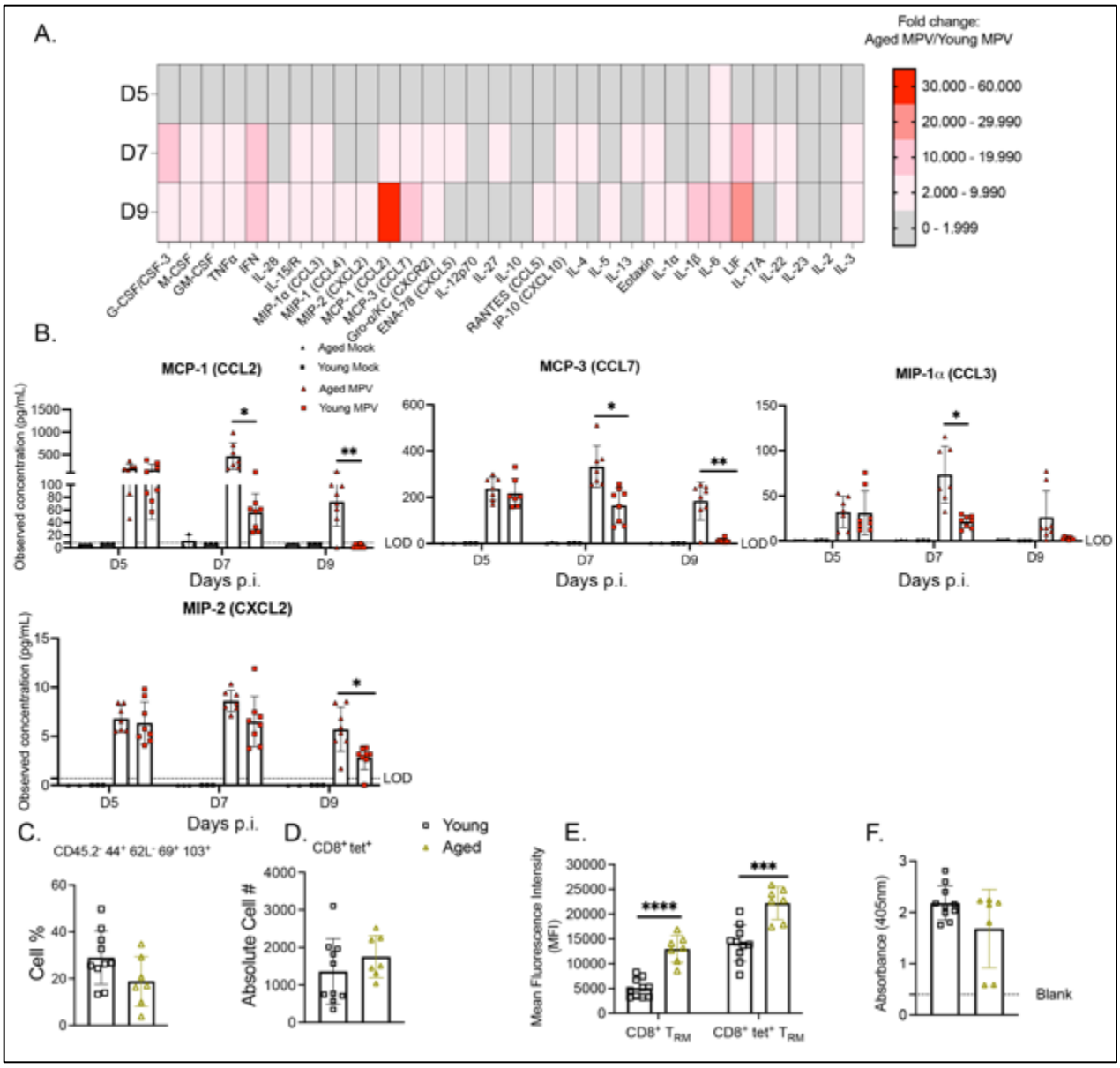

Appendix Figure 10. Aged mice had increased T cell chemoattractants in lung late during HMPV infection and had increased PD-1 expression on CD45.2$^-$ CD8$^+$ T cells in the lung 40 days p.i.

(A) Fold change aged MPV/young MPV heat map of chemokine and cytokine expression from lung homogenates. **(B)** Raw data from select chemokines. **(C)** There was no difference between age groups in cell percent of CD45.2$^-$ 44$^+$ 62L$^-$ 69$^+$ 103$^+$ T_{RM} cells. **(D)** There was also no difference in CD8$^+$ tet$^+$ absolute cell number. **(E)** Aged bulk CD8$^+$ and CD8$^+$ tet$^+$ T_{RM}s had increased cell percent PD-1 expression. **(F)** There was no difference in HMPV IgG production as measured by HMPV ELISA. Data represet 2 independent experiments with 3-5 mice per experiment. *P<0.05, **P<0.01, ***P<0.005, unpaired t-test or two-way ANOVA.

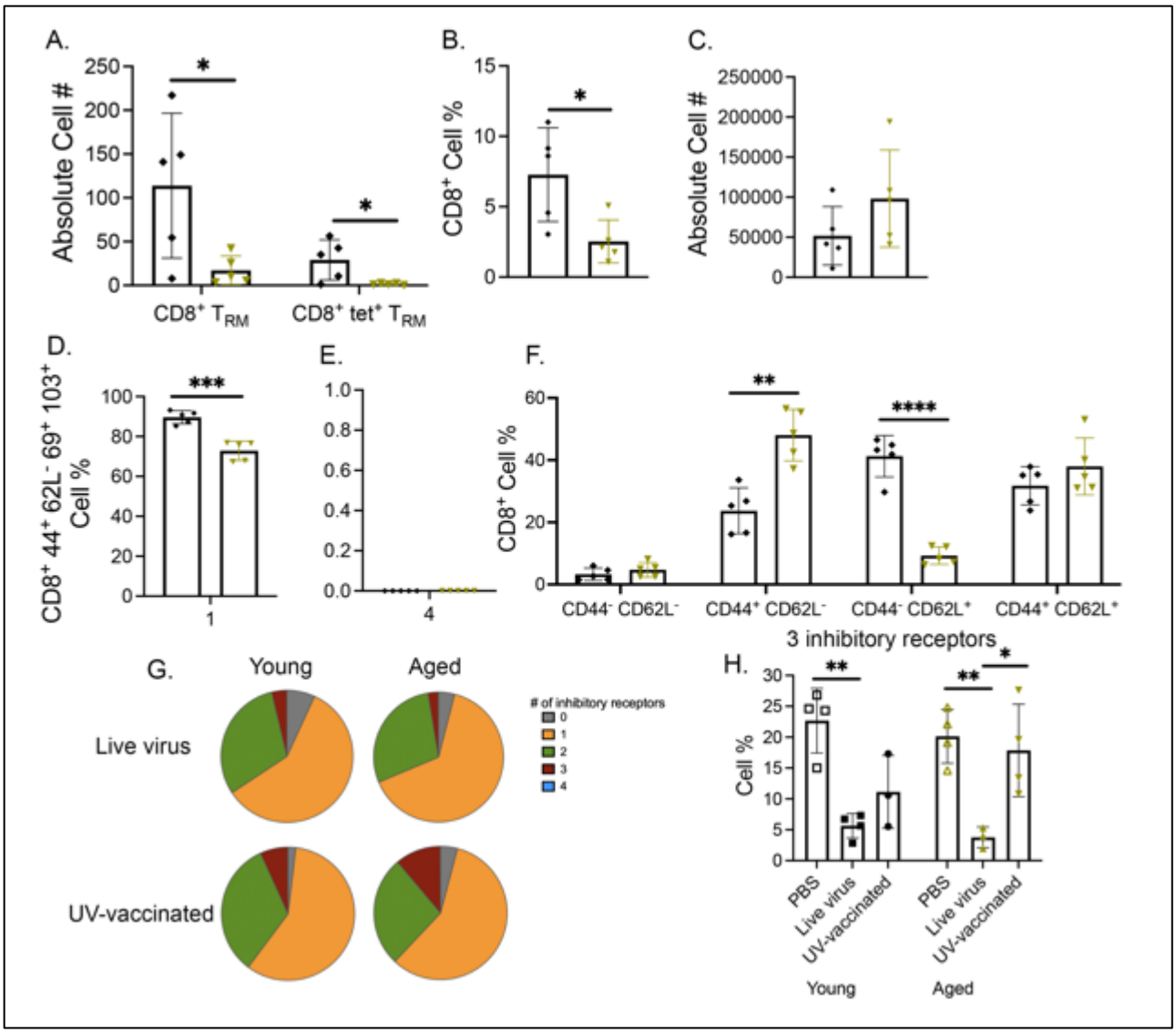

Appendix Figure 11. Aged mice re-stimulated with HMPV cognate peptide adjuvanted with LPS or vaccinated with UV-inactivated virus had impaired CD8$^+$ memory T cell response.

(A) Aged mice accumulated fewer bulk and tet$^+$ CD8$^+$ T$_{RM}$s. **(B)** Aged mice also produced fewer tet$^+$ CD8$^+$ T cells compared to young mice. **(C)** There was no difference in CD8$^+$ absolute cell number between the age groups. **(D)** Young mice had increased expression of only one inhibitory receptor on CD8$^+$ T$_{RM}$s. **(E)** Neither age group expressed all four inhibitory receptors (i.e. PD-1, TIM-3, LAG-3, and 2B4) on CD8$^+$ T$_{RM}$s. **(F)** Aged mice had increased CD8$^+$ CD44$^+$ CD62L$^-$ T cells but had a smaller pool of navie CD44$^-$ CD62L$^+$ CD8$^+$ T cells compared to young mice. **(G)** SPICE pie charts of combinatorial analysis of Boolean gating of 0, 1, 2, 3, or 4 inhibitory receptor expression. Inhibitory receptors assessed: PD-1, TIM-3, LAG-3, 2B4. Aged and young vaccinated mice had increased co-

expression of 3 inhibitory receptors. **A-F** data represents 1 independent experiment with 5 mice per group. **G-H** data represents 2 independent experiments with 2-3 mice per group. *P<0.05, **P<0.01, ***P<0.005, unpaired t-test.

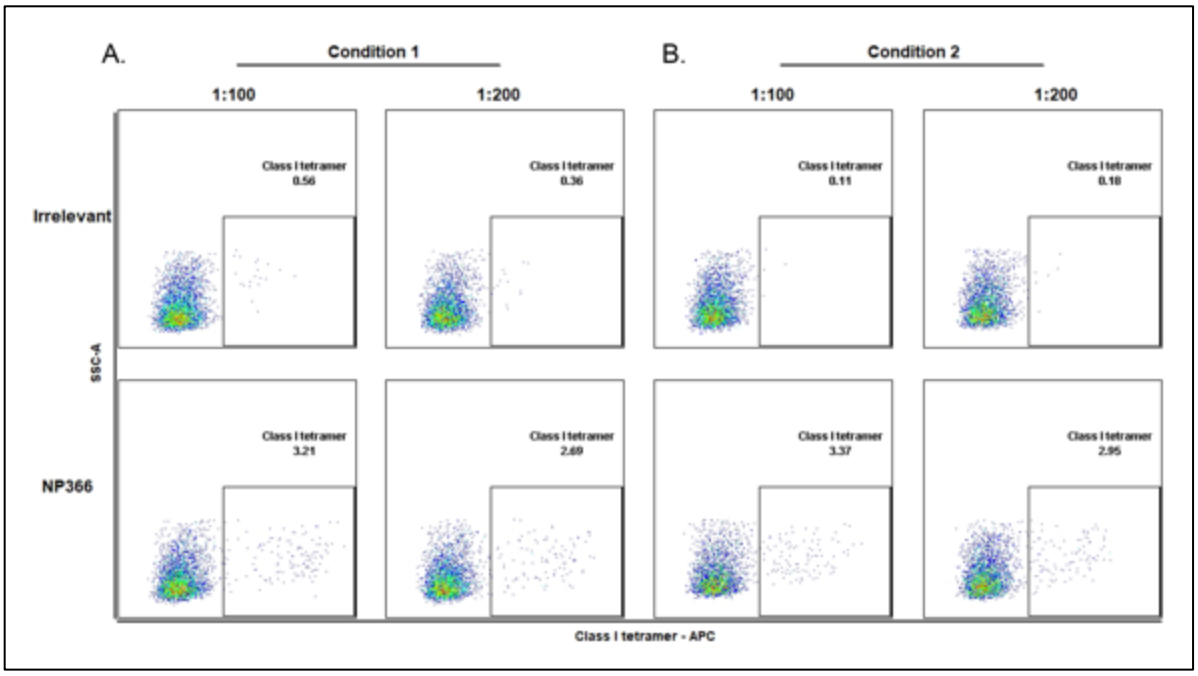

Appendix Figure 12. IAV MHC-Class I tetramer staining conditions.

For influenza virus PR8 (IAV) MHC-Class I tetramer (NP366) staining, C57BL/6 mice were infected with IAV and euthanized at day 7 post-infection (p.i.). Lung lymphocytes were stained using two different staining conditions. **(A)** Condition 1: incubate at RT for 1hr. **(B)** Condition 2: incubate at 4C for 30min. Two different dilutions were tested at each condition, 1:100 and 1:200.

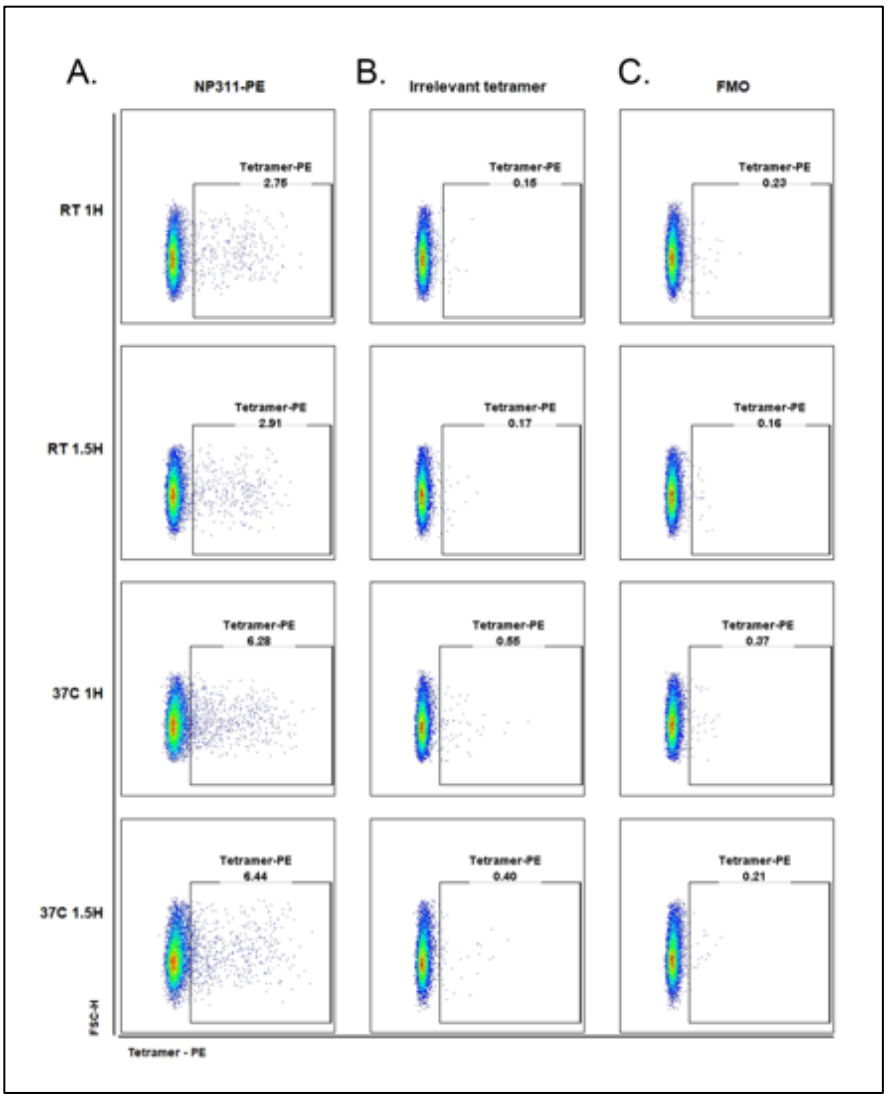

Appendix Figure 13. IAV MHC-Class II tetramer staining conditions

For IAV MHC-Class II tetramer (NP311) staining, C57BL/6 mice were infected with IAV and euthanized at day 7 (p.i.). Lung lymphocytes were stained with **(A)** NP311, **(B)** Irrelevant HMPV N37 tetramer, or **(C)** FMO at either room temperature (RT) or 37C for either 1hr or 1.5hrs.

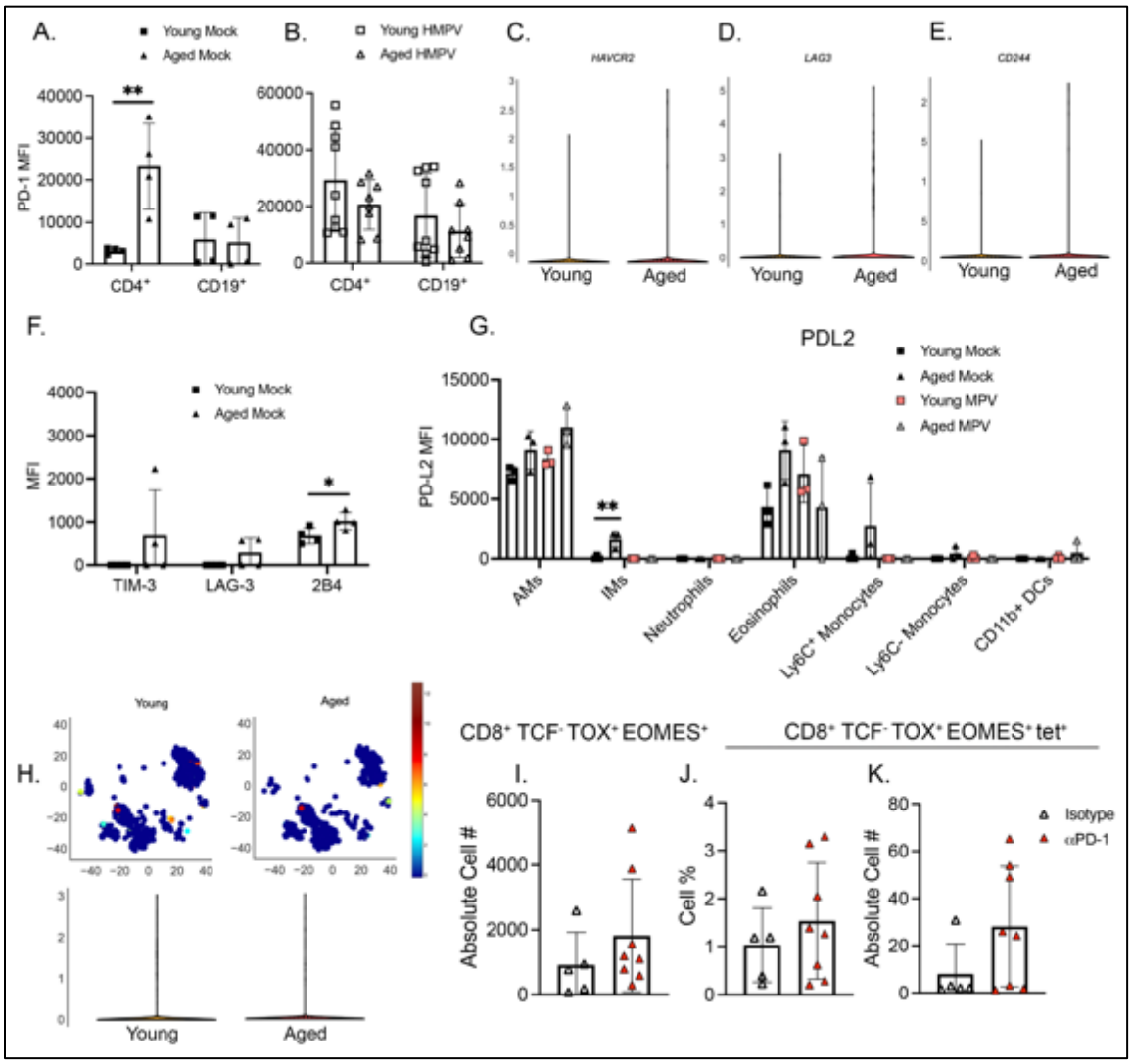

Appendix Figure 14. Minimal TIM-3, LAG-3, and 2B4 expression on aged CD8$^+$ T cells.

(A) PD-1 mean fluorescence intensity (MFI) on CD8$^+$ T cells in young and aged mock infected mice at day 7 p.i. **(B)** PD-1 MFI on CD8$^+$ T cells in young and aged HMPV infected mice at day 7 p.i. **(C-E)** Violin plots of *HAVCR2* (TIM-3), *LAG-3*, and *CD244* (2B4) expression from scRNAseq lung CD8$^+$ T cells in young and aged uninfected mice. **(F)** MFI of TIM-3, LAG-3, and 2B4 expression on lung CD8$^+$ T cells in young and aged mock infected mice. **(G)** PDL2 mean fluorescence intensity (MFI) on innate immune cells at day 1 p.i. **(H)** Heat map of *Pdcd1lg2* (PD-L2) expression in lung myeloid cells (TOP) and corresponding violin plot (BOTTOM). **(I-K)** Absolute cell number of CD8$^+$ TCF$^-$ TOX$^+$ EOMES$^+$ **(I)** or tetramer$^+$ cell percent **(J)** and absolute cell number **(K)** in isotype or PD-1 blockade treated aged HMPV-infected mice. Absolute cell number calculation by Biolegend Precision Counting Beads. *P<0.05; **P<0.01; unpaired t-test or two-way ANOVA. Data in (A; F) represents four experimental replicates, 1 mouse/group.

Data in (B) represents four experimental replicates, 2-3 mice/group. Data in (G) represents one experimental replicate, 3 mice/group. Data in (I-K) represents three experimental replicates 3-4 mice/group.

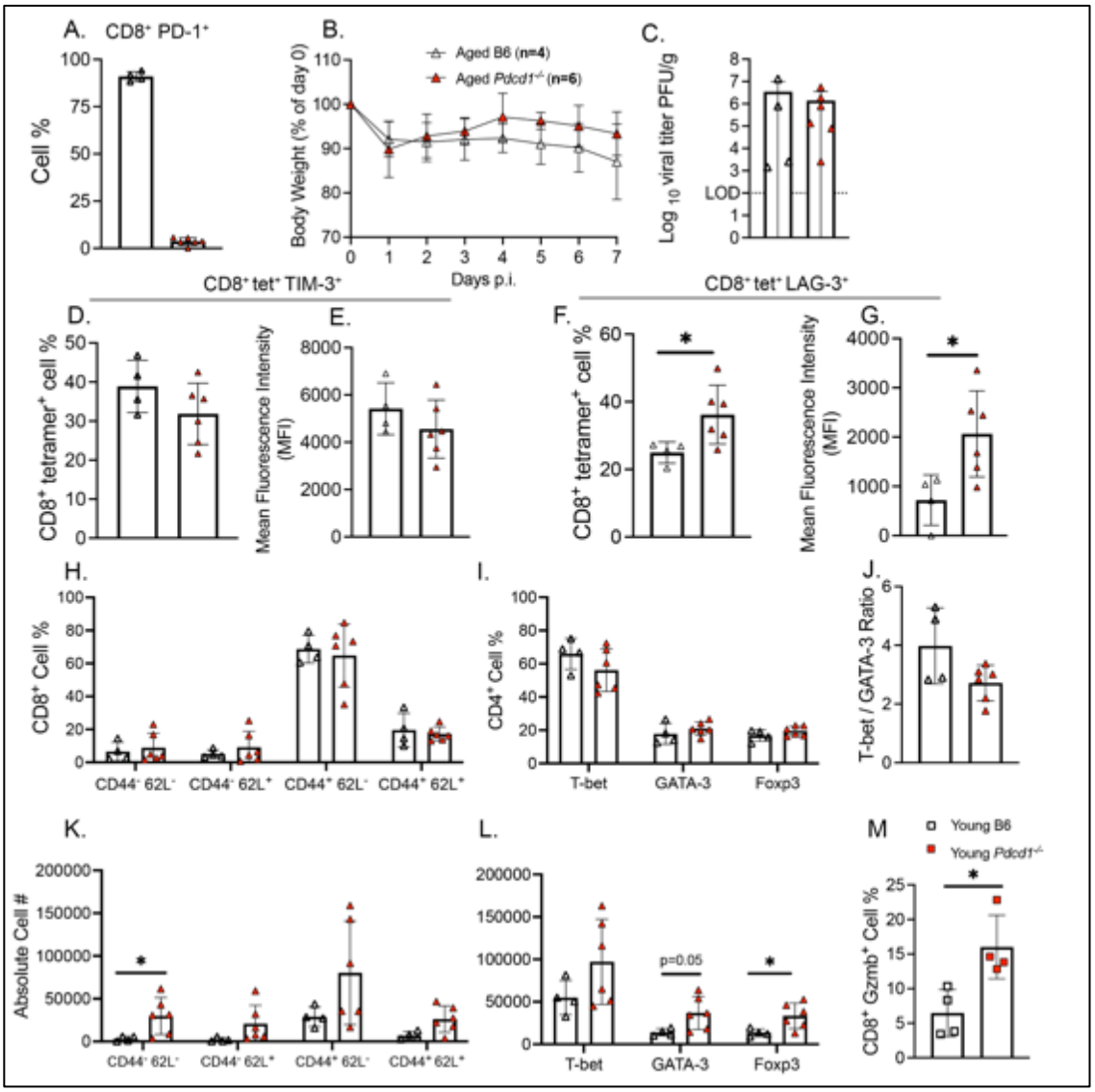

Appendix Figure 15. Aged *Pdcd1*$^{-/-}$ tet^{+} CD8^{+} T cells had a compensatory increase in LAG-3 expression.

(A) PD-1 expression on CD8^{+} tet^{+} T cells in both B6 and *Pdcd1*$^{-/-}$ groups. **(B-C)** Weight loss and viral burden, respectively between aged B6 and *Pdcd1*$^{-/-}$. **(D-E)** TIM-3 expression in cell percent and MFI on CD8^{+} tet^{+} T cells. **(F-G)** LAG-3 expression in cell percent and MFI on CD8^{+} tet^{+} T cells. **(H & K)** CD44 and 62L expression on CD8^{+} T cells in aged B6 and *Pdcd1*$^{-/-}$.mice - cell percent and absolute cell number, respectively. **(I & L)** T-bet, Foxp3, T-bet, and GATA3 expression on CD4^{+} T cells - cell percent and absolute cell number, respectively. **(J)** Th1:Th2 ratio

between aged B6 and *Pdcd1*$^{-/-}$ mice. **(M)** CD8^{+} Gzmb^{+} cell percent in young B6 and *Pdcd1*$^{-/-}$ HMPV-infected mice. *P<0.05; unpaired t-test. Data represents two experimental replicates, 2-3 mice/group.

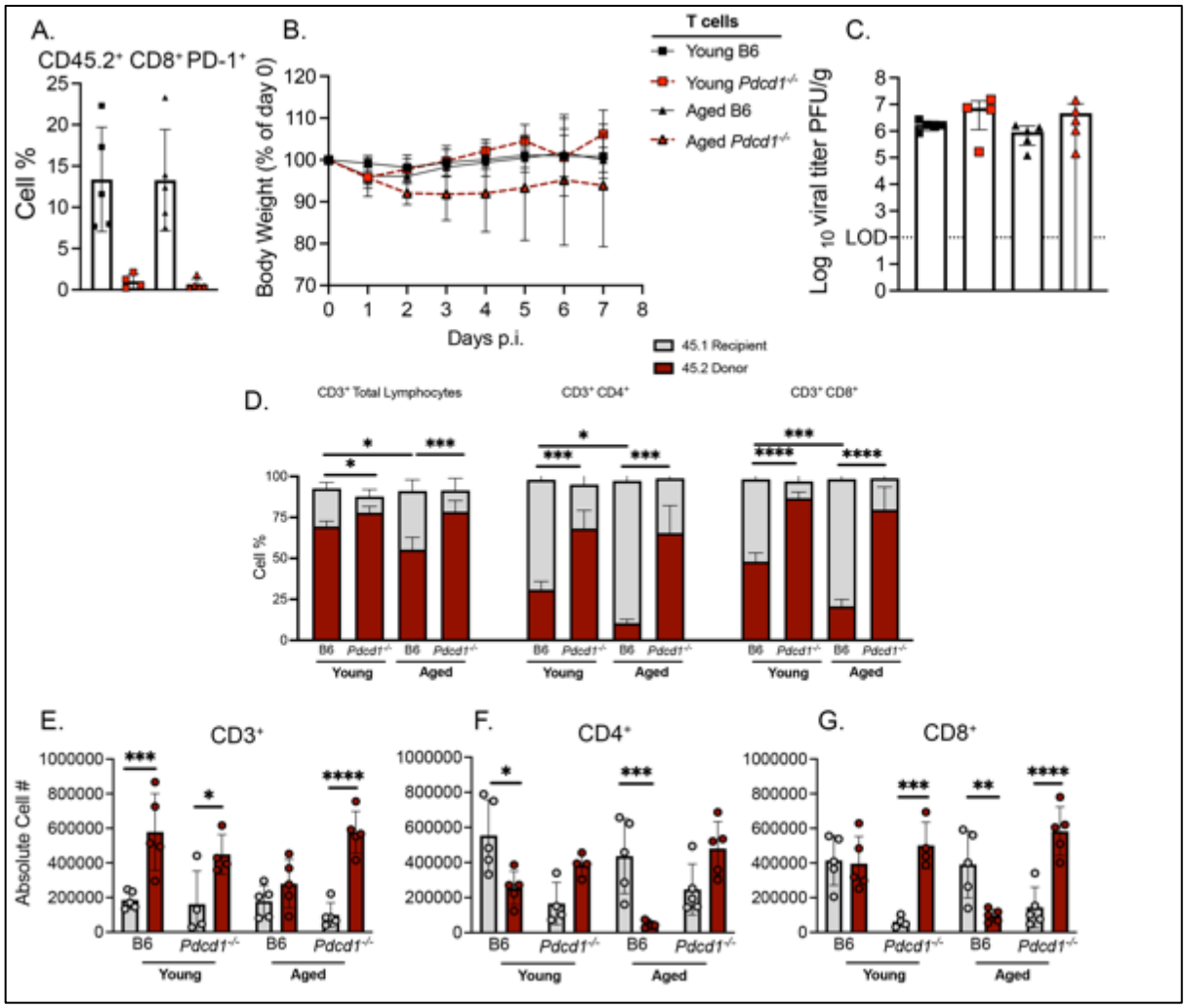

Appendix Figure 16. Aged and young *Pdcd1*$^{-/-}$ T cells had better engraftment in syngeneic transplant.

(A) PD-1 expression on donor transplanted CD8^{+} T cells. **(B)** Weight loss in the four syngeneic transplant groups during HMPV infection. **(C)** Viral titer measured in PFU/g at day 7 p.i. **(D)** Cell frequency of CD45.1 recipient (gray bars) and CD45.2 donor (red bars) in CD3^{+} total lymphocytes, CD3^{+} CD4^{+}, and CD3^{+} CD8^{+} T lymphocytes. **(E-G)** Absolute cell number of CD45.1 and CD45.2 CD3^{+}, CD4^{+}, and CD8^{+} T cells. *P<0.05; **P<0.01, ***P<0.001; ****P<0.0001, unpaired t-test or one-way ANOVA. Absolute cell number calculated by BioLegend Precision Counting Beads. Data represents one experimental replicate, 4-5 mice/group.

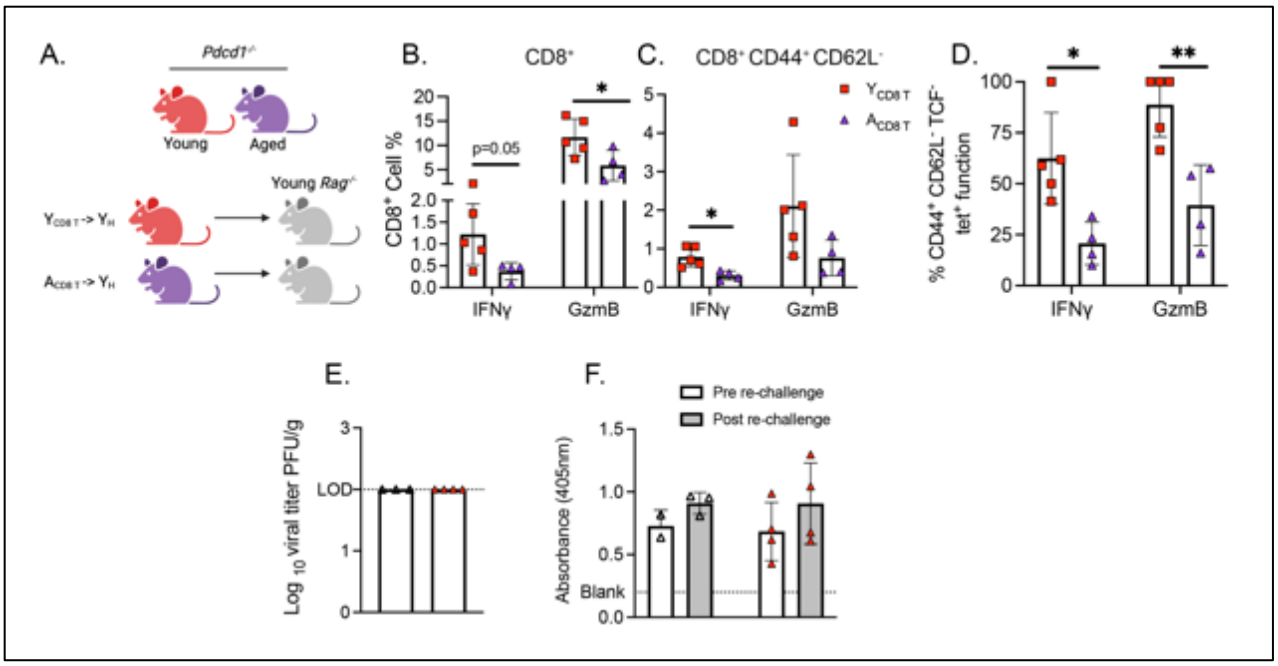

Appendix Figure 17. Young *Pdcd1*$^{-/-}$ CD8^{+} T cells produce more granzyme B in CD8^{+} adoptive transfer model. **(A)** Experimental schematic for *Pdcd1*$^{-/-}$ CD8^{+} T cells adoptive transfer. **(B)** IFN and granzyme B expression on bulk CD8^{+} T cells and **(C)** CD44^{+} CD62L^{+} CD8^{+} T cells. **(D)** Percent functional CD44^{+} CD62L^{-} TCF^{-} tet^{+} CD8^{+} T cells. **(E)** Viral titer in PFU/g in aged isotype and PD-1 blockade groups at day 7 post re-challenge. **(F)** HMPV ELISA absorbance from serum collected by submandibular bleed pre and post re-challenge. *P<0.05; **P<0.01, ***P<0.001; ****P<0.0001, unpaired t-test or one-way ANOVA. Data in (A-D) represents one experimental replicate, 4-5 mice/group. Data in (E-F) represents one experimental replicate 3-4 mice/group.

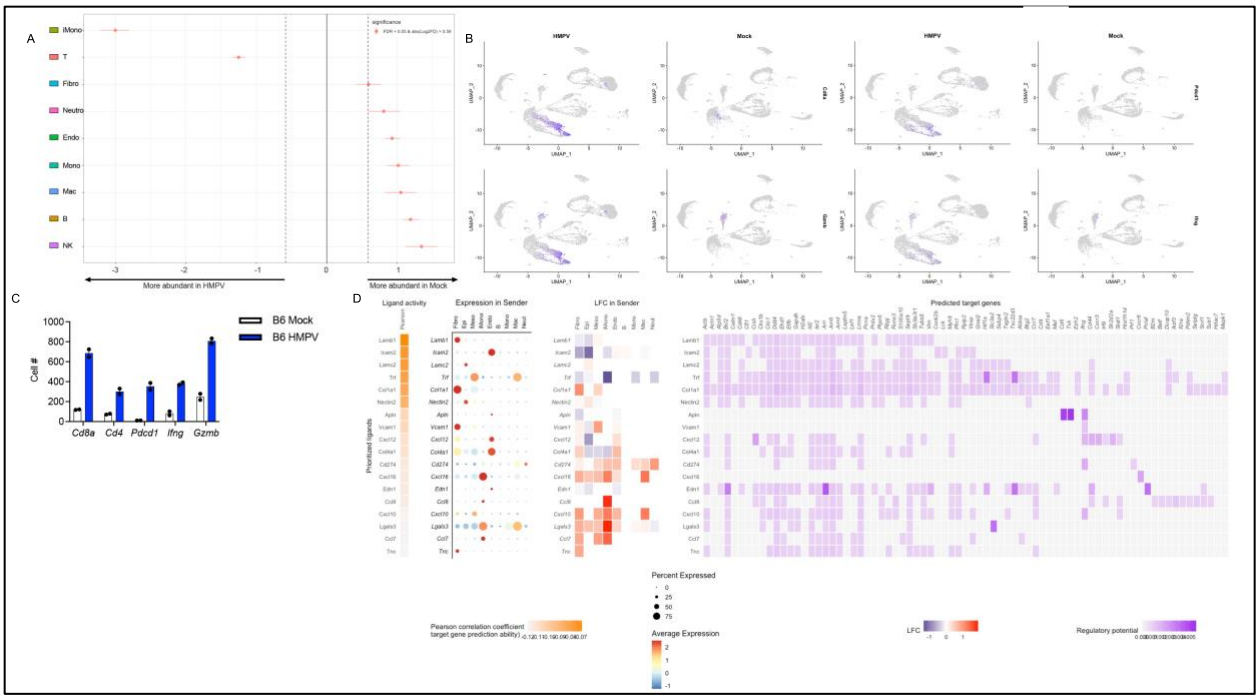

Appendix Figure 18. Validation of CD8 effector function and inhibitory receptor expression by single cell RNA sequencing.

(A) Relative abundance of cell clusters based on infection status as assessed by permutation testing. **(B)** UMAPs of *Cd8a*, *Pdcd1* (protein: PD-1), *Ifng*, and *Gzmb* showing co-expression of effector functions and PD-1 in CD8s. **(C)** Cell number based on CD8a, CD4, Pdcd1, Ifng, and Gzmb expression. **(D)** NicheNet analysis of upregulated ligands (left), including PD-L1 (gene: *Cd274*), and the relative expression in sender populations (middle). Regulation of target genes (right) by individual ligands reveals PD-L1 regulation of *Ifng*. Data represents one experimental replicate, two mice/group.

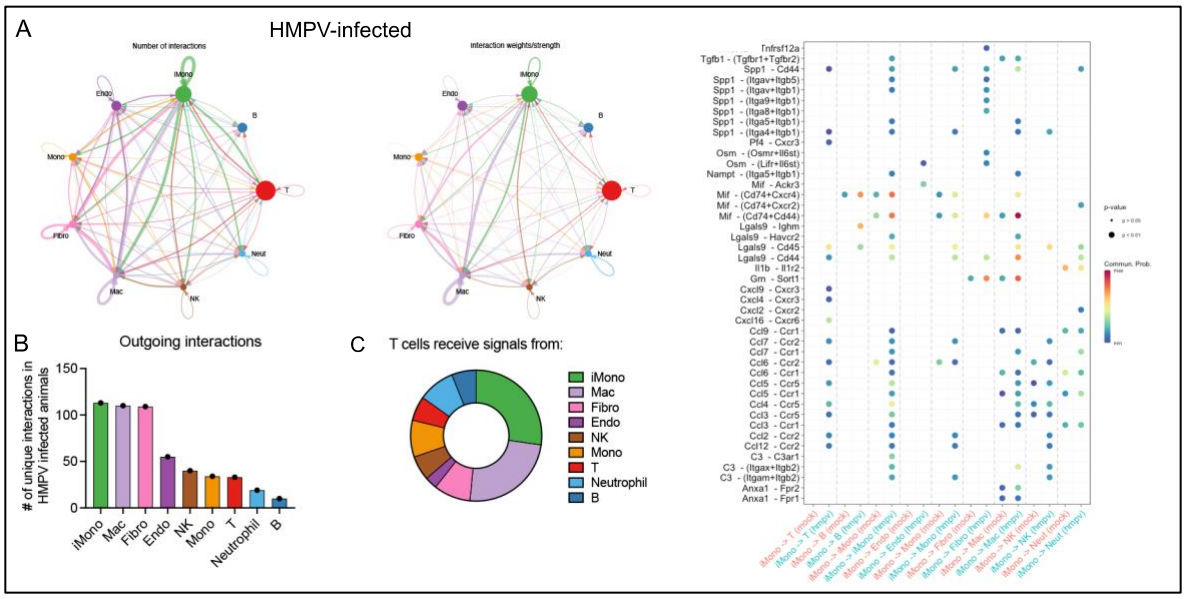

Appendix Figure 19. Cell-to-cell communication networks following HMPV infection.

(A) Number of interactions and interaction strength between 9 cell populations following HMPV infection, showing iMono-dominant communication after infection. **(B)** Quantification of unique interactions in HMPV-infected animals based on cell cluster. **(C)** Proportion of signals sent to T cells from each cell cluster. **(D)** iMono signals transmitted to other cell populations in mock infection (red) or HMPV-infection (blue). Data represents one experimental replicate, two mice/group.

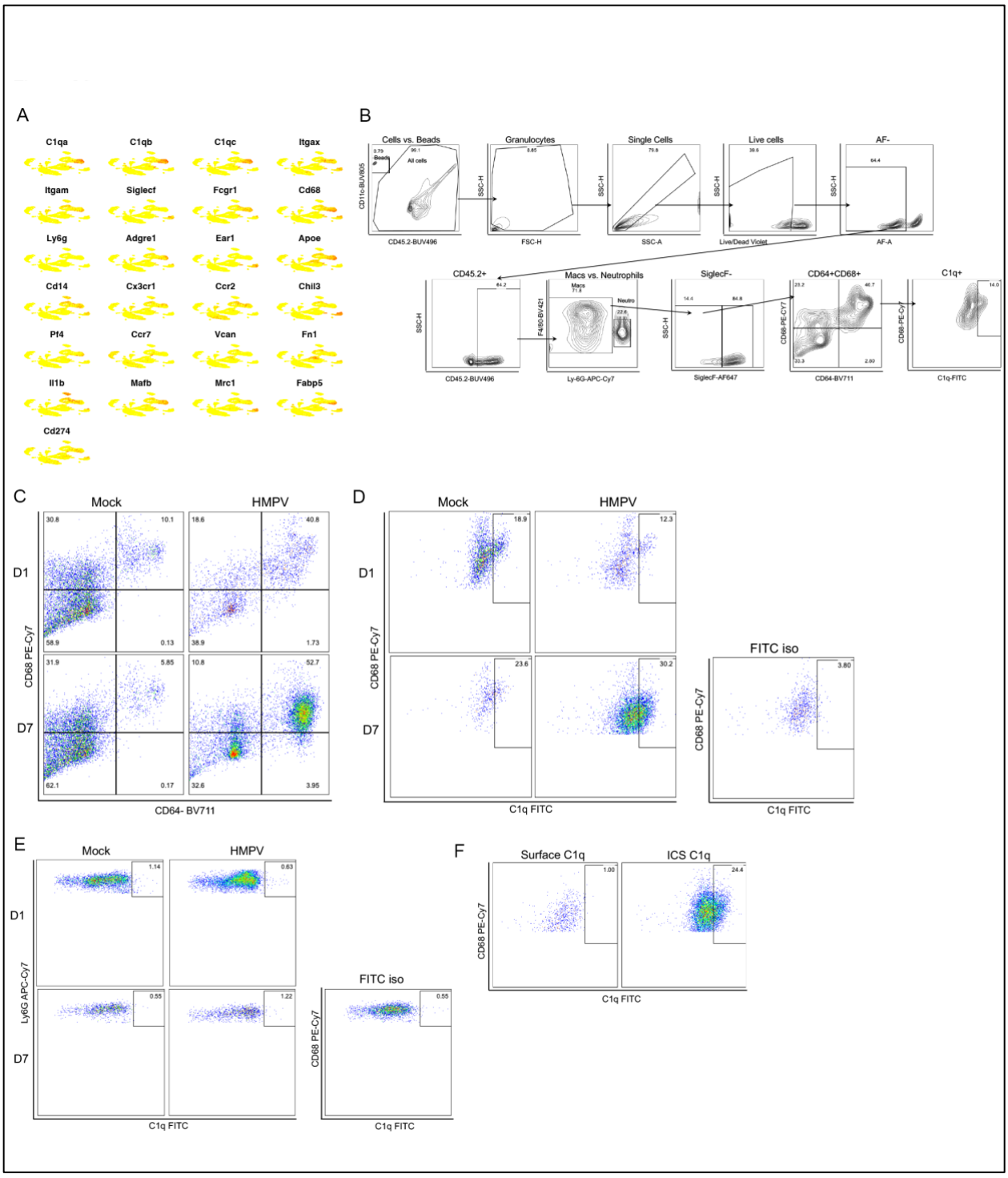

Appendix Figure 20. C1q production by inflammatory monocytes on day 7 after HMPV infection.

(A) Expression of several monocyte/macrophage gene transcripts overlaid on a UMAP, showing upregulation of CD64 (gene: *Fcgr1*) and *CD68* in C1q-producing population. **(B)** Innate panel gating strategy. **(C)** $CD64^{+}CD68^{+}$ cell recruitment in lung tissue on day 7 after HMPV infection. **(D)** C1q production in $CD64^{+}CD68^{+}$ lung cells by

intracellular staining. FITC isotype staining shown on right which was used to set gate position for $C1q^+$ staining. **(E)** C1q staining on Ly6G+ neutrophils. **(F)** Limited C1q staining without the use of permeabilization (left) compared to intracellular staining (ICS) on $CD64^+CD68^+$ cells.

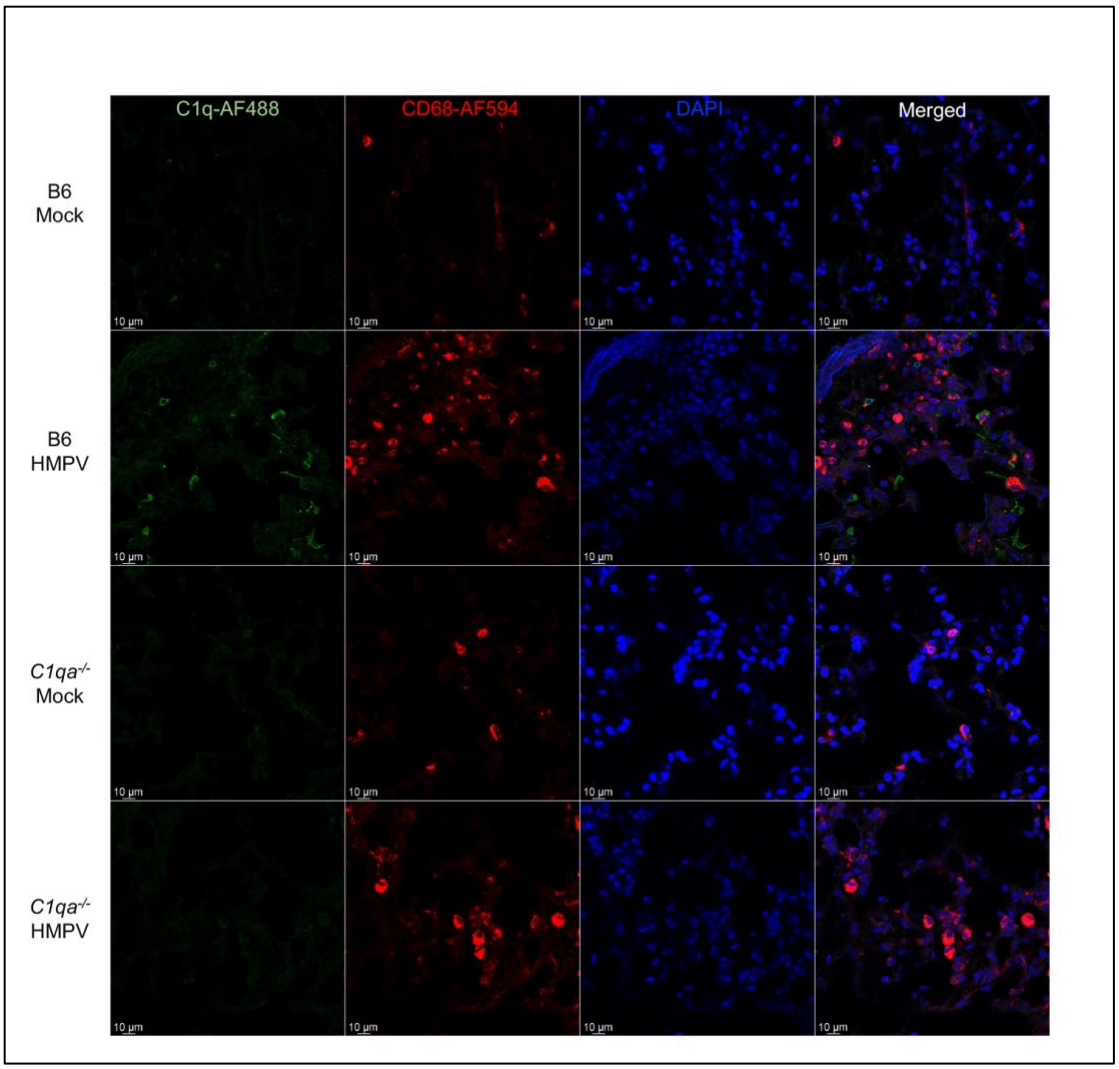

Appendix Figure 21. Immunofluorescent (IFC) staining on lung tissue showing co-localization of C1q and CD68.

Lungs were harvested 7 days post-HMPV or mock treatment, fixed with 4% paraformaldehyde, frozen, and embedded in OCT followed by IFC staining. B6 HMPV mice had a clear C1q-AF488 signal, which colocalized with CD68 cell recruitment.

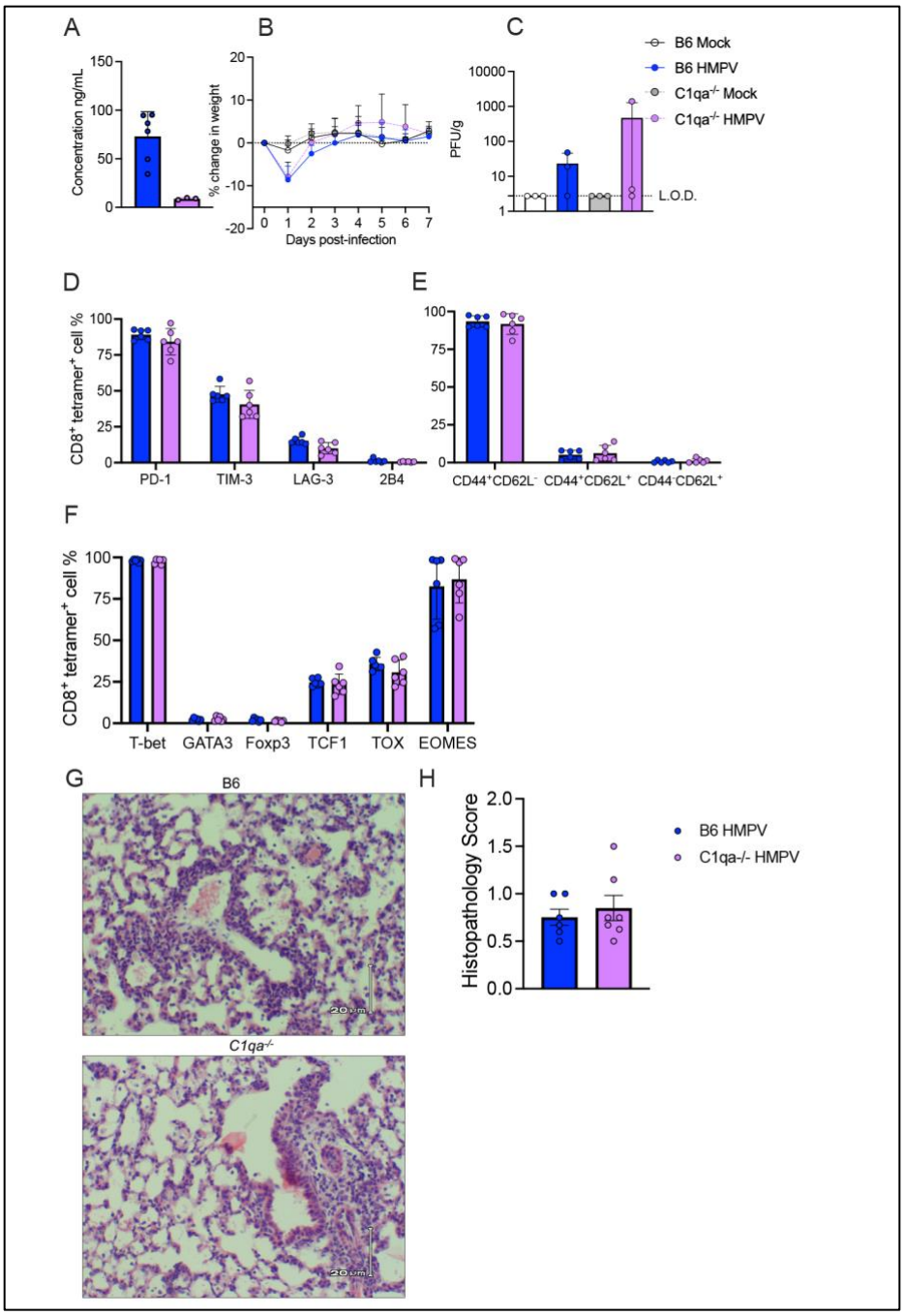

Appendix Figure 22. Inhibitory receptor, activation states, and transcription factor expression in B6 vs *C1qa*$^{-/-}$.

(A) C1q quantity in lung homogenate in B6 vs. *C1qa*$^{-/-}$ mice. **(B)** No changes in weight between groups. **(C)** Low burdens of HMPV infection in infected animals regardless of genotype. **(D)** Expression of PD-1, TIM-3, LAG-3, and 2B4 in B6 and *C1qa*$^{-/-}$ HMPV-infected mice on N11^{+} CD8^{+} T cells isolated from lung tissue. **(E)** CD44/CD62L activation states in in B6 and *C1qa*$^{-/-}$ HMPV-infected mice. **(F)** Expression of transcription factors in in B6 and *C1qa*$^{-/-}$.

$^{-/-}$ HMPV-infected mice. **(G-H)** Representative histopathology staining and quantification at day 7 post infection in in B6 and *C1qa*$^{-/-}$ HMPV-infected mice. Data in A; C represents one experimental replicate, 3-6 mice/group. Data in B; D-H represents two experimental replicates, 3 mice/group.

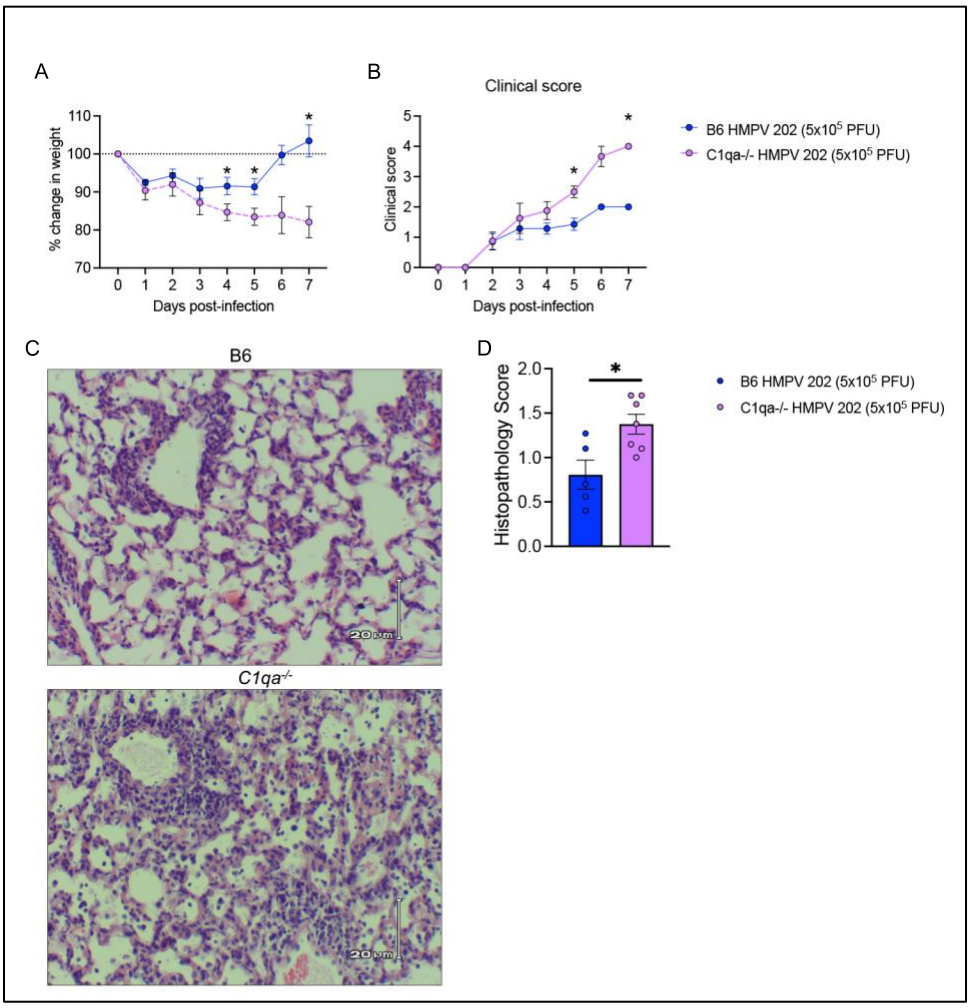

Appendix Figure 23. Virulent HMPV strain leads to enhanced disease in *C1qa*$^{-/-}$ mice.

(A) Increased weight loss in *C1qa*$^{-/-}$ mice infected with C-202. *p<0.05 by two-way ANOVA with multiple comparisons. **(B)** Increased clinical score in *C1qa*$^{-/-}$ mice infected with -202 calculated by hunched, fur grooming, respiratory rate, and activity. *p<0.05 by two-way ANOVA with multiple comparisons. **(C-D)** Representative histopathology staining and quantification at day 7 post infection in in B6 and *C1qa*$^{-/-}$ C-202-infected mice. *p<0.05 by t-test. Data represents two experimental replicate, 3-4 mice/group/replicate.

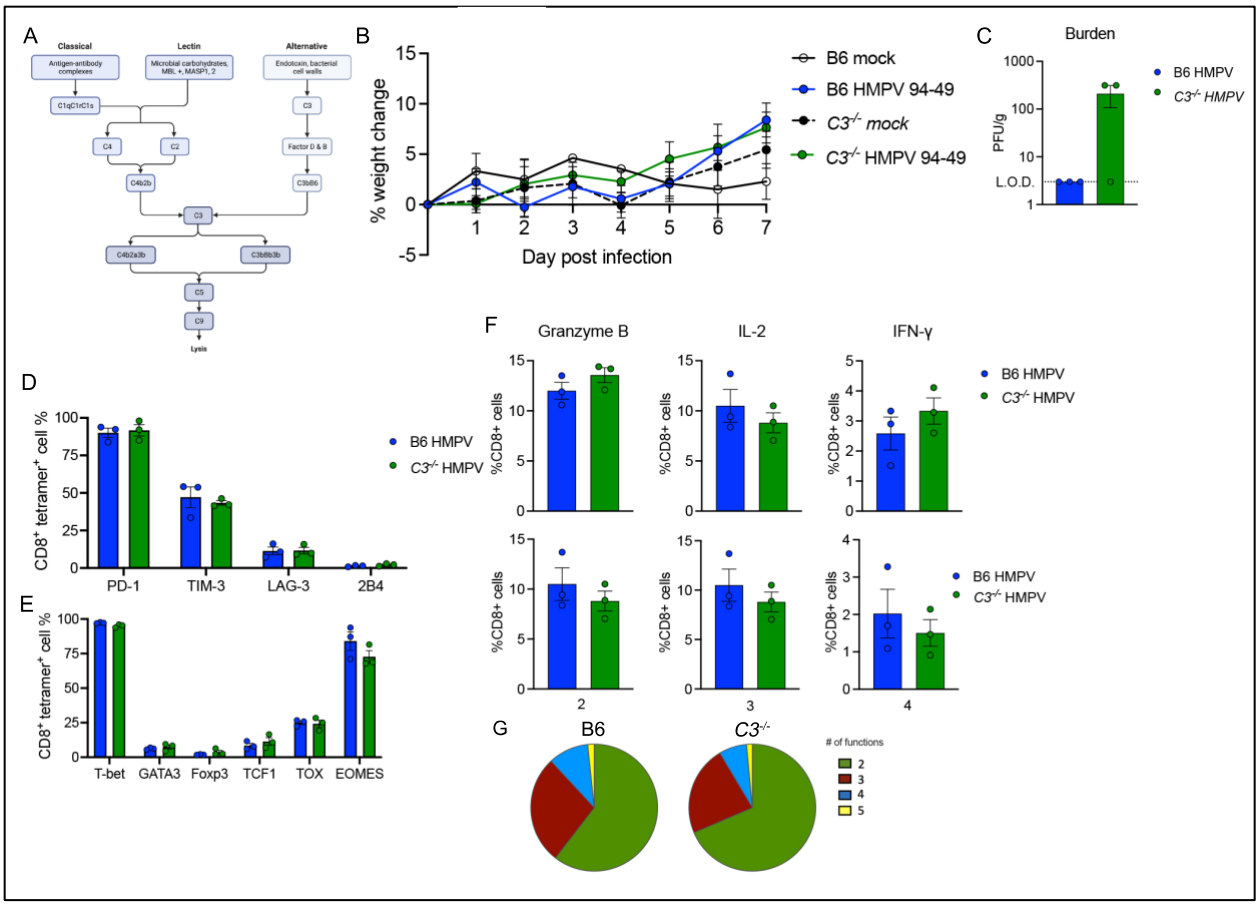

Appendix Figure 24. CD8 effector function is preserved in animals lacking C3.

(A) Schematic of complement pathways showing convergence on C3 (Biorender). **(B)** No changes in weight between groups. **(C)** Low burdens of HMPV infection in infected animals regardless of genotype. **(D)** Expression of PD-1, TIM-3, LAG-3, and 2B4 in B6 and *C3*$^{-/-}$ HMPV-infected mice. **(E)** Expression of transcription factors in B6 and *C3*$^{-/-}$ HMPV-infected mice. **(F)** No changes in effector functions (granzyme B, IL-2, and IFN-γ) in B6 and *C3*$^{-/-}$ HMPV-infected mice. **(G)** Boolean gating demonstrating similar distribution of multiple effector functions in B6 and *C3*$^{-/-}$ HMPV-infected mice. Data represents one experimental replicate, 3 mice/group.

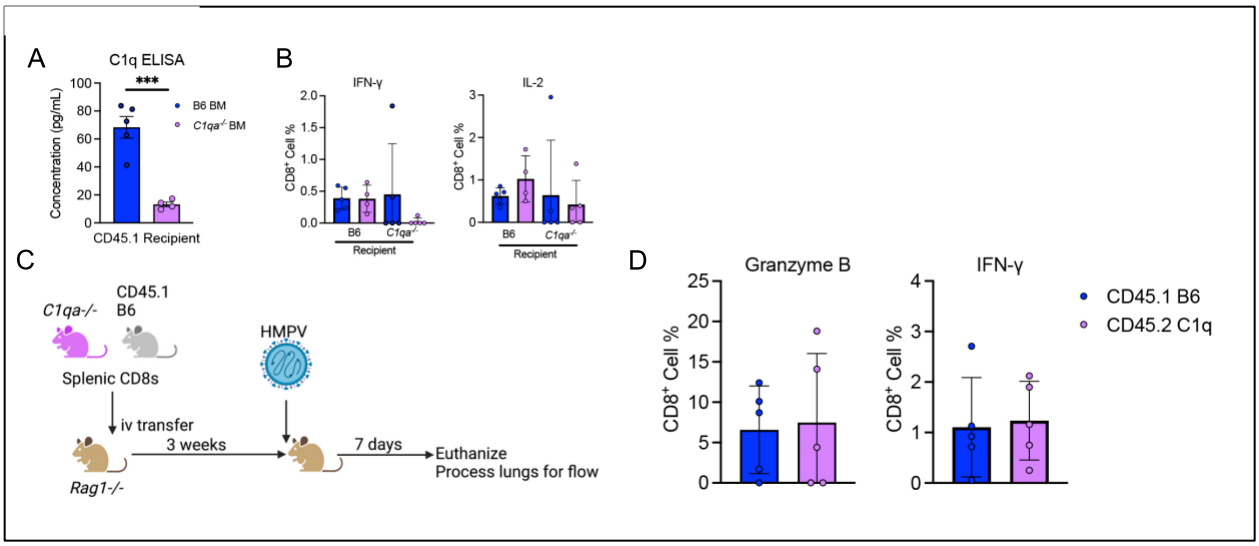

Appendix Figure 25. CD8 extrinsic requirement of C1q.

(A) C1q protein quantity from lung homogenate of CD45.1 recipient mice. *p<0.05 by t-test. **(B)** Four-way adoptive transfer experiments showing no difference in IL-2 or IFN-γ. **(C)** Adoptive transfer schematic of either CD8s from B6 or *C1qa*$^{-/-}$ mice into *Rag1*$^{-/-}$ recipients followed by HMPV infection. **(D)** No change in granzyme B or IFN-γ production by B6 or *C1qa*$^{-/-}$ CD8s. Data represents one experimental replicate, 5 mice/group.

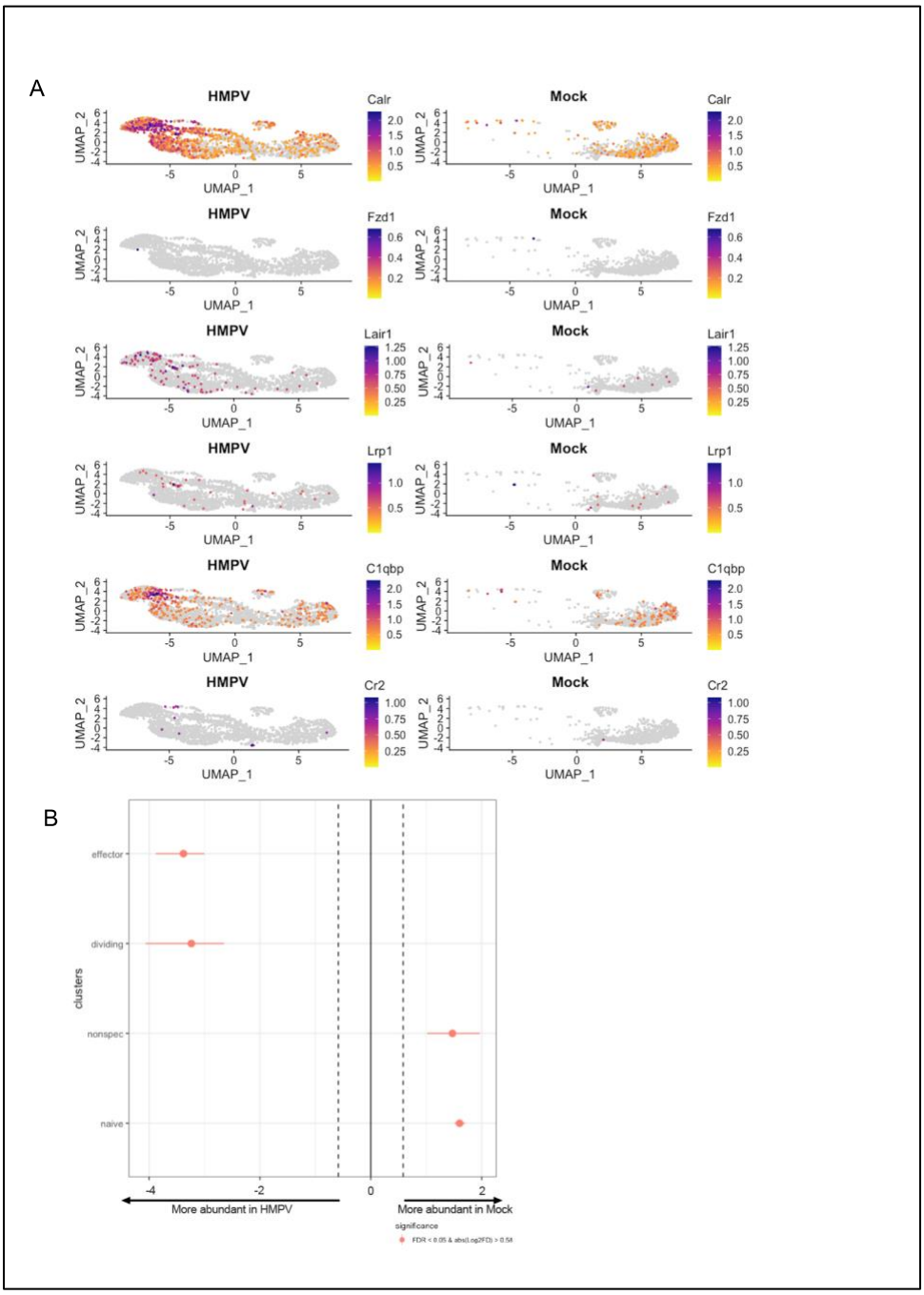

Appendix Figure 26. C1q receptor expression on CD8 T cells after HMPV infection.

(A) Expression of various C1q receptors on $CD8^+$ T cells by single cell RNA sequencing. **(B)** Permutation testing showing significant increase in effector and dividing T cells after HMPV infection.

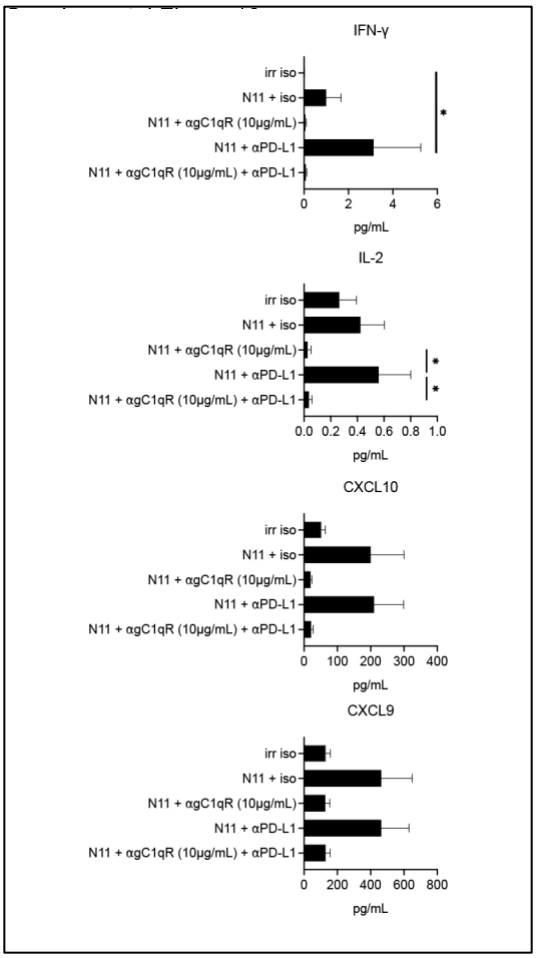

Appendix Figure 27. αgC1qR treatment abrogates cytokine production regardless of PD-L1 blockade.

IFN-γ, IL-2, CXCL10, and CXCL9 production following 48 hours of *ex vivo* stimulation with reduced cytokine production when treated with αgC1qR. *$p<0.05$ by one-way ANOVA with multiple comparisons. Data represents one experimental replicate, 3 mice/group.

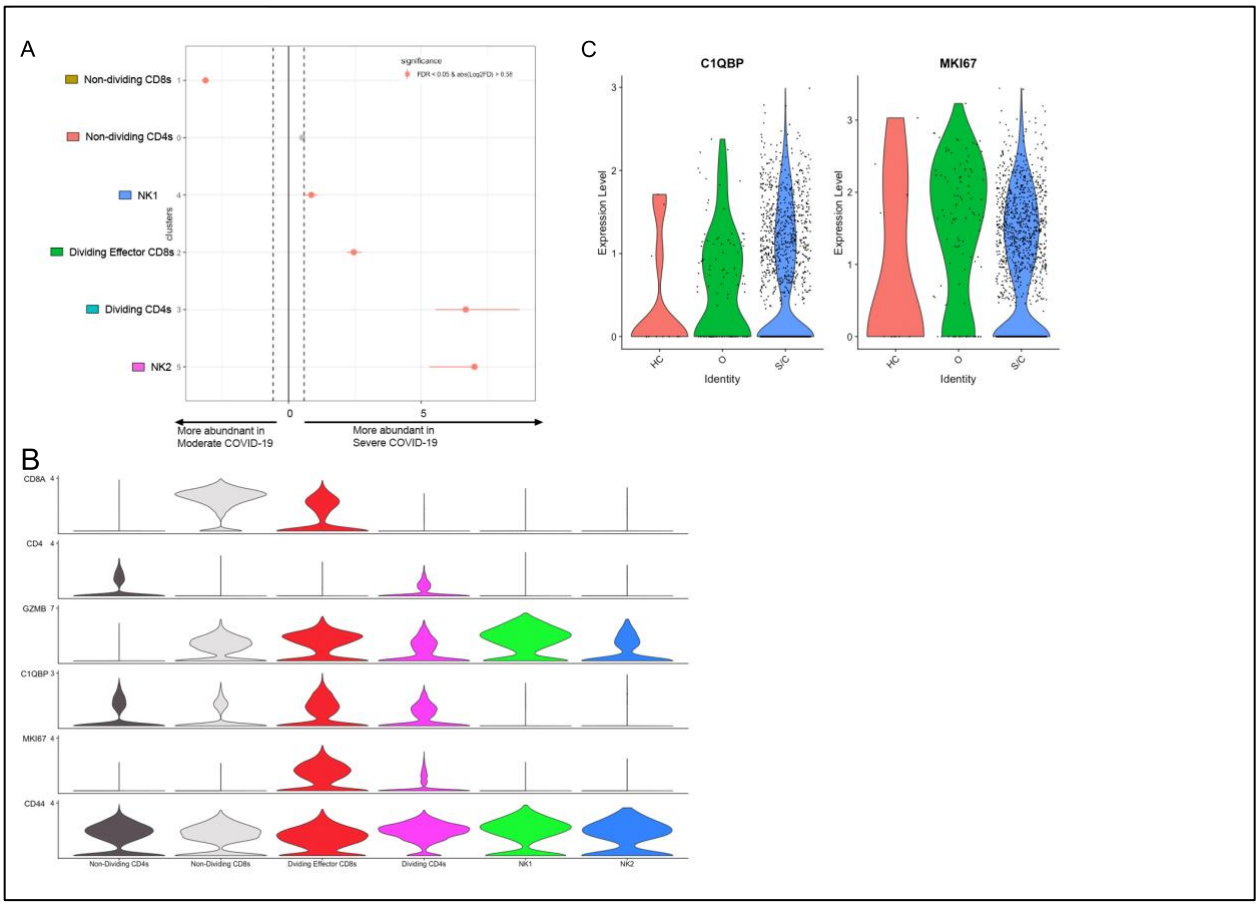

Appendix Figure 28. C1QBP expression on rapidly dividing CD8s with severe COVID-19 infection.

(A) Permutation testing for abundance of cell clusters in moderate vs. severe COVID-19 disease. **(B)** Stacked violin plots demonstrating expression of various T cell markers, including *C1QBP* and *MKI67* abundantly expressed in rapidly dividing CD8s. **(C)** Violin plot of *C1QBP* and *MKI67* expression by disease state (healthy control =HC, moderate = O, severe = S/C). Both *C1QBP* and *MKI67* were significantly upregulated in S/C patients by differential gene expression analysis.

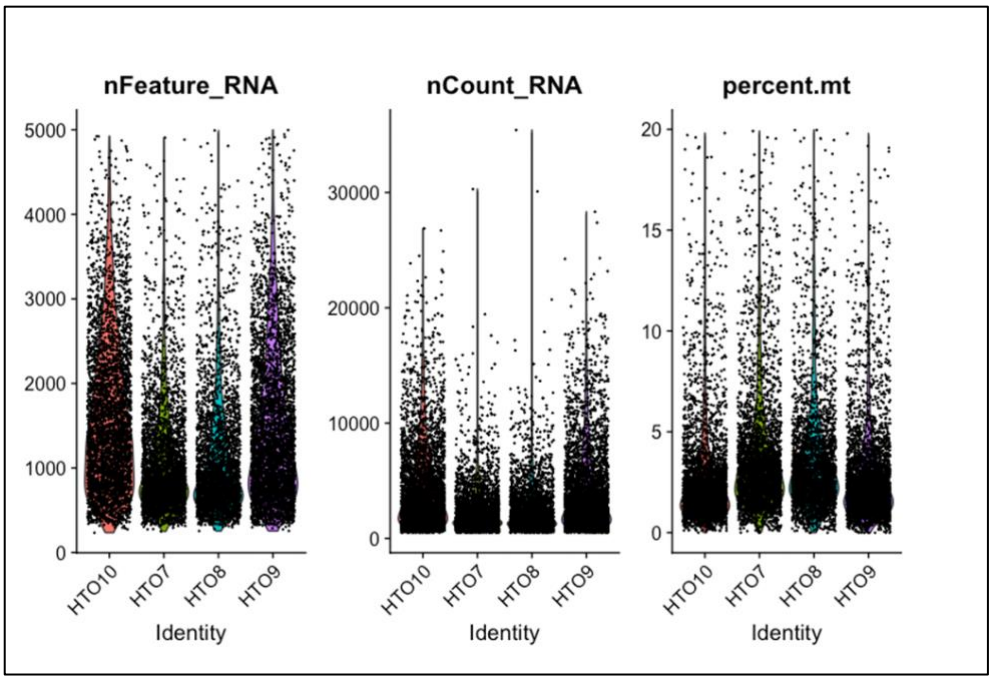

Appendix Figure 29. Quality control metrics per HTO for single cell RNA sequencing run.

Bibliography

1.Shafagati N, Williams J. Human metapneumovirus - what we know now. F1000Res. 2018;7:135.
2.Haas LE, Thijsen SF, van Elden L, Heemstra KA. Human metapneumovirus in adults. Viruses. 2013;5(1):87-110.
3.Eddens T, Parks OB, Williams JV. Neonatal Immune Responses to Respiratory Viruses. Front Immunol. 2022;13:863149.
4.Scheuerman O, Barkai G, Mandelboim M, Mishali H, Chodick G, Levy I. Human metapneumovirus (hMPV) infection in immunocompromised children. J Clin Virol. 2016;83:12-6.
5.Williams JV, Crowe JE, Jr., Enriquez R, Minton P, Peebles RS, Jr., Hamilton RG, et al. Human metapneumovirus infection plays an etiologic role in acute asthma exacerbations requiring hospitalization in adults. J Infect Dis. 2005;192(7):1149-53.
6.Walsh EE, Peterson DR, Falsey AR. Human metapneumovirus infections in adults: another piece of the puzzle. Arch Intern Med. 2008;168(22):2489-96.
7.Edwards KM, Zhu Y, Griffin MR, Weinberg GA, Hall CB, Szilagyi PG, et al. Burden of human metapneumovirus infection in young children. N Engl J Med. 2013;368(7):633-43.
8.Boivin G, Abed Y, Pelletier G, Ruel L, Moisan D, Cote S, et al. Virological features and clinical manifestations associated with human metapneumovirus: a new paramyxovirus responsible for acute respiratory-tract infections in all age groups. J Infect Dis. 2002;186(9):1330-4.
9.van den Hoogen BG, van Doornum GJ, Fockens JC, Cornelissen JJ, Beyer WE, de Groot R, et al. Prevalence and clinical symptoms of human metapneumovirus infection in hospitalized patients. J Infect Dis. 2003;188(10):1571-7.
10.Te Wierik MJ, Nguyen DT, Beersma MF, Thijsen SF, Heemstra KA. An outbreak of severe respiratory tract infection caused by human metapneumovirus in a residential care facility for elderly in Utrecht, the Netherlands, January to March 2010. Euro Surveill. 2012;17(13).
11.van den Hoogen BG, Osterhaus DM, Fouchier RA. Clinical impact and diagnosis of human metapneumovirus infection. Pediatr Infect Dis J. 2004;23(1 Suppl):S25-32.
12.Williams JV, Harris PA, Tollefson SJ, Halburnt-Rush LL, Pingsterhaus JM, Edwards KM, et al. Human metapneumovirus and lower respiratory tract disease in otherwise healthy infants and children. N Engl J Med. 2004;350(5):443-50.
13.Spaeder MC, Custer JW, Bembea MM, Aganga DO, Song X, Scafidi S. A multicenter outcomes analysis of children with severe viral respiratory infection due to human metapneumovirus. Pediatr Crit Care Med. 2013;14(3):268-72.
14.Ampofo K, Bender J, Sheng X, Korgenski K, Daly J, Pavia AT, et al. Seasonal invasive pneumococcal disease in children: role of preceding respiratory viral infection. Pediatrics. 2008;122(2):229-37.
15.Seki M, Yoshida H, Gotoh K, Hamada N, Motooka D, Nakamura S, et al. Severe respiratory failure due to co-infection with human metapneumovirus and Streptococcus pneumoniae. Respir Med Case Rep. 2014;12:13-5.
16.Chiu CY, Alizadeh AA, Rouskin S, Merker JD, Yeh E, Yagi S, et al. Diagnosis of a critical respiratory illness caused by human metapneumovirus by use of a pan-virus microarray. J Clin Microbiol. 2007;45(7):2340-3.

17.Cote S, Abed Y, Boivin G. Comparative evaluation of real-time PCR assays for detection of the human metapneumovirus. J Clin Microbiol. 2003;41(8):3631-5.
18.Maertzdorf J, Wang CK, Brown JB, Quinto JD, Chu M, de Graaf M, et al. Real-time reverse transcriptase PCR assay for detection of human metapneumoviruses from all known genetic lineages. J Clin Microbiol. 2004;42(3):981-6.
19.Klemenc J, Asad Ali S, Johnson M, Tollefson SJ, Talbot HK, Hartert TV, et al. Real-time reverse transcriptase PCR assay for improved detection of human metapneumovirus. J Clin Virol. 2012;54(4):371-5.
20.Tollefson SJ, Cox RG, Williams JV. Studies of culture conditions and environmental stability of human metapneumovirus. Virus Res. 2010;151(1):54-9.
21.Kim JI, Park S, Lee I, Park KS, Kwak EJ, Moon KM, et al. Genome-Wide Analysis of Human Metapneumovirus Evolution. PLoS One. 2016;11(4):e0152962.
22.de Graaf M, Osterhaus A, Fouchier RAM, Holmes EC. Evolutionary dynamics of human and avian metapneumoviruses. J Gen Virol. 2008;89(Pt 12):2933-42.
23.Yang CF, Wang CK, Tollefson SJ, Lintao LD, Liem A, Chu M, et al. Human metapneumovirus G protein is highly conserved within but not between genetic lineages. Arch Virol. 2013;158(6):1245-52.
24.Yang CF, Wang CK, Tollefson SJ, Piyaratna R, Lintao LD, Chu M, et al. Genetic diversity and evolution of human metapneumovirus fusion protein over twenty years. Virol J. 2009;6:138.
25.Easton AJ, Domachowske JB, Rosenberg HF. Animal pneumoviruses: molecular genetics and pathogenesis. Clin Microbiol Rev. 2004;17(2):390-412.
26.Seal BS. Matrix protein gene nucleotide and predicted amino acid sequence demonstrate that the first US avian pneumovirus isolate is distinct from European strains. Virus Res. 1998;58(1-2):45-52.
27.van den Hoogen BG, Herfst S, Sprong L, Cane PA, Forleo-Neto E, de Swart RL, et al. Antigenic and genetic variability of human metapneumoviruses. Emerg Infect Dis. 2004;10(4):658-66.
28.Skiadopoulos MH, Biacchesi S, Buchholz UJ, Riggs JM, Surman SR, Amaro-Carambot E, et al. The two major human metapneumovirus genetic lineages are highly related antigenically, and the fusion (F) protein is a major contributor to this antigenic relatedness. J Virol. 2004;78(13):6927-37.
29.MacPhail M, Schickli JH, Tang RS, Kaur J, Robinson C, Fouchier RAM, et al. Identification of small-animal and primate models for evaluation of vaccine candidates for human metapneumovirus (hMPV) and implications for hMPV vaccine design. J Gen Virol. 2004;85(Pt 6):1655-63.
30.Williams JV, Edwards KM, Weinberg GA, Griffin MR, Hall CB, Zhu Y, et al. Population-based incidence of human metapneumovirus infection among hospitalized children. J Infect Dis. 2010;201(12):1890-8.
31.Soto JA, Galvez NMS, Benavente FM, Pizarro-Ortega MS, Lay MK, Riedel C, et al. Human Metapneumovirus: Mechanisms and Molecular Targets Used by the Virus to Avoid the Immune System. Front Immunol. 2018;9:2466.
32.Andrade CA, Pacheco GA, Galvez NMS, Soto JA, Bueno SM, Kalergis AM. Innate Immune Components that Regulate the Pathogenesis and Resolution of hRSV and hMPV Infections. Viruses. 2020;12(6).
33.Cox RG, Mainou BA, Johnson M, Hastings AK, Schuster JE, Dermody TS, et al. Human Metapneumovirus Is Capable of Entering Cells by Fusion with Endosomal Membranes. PLoS Pathog. 2015;11(12):e1005303.

34.Cox RG, Livesay SB, Johnson M, Ohi MD, Williams JV. The human metapneumovirus fusion protein mediates entry via an interaction with RGD-binding integrins. J Virol. 2012;86(22):12148-60.
35.Kolli D, Bao X, Casola A. Human metapneumovirus antagonism of innate immune responses. Viruses. 2012;4(12):3551-71.
36.Cavallaro EC, Liang KK, Lawrence MD, Forsyth KD, Dixon DL. Neutrophil infiltration and activation in bronchiolitic airways are independent of viral etiology. Pediatr Pulmonol. 2017;52(2):238-46.
37.Vargas SO, Kozakewich HP, Perez-Atayde AR, McAdam AJ. Pathology of human metapneumovirus infection: insights into the pathogenesis of a newly identified respiratory virus. Pediatr Dev Pathol. 2004;7(5):478-86; discussion 21.
38.Kim CK, Choi J, Callaway Z, Kim HB, Chung JY, Koh YY, et al. Clinical and epidemiological comparison of human metapneumovirus and respiratory syncytial virus in seoul, Korea, 2003-2008. J Korean Med Sci. 2010;25(3):342-7.
39.Chakraborty K, Zhou Z, Wakamatsu N, Guerrero-Plata A. Interleukin-12p40 modulates human metapneumovirus-induced pulmonary disease in an acute mouse model of infection. PLoS One. 2012;7(5):e37173.
40.Kolli D, Gupta MR, Sbrana E, Velayutham TS, Chao H, Casola A, et al. Alveolar macrophages contribute to the pathogenesis of human metapneumovirus infection while protecting against respiratory syncytial virus infection. Am J Respir Cell Mol Biol. 2014;51(4):502-15.
41.Wen SC, Tollefson SJ, Johnson M, Gilchuk P, Boyd KL, Shepherd B, et al. Acute clearance of human metapneumovirus occurs independently of natural killer cells. J Virol. 2014;88(18):10963-9.
42.Galvez NMS, Andrade CA, Pacheco GA, Soto JA, Stranger V, Rivera T, et al. Host Components That Modulate the Disease Caused by hMPV. Viruses. 2021;13(3).
43.Hastings AK, Erickson JJ, Schuster JE, Boyd KL, Tollefson SJ, Johnson M, et al. Role of type I interferon signaling in human metapneumovirus pathogenesis and control of viral replication. J Virol. 2015;89(8):4405-20.
44.Hastings AK, Amato KR, Wen SC, Peterson LS, Williams JV. Human metapneumovirus small hydrophobic (SH) protein downregulates type I IFN pathway signaling by affecting STAT1 expression and phosphorylation. Virology. 2016;494:248-56.
45.Bao X, Kolli D, Esham D, Velayutham TS, Casola A. Human Metapneumovirus Small Hydrophobic Protein Inhibits Interferon Induction in Plasmacytoid Dendritic Cells. Viruses. 2018;10(6).
46.Erickson JJ, Gilchuk P, Hastings AK, Tollefson SJ, Johnson M, Downing MB, et al. Viral acute lower respiratory infections impair CD8+ T cells through PD-1. J Clin Invest. 2012;122(8):2967-82.
47.Xiao X, Fridman A, Zhang L, Pristatsky P, Durr E, Minnier M, et al. Profiling of hMPV F-specific antibodies isolated from human memory B cells. Nat Commun. 2022;13(1):2546.
48.Okamoto M, Sugawara K, Takashita E, Muraki Y, Hongo S, Nishimura H, et al. Longitudinal course of human metapneumovirus antibody titers and reinfection in healthy adults. J Med Virol. 2010;82(12):2092-6.
49.Falsey AR, Erdman D, Anderson LJ, Walsh EE. Human metapneumovirus infections in young and elderly adults. J Infect Dis. 2003;187(5):785-90.

50.Williams JV, Wang CK, Yang CF, Tollefson SJ, House FS, Heck JM, et al. The role of human metapneumovirus in upper respiratory tract infections in children: a 20-year experience. J Infect Dis. 2006;193(3):387-95.
51.Kolli D, Bataki EL, Spetch L, Guerrero-Plata A, Jewell AM, Piedra PA, et al. T lymphocytes contribute to antiviral immunity and pathogenesis in experimental human metapneumovirus infection. J Virol. 2008;82(17):8560-9.
52.Erickson JJ, Lu P, Wen S, Hastings AK, Gilchuk P, Joyce S, et al. Acute Viral Respiratory Infection Rapidly Induces a CD8+ T Cell Exhaustion-like Phenotype. J Immunol. 2015;195(9):4319-30.
53.Wen SC, Schuster JE, Gilchuk P, Boyd KL, Joyce S, Williams JV. Lung CD8+ T Cell Impairment Occurs during Human Metapneumovirus Infection despite Virus-Like Particle Induction of Functional CD8+ T Cells. J Virol. 2015;89(17):8713-26.
54.McLane LM, Abdel-Hakeem MS, Wherry EJ. CD8 T Cell Exhaustion During Chronic Viral Infection and Cancer. Annu Rev Immunol. 2019;37:457-95.
55.Day CL, Kaufmann DE, Kiepiela P, Brown JA, Moodley ES, Reddy S, et al. PD-1 expression on HIV-specific T cells is associated with T-cell exhaustion and disease progression. Nature. 2006;443(7109):350-4.
56.Budimir N, Thomas GD, Dolina JS, Salek-Ardakani S. Reversing T-cell Exhaustion in Cancer: Lessons Learned from PD-1/PD-L1 Immune Checkpoint Blockade. Cancer Immunol Res. 2022;10(2):146-53.
57.Barber DL, Wherry EJ, Masopust D, Zhu B, Allison JP, Sharpe AH, et al. Restoring function in exhausted CD8 T cells during chronic viral infection. Nature. 2006;439(7077):682-7.
58.Arasanz H, Gato-Canas M, Zuazo M, Ibanez-Vea M, Breckpot K, Kochan G, et al. PD1 signal transduction pathways in T cells. Oncotarget. 2017;8(31):51936-45.
59.Wu Y, Chen W, Xu ZP, Gu W. PD-L1 Distribution and Perspective for Cancer Immunotherapy-Blockade, Knockdown, or Inhibition. Front Immunol. 2019;10:2022.
60.Philips EA, Garcia-Espana A, Tocheva AS, Ahearn IM, Adam KR, Pan R, et al. The structural features that distinguish PD-L2 from PD-L1 emerged in placental mammals. J Biol Chem. 2020;295(14):4372-80.
61.Erickson JJ, Rogers MC, Hastings AK, Tollefson SJ, Williams JV. Programmed death-1 impairs secondary effector lung CD8(+) T cells during respiratory virus reinfection. J Immunol. 2014;193(10):5108-17.
62.Erickson JJ, Rogers MC, Tollefson SJ, Boyd KL, Williams JV. Multiple Inhibitory Pathways Contribute to Lung CD8+ T Cell Impairment and Protect against Immunopathology during Acute Viral Respiratory Infection. J Immunol. 2016;197(1):233-43.
63.Rogers MC, Lamens KD, Shafagati N, Johnson M, Oury TD, Joyce S, et al. CD4(+) Regulatory T Cells Exert Differential Functions during Early and Late Stages of the Immune Response to Respiratory Viruses. J Immunol. 2018;201(4):1253-66.
64.Williams JV, Chen Z, Cseke G, Wright DW, Keefer CJ, Tollefson SJ, et al. A recombinant human monoclonal antibody to human metapneumovirus fusion protein that neutralizes virus in vitro and is effective therapeutically in vivo. J Virol. 2007;81(15):8315-24.
65.Hamelin ME, Gagnon C, Prince GA, Kiener P, Suzich J, Ulbrandt N, et al. Prophylactic and therapeutic benefits of a monoclonal antibody against the fusion protein of human metapneumovirus in a mouse model. Antiviral Res. 2010;88(1):31-7.

66.Ulbrandt ND, Ji H, Patel NK, Riggs JM, Brewah YA, Ready S, et al. Isolation and characterization of monoclonal antibodies which neutralize human metapneumovirus in vitro and in vivo. J Virol. 2006;80(16):7799-806.
67.Hamelin ME, Couture C, Sackett M, Kiener P, Suzich J, Ulbrandt N, et al. The prophylactic administration of a monoclonal antibody against human metapneumovirus attenuates viral disease and airways hyperresponsiveness in mice. Antivir Ther. 2008;13(1):39-46.
68.Wen X, Krause JC, Leser GP, Cox RG, Lamb RA, Williams JV, et al. Structure of the human metapneumovirus fusion protein with neutralizing antibody identifies a pneumovirus antigenic site. Nat Struct Mol Biol. 2012;19(4):461-3.
69.Deffrasnes C, Hamelin ME, Prince GA, Boivin G. Identification and evaluation of a highly effective fusion inhibitor for human metapneumovirus. Antimicrob Agents Chemother. 2008;52(1):279-87.
70.Miller SA, Tollefson S, Crowe JE, Jr., Williams JV, Wright DW. Examination of a fusogenic hexameric core from human metapneumovirus and identification of a potent synthetic peptide inhibitor from the heptad repeat 1 region. J Virol. 2007;81(1):141-9.
71.Shahda S, Carlos WG, Kiel PJ, Khan BA, Hage CA. The human metapneumovirus: a case series and review of the literature. Transpl Infect Dis. 2011;13(3):324-8.
72.Wyde PR, Moylett EH, Chetty SN, Jewell A, Bowlin TL, Piedra PA. Comparison of the inhibition of human metapneumovirus and respiratory syncytial virus by NMSO3 in tissue culture assays. Antiviral Res. 2004;63(1):51-9.
73.Hamelin ME, Prince GA, Boivin G. Effect of ribavirin and glucocorticoid treatment in a mouse model of human metapneumovirus infection. Antimicrob Agents Chemother. 2006;50(2):774-7.
74.Kilham L, Ferm VH. Congenital anomalies induced in hamster embryos with ribavirin. Science. 1977;195(4276):413-4.
75.Lee J, Son W, Hong J, Song Y, Yang CS, Kim YH. Down-regulation of TNF-alpha via macrophage-targeted RNAi system for the treatment of acute inflammatory sepsis. J Control Release. 2021;336:344-53.
76.Deffrasnes C, Cavanagh MH, Goyette N, Cui K, Ge Q, Seth S, et al. Inhibition of human metapneumovirus replication by small interfering RNA. Antivir Ther. 2008;13(6):821-32.
77.Miranda-Katz M, Erickson JJ, Lan J, Ecker A, Zhang Y, Joyce S, et al. Novel HLA-B7-restricted human metapneumovirus epitopes enhance viral clearance in mice and are recognized by human CD8(+) T cells. Sci Rep. 2021;11(1):20769.
78.Hamelin ME, Couture C, Sackett MK, Boivin G. Enhanced lung disease and Th2 response following human metapneumovirus infection in mice immunized with the inactivated virus. J Gen Virol. 2007;88(Pt 12):3391-400.
79.Yim KC, Cragin RP, Boukhvalova MS, Blanco JC, Hamlin ME, Boivin G, et al. Human metapneumovirus: enhanced pulmonary disease in cotton rats immunized with formalin-inactivated virus vaccine and challenged. Vaccine. 2007;25(27):5034-40.
80.Levy C, Aerts L, Hamelin ME, Granier C, Szecsi J, Lavillette D, et al. Virus-like particle vaccine induces cross-protection against human metapneumovirus infections in mice. Vaccine. 2013;31(25):2778-85.
81.Talaat KR, Karron RA, Thumar B, McMahon BA, Schmidt AC, Collins PL, et al. Experimental infection of adults with recombinant wild-type human metapneumovirus. J Infect Dis. 2013;208(10):1669-78.

82.Johnstone J, Parsons R, Botelho F, Millar J, McNeil S, Fulop T, et al. Immune biomarkers predictive of respiratory viral infection in elderly nursing home residents. PLoS One. 2014;9(9):e108481.
83.Flamaing J, Engelmann I, Joosten E, Van Ranst M, Verhaegen J, Peetermans WE. Viral lower respiratory tract infection in the elderly: a prospective in-hospital study. Eur J Clin Microbiol Infect Dis. 2003;22(12):720-5.
84.Talbot HK, Falsey AR. The diagnosis of viral respiratory disease in older adults. Clin Infect Dis. 2010;50(5):747-51.
85.Kobashi Y, Okimoto N, Matsushima T, Soejima R. Clinical analysis of community-acquired pneumonia in the elderly. Intern Med. 2001;40(8):703-7.
86.Boe DM, Boule LA, Kovacs EJ. Innate immune responses in the ageing lung. Clin Exp Immunol. 2017;187(1):16-25.
87.Molinari NA, Ortega-Sanchez IR, Messonnier ML, Thompson WW, Wortley PM, Weintraub E, et al. The annual impact of seasonal influenza in the US: measuring disease burden and costs. Vaccine. 2007;25(27):5086-96.
88.Pollard CA, Morran MP, Nestor-Kalinoski AL. The COVID-19 pandemic: a global health crisis. Physiol Genomics. 2020;52(11):549-57.
89.Tsai Y, Vogt TM, Zhou F. Patient Characteristics and Costs Associated With COVID-19-Related Medical Care Among Medicare Fee-for-Service Beneficiaries. Ann Intern Med. 2021;174(8):1101-9.
90.Thompson WW, Shay DK, Weintraub E, Brammer L, Cox N, Anderson LJ, et al. Mortality associated with influenza and respiratory syncytial virus in the United States. JAMA. 2003;289(2):179-86.
91.Oh SJ, Lee JK, Shin OS. Aging and the Immune System: the Impact of Immunosenescence on Viral Infection, Immunity and Vaccine Immunogenicity. Immune Netw. 2019;19(6):e37.
92.Greenberg SB. Respiratory viral infections in adults. Curr Opin Pulm Med. 2002;8(3):201-8.
93.Loeb M, McGeer A, McArthur M, Peeling RW, Petric M, Simor AE. Surveillance for outbreaks of respiratory tract infections in nursing homes. CMAJ. 2000;162(8):1133-7.
94.Walsh EE. Respiratory Syncytial Virus Infection: An Illness for All Ages. Clin Chest Med. 2017;38(1):29-36.
95.Sundaram ME, Meece JK, Sifakis F, Gasser RA, Jr., Belongia EA. Medically attended respiratory syncytial virus infections in adults aged >/= 50 years: clinical characteristics and outcomes. Clin Infect Dis. 2014;58(3):342-9.
96.Bellmann-Weiler R, Weiss G. Pitfalls in the diagnosis and therapy of infections in elderly patients--a mini-review. Gerontology. 2009;55(3):241-9.
97.Jongbloed M, Leijte WT, Linssen CFM, van den Hoogen BG, van Gorp ECM, de Kruif MD. Clinical impact of human metapneumovirus infections before and during the COVID-19 pandemic. Infect Dis (Lond). 2021:1-10.
98.Falsey AR, Walsh EE. Respiratory syncytial virus infection in elderly adults. Drugs Aging. 2005;22(7):577-87.
99.Morales F, Calder MA, Inglis JM, Murdoch PS, Williamson J. A study of respiratory infections in the elderly to assess the role of respiratory syncytial virus. J Infect. 1983;7(3):236-47.
100.Vikerfors T, Grandien M, Olcen P. Respiratory syncytial virus infections in adults. Am Rev Respir Dis. 1987;136(3):561-4.

101.Falsey AR, Cunningham CK, Barker WH, Kouides RW, Yuen JB, Menegus M, et al. Respiratory syncytial virus and influenza A infections in the hospitalized elderly. J Infect Dis. 1995;172(2):389-94.
102.Zaroukian MH, Leader I. Community-acquired pneumonia and infection with respiratory syncytial virus. Ann Intern Med. 1988;109(6):515-6.
103.Linehan E, Fitzgerald DC. Ageing and the immune system: focus on macrophages. Eur J Microbiol Immunol (Bp). 2015;5(1):14-24.
104.Ogawa T, Kitagawa M, Hirokawa K. Age-related changes of human bone marrow: a histometric estimation of proliferative cells, apoptotic cells, T cells, B cells and macrophages. Mech Ageing Dev. 2000;117(1-3):57-68.
105.Mogilenko DA, Shchukina I, Artyomov MN. Immune ageing at single-cell resolution. Nat Rev Immunol. 2021.
106.Herrero C, Marques L, Lloberas J, Celada A. IFN-gamma-dependent transcription of MHC class II IA is impaired in macrophages from aged mice. J Clin Invest. 2001;107(4):485-93.
107.Hearps AC, Martin GE, Angelovich TA, Cheng WJ, Maisa A, Landay AL, et al. Aging is associated with chronic innate immune activation and dysregulation of monocyte phenotype and function. Aging Cell. 2012;11(5):867-75.
108.Nyugen J, Agrawal S, Gollapudi S, Gupta S. Impaired functions of peripheral blood monocyte subpopulations in aged humans. J Clin Immunol. 2010;30(6):806-13.
109.Seidler S, Zimmermann HW, Bartneck M, Trautwein C, Tacke F. Age-dependent alterations of monocyte subsets and monocyte-related chemokine pathways in healthy adults. BMC Immunol. 2010;11:30.
110.Franke-Ullmann G, Pfortner C, Walter P, Steinmuller C, Lohmann-Matthes ML, Kobzik L. Characterization of murine lung interstitial macrophages in comparison with alveolar macrophages in vitro. J Immunol. 1996;157(7):3097-104.
111.Eichinger KM, Egana L, Orend JG, Resetar E, Anderson KB, Patel R, et al. Alveolar macrophages support interferon gamma-mediated viral clearance in RSV-infected neonatal mice. Respir Res. 2015;16:122.
112.Kuwano K, Kawashima T, Arai S. Antiviral effect of TNF-alpha and IFN-gamma secreted from a CD8+ influenza virus-specific CTL clone. Viral Immunol. 1993;6(1):1-11.
113.Ardain A, Marakalala MJ, Leslie A. Tissue-resident innate immunity in the lung. Immunology. 2020;159(3):245-56.
114.Wong CK, Smith CA, Sakamoto K, Kaminski N, Koff JL, Goldstein DR. Aging Impairs Alveolar Macrophage Phagocytosis and Increases Influenza-Induced Mortality in Mice. J Immunol. 2017;199(3):1060-8.
115.McQuattie-Pimentel AC, Ren Z, Joshi N, Watanabe S, Stoeger T, Chi M, et al. The lung microenvironment shapes a dysfunctional response of alveolar macrophages in aging. J Clin Invest. 2021;131(4).
116.Blacher E, Tsai C, Litichevskiy L, Shipony Z, Iweka CA, Schneider KM, et al. Aging disrupts circadian gene regulation and function in macrophages. Nat Immunol. 2022;23(2):229-36.
117.Minciullo PL, Catalano A, Mandraffino G, Casciaro M, Crucitti A, Maltese G, et al. Inflammaging and Anti-Inflammaging: The Role of Cytokines in Extreme Longevity. Arch Immunol Ther Exp (Warsz). 2016;64(2):111-26.
118.Singh T, Newman AB. Inflammatory markers in population studies of aging. Ageing Res Rev. 2011;10(3):319-29.

119.Franceschi C, Bonafe M, Valensin S, Olivieri F, De Luca M, Ottaviani E, et al. Inflamm-aging. An evolutionary perspective on immunosenescence. Ann N Y Acad Sci. 2000;908:244-54.
120.Weissberg PL, Bennett MR. Atherosclerosis--an inflammatory disease. N Engl J Med. 1999;340(24):1928-9.
121.Eikelenboom P, Veerhuis R. The importance of inflammatory mechanisms for the development of Alzheimer's disease. Exp Gerontol. 1999;34(3):453-61.
122.Giunta S. Exploring the complex relations between inflammation and aging (inflamm-aging): anti-inflamm-aging remodelling of inflamm- aging, from robustness to frailty. Inflammation research : official journal of the European Histamine Research Society [et al]. 2008;57(12):558-63.
123.Boule LA, Kovacs EJ. Alcohol, aging, and innate immunity. J Leukoc Biol. 2017;102(1):41-55.
124.Fedullo AJ, Swinburne AJ. Relationship of patient age to clinical features and outcome for in-hospital treatment of pneumonia. J Gerontol. 1985;40(1):29-33.
125.Park H, Adeyemi AO, Rascati KL. Direct Medical Costs and Utilization of Health Care Services to Treat Pneumonia in the United States: An Analysis of the 2007-2011 Medical Expenditure Panel Survey. Clin Ther. 2015;37(7):1466-76 e1.
126.Boyd AR, Orihuela CJ. Dysregulated inflammation as a risk factor for pneumonia in the elderly. Aging Dis. 2011;2(6):487-500.
127.Lowery EM, Brubaker AL, Kuhlmann E, Kovacs EJ. The aging lung. Clin Interv Aging. 2013;8:1489-96.
128.Kovacs EJ, Grabowski KA, Duffner LA, Plackett TP, Gregory MS. Survival and cell mediated immunity after burn injury in aged mice. J Am Aging Assoc. 2002;25(1):3-9.
129.Castelo-Branco C, Soveral I. The immune system and aging: a review. Gynecol Endocrinol. 2014;30(1):16-22.
130.Franceschi C, Garagnani P, Parini P, Giuliani C, Santoro A. Inflammaging: a new immune-metabolic viewpoint for age-related diseases. Nat Rev Endocrinol. 2018;14(10):576-90.
131.Baggio G, Donazzan S, Monti D, Mari D, Martini S, Gabelli C, et al. Lipoprotein(a) and lipoprotein profile in healthy centenarians: a reappraisal of vascular risk factors. FASEB J. 1998;12(6):433-7.
132.Hitt R, Young-Xu Y, Silver M, Perls T. Centenarians: the older you get, the healthier you have been. Lancet. 1999;354(9179):652.
133.Bruunsgaard H, Andersen-Ranberg K, Jeune B, Pedersen AN, Skinhoj P, Pedersen BK. A high plasma concentration of TNF-alpha is associated with dementia in centenarians. J Gerontol A Biol Sci Med Sci. 1999;54(7):M357-64.
134.Ebersole JL, Graves CL, Gonzalez OA, Dawson D, 3rd, Morford LA, Huja PE, et al. Aging, inflammation, immunity and periodontal disease. Periodontol 2000. 2016;72(1):54-75.
135.Almanzar G, Schwaiger S, Jenewein B, Keller M, Herndler-Brandstetter D, Wurzner R, et al. Long-term cytomegalovirus infection leads to significant changes in the composition of the CD8+ T-cell repertoire, which may be the basis for an imbalance in the cytokine production profile in elderly persons. J Virol. 2005;79(6):3675-83.
136.Gay NJ, Gangloff M. Structure and function of Toll receptors and their ligands. Annu Rev Biochem. 2007;76:141-65.
137.Bekkering S, Dominguez-Andres J, Joosten LAB, Riksen NP, Netea MG. Trained Immunity: Reprogramming Innate Immunity in Health and Disease. Annual review of immunology. 2021;39:667-93.

138.Bulut O, Kilic G, Dominguez-Andres J. Immune Memory in Aging: a Wide Perspective Covering Microbiota, Brain, Metabolism, and Epigenetics. Clin Rev Allergy Immunol. 2021.
139.Zhou H, Thompson WW, Viboud CG, Ringholz CM, Cheng PY, Steiner C, et al. Hospitalizations associated with influenza and respiratory syncytial virus in the United States, 1993-2008. Clin Infect Dis. 2012;54(10):1427-36.
140.Lee JB, Oelke M, Ramachandra L, Canaday DH, Schneck JP. Decline of influenza-specific CD8+ T cell repertoire in healthy geriatric donors. Immun Ageing. 2011;8:6.
141.Telcian AG, Laza-Stanca V, Edwards MR, Harker JA, Wang H, Bartlett NW, et al. RSV-induced bronchial epithelial cell PD-L1 expression inhibits CD8+ T cell nonspecific antiviral activity. J Infect Dis. 2011;203(1):85-94.
142.Suvas S, Joo HM, Sehrawat S, Suvas PK, Sangster MY, Yagita H, et al. Functional Significance of PD-1 expression on aging T cells (85.4). The Journal of Immunology. 2007;178(1 Supplement):S118-S.
143.Yager EJ, Ahmed M, Lanzer K, Randall TD, Woodland DL, Blackman MA. Age-associated decline in T cell repertoire diversity leads to holes in the repertoire and impaired immunity to influenza virus. J Exp Med. 2008;205(3):711-23.
144.Desai A, Grolleau-Julius A, Yung R. Leukocyte function in the aging immune system. J Leukoc Biol. 2010;87(6):1001-9.
145.Quinn KM, Fox A, Harland KL, Russ BE, Li J, Nguyen THO, et al. Age-Related Decline in Primary CD8(+) T Cell Responses Is Associated with the Development of Senescence in Virtual Memory CD8(+) T Cells. Cell Rep. 2018;23(12):3512-24.
146.Hasvold J, Sjoding M, Pohl K, Cooke C, Hyzy RC. The role of human metapneumovirus in the critically ill adult patient. J Crit Care. 2016;31(1):233-7.
147.Widmer K, Zhu Y, Williams JV, Griffin MR, Edwards KM, Talbot HK. Rates of hospitalizations for respiratory syncytial virus, human metapneumovirus, and influenza virus in older adults. J Infect Dis. 2012;206(1):56-62.
148.Holzemer NF, Hasvold JJ, Pohl KJ, Ashbrook MJ, Meert KL, Quasney MW. Human Metapneumovirus Infection in Hospitalized Children. Respir Care. 2020;65(5):650-7.
149.Syha R, Beck R, Hetzel J, Ketelsen D, Grosse U, Springer F, et al. Human metapneumovirus (HMPV) associated pulmonary infections in immunocompromised adults--initial CT findings, disease course and comparison to respiratory-syncytial-virus (RSV) induced pulmonary infections. Eur J Radiol. 2012;81(12):4173-8.
150.Mogilenko DA, Shpynov O, Andhey PS, Arthur L, Swain A, Esaulova E, et al. Comprehensive Profiling of an Aging Immune System Reveals Clonal GZMK(+) CD8(+) T Cells as Conserved Hallmark of Inflammaging. Immunity. 2021;54(1):99-115 e12.
151.Angelidis I, Simon LM, Fernandez IE, Strunz M, Mayr CH, Greiffo FR, et al. An atlas of the aging lung mapped by single cell transcriptomics and deep tissue proteomics. Nat Commun. 2019;10(1):963.
152.Li J, He Y, Hao J, Ni L, Dong C. High Levels of Eomes Promote Exhaustion of Anti-tumor CD8(+) T Cells. Front Immunol. 2018;9:2981.
153.Hu B, Jadhav RR, Gustafson CE, Le Saux S, Ye Z, Li X, et al. Distinct Age-Related Epigenetic Signatures in CD4 and CD8 T Cells. Front Immunol. 2020;11:585168.
154.Goplen NP, Wu Y, Son YM, Li C, Wang Z, Cheon IS, et al. Tissue-resident CD8(+) T cells drive age-associated chronic lung sequelae after viral pneumonia. Sci Immunol. 2020;5(53).

155.Po JL, Gardner EM, Anaraki F, Katsikis PD, Murasko DM. Age-associated decrease in virus-specific CD8+ T lymphocytes during primary influenza infection. Mech Ageing Dev. 2002;123(8):1167-81.
156.Jiang J, Bennett AJ, Fisher E, Williams-Bey Y, Shen H, Murasko DM. Limited expansion of virus-specific CD8 T cells in the aged environment. Mech Ageing Dev. 2009;130(11-12):713-21.
157.Verschoor CP, Pawelec G, Haynes L, Loeb M, Andrew MK, Kuchel GA, et al. Granzyme B: a double-edged sword in the response to influenza infection in vaccinated older adults. Front Aging. 2021;2.
158.McElhaney JE, Ewen C, Zhou X, Kane KP, Xie D, Hager WD, et al. Granzyme B: Correlates with protection and enhanced CTL response to influenza vaccination in older adults. Vaccine. 2009;27(18):2418-25.
159.Dolfi DV, Mansfield KD, Polley AM, Doyle SA, Freeman GJ, Pircher H, et al. Increased T-bet is associated with senescence of influenza virus-specific CD8 T cells in aged humans. J Leukoc Biol. 2013;93(6):825-36.
160.Williams JV, Tollefson SJ, Johnson JE, Crowe JE, Jr. The cotton rat (Sigmodon hispidus) is a permissive small animal model of human metapneumovirus infection, pathogenesis, and protective immunity. J Virol. 2005;79(17):10944-51.
161.Xu J, Zhang Y, Williams JV. Development and optimization of a direct plaque assay for trypsin-dependent human metapneumovirus strains. J Virol Methods. 2018;259:1-9.
162.Busch CJ, Favret J, Geirsdottir L, Molawi K, Sieweke MH. Isolation and Long-term Cultivation of Mouse Alveolar Macrophages. Bio Protoc. 2019;9(14).
163.Rock MT, Crowe JE, Jr. Identification of a novel human leucocyte antigen-A*01-restricted cytotoxic T-lymphocyte epitope in the respiratory syncytial virus fusion protein. Immunology. 2003;108(4):474-80.
164.Khan O, Giles JR, McDonald S, Manne S, Ngiow SF, Patel KP, et al. TOX transcriptionally and epigenetically programs CD8(+) T cell exhaustion. Nature. 2019;571(7764):211-8.
165.Lu YJ, Barreira-Silva P, Boyce S, Powers J, Cavallo K, Behar SM. CD4 T cell help prevents CD8 T cell exhaustion and promotes control of Mycobacterium tuberculosis infection. Cell Rep. 2021;36(11):109696.
166.Khan SM, Desai R, Coxon A, Livingstone A, Dunn GP, Petti A, et al. Impact of CD4 T cells on intratumoral CD8 T-cell exhaustion and responsiveness to PD-1 blockade therapy in mouse brain tumors. J Immunother Cancer. 2022;10(12).
167.Menk AV, Scharping NE, Rivadeneira DB, Calderon MJ, Watson MJ, Dunstane D, et al. 4-1BB costimulation induces T cell mitochondrial function and biogenesis enabling cancer immunotherapeutic responses. J Exp Med. 2018;215(4):1091-100.
168.Forde PM, Chaft JE, Smith KN, Anagnostou V, Cottrell TR, Hellmann MD, et al. Neoadjuvant PD-1 Blockade in Resectable Lung Cancer. N Engl J Med. 2018;378(21):1976-86.
169.Darniot M, Pitoiset C, Petrella T, Aho S, Pothier P, Manoha C. Age-associated aggravation of clinical disease after primary metapneumovirus infection of BALB/c mice. J Virol. 2009;83(7):3323-32.
170.Westmeier J, Paniskaki K, Karakose Z, Werner T, Sutter K, Dolff S, et al. Impaired Cytotoxic CD8(+) T Cell Response in Elderly COVID-19 Patients. mBio. 2020;11(5).
171.Mattoo H, Faulkner M, Kandpal U, Das R, Lewis V, George A, et al. Naive CD4 T cells from aged mice show enhanced death upon primary activation. Int Immunol. 2009;21(11):1277-89.
172.Saule P, Trauet J, Dutriez V, Lekeux V, Dessaint JP, Labalette M. Accumulation of memory T cells from childhood to old age: central and effector memory cells in CD4(+) versus effector

memory and terminally differentiated memory cells in CD8(+) compartment. Mech Ageing Dev. 2006;127(3):274-81.
173.Gilchuk P, Spencer CT, Conant SB, Hill T, Gray JJ, Niu X, et al. Discovering naturally processed antigenic determinants that confer protective T cell immunity. J Clin Invest. 2013;123(5):1976-87.
174.Martinez-Perez AG, Perez-Trujillo JJ, Garza-Morales R, Loera-Arias MJ, Saucedo-Cardenas O, Garcia-Garcia A, et al. 4-1BBL as a Mediator of Cross-Talk between Innate, Adaptive, and Regulatory Immunity against Cancer. Int J Mol Sci. 2021;22(12).
175.Kuribayashi W, Oshima M, Itokawa N, Koide S, Nakajima-Takagi Y, Yamashita M, et al. Limited rejuvenation of aged hematopoietic stem cells in young bone marrow niche. J Exp Med. 2021;218(3).
176.Wherry EJ, Ha SJ, Kaech SM, Haining WN, Sarkar S, Kalia V, et al. Molecular signature of CD8+ T cell exhaustion during chronic viral infection. Immunity. 2007;27(4):670-84.
177.Forde PM, Chaft JE, Pardoll DM. Neoadjuvant PD-1 Blockade in Resectable Lung Cancer. N Engl J Med. 2018;379(9):e14.
178.Tserel L, Kolde R, Limbach M, Tretyakov K, Kasela S, Kisand K, et al. Age-related profiling of DNA methylation in CD8+ T cells reveals changes in immune response and transcriptional regulator genes. Sci Rep. 2015;5:13107.
179.Im SJ, Hashimoto M, Gerner MY, Lee J, Kissick HT, Burger MC, et al. Defining CD8+ T cells that provide the proliferative burst after PD-1 therapy. Nature. 2016;537(7620):417-21.
180.Ford BR, Vignali PDA, Rittenhouse NL, Scharping NE, Peralta R, Lontos K, et al. Tumor microenvironmental signals reshape chromatin landscapes to limit the functional potential of exhausted T cells. Sci Immunol. 2022;7(74):eabj9123.
181.Schuster JE, Williams JV. Human metapneumovirus. Pediatr Rev. 2013;34(12):558-65.
182.Collaborators GBDLRI. Estimates of the global, regional, and national morbidity, mortality, and aetiologies of lower respiratory infections in 195 countries, 1990-2016: a systematic analysis for the Global Burden of Disease Study 2016. Lancet Infect Dis. 2018;18(11):1191-210.
183.Widmer K, Griffin MR, Zhu Y, Williams JV, Talbot HK. Respiratory syncytial virus- and human metapneumovirus-associated emergency department and hospital burden in adults. Influenza Other Respir Viruses. 2014;8(3):347-52.
184.Falsey AR, Walsh EE, House S, Vandenijck Y, Ren X, Keim S, et al. Risk Factors and Medical Resource Utilization of Respiratory Syncytial Virus, Human Metapneumovirus, and Influenza-Related Hospitalizations in Adults-A Global Study During the 2017-2019 Epidemic Seasons (Hospitalized Acute Respiratory Tract Infection [HARTI] Study). Open Forum Infect Dis. 2021;8(11):ofab491.
185.Team CC-R. Severe Outcomes Among Patients with Coronavirus Disease 2019 (COVID-19) - United States, February 12-March 16, 2020. MMWR Morb Mortal Wkly Rep. 2020;69(12):343-6.
186.Lopez-Otin C, Blasco MA, Partridge L, Serrano M, Kroemer G. The hallmarks of aging. Cell. 2013;153(6):1194-217.
187.Linton PJ, Dorshkind K. Age-related changes in lymphocyte development and function. Nat Immunol. 2004;5(2):133-9.
188.Thome JJ, Yudanin N, Ohmura Y, Kubota M, Grinshpun B, Sathaliyawala T, et al. Spatial map of human T cell compartmentalization and maintenance over decades of life. Cell. 2014;159(4):814-28.

189.Cookenham T, Lanzer KG, Tighe M, Ward JM, Reiley WW, Blackman MA. Visualization of Resident Memory CD8 T Cells in the Lungs of Young and Aged Influenza Memory Mice and after Heterosubtypic Challenge. Immunohorizons. 2021;5(7):543-56.
190.Sasaki S, Sullivan M, Narvaez CF, Holmes TH, Furman D, Zheng NY, et al. Limited efficacy of inactivated influenza vaccine in elderly individuals is associated with decreased production of vaccine-specific antibodies. J Clin Invest. 2011;121(8):3109-19.
191.Baldwin SL, Hsu FC, Van Hoeven N, Gage E, Granger B, Guderian JA, et al. Improved Immune Responses in Young and Aged Mice with Adjuvanted Vaccines against H1N1 Influenza Infection. Front Immunol. 2018;9:295.
192.Lee JKH, Lam GKL, Shin T, Samson SI, Greenberg DP, Chit A. Efficacy and effectiveness of high-dose influenza vaccine in older adults by circulating strain and antigenic match: An updated systematic review and meta-analysis. Vaccine. 2021;39 Suppl 1:A24-A35.
193.Falsey AR, Hennessey PA, Formica MA, Criddle MM, Biear JM, Walsh EE. Humoral immunity to human metapneumovirus infection in adults. Vaccine. 2010;28(6):1477-80.
194.Malloy AM, Falsey AR, Ruckwardt TJ. Consequences of immature and senescent immune responses for infection with respiratory syncytial virus. Curr Top Microbiol Immunol. 2013;372:211-31.
195.Dutta S, Sengupta P. Men and mice: Relating their ages. Life Sci. 2016;152:244-8.
196.Alvarez R, Tripp RA. The immune response to human metapneumovirus is associated with aberrant immunity and impaired virus clearance in BALB/c mice. J Virol. 2005;79(10):5971-8.
197.Elsegeiny W, Eddens T, Chen K, Kolls JK. Anti-CD20 antibody therapy and susceptibility to Pneumocystis pneumonia. Infect Immun. 2015;83(5):2043-52.
198.Masopust D, Schenkel JM. The integration of T cell migration, differentiation and function. Nat Rev Immunol. 2013;13(5):309-20.
199.Henry C, Zheng NY, Huang M, Cabanov A, Rojas KT, Kaur K, et al. Influenza Virus Vaccination Elicits Poorly Adapted B Cell Responses in Elderly Individuals. Cell Host Microbe. 2019;25(3):357-66 e6.
200.Gibson KL, Wu YC, Barnett Y, Duggan O, Vaughan R, Kondeatis E, et al. B-cell diversity decreases in old age and is correlated with poor health status. Aging Cell. 2009;8(1):18-25.
201.Frasca D, Blomberg BB. Aging affects human B cell responses. J Clin Immunol. 2011;31(3):430-5.
202.Cox RG, Erickson JJ, Hastings AK, Becker JC, Johnson M, Craven RE, et al. Human metapneumovirus virus-like particles induce protective B and T cell responses in a mouse model. J Virol. 2014;88(11):6368-79.
203.Dockman RL, Carpenter JM, Diaz AN, Benbow RA, Filipov NM. Sex differences in behavior, response to LPS, and glucose homeostasis in middle-aged mice. Behav Brain Res. 2022;418:113628.
204.Wei Y, Zhang Y, Cai H, Mirza AM, Iorio RM, Peeples ME, et al. Roles of the putative integrin-binding motif of the human metapneumovirus fusion (f) protein in cell-cell fusion, viral infectivity, and pathogenesis. J Virol. 2014;88(8):4338-52.
205.Herfst S, Schrauwen EJ, de Graaf M, van Amerongen G, van den Hoogen BG, de Swart RL, et al. Immunogenicity and efficacy of two candidate human metapneumovirus vaccines in cynomolgus macaques. Vaccine. 2008;26(33):4224-30.
206.Biacchesi S, Pham QN, Skiadopoulos MH, Murphy BR, Collins PL, Buchholz UJ. Infection of nonhuman primates with recombinant human metapneumovirus lacking the SH, G, or M2-2

protein categorizes each as a nonessential accessory protein and identifies vaccine candidates. J Virol. 2005;79(19):12608-13.
207.Ogonczyk Makowska D, Hamelin ME, Boivin G. Engineering of Live Chimeric Vaccines against Human Metapneumovirus. Pathogens. 2020;9(2).
208.Karron RA, San Mateo J, Wanionek K, Collins PL, Buchholz UJ. Evaluation of a Live Attenuated Human Metapneumovirus Vaccine in Adults and Children. J Pediatric Infect Dis Soc. 2018;7(1):86-9.
209.Baek K, Maharjan S, Akauliya M, Thapa B, Kim D, Kim J, et al. Comparison of vaccination efficacy using live or ultraviolet-inactivated influenza viruses introduced by different routes in a mouse model. PLoS One. 2022;17(10):e0275722.
210.Iwata-Yoshikawa N, Uda A, Suzuki T, Tsunetsugu-Yokota Y, Sato Y, Morikawa S, et al. Effects of Toll-like receptor stimulation on eosinophilic infiltration in lungs of BALB/c mice immunized with UV-inactivated severe acute respiratory syndrome-related coronavirus vaccine. J Virol. 2014;88(15):8597-614.
211.Papi A, Ison MG, Langley JM, Lee DG, Leroux-Roels I, Martinon-Torres F, et al. Respiratory Syncytial Virus Prefusion F Protein Vaccine in Older Adults. N Engl J Med. 2023;388(7):595-608.
212.Bender BS, Johnson MP, Small PA. Influenza in senescent mice: impaired cytotoxic T-lymphocyte activity is correlated with prolonged infection. Immunology. 1991;72(4):514-9.
213.Parks OB, Eddens T, Sojati J, Lan J, Zhang Y, Oury TD, et al. Terminally exhausted CD8(+) T cells contribute to age-dependent severity of respiratory virus infection. Immun Ageing. 2023;20(1):40.
214.Parks OB, Eddens T, Zhang Y, Oury TD, McElroy A, Williams JV. Human Metapneumovirus Reinfection in Aged Mice Recapitulates Increased Disease Severity in Elderly Humans Infected with Human Metapneumovirus. Immunohorizons. 2023;7(6):398-411.
215.Hashimoto M, Araki K, Cardenas MA, Li P, Jadhav RR, Kissick HT, et al. PD-1 combination therapy with IL-2 modifies CD8(+) T cell exhaustion program. Nature. 2022;610(7930):173-81.
216.Miller BC, Sen DR, Al Abosy R, Bi K, Virkud YV, LaFleur MW, et al. Subsets of exhausted CD8(+) T cells differentially mediate tumor control and respond to checkpoint blockade. Nat Immunol. 2019;20(3):326-36.
217.Geng Y, Zhang Q, Feng S, Li C, Wang L, Zhao X, et al. Safety and Efficacy of PD-1/PD-L1 inhibitors combined with radiotherapy in patients with non-small-cell lung cancer: a systematic review and meta-analysis. Cancer Med. 2021;10(4):1222-39.
218.Elias R, Giobbie-Hurder A, McCleary NJ, Ott P, Hodi FS, Rahma O. Efficacy of PD-1 & PD-L1 inhibitors in older adults: a meta-analysis. J Immunother Cancer. 2018;6(1):26.
219.McNally B, Ye F, Willette M, Flano E. Local blockade of epithelial PDL-1 in the airways enhances T cell function and viral clearance during influenza virus infection. J Virol. 2013;87(23):12916-24.
220.Pauken KE, Godec J, Odorizzi PM, Brown KE, Yates KB, Ngiow SF, et al. The PD-1 Pathway Regulates Development and Function of Memory CD8(+) T Cells following Respiratory Viral Infection. Cell Rep. 2020;31(13):107827.
221.Strohacker K, Breslin WL, Carpenter KC, McFarlin BK. Aged mice have increased inflammatory monocyte concentration and altered expression of cell-surface functional receptors. J Biosci. 2012;37(1):55-62.

222.Duong L, Pixley FJ, Nelson DJ, Jackaman C. Aging Leads to Increased Monocytes and Macrophages With Altered CSF-1 Receptor Expression and Earlier Tumor-Associated Macrophage Expansion in Murine Mesothelioma. Front Aging. 2022;3:848925.
223.Odorizzi PM, Pauken KE, Paley MA, Sharpe A, Wherry EJ. Genetic absence of PD-1 promotes accumulation of terminally differentiated exhausted CD8+ T cells. J Exp Med. 2015;212(7):1125-37.
224.Ahn E, Araki K, Hashimoto M, Li W, Riley JL, Cheung J, et al. Role of PD-1 during effector CD8 T cell differentiation. Proc Natl Acad Sci U S A. 2018;115(18):4749-54.
225.Kamada T, Togashi Y, Tay C, Ha D, Sasaki A, Nakamura Y, et al. PD-1(+) regulatory T cells amplified by PD-1 blockade promote hyperprogression of cancer. Proc Natl Acad Sci U S A. 2019;116(20):9999-10008.
226.Gianchecchi E, Fierabracci A. Inhibitory Receptors and Pathways of Lymphocytes: The Role of PD-1 in Treg Development and Their Involvement in Autoimmunity Onset and Cancer Progression. Front Immunol. 2018;9:2374.
227.Rafiq S, Yeku OO, Jackson HJ, Purdon TJ, van Leeuwen DG, Drakes DJ, et al. Targeted delivery of a PD-1-blocking scFv by CAR-T cells enhances anti-tumor efficacy in vivo. Nat Biotechnol. 2018;36(9):847-56.
228.Cherkassky L, Morello A, Villena-Vargas J, Feng Y, Dimitrov DS, Jones DR, et al. Human CAR T cells with cell-intrinsic PD-1 checkpoint blockade resist tumor-mediated inhibition. J Clin Invest. 2016;126(8):3130-44.
229.Kalia V, Yuzefpolskiy Y, Vegaraju A, Xiao H, Baumann F, Jatav S, et al. Metabolic regulation by PD-1 signaling promotes long-lived quiescent CD8 T cell memory in mice. Sci Transl Med. 2021;13(615):eaba6006.
230.Wang Z, Wang S, Goplen NP, Li C, Cheon IS, Dai Q, et al. PD-1(hi) CD8(+) resident memory T cells balance immunity and fibrotic sequelae. Sci Immunol. 2019;4(36).
231.Bach FH, Grillot-Courvalin C, Kuperman OJ, Sollinger HW, Hayes C, Sondel PM, et al. Antigenic requirements for triggering of cytotoxic T lymphocytes. Immunol Rev. 1977;35:76-96.
232.Bennett SR, Carbone FR, Karamalis F, Miller JF, Heath WR. Induction of a CD8+ cytotoxic T lymphocyte response by cross-priming requires cognate CD4+ T cell help. J Exp Med. 1997;186(1):65-70.
233.Wang JC, Livingstone AM. Cutting edge: CD4+ T cell help can be essential for primary CD8+ T cell responses in vivo. J Immunol. 2003;171(12):6339-43.
234.Buller RM, Holmes KL, Hugin A, Frederickson TN, Morse HC, 3rd. Induction of cytotoxic T-cell responses in vivo in the absence of CD4 helper cells. Nature. 1987;328(6125):77-9.
235.Deeths MJ, Kedl RM, Mescher MF. CD8+ T cells become nonresponsive (anergic) following activation in the presence of costimulation. J Immunol. 1999;163(1):102-10.
236.Feau S, Facchinetti V, Granucci F, Citterio S, Jarrossay D, Seresini S, et al. Dendritic cell-derived IL-2 production is regulated by IL-15 in humans and in mice. Blood. 2005;105(2):697-702.
237.Granucci F, Feau S, Angeli V, Trottein F, Ricciardi-Castagnoli P. Early IL-2 production by mouse dendritic cells is the result of microbial-induced priming. J Immunol. 2003;170(10):5075-81.
238.Granucci F, Vizzardelli C, Pavelka N, Feau S, Persico M, Virzi E, et al. Inducible IL-2 production by dendritic cells revealed by global gene expression analysis. Nat Immunol. 2001;2(9):882-8.

239.Rogers NC, Slack EC, Edwards AD, Nolte MA, Schulz O, Schweighoffer E, et al. Syk-dependent cytokine induction by Dectin-1 reveals a novel pattern recognition pathway for C type lectins. Immunity. 2005;22(4):507-17.
240.Battegay M, Moskophidis D, Rahemtulla A, Hengartner H, Mak TW, Zinkernagel RM. Enhanced establishment of a virus carrier state in adult CD4+ T-cell-deficient mice. J Virol. 1994;68(7):4700-4.
241.Matloubian M, Concepcion RJ, Ahmed R. CD4+ T cells are required to sustain CD8+ cytotoxic T-cell responses during chronic viral infection. J Virol. 1994;68(12):8056-63.
242.Moskophidis D, Lechner F, Pircher H, Zinkernagel RM. Virus persistence in acutely infected immunocompetent mice by exhaustion of antiviral cytotoxic effector T cells. Nature. 1993;362(6422):758-61.
243.Zajac AJ, Blattman JN, Murali-Krishna K, Sourdive DJ, Suresh M, Altman JD, et al. Viral immune evasion due to persistence of activated T cells without effector function. J Exp Med. 1998;188(12):2205-13.
244.Hewitt EW. The MHC class I antigen presentation pathway: strategies for viral immune evasion. Immunology. 2003;110(2):163-9.
245.Wieczorek M, Abualrous ET, Sticht J, Alvaro-Benito M, Stolzenberg S, Noe F, et al. Major Histocompatibility Complex (MHC) Class I and MHC Class II Proteins: Conformational Plasticity in Antigen Presentation. Front Immunol. 2017;8:292.
246.Norden DM, Bethea JR, Jiang J. Impaired CD8 T cell antiviral immunity following acute spinal cord injury. J Neuroinflammation. 2018;15(1):149.
247.Shane HL, Reagin KL, Klonowski KD. The Respiratory Environment Diverts the Development of Antiviral Memory CD8 T Cells. J Immunol. 2018;200(11):3752-61.
248.Brincks EL, Roberts AD, Cookenham T, Sell S, Kohlmeier JE, Blackman MA, et al. Antigen-specific memory regulatory CD4+Foxp3+ T cells control memory responses to influenza virus infection. J Immunol. 2013;190(7):3438-46.
249.Hornick EE, Zacharias ZR, Legge KL. Kinetics and Phenotype of the CD4 T Cell Response to Influenza Virus Infections. Front Immunol. 2019;10:2351.
250.Lee W, Kingstad-Bakke B, Kedl RM, Kawaoka Y, Suresh M. CCR2 Regulates Vaccine-Induced Mucosal T-Cell Memory to Influenza A Virus. J Virol. 2021;95(15):e0053021.
251.Martinez RJ, Andargachew R, Martinez HA, Evavold BD. Low-affinity CD4+ T cells are major responders in the primary immune response. Nat Commun. 2016;7:13848.
252.Munoz-Wolf N, Ward RW, Hearnden CH, Sharp FA, Geoghegan J, O'Grady K, et al. Non-canonical inflammasome activation mediates the adjuvanticity of nanoparticles. Cell Rep Med. 2023;4(1):100899.
253.Ostroumov D, Fekete-Drimusz N, Saborowski M, Kuhnel F, Woller N. CD4 and CD8 T lymphocyte interplay in controlling tumor growth. Cell Mol Life Sci. 2018;75(4):689-713.
254.Natalini A, Simonetti S, Favaretto G, Peruzzi G, Antonangeli F, Santoni A, et al. OMIP-079: Cell cycle of CD4(+) and CD8(+) naive/memory T cell subsets, and of Treg cells from mouse spleen. Cytometry A. 2021;99(12):1171-5.
255.Kishore U, Reid KB. C1q: structure, function, and receptors. Immunopharmacology. 2000;49(1-2):159-70.
256.Bulla R, Tripodo C, Rami D, Ling GS, Agostinis C, Guarnotta C, et al. C1q acts in the tumour microenvironment as a cancer-promoting factor independently of complement activation. Nat Commun. 2016;7:10346.

257.Ling GS, Crawford G, Buang N, Bartok I, Tian K, Thielens NM, et al. C1q restrains autoimmunity and viral infection by regulating CD8(+) T cell metabolism. Science. 2018;360(6388):558-63.
258.Ogawa T, Shichino S, Ueha S, Bando K, Matsushima K. Profibrotic properties of C1q(+) interstitial macrophages in silica-induced pulmonary fibrosis in mice. Biochemical and biophysical research communications. 2022;599:113-9.
259.Roumenina LT, Daugan MV, Noe R, Petitprez F, Vano YA, Sanchez-Salas R, et al. Tumor Cells Hijack Macrophage-Produced Complement C1q to Promote Tumor Growth. Cancer Immunol Res. 2019;7(7):1091-105.
260.Reid KBM. Complement Component C1q: Historical Perspective of a Functionally Versatile, and Structurally Unusual, Serum Protein. Front Immunol. 2018;9:764.
261.Petry F, Botto M, Holtappels R, Walport MJ, Loos M. Reconstitution of the complement function in C1q-deficient (C1qa-/-) mice with wild-type bone marrow cells. J Immunol. 2001;167(7):4033-7.
262.Coss SL, Zhou D, Chua GT, Aziz RA, Hoffman RP, Wu YL, et al. The complement system and human autoimmune diseases. J Autoimmun. 2023;137:102979.
263.Zeerleder S, Levi M. Hereditary and acquired C1-inhibitor-dependent angioedema: from pathophysiology to treatment. Ann Med. 2016;48(4):256-67.
264.Kochvar AP, Cobb G, Bernabe CC, Levine T. Acquired Non-histaminergic Angioedema With C1q Autoantibody and Urticaria: A Case Report. Cureus. 2023;15(8):e43841.
265.Bucher MC, Petkovic T, Helbling A, Steiner UC. Idiopathic non-histaminergic acquired angioedema: a case series and discussion of published clinical trials. Clin Transl Allergy. 2017;7:27.
266.Lei Y, Li X, Qin D, Zhang Y, Wang Y. gC1qR: A New Target for Cancer Immunotherapy. Front Immunol. 2023;14:1095943.
267.Zhang Y, Vontz AJ, Kallenberger EM, Xu X, Ploscariu NT, Ramyar KX, et al. gC1qR/C1qBP/HABP-1: Structural Analysis of the Trimeric Core Region, Interactions With a Novel Panel of Monoclonal Antibodies, and Their Influence on Binding to FXII. Front Immunol. 2022;13:887742.
268.Yao ZQ, Eisen-Vandervelde A, Waggoner SN, Cale EM, Hahn YS. Direct binding of hepatitis C virus core to gC1qR on CD4+ and CD8+ T cells leads to impaired activation of Lck and Akt. J Virol. 2004;78(12):6409-19.
269.Tian H, Wang G, Wang Q, Zhang B, Jiang G, Li H, et al. Complement C1q binding protein regulates T cells' mitochondrial fitness to affect their survival, proliferation, and anti-tumor immune function. Cancer Sci. 2022;113(3):875-90.
270.Liao M, Liu Y, Yuan J, Wen Y, Xu G, Zhao J, et al. Single-cell landscape of bronchoalveolar immune cells in patients with COVID-19. Nat Med. 2020;26(6):842-4.
271.Zhou X, Moore BB. Lung Section Staining and Microscopy. Bio Protoc. 2017;7(10).
272.Aguglia G, Coyne CB, Dermody TS, Williams JV, Freeman MC. Contemporary enterovirus-D68 isolates infect human spinal cord organoids. mBio. 2023;14(4):e0105823.
273.Browaeys R, Saelens W, Saeys Y. NicheNet: modeling intercellular communication by linking ligands to target genes. Nat Methods. 2020;17(2):159-62.
274.Jin S, Guerrero-Juarez CF, Zhang L, Chang I, Ramos R, Kuan CH, et al. Inference and analysis of cell-cell communication using CellChat. Nat Commun. 2021;12(1):1088.
275.Ghebrehiwet B, Geisbrecht BV, Xu X, Savitt AG, Peerschke EIB. The C1q Receptors: Focus on gC1qR/p33 (C1qBP, p32, HABP-1)(1). Semin Immunol. 2019;45:101338.

276.Steino A, Jorgensen CS, Laursen I, Houen G. Interaction of C1q with the receptor calreticulin requires a conformational change in C1q. Scand J Immunol. 2004;59(5):485-95.
277.Verneret M, Tacnet-Delorme P, Osman R, Awad R, Grichine A, Kleman JP, et al. Relative contribution of c1q and apoptotic cell-surface calreticulin to macrophage phagocytosis. J Innate Immun. 2014;6(4):426-34.
278.Aegerter H, Lambrecht BN, Jakubzick CV. Biology of lung macrophages in health and disease. Immunity. 2022;55(9):1564-80.
279.Leach SM, Gibbings SL, Tewari AD, Atif SM, Vestal B, Danhorn T, et al. Human and Mouse Transcriptome Profiling Identifies Cross-Species Homology in Pulmonary and Lymph Node Mononuclear Phagocytes. Cell Rep. 2020;33(5):108337.
280.Li Y, Nair H. Trends in the global burden of lower respiratory infections: the knowns and the unknowns. Lancet Infect Dis. 2022;22(11):1523-5.
281.Son M. Understanding the contextual functions of C1q and LAIR-1 and their applications. Exp Mol Med. 2022;54(5):567-72.
282.Melms JC, Biermann J, Huang H, Wang Y, Nair A, Tagore S, et al. Author Correction: A molecular single-cell lung atlas of lethal COVID-19. Nature. 2021;598(7882):E2.
283.Chen A, Gaddipati S, Hong Y, Volkman DJ, Peerschke EI, Ghebrehiwet B. Human T cells express specific binding sites for C1q. Role in T cell activation and proliferation. J Immunol. 1994;153(4):1430-40.
284.Kouser L, Madhukaran SP, Shastri A, Saraon A, Ferluga J, Al-Mozaini M, et al. Emerging and Novel Functions of Complement Protein C1q. Front Immunol. 2015;6:317.
285.Thielens NM, Tedesco F, Bohlson SS, Gaboriaud C, Tenner AJ. C1q: A fresh look upon an old molecule. Mol Immunol. 2017;89:73-83.
286.Markarian M, Krattli RP, Jr., Baddour JD, Alikhani L, Giedzinski E, Usmani MT, et al. Glia-Selective Deletion of Complement C1q Prevents Radiation-Induced Cognitive Deficits and Neuroinflammation. Cancer Res. 2021;81(7):1732-44.
287.Hu B, Jadhav RR, Gustafson CE, Le Saux S, Ye Z, Li X, et al. Corrigendum: Distinct Age-Related Epigenetic Signatures in CD4 and CD8 T Cells. Front Immunol. 2022;13:911132.
288.Farisoglu U, Balcioglu O, Ozcem B, Kilic AO, Soyler G, Nasircilar Ulker S, et al. Parabiosis Improves Endothelial Dysfunction in Aged Female Mice. J Surg Res. 2022;278:119-31.
289.Ambrosi TH, Marecic O, McArdle A, Sinha R, Gulati GS, Tong X, et al. Aged skeletal stem cells generate an inflammatory degenerative niche. Nature. 2021;597(7875):256-62.
290.Salam N, Rane S, Das R, Faulkner M, Gund R, Kandpal U, et al. T cell ageing: effects of age on development, survival & function. Indian J Med Res. 2013;138(5):595-608.
291.Yousefzadeh MJ, Flores RR, Zhu Y, Schmiechen ZC, Brooks RW, Trussoni CE, et al. An aged immune system drives senescence and ageing of solid organs. Nature. 2021;594(7861):100-5.
292.Ballou LM, Lin RZ. Rapamycin and mTOR kinase inhibitors. J Chem Biol. 2008;1(1-4):27-36.
293.Saccon TD, Nagpal R, Yadav H, Cavalcante MB, Nunes ADC, Schneider A, et al. Senolytic Combination of Dasatinib and Quercetin Alleviates Intestinal Senescence and Inflammation and Modulates the Gut Microbiome in Aged Mice. J Gerontol A Biol Sci Med Sci. 2021;76(11):1895-905.
294.Yang D, Sun B, Li S, Wei W, Liu X, Cui X, et al. NKG2D-CAR T cells eliminate senescent cells in aged mice and nonhuman primates. Sci Transl Med. 2023;15(709):eadd1951.

295.Amor C, Fernandez-Maestre I, Chowdhury S, Ho YJ, Nadella S, Graham C, et al. Prophylactic and long-lasting efficacy of senolytic CAR T cells against age-related metabolic dysfunction. Res Sq. 2023.
296.Chung JH, Ha JS, Choi J, Kwon SM, Yun MS, Kim T, et al. Granzyme B for predicting the durable clinical benefit of anti-PD-1/PD-L1 immunotherapy in patients with non-small cell lung cancer. Transl Cancer Res. 2022;11(2):316-26.
297.August A, Shaw CA, Lee H, Knightly C, Kalidindia S, Chu L, et al. Safety and Immunogenicity of an mRNA-Based Human Metapneumovirus and Parainfluenza Virus Type 3 Combined Vaccine in Healthy Adults. Open Forum Infect Dis. 2022;9(7):ofac206.